ADVANCES IN ORGANOMETALLIC AND PROTEIN CHEMISTRY

Christopher Patrick Ryan

Department of Chemistry, University College London

Doctor of Philosophy

DECLARATION

The work described in this thesis is the work of the author and has not previously been submitted to this or any other university for any other degree.

Christopher Patrick Ryan

June 2010

ACKNOWLEDGEMENTS

First I would like to thank my supervisor Prof. Steve Caddick for giving me the opportunity to carry out a variety of exciting research, and for his enthusiasm, motivation and support throughout my PhD. Second I would like to thank Prof. Nik Kaltsoyannis for his invaluable help concerning all things DFT related.

I would also like to thank past and present members of the Caddick group for making my time at UCL as fun as it was; in particular Jack, James, Mark, Nuj, Tom and Vijay. I would also like to thank Dr. Jamie Baker, Richard Fitzmaurice, Alex Lewis, Frank King, Tom Sheppard, Mark Smith and John Wilden for all the excellent help and advice they gave me.

A big thank you goes to Dr. Abel Aliev for his continued interest and help with all NMR related issues and to Dr. Lisa Harris for her invaluable Mass Spec support.

Finally I would like to thank my family, friends and housemates for their support throughout my studies.

ABSTRACT

This thesis describes two areas of scientific investigation. The first contains a description of a study on the synthesis of biotinylated and fluoresceinylated bromomaleimide based reagents. Upon synthesis, the ability of these reagents to add reversibly to cysteine containing proteins is investigated by a series of LCMS experiments. A single point mutant (L111C) of the SH2 domain of the Grb2 adaptor protein, containing a single cysteine residue, is chosen as an ideal protein for study. Thus biotinylated and fluoresceinylated mono and dibromomaleimide reagents are added to Grb2 at 0°C, 21 °C and 37 °C for 2 h at pH 7 and 8 to give protected Grb2-bromomaleimide adducts in high yield and removed using 100 eq of beta-mecaptoethanol for 4 h to return original Grb2 protein intact. Reversibility is shown to be abolished by hydrolysis of the maleimide motif, a process more prevalent in the fluoresceinylated and dibrominated maleimide reagents than for the biotinylated and monobrominated reagents. LCMS is used to investigate the insertion of these reagents reversibly into the single disulfide bridge of somatostatin, a process shown to be complete within 1 h at 21 °C and pH 6. Reduction using 100 eq of beta-mecaptoethanol is shown to take place within 1 h. Additionally no hydrolysis is observed at pH 6, suggesting that with careful control of pH, reversibility of the bromomaleimide reagents can be switched on and off.

The second part of the thesis contains a study on mechanistic aspects of organopalladium catalysis, particularly the factors affecting the final reductive elimination stage of the palladium catalysed alkyl amination reaction. DFT calculations have been used to obtain a number of energy level diagrams for the potential energy surface of Pd(IBu)(neopentyl)(morpholide), the three coordinate palladium complex believed to be the species from which reductive elimination takes place. From this it has been found that two different pathways are available; reductive elimination or morpholide promoted C-H activation of the neopentyl motif, the latter of which was favoured. The reaction pathway for reductive elimination from Pd(IBu)(neopentyl)(morpholide) is compared with Pd(IBu)(phenyl)(morpholide), Pd($PCyp_3$)(neopentyl)(morpholide) and Pd(IBu)(methyl)(morpholide), to show that the phenyl system is considerably lower

in energy. The energy requirements for (i) reductive elimination, (ii) morpholide promoted C-H activation and (iii) β-hydride elimination from Pd(IBu)(2-dimethylpropyl)(morpholide) are compared, and shown to be in the order of energy (i)>(ii)>(iii). Additionally, the rate of reaction increases as the number of available reaction sites increases, again making reductive elimination the least favoured process.

Offline ESI(+)-MS analysis have been used to monitor the reaction progress of Pd(IBu)(neopentyl)(morpholide) and Pd(IBu)(phenyl)(morpholide) three coordinate complexes. Whilst transient palladium-bound species can be observed for Pd(IBu)(phenyl)(morpholide), for Pd(IBu)(neopentyl)(morpholide) this is not the case, an artefact of the superiority of the sp^2 phenyl system over the sp^3 alkyl system.

CONTENTS

Abbreviations

Ad – Adamantyl

AcOH – Acetic acid

ADF – Amsterdam density functional

API – Atmospheric pressure ionisation

ATP – Adenosine triphosphate

BDE – Bond dissociation energy

BME – β-Mercaptoethanol

Boc – *tert*-Butoxycarbonyl

Bz – Benzyl

CI – Chemical ionisation

COSMO - Conductor-like screening model

DDT - Dithiothreitol

DEAD – Diethyl azodicarboxylate

DFT – Density functional theory

Dha - Dehydroalanine

DIAD – Diisopropyl azodicarboxylate

DIPEA – *N*,*N*'-Diisopropylethylamine

DMAP – Dimethylaminopyridine

DMF – Dimethylformaldehyde

DMPM – 1,1-Bis(dimethylphosphino)methane

DMSO – Dimethyl sulfoxide

DNA – Deoxyribonucleic acid

DPPM – 1,1-Bis(diphenylphosphino)methane

DPPP – 1,3-Bis(diphenylphosphino)propane

EDC.HCl - 1-Ethyl-3-(3-dimethyllaminopropyl)carbodiimide hydrochloride

ESI – Electrospray ionisation

ELISA - Enzyme-linked immunosorbent assay

eq – Equivalent

GBL - γ-Butyrlactone

Grb2 - Growth factor receptor-bound protein 2

GTO – Gaussian type orbital

HBTU - O-Benzotriazole-*N*,*N*,*N'*,*N'*-tetramethyl-uronium-hexafluoro-phosphate

HMDS - Hexamethyldisilazane

HOBt – 1-Hydroxybenzotriazole

HOMO – Highest occupied molecular orbital

HRMS – High resolution mass spectrum

IBu – 1,3 –di-*tert*-butyl-imidazol-2-ylidene

IMe – 1,3-dimesityl-imidazol-2-ylidene

IPr – 1,3-di-*iso*-propyl-imidazol-2-ylidene

IR – Infra-red

K_d – Dissociation equilibrium constant

LCMS – Liquid chromatography mass spectrometry

LMDS – Lithium hexamethyldisilazide

LUMO – Lowest unoccupied molecular orbital

MBO – Mayer bond order

MEA – 2-Mercaptoethylamine.hydrochloric acid

mp – Melting point

Ms - Mesityl

MS – Mass spectrometry

MSH - *o*-Mesitylenesulfonylhydroxylamine

MSS - *m*-Maleimidobenzoyl-*N*-hydroxysuccinimidyl ester

NHC – *N*-Heterocyclic carbene

NEM – *N*-Ethyl maleimide

NHS – *N*-Hydroxysuccinimide

NMM – *N*-Methyl maleimide

NMR – Nuclear magnetic resonance

OEG - Oligoethyleneglycol

ppm – Parts per million

PTM – Post translational modification

RT – Room temperature

SIBu – 1,3-di-*tert*-butyl-imidazol-4,5-dihydro-2-ylidene

SIPr – 1,3-di-*iso*-propyl-imidazol-4,5-dihydro-2-ylidene

SMCC - Succinimidyl-4-(*N*-maleimidomethyl)cyclohexane-1-carboxylate)

SMPB - Succinimidyl-4-(-*p*-maleimidophenyl)butyrate

SST - Somatostatin

STO – Slater type orbital

sulfo-SMPB - sulfosuccinimidyl-4-(-*p*-maleimidophenyl)butyrate

TCEP - *tris*(2-Carboxyethyl)phosphine

TFA – Trifluoroacetic acid

THF – Tetrahydrofuran

TLC – Thin layer chromatography

UV – Ultraviolet

ZORA – Zero-order regular approximation

1 Post translational modification of cysteine

1.1 Protein modification

Proteins are responsible for the majority of functional attributes of all living organisms. They act as building blocks of the cell structure and as catalysts in the metabolism of cells. Furthermore, signal transduction within and between cells, as well as cell morphology and stability, are dependent on a large number of proteins. Many of these functions are dependent on post-translational modifications (e.g. glycosylation or lipidation) at specific sites of the proteins involved.[1]

A post translational modification (PTM) is a chemical modification of a protein after its translation and can be thought of as one of the later steps in protein biosynthesis for many proteins. The PTM of amino acids extends the range of functions of the protein by attaching different chemical groups such as phosphates, acetates, lipids and carbohydrates, which changes the structure and reactivity of the amino acids. Being able to mimic this action in the laboratory is thus very desirable from a medicinal and therapeutic perspective and much research has gone into developing such strategies.

For a reaction in the laboratory to be of general use in protein modification, it must selectively modify a residue of interest in the presence of hundreds of competing side chains of the unprotected polypeptide.[2] This selectivity must also be realised in conditions required to prevent denaturation; aqueous media, low to ambient temperature, and at or near neutral pH. The reactions must also tolerate salts and surfactants needed for protein stability and the reactions must be rapid to achieve full conversion.

Of the twenty two different amino acids that are commonly found in proteins, there are ten that may in principle be derivatised at their side chains, since these amino acids possess functional groups (figure 1).[3]

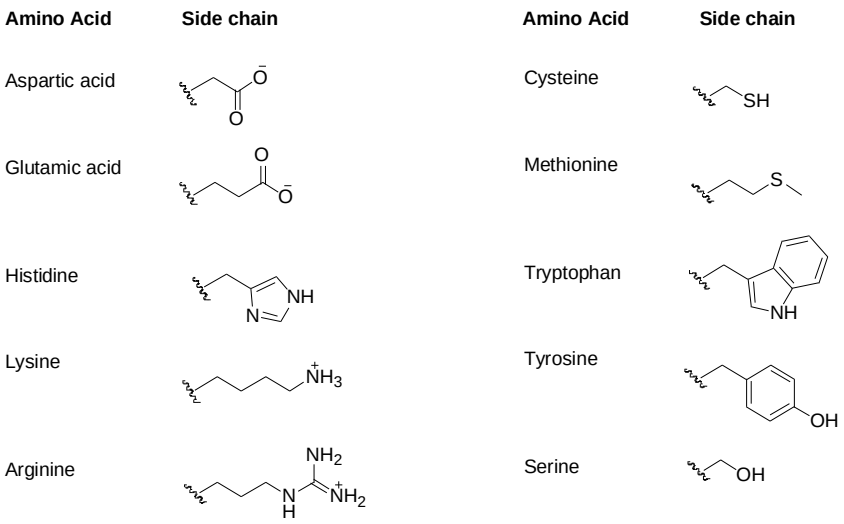

Figure 1. The ten canonical amino acids.

The most chemically reactive of these groups are the amines and thiols (scheme 1). Aldehydes, for instance, can be coupled with exposed amines on the lysine and arginine residues of the protein[4,5] and then reduced with sodium borohydride or other reagents to form a stable secondary amine linkage. Alternatively epoxides can be employed as the amine reactive electrophile which have the advantage of the resultant products being relatively stable to hydrolysis at neutral pH, allowing easier handling of the materials but slower or incomplete coupling.[5] Amides can also be formed from the reaction of activated acid with amine.

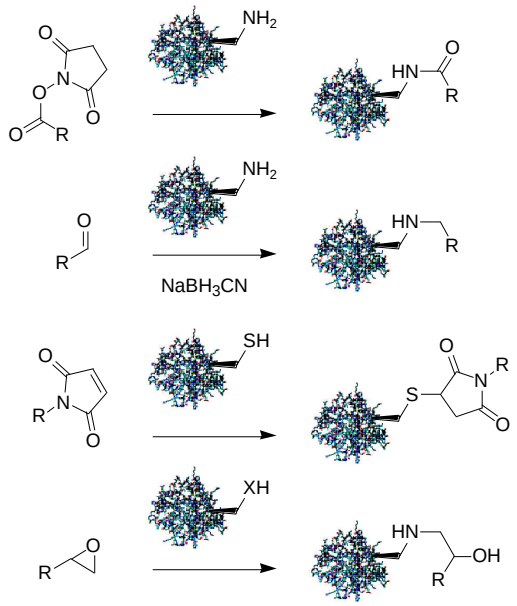

Scheme 1. Common modifications of amine and thiol amino acid side chains. X = NH_2, SH.

Of all the chemical groups present in the ten amino acids above, the thiols of cysteines are found to be most reactive and are considered better targets for site-specific labelling than the amines of the amino terminus and lysine side chains. It has been shown that conjugate addition strongly favours the thiolate group at physiological pH (6.5-7.5) since under these conditions the amines of lysine and arginine are predominantly protonated: a result of the lower pKa of cysteine (8.3) compared with lysine (10.5) and arginine (12.0). Maleimides, for instance, react approximately 1000 times faster with thiols than with amines at neutral pH and below.[6] Additionally as proteins generally have very few surface-exposed cysteine residues,[7] it is possible to achieve site-selective modification, especially if the protein of interest is engineered to remove all but one surface cysteine residue or to insert a single cysteine on the surface where none previously existed.[8-10] If no free cysteine is available, then any present disulfide bridge could take its place, although this would first need to be reduced to form the free sulfhydryls before reaction with any cysteine modifying reagent. To these ends, reducing agents such as 2-mercaptoethylamine.HCl (MEA), *β*-mercaptoethanol (BME), *tris*(2-carboxyethyl)phosphine (TCEP) or dithiothreitol (DTT) have all been used.[11]

1.2 Reactions for cysteine modification

Cysteine can be considered very useful for introducing protein-modifying agents such as fluorophores,[12,13] cross linkers[14,15] and peptide/DNA cleavage reagents[16,17] including α-halocarbonyl bound iron-chelate (section 1.2.3) into proteins.[18] Today a variety of cysteine modifying reagents are available from a number of leading biochemical companies (e.g. Pierce, Aldrich) with even more being synthesised in laboratories around the world for specific applications. The main reaction types that are employed to modify cysteine residues are alkylation, disulfide formation and oxidation and these are considered in turn (scheme 2).

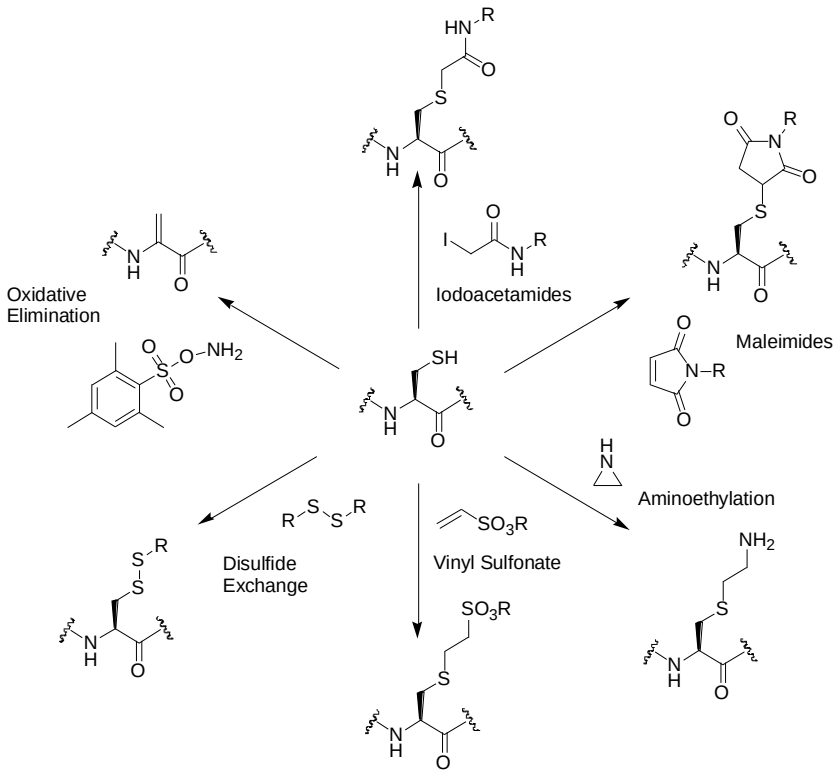

Scheme 2. Reactions for cysteine modification.

1.2.1 Oxidative elimination

The oxidative elimination of cysteine has been shown to be a useful tool for the removal of sulfur to give the unsaturated amino acid dehydroalanine, Dha **1**.[2,19] The simplest method for formation of **1** is the oxidation in air to give the disulfide species, followed by elimination with base. In many instances, simply mixing of cysteine in basic buffer open to air would be enough to carry out the transformation, although reaction times can be slow and dimer formation a potential problem. More recent desulfurisations rely on the addition of cysteine to an electrophile, where elimination of hydrogen from the intermediate would give Dha **1** (scheme 3).

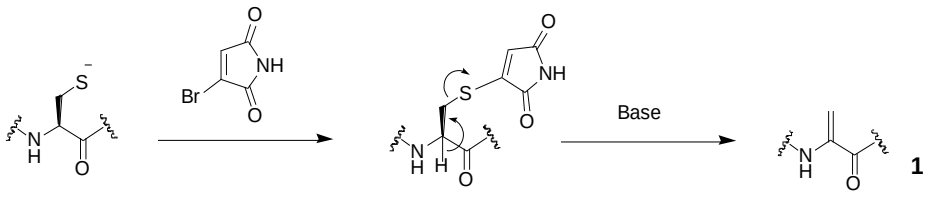

Scheme 3. An example of a new method for the desulfurisation of cysteine, using bromomaleimide.

From **1** a considerable number of chemical transformations have been carried out to derivatise the structure further, such as Pd and Rh catalysed reactions,[20-23] hydroboration[24] and alkylation.[19] Recent efforts have focused on finding milder conditions to carry out these desulfurisations, with *o*-mesitylenesulfonylhydroxylamine[2] (MSH **2**) and then bromomaleimides[25] **3** finding use (figure 2).

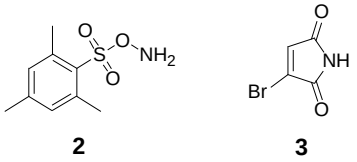

2 **3**

Figure 2. Reagents recently used in the desulfurisation of cysteine to dehydroalanine (Dha), MSH **2** and bromomaleimide **3**.

1.2.2 Disulfide exchange

Compounds possessing a disulfide group have been shown to take part in disulfide exchange reactions with other thiols. This process involves attack of the thiol at the disulfide, breaking the S-S bond, with subsequent formation of a new mixed disulfide containing a portion of the original disulfide compound **5** (scheme 4).[26] If the thiol is present in excess, the mixed disulfide can go on to form a symmetrical disulfide consisting entirely of the thiol reducing agent, thus completely reducing the original disulfide to free sulfhydryls. However, if an excess of thiol is not used, the mixed disulfide is the end product.

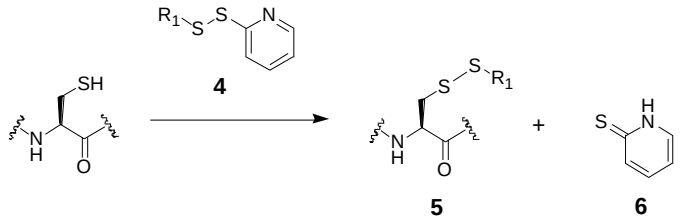

4 **5** **6**

Scheme 4. Disulfide exchange of cysteine using pyridyl disulfide **4**.

Many activated or activating reagents for disulfide exchange are available today and it is through these reagents that disulfide modification for functional purposes has become common. A popular reagent is pyridyl dithiol **4** (figure 3). This readily undergoes an interchange reaction with a free sulfhydryl to yield a single mixed disulfide product. The presence of a good leaving group not capable of taking part in

further reactions, in this case pyridine-2-thione, is key to success of these reactions. Another well known reagent is 5,5-dithiobis(2-nitrobenzoate) (Ellman's reagent 7).[27,28] This reagent is predominantly used to measure protein cysteine content and as a way of blocking free thiol groups.

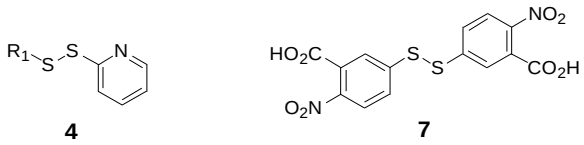

4 **7**

Figure 3. Pyridyl thiol **4** and Ellman's reagent **7**, two common reagents used in disulfide exchange reactions.

An additional factor that has made disulfide exchange such a popular modification is the reversibility it affords. Therefore treatment of disulfides with reducing agents such as dithiothrietol (DTT **8**), *β*-mercaptoethanol (BME **9**) or 2-mercaptoethylamine (MEA **10**) results in reduction of the disulfide to give back free cysteine. This process works in two stages. First, one molecule of the reducing agent (**8**, **9** or **10**) undergoes disulfide exchange, cleaving the disulfide and forming a new, mixed disulfide **13**. In the second stage, another molecule of the thiol cleaves this new mixed disulfide, releasing a free sulfhydryl and forming a molecule of oxidised reducing agent **15** (scheme 5).

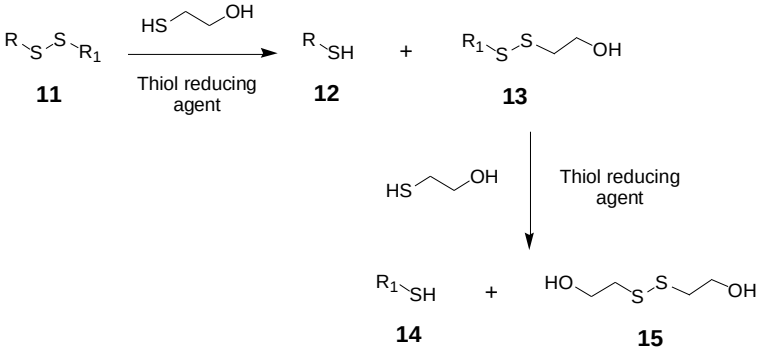

11 **12** **13** **14** **15**

Scheme 5. Reduction of disulfides, in this example using BME **9**.

1.2.3 Alkylation

Of all the potential reagents for cysteine modification, α-halocarbonyls, such as iodo[29] and chloroacetamides,[30] were among the first reagents used for the direct alkylation of cysteine in 1935 and have remained useful and commercially available still today (scheme 6). They allow the direct displacement of the halide centre by the soft nucleophilic sulfhydryl group and have been used to produce mimics of natural asparagine-linked glycoproteins[31] to assess homogenously glycosylated samples of human erythropoietin.[32] They have also been used as DNA/peptide cleavage reagents, such as α-halocarbonyl bound iron-chelates, which induces cleavage at cysteine upon treatment with H_2O_2/ascorbate.[16,17]

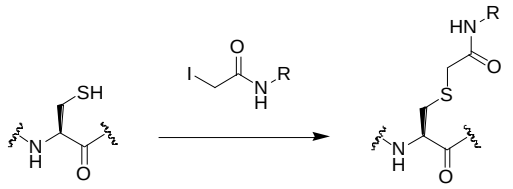

16

Scheme 6. Cysteine modification using α-halocarbonyls.

Aminoethylation of cysteine using aziridine is another example of alkylation and has been used for over half a century for the conversion of cysteine to lysine mimics.[33,34] The aziridine functional group is a small ring system composed of one nitrogen and two carbon atoms, whose highly hindered nature lends strong reactivity towards nucleophiles. Sulfhydryls will react with aziridine-containing reagents in a ring-opening process to form a thioether bond **17** (scheme 7). In slightly alkaline pH the reaction is highly specific although in aqueous solution the major side reaction is hydrolysis.[26]

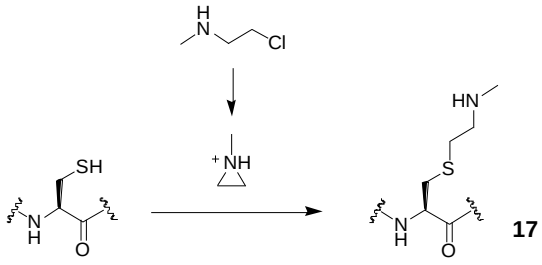

17

Scheme 7. Aminoethylation of cysteine to form methylated lysine mimic.

The conjugate addition of cysteine to Michael acceptors such as vinyl sulfonates, maleimides and related α,β-unsaturated systems has also been established as a reliable way of alkylating cysteine and have emerged as the reagents of choice in these reactions. They have been shown to be very fast, reliable and robust in their selective alkylation of the cysteine side chain. Of these reagents, however, the maleimide functional group is of paramount importance due to its highly specific affinity for free sulfhydryl groups. The double bond of maleimide may undergo an alkylation reaction with sulfhydryls to form stable thioether bonds **18** (scheme 8). This reaction is specific for sulfhydryl groups in the pH range 6.5-7.5, whilst at higher pH values some cross-reactivity with amino groups is known to take place. Additionally, when a sufficient quantity of SH groups have been alkylated, the reaction may be followed spectrophotometrically by the decrease in absorbance at 300 nm as the double bond reacts and disappears.

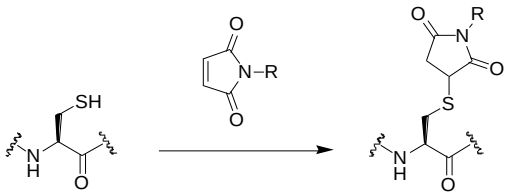

18

Scheme 8. Reaction of cysteine with maleimide. R = H, Me, Et.

The maleimide group can undergo hydrolysis to an open maleimic acid form that is unreactive toward sulfhydryls,[26] which can also occur after sulfhydryl coupling to the maleimide **19** (scheme 9). This ring-opening reaction typically becomes faster with increasing pH. Hydrolysis is also dependant on the type of chemical group adjacent to the maleimide motif. For example, the cyclohexane ring of SMCC **20** provides increased stability to maleimide hydrolysis due to its steric effects and its lack of aromatic character. However, the adjacent phenyl ring of MBS **21** allows much greater rates of hydrolysis to occur at the maleimide ring (figure 4).

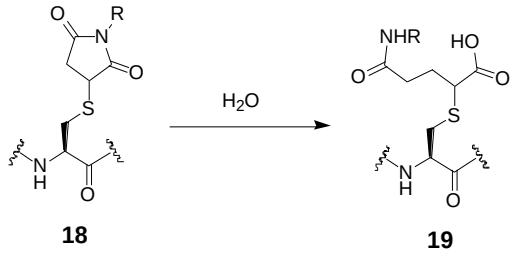

18 **19**

Scheme 9. Hydrolysis of maleimide ring.

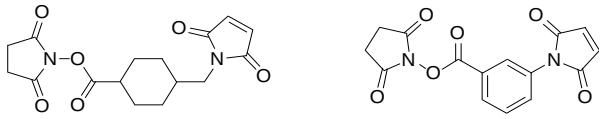

20 **21**

Figure 4. SMCC (Succinimidyl-4-(*N*-maleimidomethyl)cyclohexane-1-carboxylate) **20** and MBS (*m*-maleimidobenzoyl-*N*-hydroxysuccinimidyl ester) **21**.

1.3 Maleimides as reagents in protein modification

1.3.1 Fluorescent probes

The fluorescent labelling of peptides and proteins is usually performed through either the side chain amino group of a lysine residue or the side chain sulfhydryl group of a cysteine residue, using commercially available linkers.[35] The key requirement when incorporating these fluorescent tags on to the protein of interest is to find a site of modification that will not adversely affect the proteins function. Sulfhydryls are smaller in number compared to amine side groups and tend to be situated away from the proteins active site. This is due to the evolutionary pressure associated with not having a highly reactive amino acid residue at a biologically important site of a protein; modification of this highly reactive residue could change the function of the protein, adversely affecting the cells chances of survival. The smaller number of sulfhydryl residues and their position in the protein means that their directed modification usually helps to preserve activity in the fluorescent probe complex.

Fluorescein-5-maleimide **22** is one such fluorescent probe containing a sulfhydryl reactive maleimide group on its lower ring structure (figure 5). Addition of this reagent to sulfhydryl containing proteins under physiological conditions results in

derivatives possessing fluorescent properties characteristic of fluorescein molecules: excitation wavelength = 490 nm; emission wavelength = 515 nm, in the green spectral region.

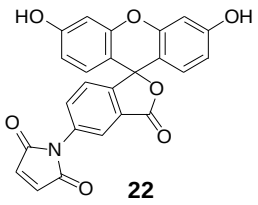

22

Figure 5. Fluorescein-5-maleimide **22**.

Fluorescein-5-maleimide **22** has been employed in many experiments, such as in labelling the transmembrane glycoprotein H-2K^{k} on both N and C terminal regions to investigate molecular structure,[36] in the determination of two different conformations of the protein actin[37] and the investigation of the calcium-dependent ATPase protein structure of the sarcoplasmic reticulum.[38]

1.3.2 Blocking agents and the inhibition of cellular processes

It has been known for a long time that disulfide bond formation between cysteine sulfhydryls is critical for protein structure and function.[39] However, the sulfhydryl group is among the most highly reactive of nucleophiles found in biological systems and undergoes covalent reactions rapidly with most of the reactive groups utilised in protein modification and conjugation. To prevent this from happening it is often necessary to block these sites and render them inert to further reaction. Two types of cysteine modifying reagents are employed as blocking agents today; permanent (maleimide group) and reversible (disulfide exchange).

N-Ethylmaleimide **23** (NEM) is one such permanent reagent which reacts with and blocks sulfhydryl groups by formation of stable thioether bonds (figure 6).[40] It has found use in the modification of sulfhydryl groups essential in the interaction of ATP with its regulatory site(s) in transport ATPases such as the (Na^{+},K^{+})-ATPase[41] and inactivation of the clathrin-coated vesicle (H+)-ATPase.[42] *N*-Methylmaleimide **24** (NMM), another irreversible blocking agent, has been found to completely abolish

K_{ATP} channel activity if applied to the cytoplasmic face of membrane patches from skeletal muscle.[43]

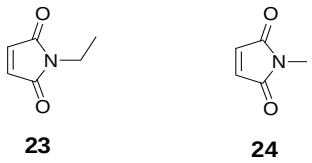

23 **24**

Figure 6. Irreversible sulfhydryl blocking agents; *N*-ethyl maleimide **23** (NEM) and *N*-methyl maleimide **24** (NMM).

1.3.3 Bifunctional reagents

There are two main types of bifunctional reagent used in bioconjugation chemistry today: those with the same function group at either end of the molecule (homobifunctional) and those with different functional groups (heterobifunctional). Major sulfhydryl reactive homobifunctional reagents in use include 1,8-bis-maleimidotriethyleneglycol **25** and 1,11-bis-maleimidotriethyleneglycol. These contain a maleimide group at either end of the reagent and allow cross linking with a variety of sulfhydryl containing molecules. However, here lies an inherent problem in their applicability: the potential for dimer formation **27**, i.e. the cross linking of homobifunctional reagents with two molecules of sulfhydryl containing protein, often results in a complex reaction mixture, low in yield of the wanted monofunctionalised protein **26** (scheme 10).

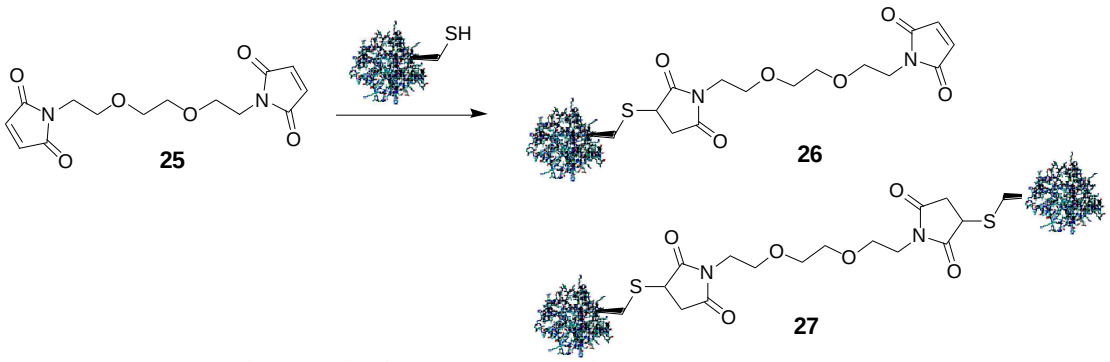

25 **26** **27**

Scheme 10. Potential dimer formation of sulfhydryl reactive homobifunctional reagents.

Heterobifunctional reagents do not exhibit any dimer formation and as a result play a key role in many bioconjugate reactions due to the greater control afforded to product formation. The most popular heterobifunctional reagents are those that contain amine-reactive and sulfhydryl-reactive ends (figure 7). The amine reactive

group is usually an active ester, most often an NHS ester, whilst the sulfhydryl-reactive portion may be one of several, in this case a maleimide motif. These reagents are very good for the selective and controlled addition of substrates to either end of the reagent. The NHS ester end of the reagent can react with primary amine groups on proteins to form stable amide bonds, whilst the maleimide functionality allows for reaction of sulfhydryls at the other end. The nature of the reactive groups allows for highly controlled cross-linking procedures to be performed.

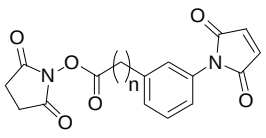

28

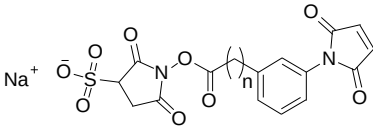

29

Figure 7. Heterobifunctional reagents; succinimidyl-4-(-*p*-maleimidophenyl)butyrate (SMPB) **28** and sulfosuccinimidyl-4-(-*p*-maleimidophenyl)butyrate (sulfo-SMPB) **29**.

A major use of heterobifunctional reagents is in the preparation of antibody-enzyme and hapten-carrier conjugates, such as those found in Enzyme-Linked ImmunoSorbent Assays (ELISA). ELISA is a biochemical technique used mainly in immunology to detect the presence of an antibody or an antigen in a sample. The procedure for this process is relatively simple; first an unknown amount of antigen is affixed to a surface and then a specific antibody is washed over the surface so that it can bind to the antigen. This antibody is linked to an enzyme, so that addition of a second substance to the antigen-antibody-enzyme conjugate would illicit some sort of detectable signal (e.g. fluorescence).

Taking the HIV ELISA (HIV enzyme immunoassay) as an example; a plastic plate containing a series of wells, each about 1.0 cm high and 0.7 cm in diameter, is first coated with inactivated HIV antigens. A patient's serum is then applied to the plate to which the HIV antigens have previously been attached. If the patient is HIV positive, then their serum will contain antibodies to HIV, and these antibodies will bind to the HIV antigens attached to the plate. The plate is then washed to remove all other components of the serum, leaving only the HIV antibodies bound to the HIV antigens. Following this, a specially prepared secondary antibody is added. This secondary antibody is usually an anti-human immunoglobulin (anti-human Ig)

coupled to an enzyme (usually horseradish peroxidase, β-galactosidase or glucose oxidase) and is designed to bind specifically to other human antibodies, in this case the HIV antibodies.

Therefore upon addition of this secondary antibody, the plate will contain an enzyme whose concentration is proportional to the amount of secondary antibody bound to the HIV antibody-antigen conjugate. A substrate for this enzyme can then be applied, so that catalysis by the enzyme leads to a change in colour. In the case of HIV ELISA studies, horseradish peroxidase (HRP) is used; HRP reacts with its fundamental substrate H_2O_2 to form a stable intermediate that will dissociate in the presence of certain electron donors (ascorbate, cytochrome *c*, ferrocyanide), oxidising the donor and creating a colour change in the process. The optical density of this colour change can then be measured, and compared to both.negative (healthy) and positive (HIV sufferer) controls, to determine whether the patient is infected with HIV.

Maleimide-containing heterobifunctional reagents, such as SMCC **20**, are relevant because they have been used in the synthesis of the antibody-enzyme conjugates **31** used in ELISA studies (scheme 11), including the peroxidase-conjugated anti-human immunoglobulin antibody used in HIV enzyme immunoassays; the NHS ester is reacted with the enzyme to give **30** and then the sulfhydryl-containing antibody is added. This two-step reaction scheme results in the formation of the specific antibody-enzyme conjugates **31**.

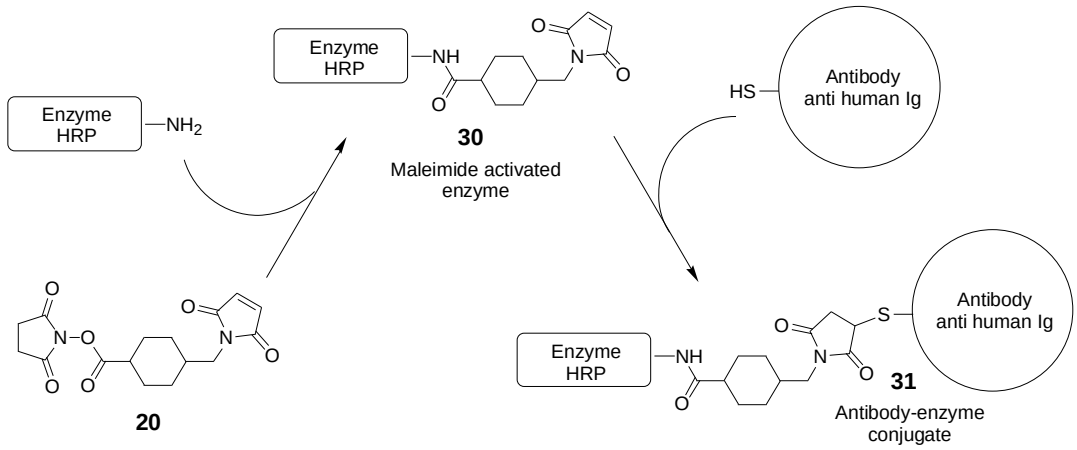

Scheme 11. Use of heterobifunctional reagent SMCC **20** in antibody-enzyme conjugate formation.

1.3.4 The use of maleimides in surface immobilisation

Today the immobilisation of biomolecules to solid phase materials is a frequently used procedure to confer a specific affinity or enzymatic activity on the surface. The development of biosensor devices typically requires the encapsulation or surface immobilisation of a molecular recognition element onto a surface for interfacing with a signal detector.[44] This has led to an explosion in the use of microarray technology (biochip) as a promising tool for gene discovery, genome analysis, medical diagnostics for genetic diseases, detection of single nucleotide polymorphism, nucleic acid-ligand interactions, DNA sequencing by hybridisation and DNA coupling,[45] as well as the discovery and mapping of novel protein-protein, protein-DNA, protein-drug, and protein-lipid function.[46-48]

In performing these immobilisation reactions, the aim is generally to attach the often fragile ligands in such a way as to leave them structurally intact with their active sites easily accessible to specifically binding reactants present in the surrounding fluid phase. Many of the applications demonstrated thus far have relied on protein attachment methods that result in non site-specific immobilisation, either covalently through amine, aldehyde, and epoxy-derivatised surfaces[5,49,50] or through non-covalent adsorption on nitrocellulose, hydrogel, or polylysine coated slides[51-54] by way of passive adsorption onto hydrophobic surfaces or electrostatic interactions with charged surfaces.[8] A number of more selective approaches have been demonstrated and employ affinity reagents that bind specific markers on proteins and render them in a correctly orientated manner such as (strept)avidin (figure 8).[55-57]

(Strept)avidin is a tetrameric protein able to bind biotin, a small naturally occurring vitamin, up to four times. The interaction has been shown to be stable *in vivo* and is essentially irreversible ($K_d \sim 10^{-15}$ M).[55,56] This has allowed the (strept)avidin-biotin system to emerge as an extremely powerful and versatile tool in biomedical science and clinical diagnostics.[58]

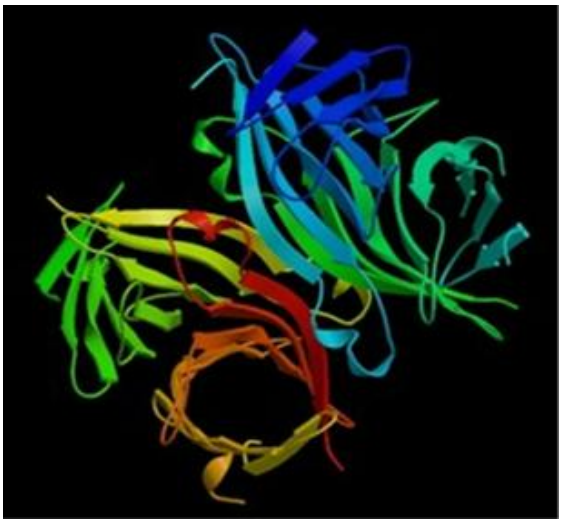

Figure 8. (Strept)avidin.

The (strept)avidin-biotin system has found considerable usage in affinity chromatography, affinity cytochemistry, cell cytometry, blotting technology, immunoassay, histopathology staining, gene probes, bioaffinity sensors and biomarker detection,[59] as well as for the targeted delivery of diagnostic and therapeutic agents.[60] For this latter purpose, a ligand is modified either with avidin or with biotin and is then allowed to accumulate in a target area. Then the pharmaceutical agent is administered as a conjugate of either biotin or avidin (depending on the corresponding subunit) and concentrates locally in the desired area due to the fast formation of the avidin-biotin complex where it can take affect. Figure 9 shows two typical sulfhydryl reactive biotinylation agents used today. Whilst one end contains the required biotin functional group, the other consists of the maleimide motif, thereby allowing specific targeting of sulfhydryl containing proteins.

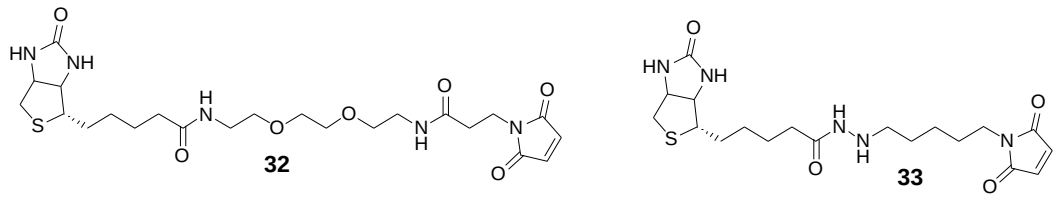

Figure 9. Maleimide-PEG_2-biotin **32** and *N*-biotinoyl-*N′*-(6-maleimidohexanoyl)hydrazide **33**.

Recently, these systems have been used for the visualisation of various pathological conditions such as tumours.[57] The approach is based on the observation that infected, inflamed, necrotic, and malignant areas are able to non-specifically accumulate large

protein molecules, such as immunoglobulin or albumin,[61,62] or even nanoparticles[63] *via* the mechanism of impaired filtration. The injection of (strept)avidin or (strept)avidin-antibody conjugates into tumour containing rats has found it too will accumulate in malignant areas. The addition of a biotin-associated label, such as radiolabel or dye, will then allow for visualisation of the infected area, due to the biotin-associated label seeking out and binding to the accumulated (strept)avidin in the rat (i.e. the tumour).

1.4 Reversible maleimide reagents

Despite the successful utilisation of maleimide as a reagent for the chemical modification of proteins, the irreversible nature of the addition prevents any possibility for controlled disassembly of the conjugate regenerating the unmodified protein, a process desirable for *in vitro* or *in vivo* applications. Furthermore there are only two points of attachment, thus limiting the number of chemical or biological entities that could be attached to a system of interest.

In 2009 Baker *et al.*[25] reported the use of monobromomaleimide, the first of a new class of reagent for the selective and reversible modification of cysteine. Previously, reversible cysteine modification could only be carried out using reagents that would form a disulfide bond, such as methanethiosulfonates,[64] and these reagents were unstable and often resulted in scrambling with respect to the disulfide bond.[65] Instead Baker incorporated a bromine onto the maleimide double bond, allowing an addition-elimination sequence to occur on reaction with *N*-Boc-Cys-OMe **34**, a model for the single amino acid cysteine in peptides (scheme 12). The product was a thiomaleimide **35**, which had retained the double bond in contrast to the succinimide product usually obtained from addition of sulfhydryl to maleimide. Addition of a second nucleophile, TCEP, yielded cysteine again plus tentatively postulated by-product **36**, thus creating a very powerful pathway for cysteine protection/deprotection and general modification.

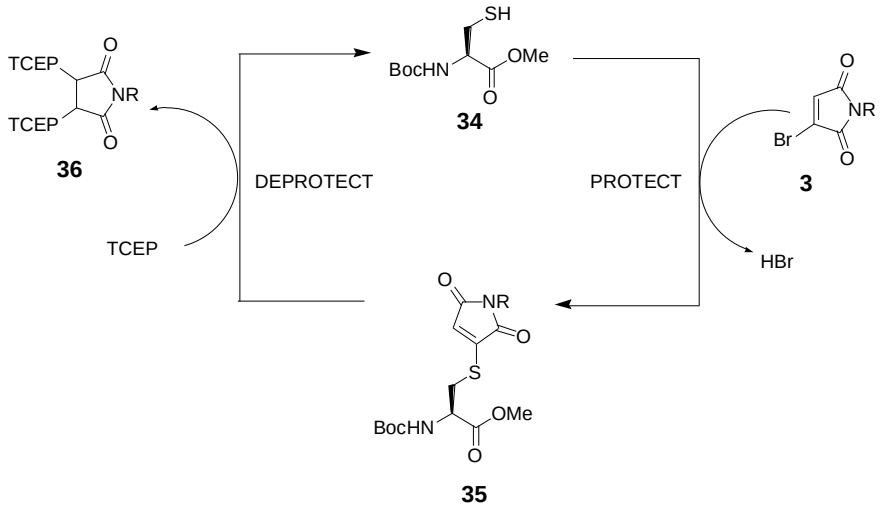

Scheme 12. Reversible addition of monobromomaleimide **3** to *N*-Boc-Cys-OMe **34**. R = H, Me.

Publication of the above results led to a collaboration between the Baker, Caddick and Waksman groups to investigate further the applicability of this reversible chemical modification on larger systems.[66] A single point mutant (L111C) of the SH2 domain of the Grb2 adaptor protein **37** was chosen as an ideal model protein for study, as it contained no disulfides and had only a single cysteine residue present.[67] Treatment of **37** with monobromomaleimide reagent **3** led to complete addition to give **38** in 1 h as observed my LCMS (scheme 13). Furthermore, 100 equivalents of TCEP (*tris*(2-carboxyethyl)phosphine) resulted in 85% conversion back to protein **37**, demonstrating the potential for reversible covalent modification of cysteine residues in proteins by the monobromomaleimide reagents.

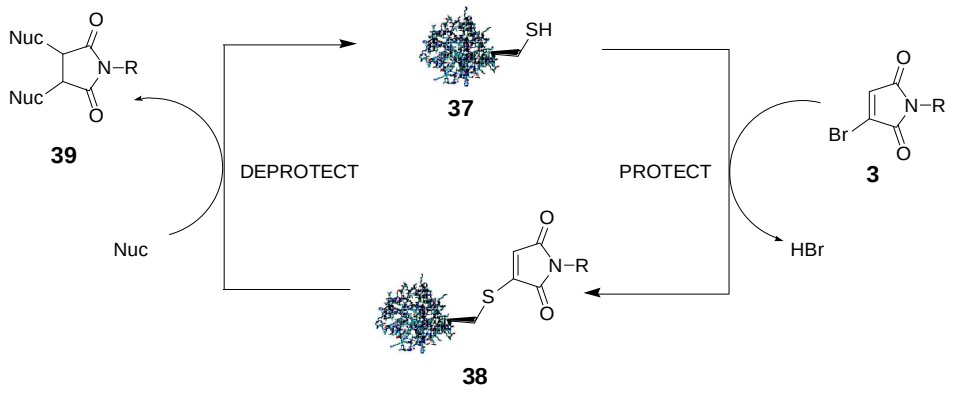

Scheme 13. Modification of the Grb2 SH2 domain (L111C) with monobromomaleimide. R = H, Me, Nuc = TCEP, BME.

Replacement of 100 eq of TCEP with 1 eq of a second nucleophilic thiol, namely glutathione or β-mercaptoethanol, led again to a second thiol conjugate addition

reaction. The resulting bis-thioether adducts **40** and **41** (figure 10) were the first examples of monobromomaleimide reagents containing three different groups and thus show the potential for three different points of attachment.

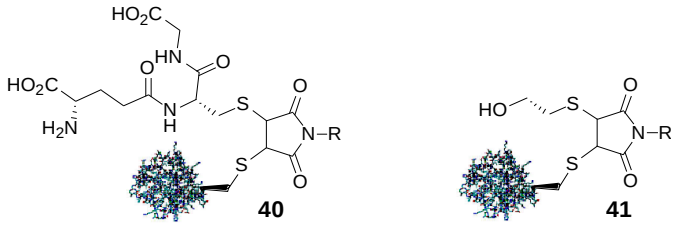

Figure 10. Examples of the first tri-substituted monobromomaleimide reagents. R = Me.

Whilst the use of monobromomaleimide as a reagent for reversible cysteine labelling and as a linker with three points of attachment is potentially very interesting, the corresponding dibromomaleimide **42** means the retention of the double bond in the maleimide moiety of bis-thioether adducts **44** and **45**, thus offering reversibility and the attachment of three different functional groups (scheme 14).

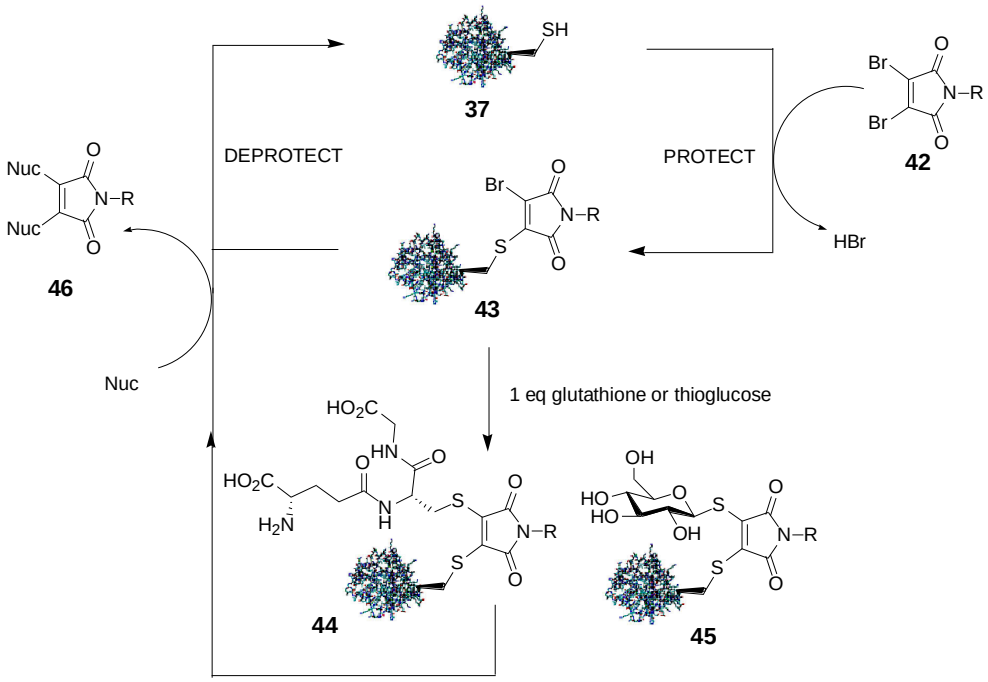

Scheme 14. Reversible modification of the Grb2 SH2 domain (L111C) **37** with 1 eq dibromomaleimide, followed by the glutathione or thioglucose, pH 8, 0 °C. R = H, Me. Nuc = 100 eq glutathione or BME, TCEP found to be unsuitable.

In order to compare the relative reactivity of the bromomaleimides with Grb2 SH2 domain **37**, Baker and Caddick *et al.* treated **37** with traditional cysteine modifying

reagents (NEM and iodoacetamide) and monitored the reaction between 5 and 30 min using LCMS (scheme 15). By comparing the percentage conversion of Grb2 SH2 **37** into Grb2-cysteine modifying reagent conjugate, the order of reactivity was found to be *N*-methylbromomaleimide ≈ NEM > dibromomaleimide >> iodoacetamide (figure 11).

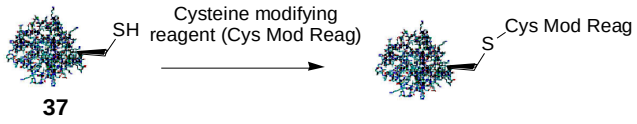

Scheme 15. Additional of different cysteine modifying reagents to cysteine; Cys Mod Reag = NEM, *N*-methylbromomaleimde, dibromomaleimde and iodoacetamide.

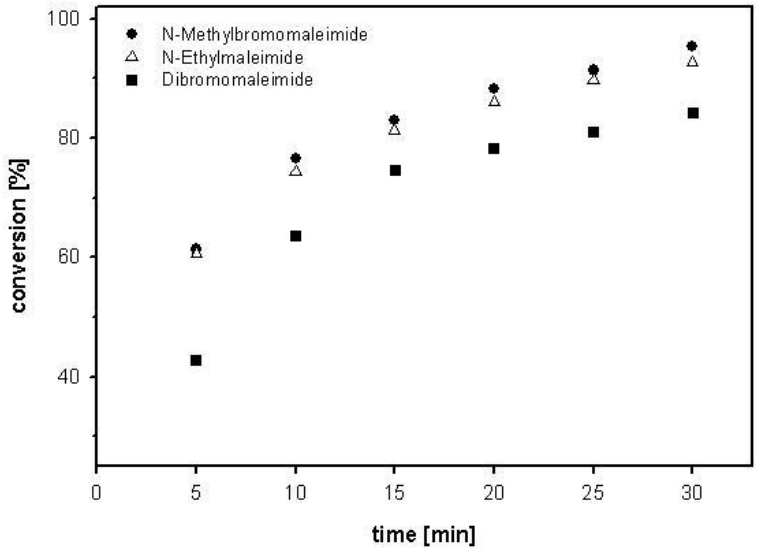

Figure 11. Relative reactivity of Grb2 SH2 domain (L111C) **37** with *N*-methylbromomaleimide, dibromomaleimide and *N*-ethylmaleimide. Iodoacetamide is not shown as < 5% reaction had taken place after 30 min.

Further work by Baker and Caddick focused on the insertion of bromomaleimide reagents into the disulfide bonds present in peptides and proteins, leading to the formation of stable bridged disulfide adducts which still retained the native proteins structure and function. Thus somatostatin **47**, a peptide consisting of 14 amino acids with a single disulfide bridge, was reduced with 1 eq of TCEP and treated with 1.1 eq of dibromomaleimide (scheme 16). The resultant product was the stable bridged SST adduct **48** which could be reduced back to unbridged SST upon addition of 100 eq of BME in 1 h at room temperature. This result demonstated that the bromomaleimides offered the first effective reagent for controlled reversible bridging

of disulfides and thus the potential offered to the world of bioconjugate and biomedicinal chemistry.

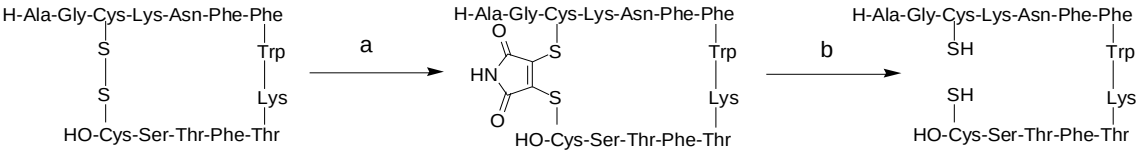

47 **48** **49**

Scheme 16. Reversible modification of the disulfide bond of somatostatin **47** (SST) by dibromomaleimide. (a) dibromommaleimide, (b) TCEP.

2 The use of functionalised bromomaleimides in cysteine labelling

2.1 Aim of project

The addition of biotin maleimide reagents to proteins can be considered irreversible **50** (scheme 17). In order to detach the constituent parts, strongly denaturing conditions, such as high detergent concentration, are required to separate the avidin-biotin complexes.[68] The development of reagents based on mono- and di-bromomaleimides make this process reversible, offering a powerful method for the isolation of complete proteins, antigens and other biological molecules of interest, without the problems of denaturation associated with existing methods (scheme 18).

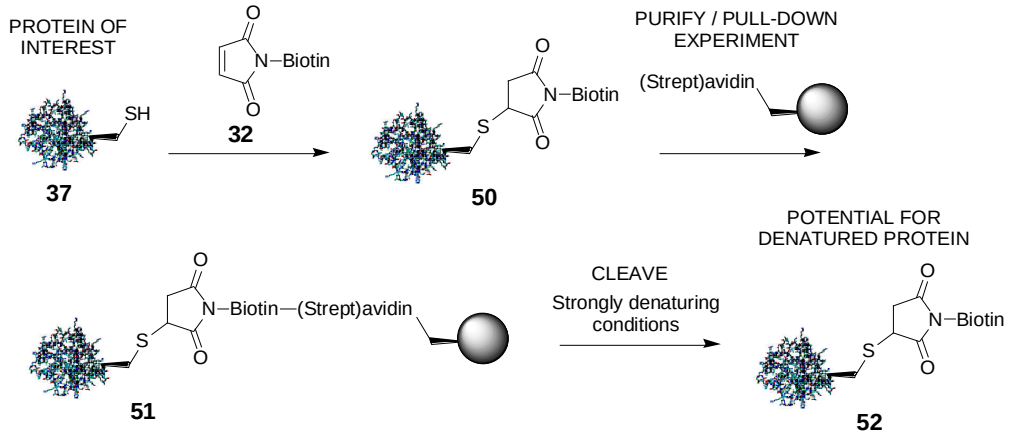

Scheme 17. Protocol for the isolation and purification of irreversibly bound biotin maleimide reagents.

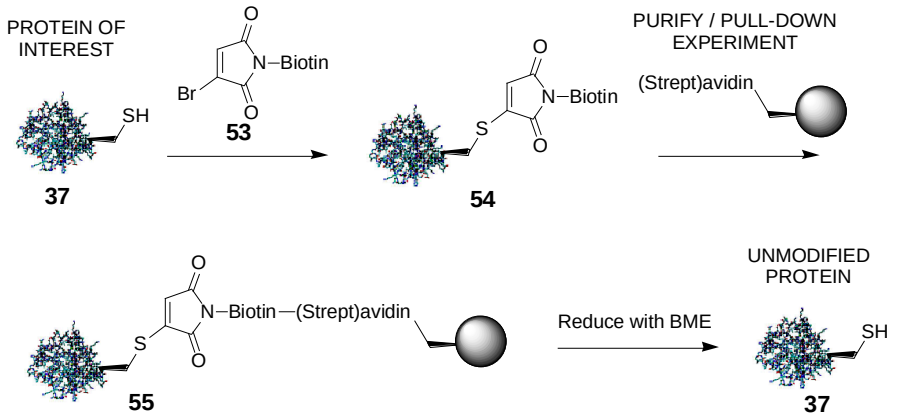

Scheme 18. Potential protocol for the isolation and purification of reversibly bound bromomaleimide reagents.

Mono- and di- bromomaleimide reagents also offer the opportunity for three points of attachment, allowing the incorporation of more functionality into the system of interest (scheme 19). For instance, the addition of a cell penetrating peptide **56**, sulfhydryl containing drug molecule **58** and fluorescent tag, to dibromomaleimide would offer the potential for a directed, biologically active and easily traceable molecule of therapeutic interest **59**. The presence of a fluorescent tag onto the bromomaleimide motif would also offer an alternative to the currently irreversible fluorescein-maleimide reagents available today.

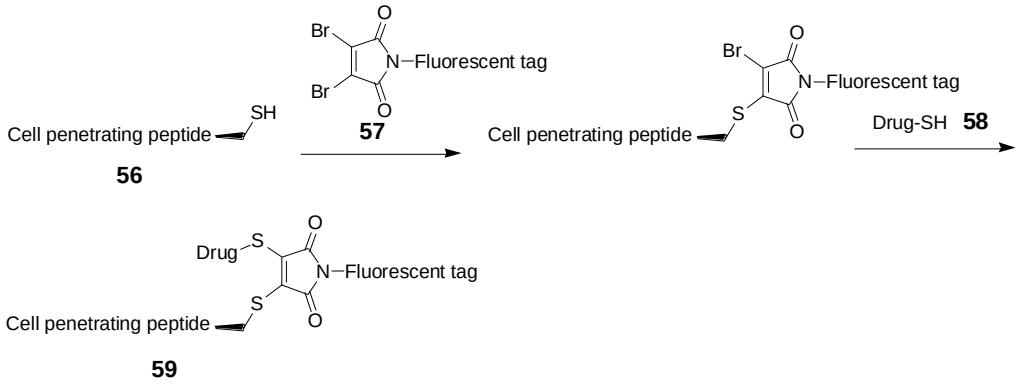

Scheme 19. Potential protocol demonstrating bromomaleimide reagents three points of attachment.

With these potential applications in mind, figure 12 shows the intended targets for this project, namely biotinylated bromomaleimide reagents **60** and **61** and fluorescein tagged bromomaleimide reagents **62** and **63**. Whilst these are similar to current reagents available today, the presence of the bromide substituents on the maleimide motif introduces some complexities for the proposed synthetic route. Current methods of maleimide synthesis (discussed in section 2.2) may not be applicable for use in the development of their bromomaleimide counterparts.

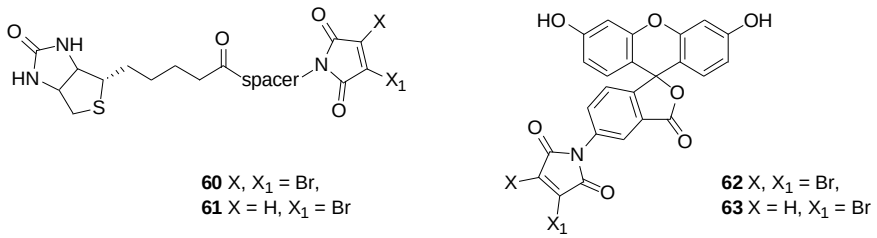

60 X, X_1 = Br,
61 X = H, X_1 = Br

62 X, X_1 = Br,
63 X = H, X_1 = Br

Figure 12. Bromomaleimide reagents targeted for study in this project.

The aims of this project are thus (1) the synthesis of elaborated mono- and di-bromomaleimide reagents;[25] (2) the incorporation of functionality useful for biomedical research applications, particularly fluorescent tagging and biotin pull-down experiments.

2.2 Previous routes to maleimide reagents

Numerous synthetic strategies have been reported for the synthesis of *N*-substituted maleimides **66**. The most commonly employed method involves the reaction of maleic anhydride **64** with primary amines leading to maleimic acid intermediates **65**, which are subsequently dehydrated into the corresponding cyclic maleimides (scheme 20).[69-72]

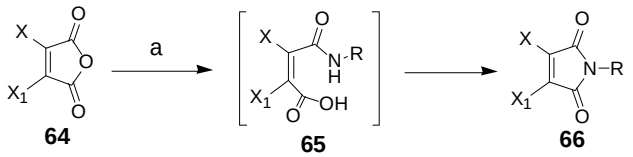

(a) RNH_2, AcOH, 21 °C, then heating with (or without) acetic anhydride and sodium acetate, X, X_1 = H; X = H, X_1 = Br.

Scheme 20. General conditions for maleimide synthesis.

Several variations using milder reagents have been described; reaction of the amine with maleic anhydride followed by dehydration with TMS-Cl/triethylamine;[6] HMDS and $ZnBr_2$ in refluxing benzene.[71,72] However, the yields when converting maleimic acid to maleimide under acidic or dehydrating conditions are generally modest and the scope of the amine is limited. Additionally the reactions preclude the use of acid labile or other sensitive functionality which limits the scope of this strategy.[73]

A variation of this approach makes use of the initial ring closure described in scheme 20 using *β*-alanine, or other similar simple amino acids, in order to generate maleimide intermediates to which further functionality can be incorporated by amide coupling reaction (scheme 21).[74] This circumvents the requirement for non-acid sensitive substrates and allows synthesis of reagents of considerable complexity.

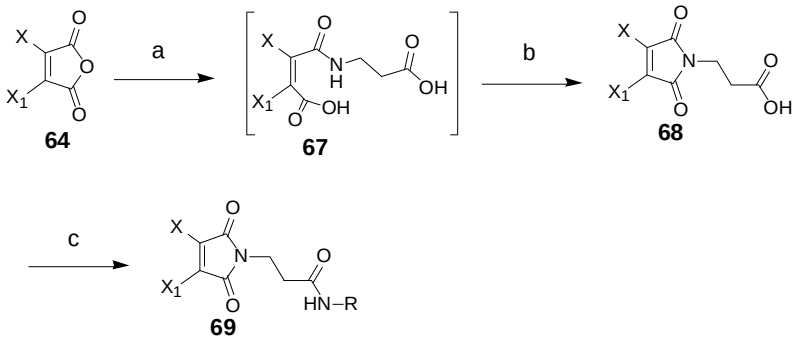

(a) AcOH, *β*-alanine, RT; (b) acetic anhydride, AcOH, 160 °C; (c) HBTU, NH_2R, *N*-methylmorpholine, DMF; X, X_1 = H; X = H, X_1 = Br.

Scheme 21. Alternative synthesis of maleimide motif using a ring closure approach

A number of other fairly conventional routes have been utilised. For example, one convenient method involves the direct reaction of primary amine derivatives with *N*-methoxycarbonyl maleimide.[75] Alternatively, an elegant Mitsunobu approach has been reported by Walker[73] in which alcohol derivatives are reacted with maleimides in the presence of triphenylphosphine and a dialkyl azodicarboxylate (scheme 22).[6,73,76] The Mitsunobu reaction is more general since it can be carried out under essentially neutral conditions and at room temperature. The starting material is also an alcohol rather than an amine which allows an alternative synthetic entry into this class of maleimide.

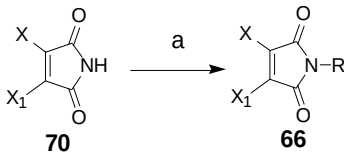

(a) PPh_3, DIAD, -78 °C, ROH, 15 h. X, X_1 = H

Scheme 22. Mitsunobu reaction.

The method employed to synthesis the reagent will need to fulfil certain criteria; (1) be simple, cost effective and straightforward methodology; (2) need for the reagent to be chemically stable and sufficiently robust for general use;[77,78] (3) need for the reagent to be hydrophilic so as to ensure complete aqueous medium solubility.[79]

2.3 Retrosynthetic analysis of biotinylated and fluoresceinylated bromomaleimide reagents

In order to develop a concise and divergent synthesis which could be used for the synthesis of a variety of bromomaleimide containing reagents, a route was conceived that would allow easy access to **71** (scheme 23), an intermediate which could then be manipulated to incorporate whichever functionality was desired.

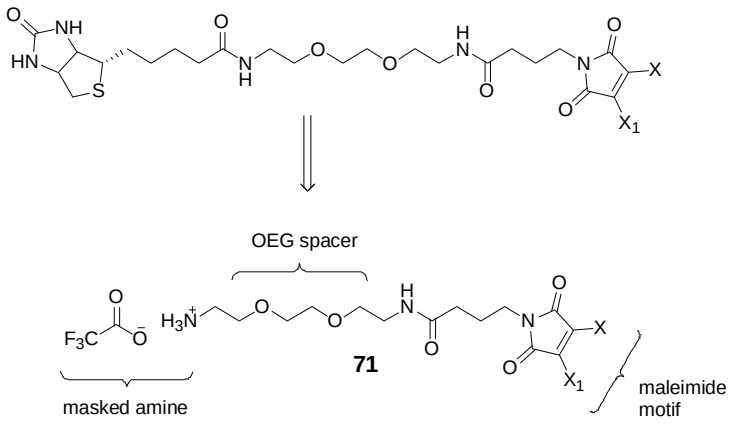

Scheme 23. Target for synthetic route; X, X_1 = Br, X = H, X_1 = Br.

The use of the TFA salt could be of importance in limiting potential degradation over time. The incorporation of an oligoethyleneglycol (OEG) spacer would be important for the biotin bromomaleimide reagents **60** and **61**, to allow access to the active site of (strept)avidin, maintaining the strong interaction upon binding. OEGylation would also give increased solubility in aqueous solution. Scheme 24 shows the possible retrosynthetic strategies for such an intermediate.

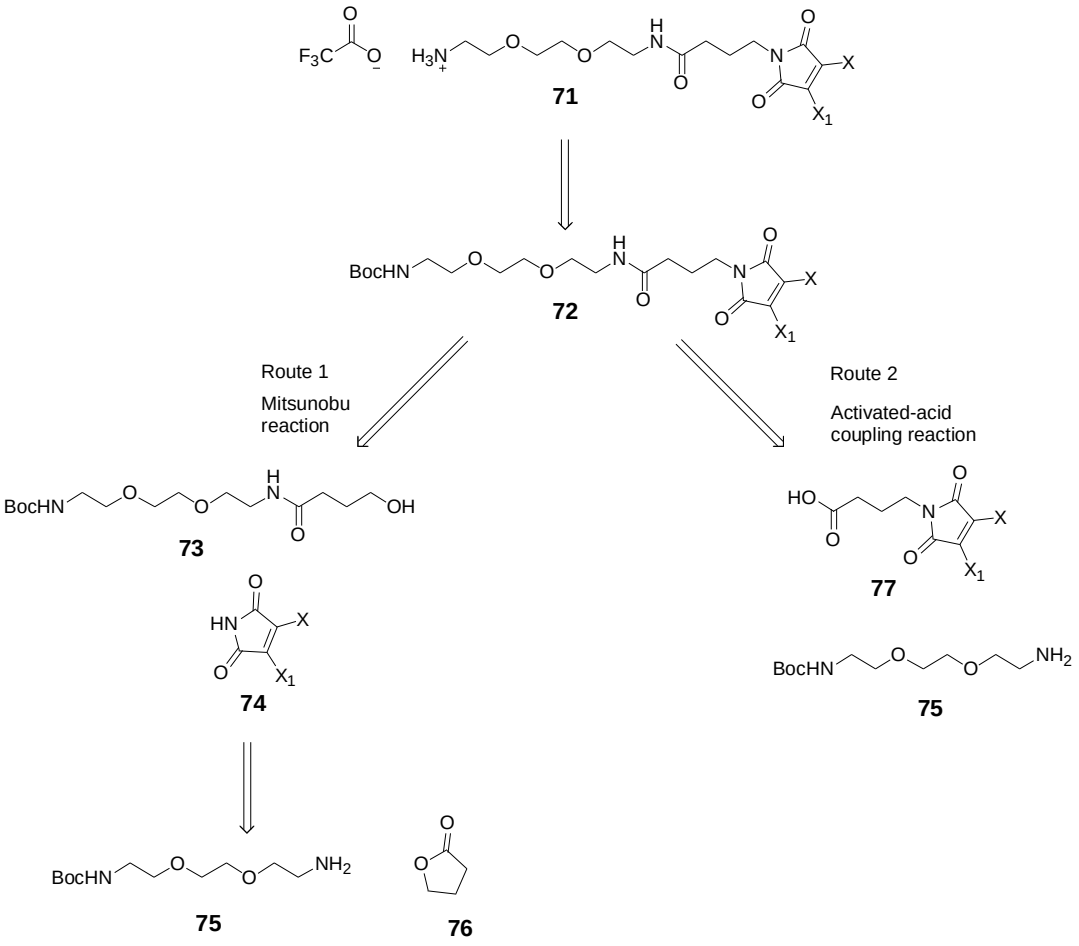

Scheme 24. Retosynthetic analysis for species **71**, the key intermediate in the synthesis of bromomaleimide reagents.

Route 1 consists of the reaction of mono-Boc protected diamine **75** with γ-butyrolactone (GBL) 76,[80] Mitsunobu coupling[73] with either mono- or di-bromomaleimides, followed by deprotection to afford **71**. Route 2, despite requiring the reaction of an activated acid **77** with an amine rather than Mitsunobu coupling, also leads to the formation of intermediate **71**. With this amine in hand, it would then be possible to attach a diverse range of functionality, including biotinylation, *via* the many amine reactive reagents commercially available.

Where there is no requirement for the incorporation of a spacer, as in the case of fluorescent bromomaleimides, the synthetic scheme can be simplified. In such instances, the retrosynthesis consists of one simple step (scheme 25), the forward synthesis of which entails acid catalysed ring-opening and closing of maleimic anhydride analogues **64** with fluoresceinamine **78** at elevated temperatures.

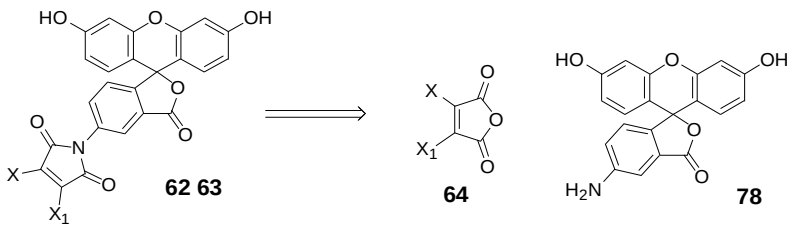

Scheme 25. Retrosynthetic analysis for fluorescein bromomaleimide reagents. **62** X, X_1 = Br; **63** X = H, X_1 = Br.

2.4 Synthesis of biotinylated bromomaleimide reagents 60 and 61

2.4.1 Route 1 to biotin bromomaleimide reagents

The investigation was initiated with an evaluation of route 1 (scheme 26). Desymmetrisation of diamine **79** with γ-butyrolactone 7**6** in the presence of H_2O led efficiently to amino alcohol **80** in 74% yield. However, Mitsunobu reaction of **80** with mono- and di- bromomaleimide failed to produce the desired amines. Rather, a complex reaction mixture resulted, from which it was not possible to determine any discrete molecular structures. As an alternative, the free amine of amino alcohol **80** was Boc-protected to give **73** and then subjected to Mitsunobu conditions, again to no avail. Replacement of the OEG-chain with a benzyl group to give **82** also failed to give the desired product under Mitsonobu conditions, suggesting that the presence of the amide group caused the reactions to fail. A possible explanation for this is the potential ring cyclisation upon ejection of triphenylphosphine oxide from the Mitsunobu intermediates **83**, although the expected lactam by-products **84** were not isolated (scheme 27).

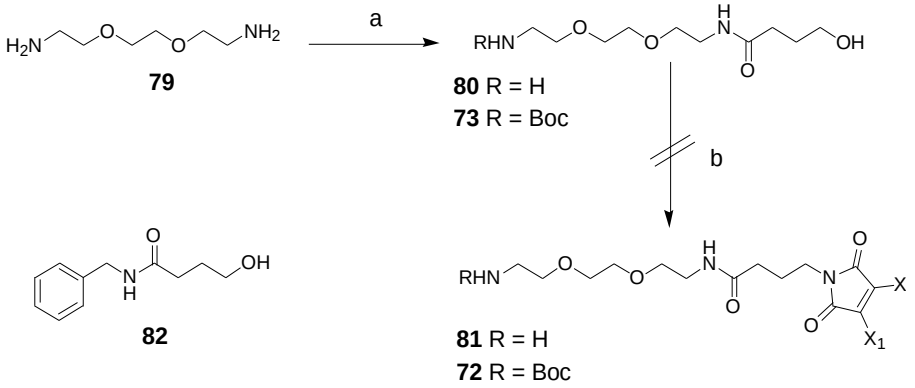

(a) γ-butyrlactone **76**, H_2O, 90 ^oC, 74% yield; (b) DIAD, PPh_3, -78 ^oC, mono- or di- bromomaleimide.

Scheme 26. Route 1 to key intermediate **71**.

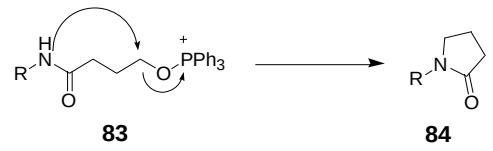

Scheme 27. Formation of lactam by-product *via* ring cyclisation. R = $(CH_2CH_2O)_2NHBoc$, $(CH_2CH_2O)_2NH_2$, Bn.

Despite the fact that the lactam by-product was not detected, it seems reasonable to assume that the presence of the amide five carbons away from the O-P bond was affecting the outcome of the Mitsunobu reaction. With this in mind, an alternative strategy was investigated which would preclude this potential cyclisation by removal of the amide bond in **73** (scheme 28). Therefore amino alcohol **85** was synthesised according the method of Lebeau,[81] and reacted with dibromomaleimide under Mitsunobu conditions, which pleasingly furnished OEG-dibromomaleimide **86**. However, this could not be isolated pure. Instead **86** was treated directly with TFA to yield amine-TFA salt **87**, a derivative of the initial key intermediate **71**.

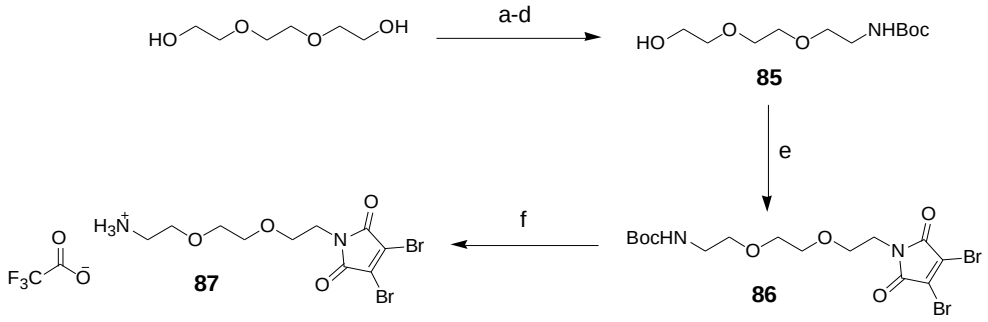

(a) Methane sulfonyl chloride, NEt_3, 21 °C, 24 h, 33% yield; (b) NaN_3, MeCN, 90 °C, 36 h, 84% yield; (c) PPh_3, H_2O, 21 °C, 4 h, 78% yield; (d) KOH, di-*tert*-butyl-di-carbonate, 21 °C, 4 h, 100% yield; (e) DIAD, PPh_3, -78 °C, 1 h, dibromomaleimide, then 21 °C, 15 h; (f) TFA/CH_2Cl_2, 21 °C, 24 h, 94% yield.

Scheme 28. Synthesis of **87**.

With the synthesis of this intermediate completed, the first of several coupling reactions was carried out with the biotin acid **88** (scheme 29). Disappointingly the coupling conditions of EDC.HCl, DMAP and *N*-methylmorpholine (2 and 5 eq); EDC.HCl, HOBt and *N*-methylmorpholine (2 and 5 eq); EDC.HCl, HOBt and NEt_3 (2 and 5 eq); HBTU and DIEA (2 and 5 eq); $SOCl_2$ and DIEA (2 and 5 eq) all led to eventual decomposition over time. Although trace amounts of product were observed spectroscopically by ^1H and ^{13}C NMR and mass spectrometry, none could be isolated.

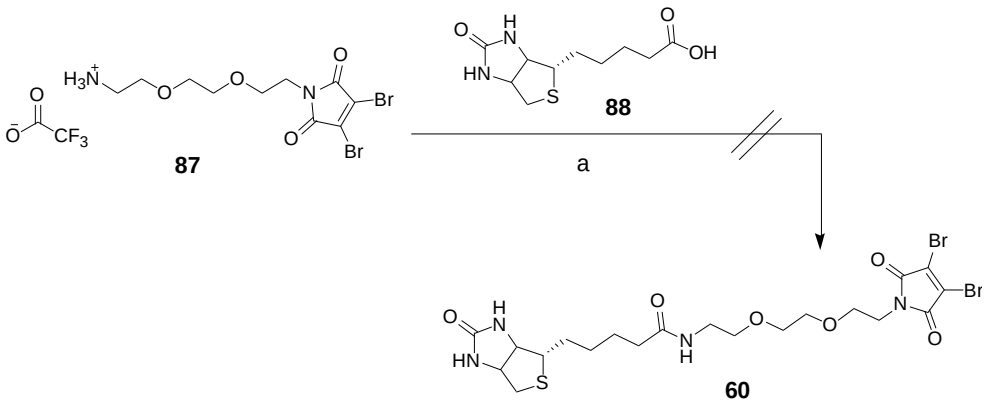

Scheme 29. Attempted amide coupling of biotin acid **88** with amine-TFA salt **87**.

It was postulated that the bromomaleimide motif could react with the amine base, leading to degradation of both **87** and **60**. Therefore to investigate whether this was the case, a ^{1}H NMR reaction of **87** with NEt_3 (two and five eq) was performed. Unfortunately the disappearance of the maleimide double bond was observed, indicating degradation of the maleimide was taking place (scheme 30).

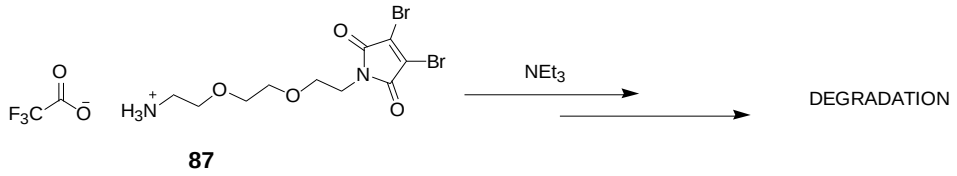

Scheme 30. Reaction of amine-TFA salt with NEt_3.

2.4.2 Route 2 to biotin bromomaleimide reagents

Despite the requirement of another amide coupling reaction in this approach, it was considered useful to determine whether the problems encountered in route 1 would still be present in route 2. Therefore in order to test whether the acid **77** (scheme 24) would suffer the same problems of degradation as encountered with amine-TFA salt **87** (scheme 30), a pilot reaction using **91** was carried out (scheme 31). Dibromomaleic anhydride **90** was synthesised using the procedure of Dubernet[69] and condensed with β-alanine in refluxing acetic acid. Unfortunately the required amide coupling reaction again led to failure with significant decomposition taking place.

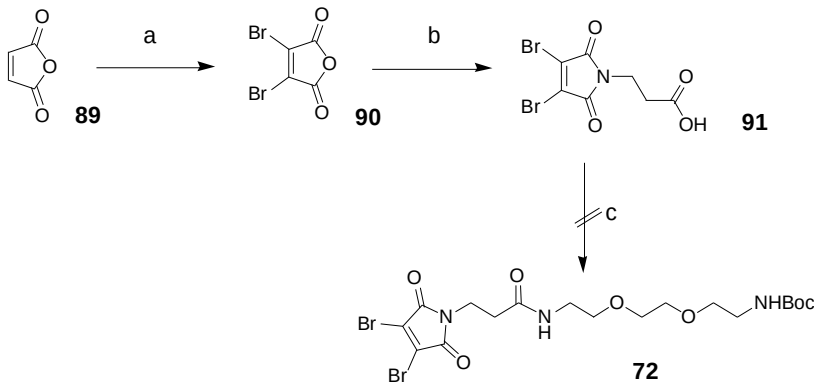

(a) Br_2, $AlCl_3$, 160 °C, 24 h, 78% yield; (b) *β*-alanine, AcOH, 150 °C, 3 h, 70% yield.

Scheme 31. Amide coupling reaction used in route 2.

2.4.3 Route 3 to biotin bromomaleimide reagents

Thus a third route was sought to circumvent the troublesome amide coupling reaction (scheme 32). No reaction involving the use of amine with bromomaleimide could be carried out. However, the reaction of *β*-alanine with bromomaleic anhydride has been shown to be a feasible alternative and high yielding (scheme 31 – formation of **91**). The third synthetic route began with the coupling of mono-Boc protected amine **75**[82] with activated biotin,[83] followed by Boc-deprotection to give **93** in excellent yield. Addition of mono- and di- bromomaleimic anhydride in acid then gave ring opened maleimic acids, which underwent ring closure by heating to 170 °C for 2 h to yield compounds **60** and **61** (figure 13 and 14).

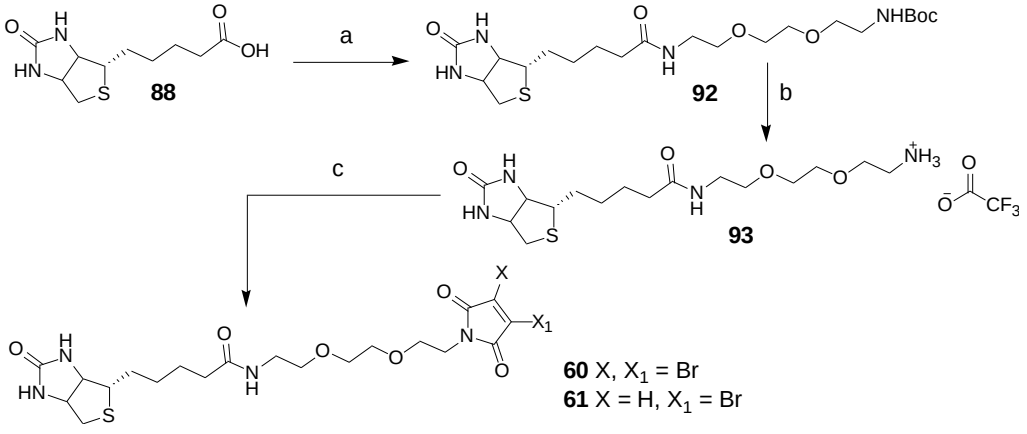

(a) HBTU, DIEA, **75**, 2 h, RT, 80% yield; (b) TFA/DCM, RT, 15 h, 100% yield; (c) mono- or di-bromomaleimic anhydride, AcOH, 170 °C, 2 h, **60** 48% and **61** 52%.

Scheme 32. Route 3 to biotin bromomaleimides **60** and **61**.

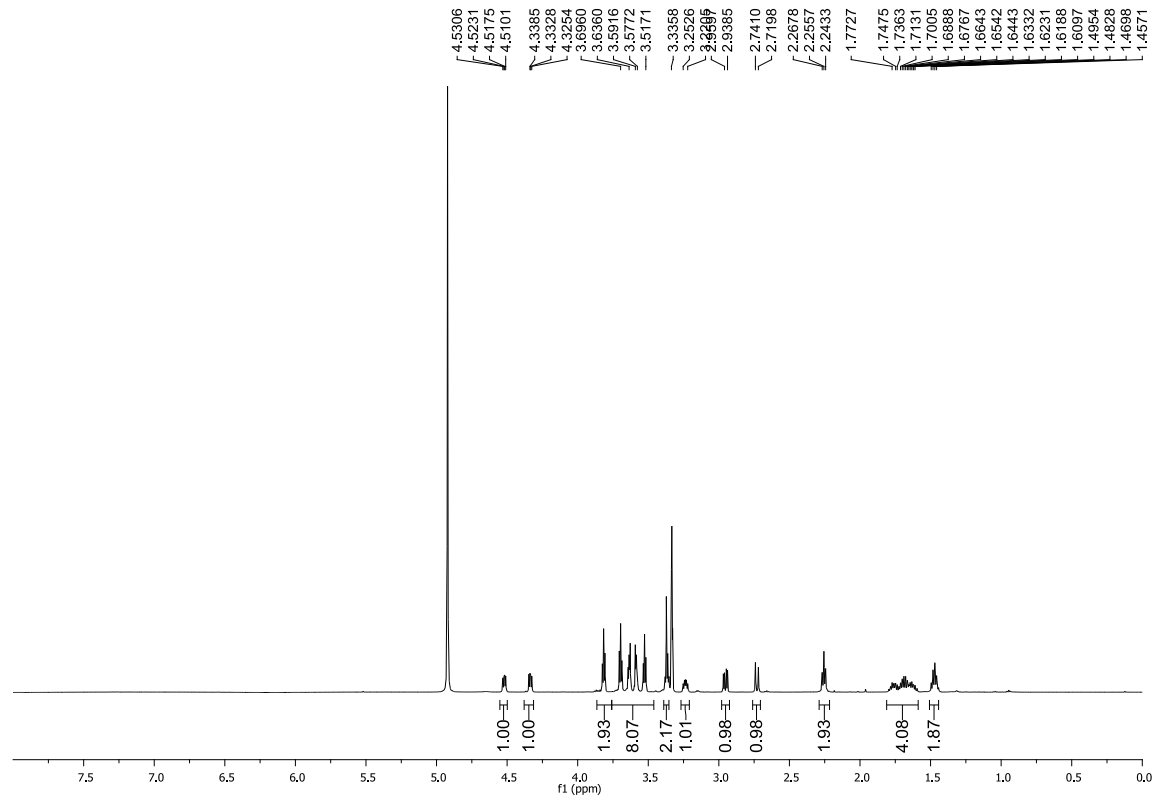

Figure 13. ^{1}H NMR of **60** in CD_3OD.

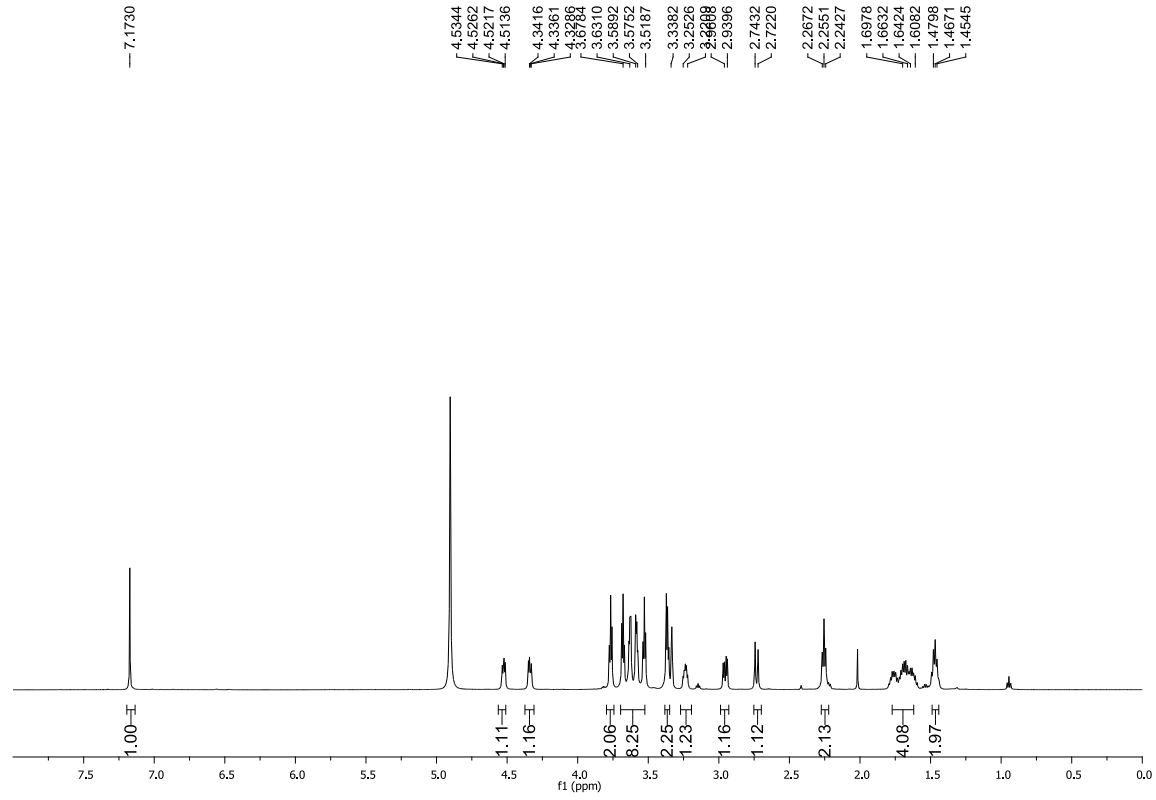

Figure 14. ^{1}H NMR of **61** in CD_3OD.

Thus we have successfully developed an efficient three step synthesis of biotin mono- and di- bromomaleimide reagents. Crucially this synthesis avoids the addition of free amine to the bromomaleimide moiety. By carrying out the reaction under strongly acidic conditions, we can ensure the amine remains protonated and therefore unable to react with the double bond of the bromomaleimide motif. Additionally, the acidic conditions do not impede formation of the maleimic acid intermediates or the ring closure to afford the biotin bromomaleimide reagents.

2.5 Synthesis of fluorescein bromomaleimide reagents 62 and 63

The attachment of biotin to bromomaleimides in section 2.4 required the use of a linker. However, in the case of the fluorescent tag a linker is not necessary. Therefore a simple acid catalysed condensation reaction was used to give fluorescein reagents **62** and **63** (scheme 33, figures 15 and 16).

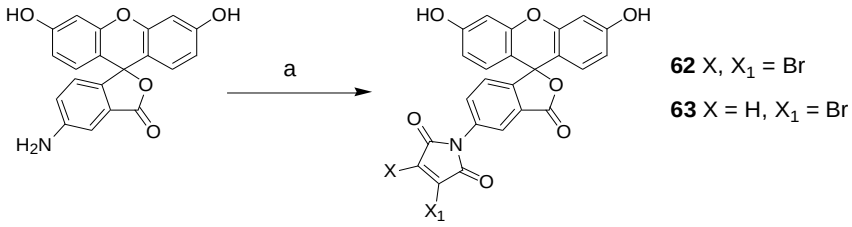

(a) Mono- or di- bromomaleimic anhydride, AcOH, 170 ^{o}C, **62** 84% yield and **63** 65% yield.

Scheme 33. Synthesis of fluorescein bromomaleimides.

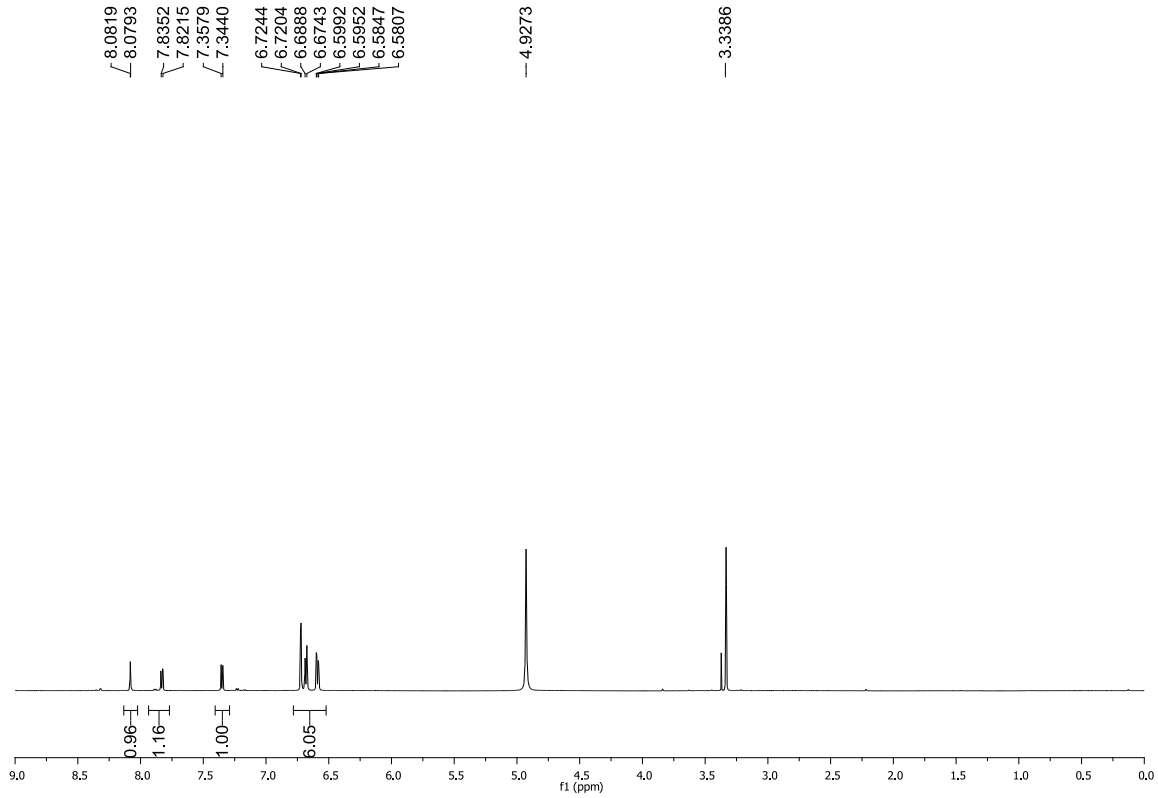

Figure 15. ^{1}H NMR of **62** in CD_3OD.

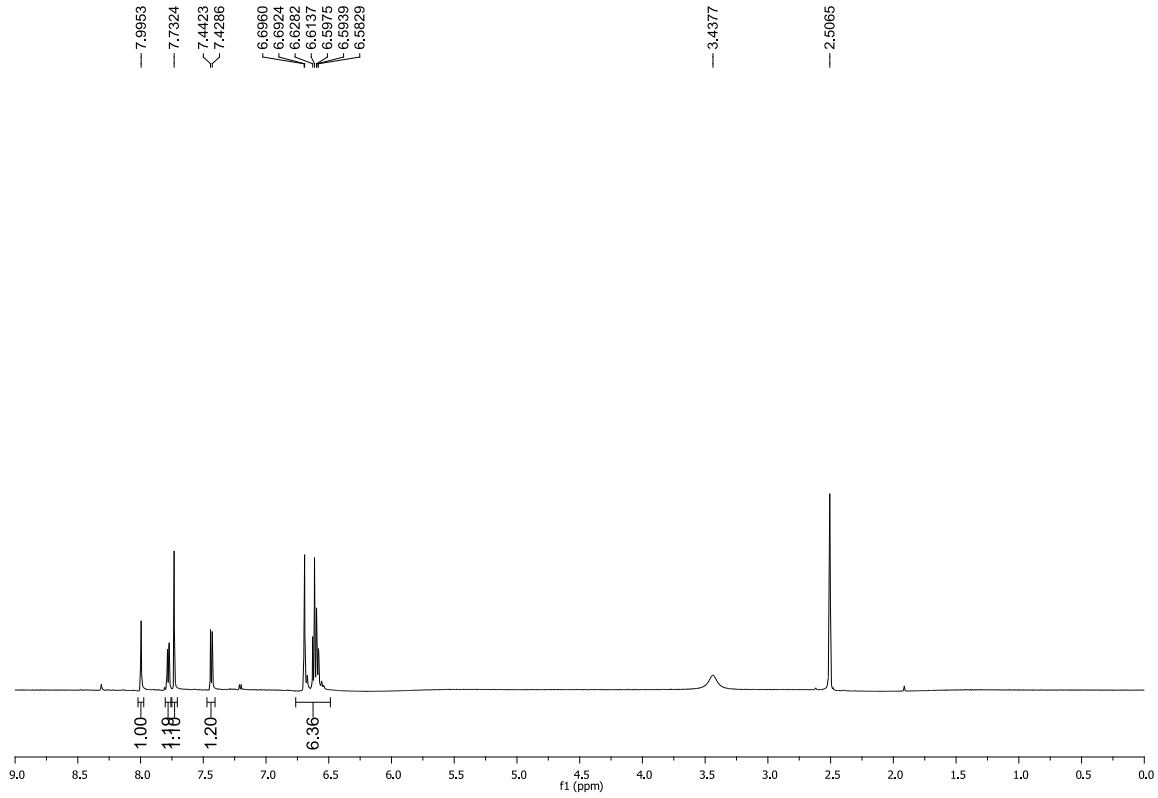

Figure 16. ^{1}H NMR of **63** in DMSO-d6.

2.6 Studies on the chemical modification of Grb2 SH2 domain 37

With the biotinylated and fluoresceinylated bromomaleimide reagents in hand, a series of experiments were carried out to investigate how well they would react with the single point mutant (L111C) of the SH2 domain of the Grb2 adaptor protein **37**, a model protein chosen due to the presence of a single cysteine residue and absence of any disulfide bonds,[67] with the reactions monitored by Liquid Chromatography Mass Spectrometry (LCMS or HPLC MS).

LCMS combines the physical separation capabilities of liquid chromatography with the mass analysis capabilities of mass spectrometry (MS) and is therefore a very powerful technique, exhibiting high sensitivity and specificity. By running samples through a column prior to MS analysis, chemically different species can be separated and then analysed by MS individually, providing sufficient separation is achieved. This separation is monitored using a chromatogram which produces absorbance peaks corresponding to all the different species present in solution and how long it takes each species to pass through the LC column (figure 17).

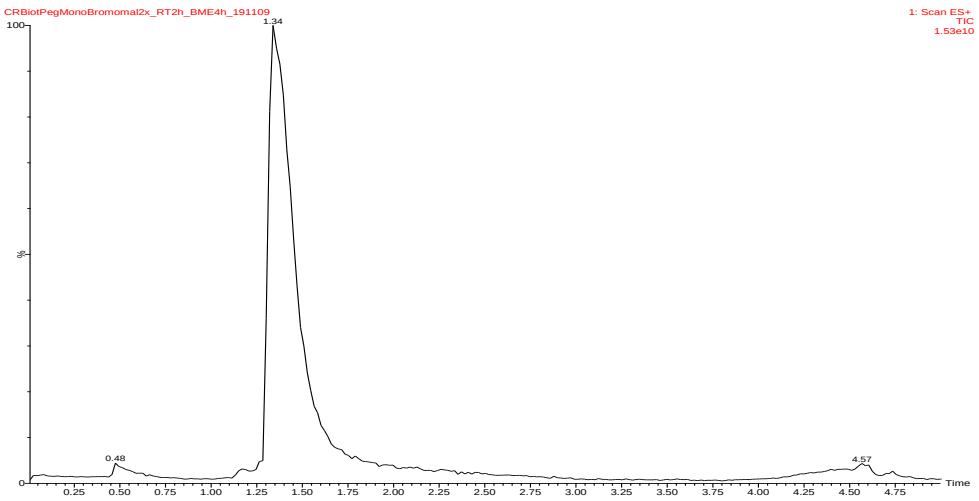

Figure 17. LCMS chromatogram showing a single molecular species.

By MS analysis of these peaks individually, the specific species present can be studied. In cases where separation is not good enough for accurate MS analysis of the individual peaks, the peaks can instead be analysed collectively (figure 18). This allows for the MS analysis of more than one species present in solution, and

providing they are of similar sensitivity to MS, a ratio of their abundance can be determined. Whilst the presence of an amine in one species and an aromatic group in another will result in different degrees of sensitivity towards MS analysis, in proteins of similar size and chemical space this is not the case.

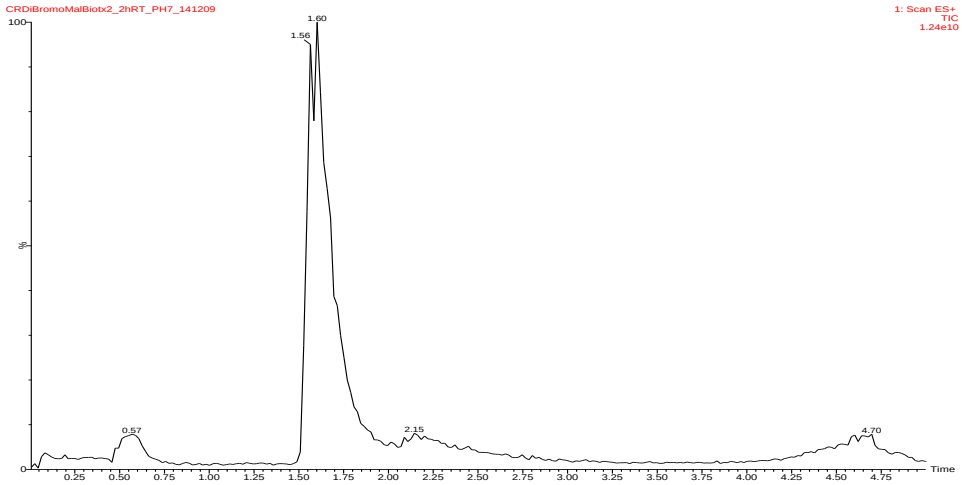

Figure 18. LCMS chromatogram showing two inseparable molecular species.

The addition of small molecules, such as bromomaleimides, to proteins can be shown not to significantly affect their chemical space, providing the modification is specific and not denaturing. For instance, the addition of bromomaleimide to the single cysteine of Grb2 SH2 domain **37** does not significantly affect its interaction and movement through the LC column or its sensitivity to MS.[66] Therefore LCMS can be used as a way of monitoring the modification of proteins with small molecules, such as bromomaleimides, *via* the collective MS analysis of the peaks observed in the LC chromatogram (e.g. figures 19 and 20), and has become an established and well accepted method of analysis.[84-86]

By taking the ratio of the abundances of unmodified and modified protein, a percentage conversion can be obtained, assuming that no decomposition of the protein has taken place. However, even if this were the case, decomposition of such a large molecule would be observed by LCMS, and has been found to small extent in the following sections (section 2.6.1 to 2.6.4, tables 1 to 8, column 7; loss of OEGbiotin, unidentifiable species, -23 m/z).

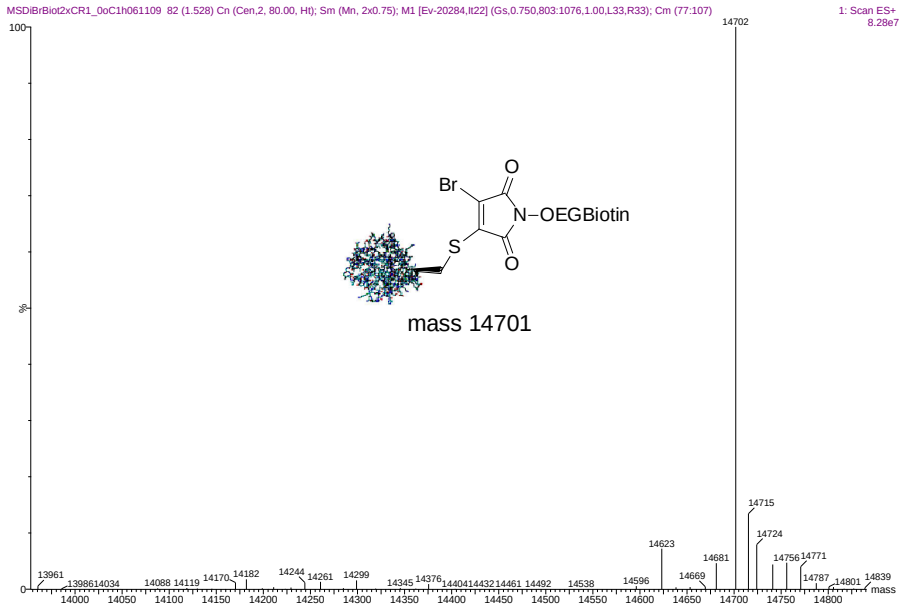

Figure 19. LCMS spectrum obtained from the addition of **60** to Grb2 SH2 domain **37**.

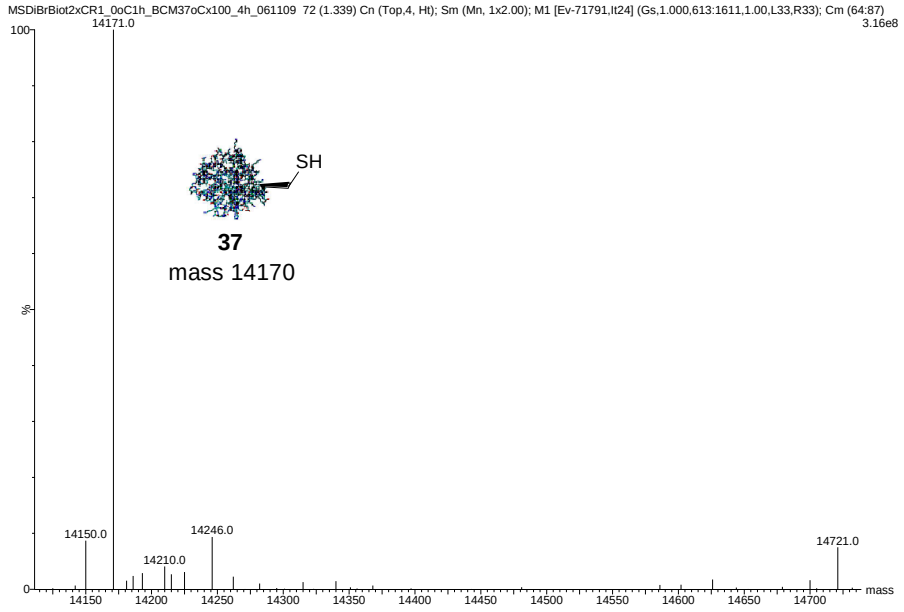

Figure 20. LCMS spectrum obtained from the addition of 100 eq of BME to Grb2-biotin dibromomaleimide conjugate.

In this way, no internal standard is used. Rather, by analysing the overlapping peaks in the chromatogram collectively (figure 18), it is assumed that all protein species present in solution are accounted for. Additionally, the presence of an internal standard of sufficient size to be of use (e.g. another protein) could be detrimental to the outcome of the reaction, by itself reacting with the other reagents present.[84] This also applies for an external standard. Studies using an external standard usually

require the addition of a known amount of a reaction mixture to a second solution containing the external standard. MS analysis can then be used to determine the percentage conversion by comparing the amount of starting material and product against the known amount of external standard. However, again this external standard would need to be of sufficient size and sensitivity towards MS analysis to be of use, and of a chemical nature that would not interact with the reagents and reactive species present in the solution.

The error associated with not having an internal and external standard will be the same throughout this study. As the reaction conditions will be set for all experiments, a comparison can be made as to the trends on changing from the biotin bromomaleimides to the fluorescein bromomaleimides, as well as changing from mono to di bromomaleimide, and changes in pH and temperature, all of which will then be used to determine the best reagent and conditions for protein modification with bromomaleimides.

If the assumption is made that the unmodified and modified Grb2 SH2 domain **37** can be used to determine the percentage conversion, an excess of the protein modifying reagent (bromomaleimides) would be needed to ensure that complete conversion can occur. In the vast majority of PTM procedures found in the literature,[26] a 100-fold excess of protein modifying reagent is the minimum that is used. However, in this study to demonstrate the specificity and reactivity of the new bromomaleimide reagents, only 2 equivalents will be used.

Three temperatures have been chosen for this study of reactivity; 0 °C, 21 °C and 37 °C. A standard time interval for each reaction is also required, in order to properly compare the results; 2 h was chosen for the addition of bromomaleimide reagent (2 eq) to Grb2 SH2 domain **37**, and 4 h for its elimination using BME (100 eq). These reactions were carried out at pH 7 and 8. It should be noted that whilst many MS studies in the literature only record species present in solution which are greater than 5 % in abundance,[87] in this study all species present in solution will be taken into account.

2.6.1 Reactivity of biotin dibromomaleimide with 37

Scheme 34 shows the protection reaction of Grb2 SH2 domain **37** with **60** and the possible intermediates formed, whilst table 1 shows the mean percentage conversion for this protection at pH 7 and 8. The standard error (i.e. standard deviation of the mean)[88] is shown in parenthesis. Note – all data is rounded to the nearest whole number.

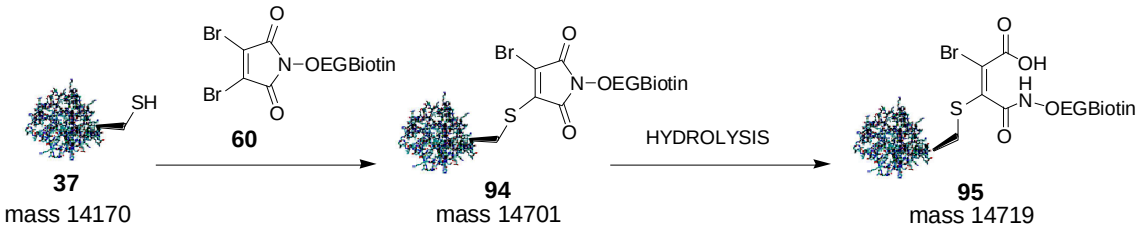

37
mass 14170

94
mass 14701

95
mass 14719

Scheme 34. Reaction of Grb2 SH2 domain **37** with dibromomaleimide reagent **60** (2 eq) for 2 h.

Entry	Temp	pH	**37**	**94**	**95**	Other
1	0 °C	8	4 (±1) %	80 (±2) %	2 (±1) %	14 (±2) %
2	0 °C$^{\omega}$	8	3 (±1) %	82 (±1) %	3 (±3) %	12 (±1) %
3	21 °C	8	3 (±2) %	43 (±2) %	41 (±1) %	14 (±3) %
4	37 °C	8	0 (±0) %	1 (±1) %	66 (±3) %	34 (±2) %
5	0 °C	7	3 (±2) %	83 (±2) %	0 (±0) %	14 (±2) %
6	21 °C	7	1 (±1) %	72 (±12) %	10 (±10) %	17 (±5) %
7	37 °C	7	2 (±1) %	0 (±0) %	80 (±5) %	18 (±4) %

Table 1. Protection of Grb2 SH2 domain with biotin dibromomaleimide **60**. Hyd = hydrolysis product **95**; other = loss of OEGbiotin section of reagent, -23 m/z; $^{\omega}$ 10eq of biotin dibromomaleimide reagent **60** used.

The best results at pH 8 were that obtained for the protection of Grb2 SH2 domain **37** with **60** at 0 °C (table 1, entries 1 and 2). At this temperature degradation was found to be minimal but became more pronounced as the reaction temperature was increased (table 1, entry 4). At the higher temperatures (table 1 entries 3 and 4)

increased amounts of hydrolysis were also observed. This is a significant result, as the hydrolysed product **95** is inactive towards reduction with BME and thus creates a 'sink' of irreversibly bound Grb2-bromomaleimide-species (scheme 35). The same observations were made when the reactions are carried out at pH 7. At 0 °C (table 1 entry 5) protection is optimal with no hydrolysis taking place. However, as the temperature is increased, both degradation and hydrolysis are again observed (table 1 entries 6 and 7).

Scheme 35 shows the conditions used for the deprotection of Grb2-biotin dibromomaleimide conjugate and table 2 the mean percentage conversions from the deprotection of Grb2-biotindibromomaleimide conjugate **94** with BME (100 eq) at pH 7 or 8 at 0 °C, 21 °C and 37 °C. The standard error is again shown in parenthesis.

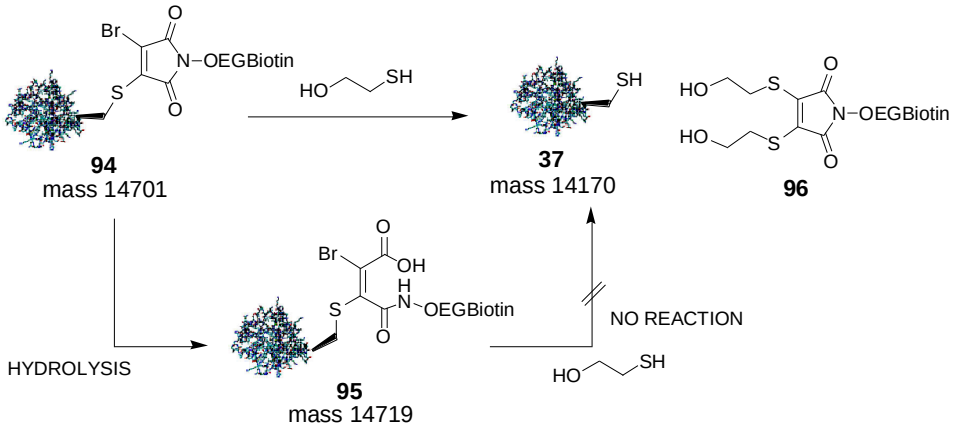

Scheme 35. Deprotection of Grb2-biotin dibromomaleimide conjugate **94** with BME (100 eq) for 4 h.

Entry	Temperature	pH	**94**	**37**	**95**	Other
1	0 °C	8	8 (±8) %	80 (±0) %	3 (±3) %	8 (±8) %
2	21 °C	8	2 (±2) %	26 (±2) %	47 (±1) %	25 (±1) %
3	37 °C	8	0 (±0) %	5 (±5) %	61 (±4) %	34 (±8) %
4	0 °C(p)/21 °C	8	10 (±3) %	85 (±5) %	2 (±2) %	4 (±4) %
5	0 °C(p)/37 °C	8	0 (±0) %	84 (±12) %	8 (±4) %	6 (±6) %
6	0 °C	7	25 (±3) %	69 (±5) %	0 (±0) %	6 (±4) %
7	21 °C	7	3 (±3) %	43 (±2) %	39 (±2) %	15 (±5) %
8	37 °C	7	0 (±) %	10 (±2) %	65 (±2) %	25 (±1) %

Table 2. Deprotection of Grb2-biotindibromomaleimide conjugate **94**. Other = loss of OEGbiotin section of reagent.

These results were obtained from taking the reaction mixture of the original protection reactions and subjecting them to the conditions required for deprotection (BME 100 eq). For instance, the product from the protection at 0 °C (table 1 entry 1) was used directly in the deprotection reaction with BME at 0 °C (table 2 entry 1). However, this means that the composition of the reaction mixture obtained from the protection reactions will directly influence the latter deprotections. To illustrate this point, let us compare table 1 entry 4 and table 2 entry 3. 66% hydrolysis was observed for the protection reaction at 37 °C (table 1 entry 4), whilst 61% hydrolysis was observed during the deprotection step at 37 °C (table 2 entry 3). These two values are very similar, suggesting that whatever was hydrolysed in the protection step remained hydrolysed and inactive during deprotection, thus demonstrating the irreversible nature of the hydrolysed products **95**. To avoid this troublesome result, the protection conditions which produced the smallest amount of hydrolysis were used (table 1 entry 1), followed by deprotection at 21 °C and 37 °C (table 2 entries 4 and 5), which pleasingly furnished the greatest yield in product **37**.

The results also differed depending on the pH, with those reactions carried out at pH 8 generally leading to poorer yields than those carried out at pH 7 (with the exception at 0 °C). This could be attributed to the increase in side reactions at higher pH, leading to decomposition rather than the return of deprotected protein **37**.

2.6.2 Reactivity of biotin monobromomaleimide with 37

The second biotin bromomaleimide reagent to be investigated was **61**, using the same conditions to those employed for the reaction of **60** with Grb2 SH2 **37** (scheme 36). Table 3 presents the mean percentage conversions for the protection of the Grb2 SH2 domain **37** with **61** (2 eq) at 0 °C, 21 °C and 37 °C, and at pH 7 and 8, with the standard error again shown in parenthesis.

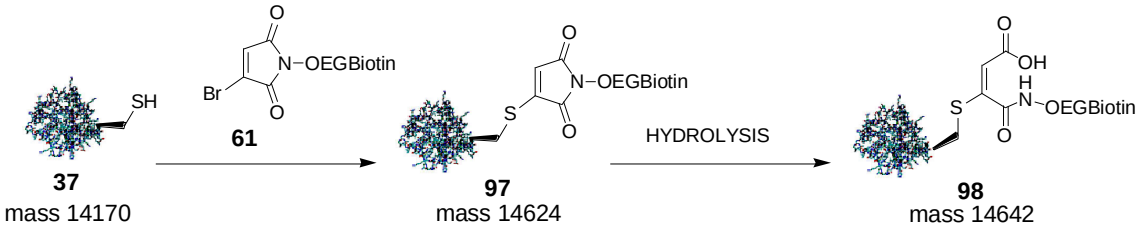

Scheme 36. Reaction of Grb2 SH2 domain protein **37** with biotin monobromomaleimide reagent **61** (2 eq) for 2 h.

Entry	Temp	pH	**37**	**97**	**98**	Other
1	0 °C	8	2 (±2) %	90 (±3) %	0 (±0) %	8 (±1) %
2	21 °C	8	0 (±0) %	90 (±2) %	3 (±3) %	7 (±4) %
3	37 °C	8	24 (±9) %	71 (±4) %	5 (±5) %	0 (±0) %
4	0 °C	7	0 (±0) %	86 (±6) %	0 (±0) %	14 (±6) %
5	21 °C	7	0 (±0) %	79 (±10) %	0 (±0) %	21 (±10) %
6	37 °C	7	0 (±0) %	76 (±5) %	11 (±11) %	13 (±6) %

Table 3. Protection of Grb2 SH2 domain with biotin monobromomaleimide. Hyd = hydrolysis product **98**; other = loss of pegbiotin section of reagent, -23 m/z.

From the entries above it can be seen that addition of **61** does react with much less hydrolysis (as determined by the mean percentage conversion of **97** and **98)**, particularly at 0 °C and 21 °C (table 3 entries 1, 2, 4 and 5). Further, a comparison of reaction rates at different pH's suggests that the reaction at pH 7 is slower than the corresponding reaction at pH 8. This is due to the increased formation of the anion of **37** at higher pH, and thus faster reaction. At pH 7 degradation is also found to be slightly more pronounced, whereas at pH 8 it is minor.

Table 4 shows the mean percentage conversion for the deprotection of Grb2 SH2 domain – biotin monobromomaleimide conjugate with BME at 0 °C, 21 °C and 37 °C (scheme 37), with standard errors shown in parenthesis.

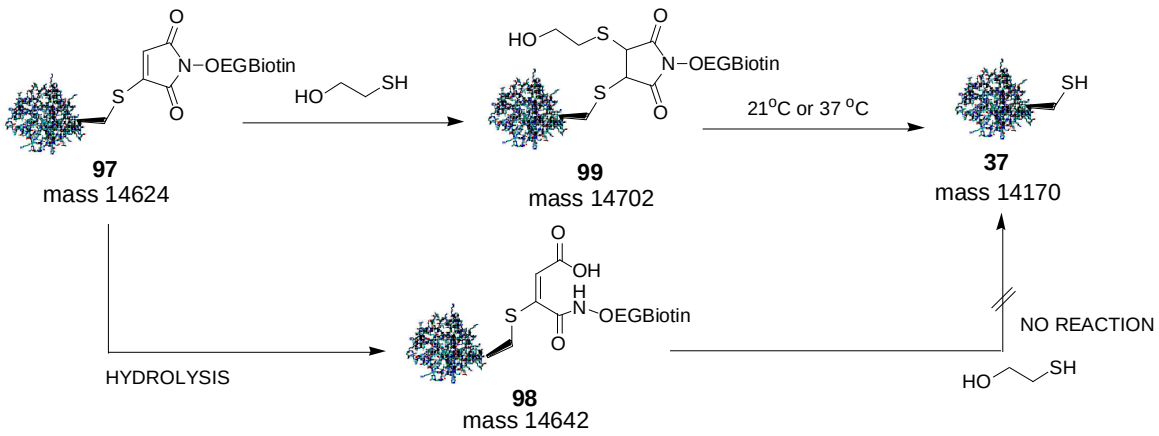

Scheme 37. Deprotection of Grb2-biotin monobromomaleimide conjugate **61** with BME (100 eq) for 4 h.

Entry	Temp	pH	**97**	**37**	**98**	Other **99**
1	0 °C	8	0 (±0) %	12 (±8) %	0 (±0) %	88 (±8) %
2	21 °C	8	2 (±2) %	30 (±1) %	0 (±0) %	65 (±3) %[ξ]
3	37 °C	8	2 (±2) %	75 (±9) %	16 (±8) %	5 (±1) %[ξ]
4	0 °C	7	0 (±0) %	5 (±5) %	0 (±) %	77 (±6) %[ξ]
5	21 °C	7	5 (±5) %	21 (±5) %	0 (±0) %	61 (±5) %[ξ]
6	37 °C	7	17 (±7) %	66 (±1) %	0 (±0) %	18 (±5) %[ξ]

Table 4. Deprotection of Grb2-biotin monobromomaleimide. Hyd = hydrolysis product **98**; other = BME addition product **99**; [ξ] remaining unaccounted mean percentage conversion is a combination of unidentifiable species.

It can be seen from table 4 that the addition of BME to Grb2-biotin monobromomaleimide conjugate **97** at pH 7 and 8 resulted in little hydrolysis (16 % conversion - table 4 entry 3). However, rather than isolating the expected product **37**, a BME-Grb2-biotin-monobromomaleimide adduct **99** was formed, whereby BME had added across the maleimide double bond.

Species **99** is a maleimide unit with three different groups attached and demonstrates that monobromomaleimide reagents offer an opportunity for the attachment of three functional groups. Interestingly, formation of species **99** was found to be reversible, thus when the temperature was increased to 37 °C (table 4 entries 3 and 6), **37** was obtained.

In conclusion it has been shown that biotin mono- and di- bromomaleimide can be used for the protection of the Grb2 SH2 domain, a single cysteine containing model protein. The optimum temperature for protection using biotin dibromomaleimide **60** was 0 °C. At higher temperature hydrolysis became an issue, leading to the formation of irreversibly bound Grb2-biotin dibromomaleimic acid conjugate **95**. The optimum temperatue for deprotection was 37 °C, although even at this temperature the hydrolysed species **95** was still found to be inactive towards deprotection.

Hydrolysis was shown to be markedly reduced by using biotin monobromomaleimide **61**, allowing higher temperatures to be used throughout. However, when using monobromomaleimide **61**, the Grb2-biotin monobromomaleimic acid intermediate **99** was observed at low temperature but was shown to react at 21 and 37 °C to yield Grb2 model protein **37** in high yield.

2.6.3 Reactivity of fluorescein dibromomaleimide with 37

With the results for the protection and deprotection of the Grb2 SH2 domain using biotin mono- and di- bromomaleimide reagents complete, attention was turned to the fluorescein bromomaleimide equivalents **62** and **63**. Scheme 38 shows the product formed from the protection of Grb2 **37** with fluorescein dibromomaleimide **62** and table 5 the mean percentage conversion for the protection reaction at 0 °C, 21 °C and 37 °C at pH 7 and 8. The standard error is shown in parenthesis.

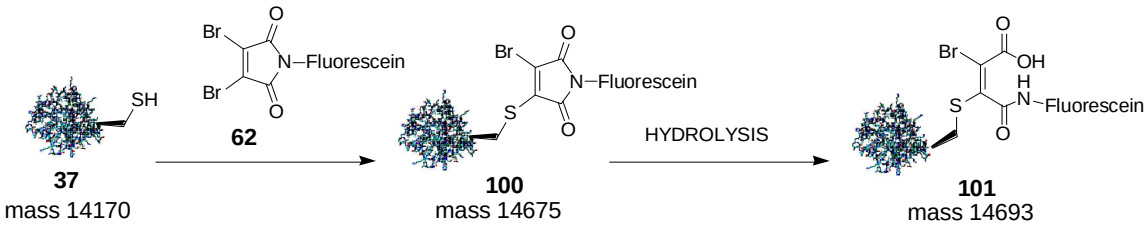

Scheme 38. Reaction of Grb2 SH2 domain **37** with fluorescein dibromomaleimide reagent **62** (2eq) for 2 h.

Entry	Temp	pH	**37**	**100**	**101**	Other
1	0 °C	8	1 (±1) %	61 (±3) %	32 (±3) %	6 (±0) %
2	21 °C	8	0 (±0) %	2 (±1) %	61 (±9) %	37 (±8) %
3	21 °C dark[κ]	8	0 %	12 %	80 %	8 %
4	37 °C	8	0 (±0) %	0 (±0) %	75 (±4) %	25 (±4) %
5	0 °C	7	0 (±0) %	57 (±4) %	43 (±4) %	0 (±0) %
6	21 °C	7	1 (±1) %	9 (±1) %	81 (±1) %	10 (±0) %
7	37 °C	7	0 (±0) %	7 (±7) %	71 (±1) %	22 (±8) %

Table 5. Protection of Grb2 SH2 domain with fluorescein dibromomaleimide. Hyd = hydrolysis product **101**; other = -23 m/z, [κ] = reaction carried out once.

The protection of Grb2 SH2 domain **37** using fluorescein dibromomalemide **62** at pH 7 and 8 was found to be most efficient at 0 °C (table 5 entries 1 and 5), with higher temperatures resulting in degradation and hydrolysis (table 5 entries 2, 4, 6 and 7). The failure of the reaction at 21 °C was also of note, due to the substantial degradation observed (37% conversion, table 5 entry 2). To investigate whether light was contributing to this degradation; the 21 °C reaction was repeated in the dark (table 5 entry 3). However, whilst this did alleviate degradation considerably, the amount of hydrolysis was seen to increase to a level comparable with that at 37 °C (table 5 entry 4). At this temperature, little product was observed, predominantly being hydrolysed species **101**.

Thus at temperatures above 0 °C and in the presence of light, hydrolysis was observed to be the major process taking place. In comparison with the biotinylated dibromomaleimide reagent **60** discussed in section 2.6.1, the fluoresceinylated analogue was found to be considerably more reactive to hydrolysis, which is in agreement with observations of *N*-aryl maleimides reported in the literature.[26]

Table 6 presents the mean percentage conversions for the deprotection of Grb2-fluorescein dibromomaleimide conjugate **100** with BME, at pH 7 and 8, and at 0 °C, 21 °C and 37 °C (scheme 39), with the standard error shown in parenthesis.

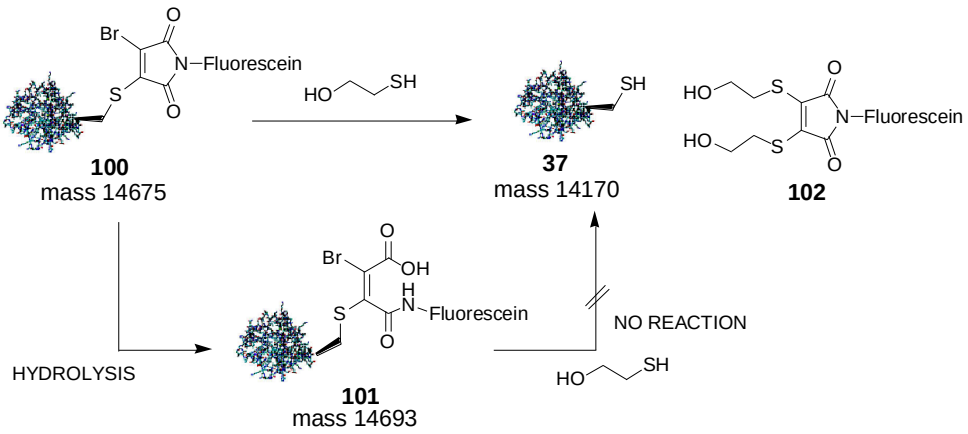

Scheme 39. Deprotection of Grb2-fluorescein dibromomaleimide **100** with BME (100 eq) for 4 h.

Entry	Temp	pH	**100**	**37**	**101**	Other
1	0 °C	8	3 (±3) %	52 (±7) %	41 (±7) %	4 (±4) %
2	21 °C$^{\tau}$	8	0 %	0 %	0 %	0 %
3	37 °C	8	0 (±0) %	0 (±) %	93 (±2) %	7 (±2) %
4	0 °C(P)/21 °C$^{\tau}$	8	0 %	0 %	0 %	0 %
5	0 °C(P)/37 °C	8	0 (±0) %	58 (±2) %	39 (±5) %	3 (±3) %
6	0 °C	7	0 (±0) %	58 (±2) %	42 (±2) %	0 (±0) %
7	21 °C$^{\tau}$	7	0 %	0 %	0 %	0 %
8	37 °C	7	6 (±1) %	0 (±0) %	93 (±2) %	1 (±1) %

Table 6. Deprotection of Grb2-fluorescein dibromomaleimide. Hyd = hydrolysis product **101**; other = -23 m/z. τ complete reaction failure.

The highest mean percentage conversion for the deprotection of Grb2-fluorescein dibromomaleimide conjugate **100** at pH 7 and 8 were both obtained at 0 °C (table 6 entries 1 and 6). At this temperature hydrolysis was also found to be of a comparable value (41% entry 1; 42% entry 6). In order to avoid this hydrolysis and hence determine an accurate mean percentage conversion for the deprotection of **100** at elevated temperature, Grb2 was first protected with fluorescein dibromomaleimide **62** at 0 °C and subsequently deprotected at 21 °C and 37 °C (table 6, entries 4 and 5). Despite this, no change in yield was observed, suggesting that the limiting factor in these reactions is the relative rates of protection and hydrolysis, and that deprotection is faster than hydrolysis.

2.6.4 Reactivity of fluorescein monobromomaleimide with 37

The major product from the protection of the Grb2 SH2 domain **37** with fluorescein dibromomaleimide **62** at elevated temperature was hydrolysed species **101**. However, as shown in section 2.6.2, hydrolysis of the maleimide motif could be subdued by replacing the dibromomaleimide motif with monobromomaleimide. Therefore, in

order to investigate whether a similar result could be achieved with the fluorescein analogues, the fluorescein dibromomaleimide was in turn replaced with fluorescein monobromomaleimide (scheme 40).

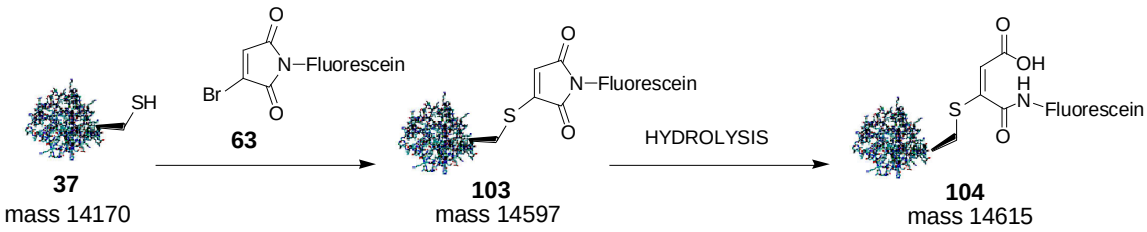

Scheme 40. Reaction of Grb2 SH2 domain **37** with fluorescein monobromomaleimide reagent **63** (2eq) for 2 h.

The results for the protection of Grb2 SH2 domain **37** with fluorescein monobromomaleimide **63,** at 0 °C, 21 °C and 37 °C and at pH's 7 and 8, are presented in table 7 as mean percentage conversions with standard errors shown in parenthesis.

Entry	Temp	pH	**37**	**103**	**104**	Other
1	0 °C	8	0 (±0) %	82 (±4) %	2 (±2) %	16 (±4) %
2	21 °C	8	0 (±0) %	78 (±5) %	9 (±9) %	13 (±13) %
3	37 °C	8	0 (±0) %	31 (±3) %	67 (±1) %	2 (±2) %
4	0 °C	7	0 (±0) %	89 (±2) %	9 (±1) %	2 (±2) %

Table 7. Protection of Grb2 SH2 domain with fluorescein monobromomaleimide. Hyd = hydrolysis product **104**; other = -23 m/z.

The protection of the Grb2 SH2 domain **37** with fluorescein monobromomaleimide **63** at 0 °C and 21 °C for pH's 7 and 8 (table 7 entries 1, 2 and 4) was shown to proceed with the desired increase in product, demonstrating the beneficial effect of using a single bromine on the maleimide motif. Unfortunately at 37 °C significant hydrolysis was observed (table 7 entry 3), but was modest by comparison with the extent of hydrolysis observed with the fluorescein dibromomaleimide derivative **62**, and so this approach is considered an improvement.

The mean percentage conversions for the deprotection of **103** using BME (scheme 41) are presented in table 8, with the standard error shown in parenthesis.

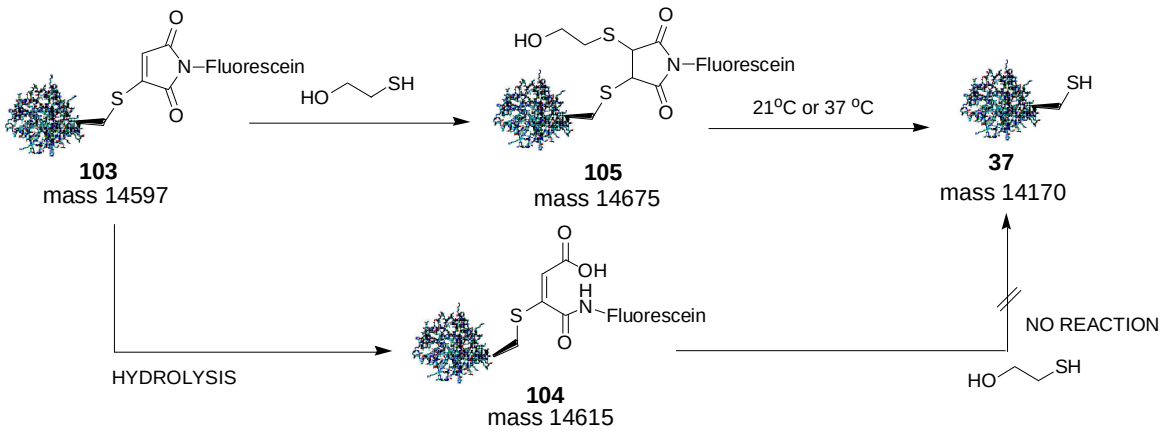

Scheme 41. Deprotection of Grb2-fluorescein monobromomaleimide conjugate with BME (100 eq) for 4 h.

Entry	Temp	pH	**103**	**37**	**104**	Other **105**
1	0 °C	8	0 (±0) %	27 (±3) %	0 (±0) %	65 (±0) %[κ]
2	21 °C	8	12 (±3) %	51 (±2) %	8 (±8) %	27 (±6) %[κ]
3	37 °C	8	7 (±7) %	23 (±9) %	70 (±2) %	0 (±0) %
4	37 °C	7	1 (±1) %	87 (±1) %	11 (±1) %	1 (±1) %

Table 8. Deprotection of Grb2-fluorescein monobromomaleimide. Other = yield corresponds to BME addition product **105**, [κ] = remaining unaccounted mean percentage conversion is a combination of unidentifiable species.

It is notable that at pH 8 there is modest product formation, irrespective of the temperature. It was also observed that the BME again reacts with the bromomaleimide double bond leading to the maleimide complex **105**. Heating of **105** at pH 8 was observed to reverse the conjugate addition, although hydrolysis of the less stable aromatic maleimide group gave the hydrolysis product **104** (table 8 entry 3), which was unreactive towards BME deprotection. However, at pH 7 a different mode of reactivity was observed with the reduced Grb2 SH2 **37** being predominantly formed, with only a minor amount of hydrolysis (11 % conversion - table 8 entry 4).

This is a result of the decreasing concentration of hydroxide ion present in solution as the pH is decreased from 8 to 7.

2.6.5 Comments and conclusions on the reactivity of mono - and di-bromomaleimides with 37

It has been shown that the reaction of Grb2 SH2 domain **37** with modified dibromomaleimides (biotin / fluorescein) occurs in high percentage conversion at low temperature (0 °C), whilst at higher temperatures (21 °C and 37 °C) hydrolysis to form the inactive hydrolysed dibromomaleimide adducts is observed. However, the rate of hydrolysis appears slower than the protection of Grb2 SH2 domain with the dibromomaleimide reagents. Optimisation studies have indicated that at pH 7 and 8, addition of the Grb2 SH2 domain to the dibromomaleimide reagents is complete within 35 min. It has previously been reported and found in this study that thiolates are unable to react with hydrolysed maleimides due to the electrostatic repulsion with the carboxylate.[26] This literature precedent along with the results from the present studies, indicate that addition of Grb2 SH2 domain to the bromomaleimide is the first step which is then followed by hydrolysis.

The monobromomaleimides appear to be a useful alternative reagent, which can be used to avoid hydrolysis of the maleimide ring. The rate of hydrolysis is increased by the presence of two bromines on the maleimide motif, but the incorporation of only one bromine leads to greater stability. Although the resistance to hydrolysis is desirable, the monobromomaleimide reagents do encounter another problem; at low temperature the intermediate from the cleavage reaction appears stable (scheme 42). Whilst this process can be reversed by heating at pH 7 or 8, this reverse reaction can also be complicated by further problems of hydrolysis, particularly at pH 8. At pH 7 reversibility is ensured, returning the Grb2 SH2 domain unprotected and in its original form (as characterised by LCMS), without undesired hydrolysis.

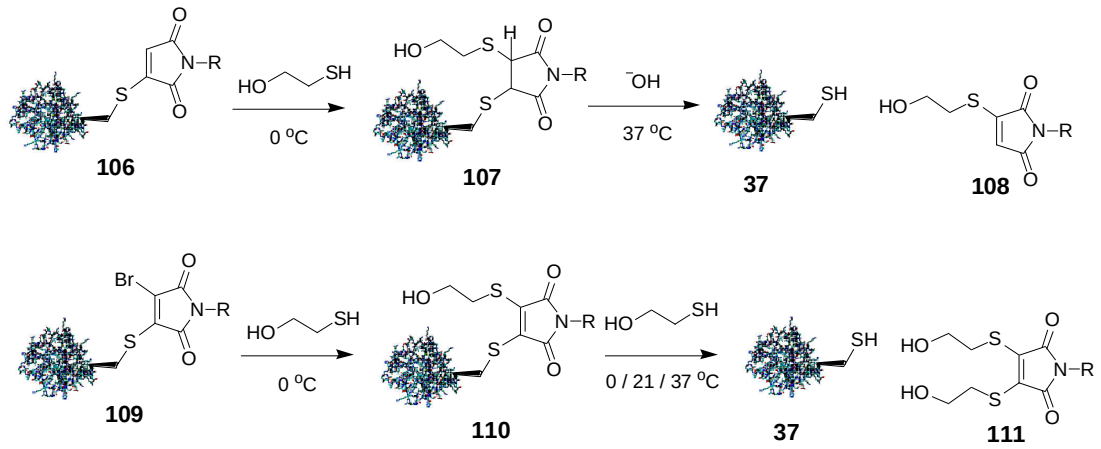

Scheme 42. Mechanism of cleavage for mono- and di- bromomaleimide reagents.

2.7 Studies on the chemical modification of Somatostatin 112

It has previously been shown that treatment of Somatostatin, a peptide containing a single disulfide bridge, with 1 eq of TCEP at pH 6.2 followed by 1.1 eq of dibromomaleimide results in the insertion of the bromomaleimide unit into the disulfide bond.[66] This modification can be reversed with the addition of 100 eq of BME.[25] Prior work had demonstrated the proof of this concept using a simple dibromomaleimide compound (*N* = H) and hence it is desirable to investigate whether this reaction can be accomplished with more complex dibromomaleimide compounds, particularly those containing useful functionality such as biotin or fluoroscein.

2.7.1 Reactivity of fluorescein dibromomaleimide with 112

Somatostatin **112** was first reduced with 1 eq of TCEP at pH 6.2 and 21 °C in 10 min. To the reduced adduct was then added 1.1 eq of fluorescein dibromomaleimide **63**, which led to the conversion into the fluorescent bridged adduct **113** in 100% percentage conversion after 1 min, as determined by LCMS (scheme 43 and figure 21). Subsequent addition of 100 eq of BME to **113** then led to the regeneration of the reduced somatostatin in 1 h.

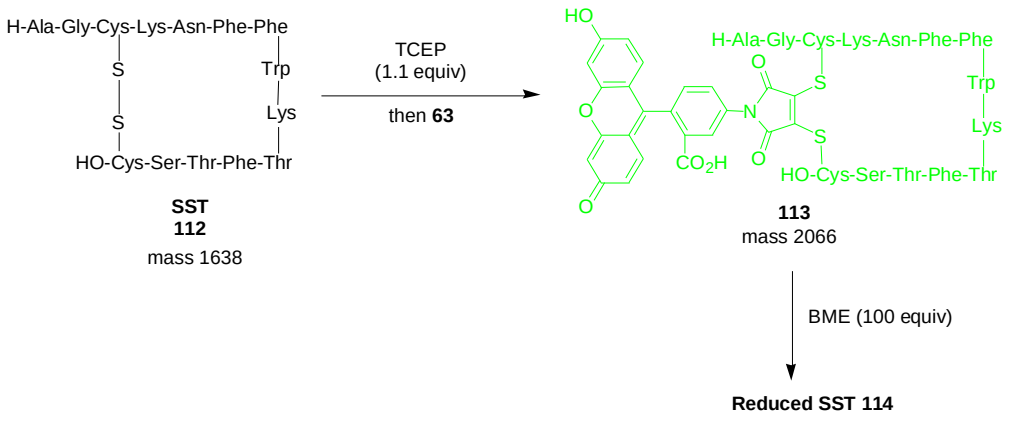

Scheme 43. Reversible modification of the disulfide bond of SST by fluorescein dibromomaleimide reagent **63**. Reactions carried out at 21 °C.

It is notable that there is a complete lack of maleimide hydrolysis under these reaction conditions; perhaps because (1) the dibromomaleimide motif is more stable

at pH 6.2 or (2) hydrolysis would result in an unfavourable conformation of the maleimide in the region of the initial disulfide bridge **115** (figure 22).

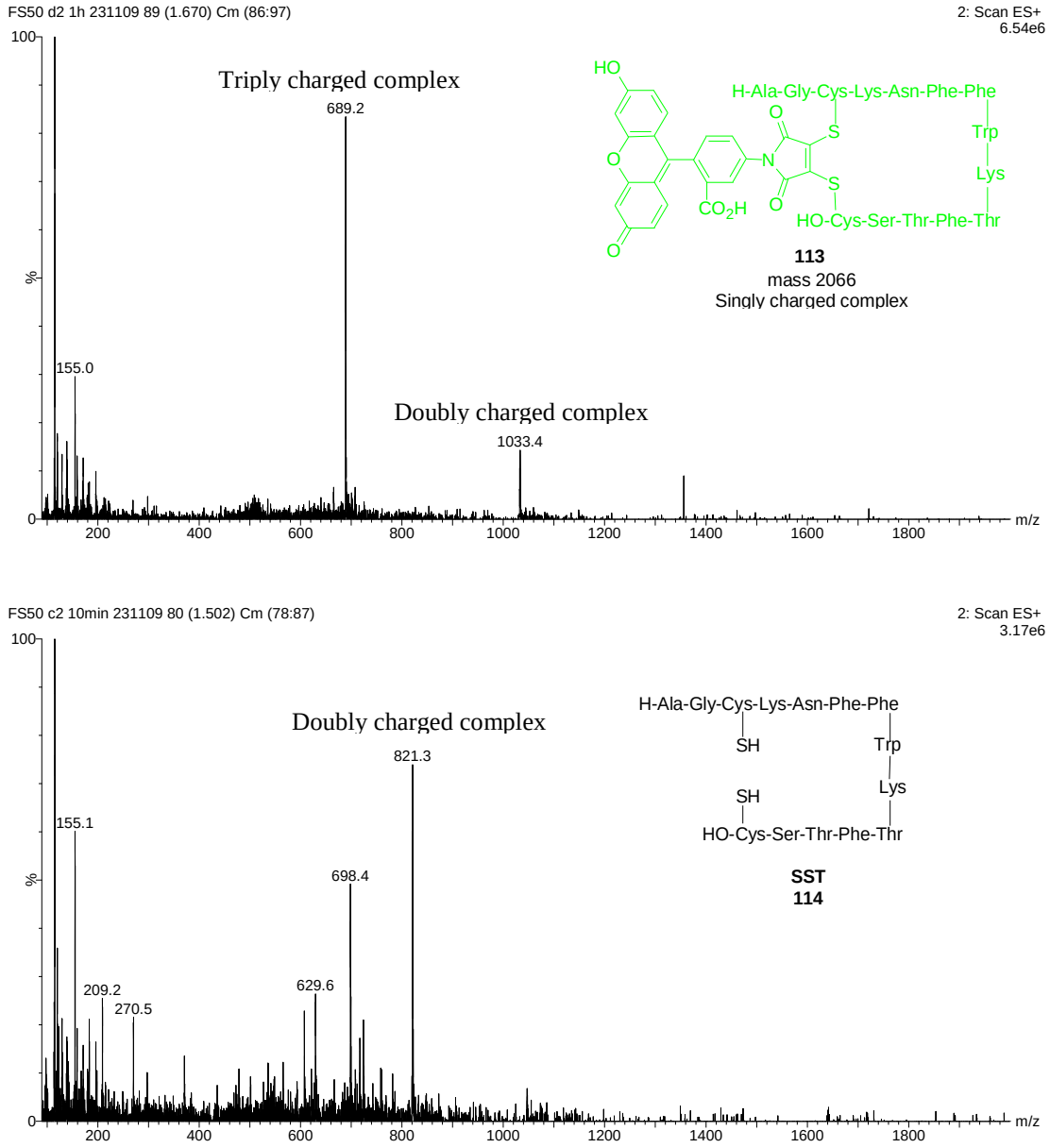

Figure 21. LCMS spectrums for reaction of fluorescein dibromomaleimide reagent **50** plus SST peptide.

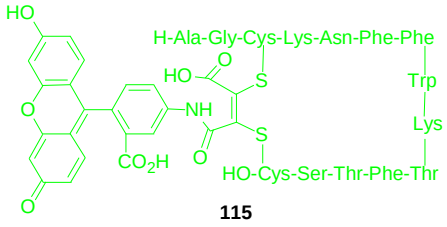

Figure 22. Potential hydrolysis product of SST bound fluorescein maleimide.

2.7.2 Reactivity of biotin dibromomaleimide with 112

Reduction of the Somatostatin **112** with 1 eq TCEP (pH 6.2, 21 °C, 10 min), followed by treatment with 1.1 eq of biotinylated dibromomaleimide **61** led to a biotinylated, bridged construct **116** in 65% percentage conversion after 1 min and 87 % after 1 h (scheme 44). Addition of 100 eq of BME reversed the modification and regenerated the reduced SST in 92% percentage conversion after 1 h, again with complete absence of hydrolysis.

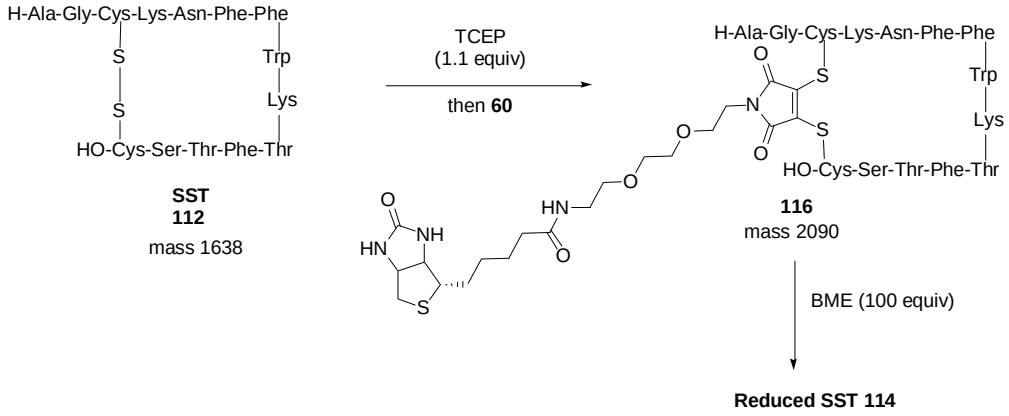

Scheme 44. Reversible modification of the disulfide bond of SST by biotin dibromomaleimide reagent **61**. Reactions carried out at 21 °C.

2.7.3 Comments and conclusions on the reactivity of fluorescein and biotin dibromomaleimides with 112

From this study it appears that functionalized dibromomaleimide reagents **63** and **60** can be used for the rapid, reversible chemical modification of the peptide Somatostatin. These compounds were found to be stable at pH 6.2 and at 21 °C and did not undergo hydrolysis in the way that was observed in the Grb2 studies. This may be due to differences in the peptide structure, but could be more likely attributable to an increased stability at pH 6.2.

Significant differences in reactivity were observed between the biotin and fluorescein dibromomaleimide reagents, with the latter being considerably more reactive (addition of fluorescein to Somatostatin complete in 1 min, as opposed to 1 h for biotin dibromomaleimide). This is most likely due to the fluorescein dibromomaleimide *N*-nitrogen's lone pair being conjugated into the fluorescein π-

system, resulting in less electron density in the amide bond and thus favouring 1,4-addition of somatostatin.

2.8 General conclusions

Previous work by Baker and Caddick *et al.* investigated the ability of simple mono- and di- bromomaleimide reagents to modify single sulfhydryl containing proteins, and found such modifications to be mild, selective, reversible and thus useful to the wider scientific community. However, other than acting as either protecting groups or blocking agents for sulfhydryl containing proteins, these reagents were limited in use. It has been shown in section 2 of this thesis that the reversible modification of sulfhydryl containing proteins can be extended to include mono- and di-bromomaleimide reagents more functionally diverse than the simple maleimides previously reported, such as the biotin and fluorescein bromomaleimides used here.

Whilst the synthesis of fluorescein mono- and di- bromomaleimide was found to be straightforward, this was not the case for the biotin analogues; the presence of the bromine on the maleimide motif leads to decomposition under basic conditions. Therefore a synthetic route was employed that kept to either neutral or acidic conditions, enabling the formation of biotin mono- and di- bromomaleimide in three efficient steps.

With the biotin and fluorescein bromomaleimide reagents complete, a number of LCMS experiments were carried out to investigate how well they would react with the single point mutant (L111C) of the SH2 domain of the Grb2 adaptor protein and with Somatostatin, a peptide containing a single disulfide bridge. In both cases it was found that the biotin and fluorescein mono- and di-bromomaleimide reagents reacted selectively and efficiently. However, a complicating factor not observed with bromomaleimide and *N*-methyl-bromomaleimide by Baker and Caddick was the issue of hydrolysis. Whilst protection of the protein and peptide with biotin and fluorescein dibromomaleimide occurred in high yield, hydrolysis of the protein-bromomaleimide conjugate yielded protein-bromomaleimic acid, a species inactive towards deprotection with BME. Hydrolysis was also found to be more pronounced for the aromatic fluorescein mono- and di-bromomaleimides, in line with the

literature, yet could be overcome at higher temperatures or by lowering the pH (as observed for reaction with Somatostatin at pH 6.2).Hydrolysis could additionally be overcome by switching to the monobromomaleimide reagents, although higher temperatures were needed to deprotect with BME in order to overcome the formation of intermediates stable at low temperature.

Further research into the reversible modification of sulfhydryl containing proteins will need to take both the potential hydrolysis and formation of stable intermediates into account. Whilst the extension of the linker between the bromomaleimide motif and biotin/fluorescein functionality could feasible reduce hydrolysis, the formation of stable reaction intermediates will need to be more carefully considered. Further investigations are thus needed to ascertain what factors are involved and how they can overcome the formation of these stable intermediates, without affecting the efficiency and selectivity of reversible bromomaleimide modification.

3 Pd catalysis and DFT

3.1 Palladium catalysed reactions

Carbon-carbon and carbon-nitrogen bond forming reactions are the key steps in the synthesis of many organic substances.[89,90] The use of palladium in catalysing these types of reactions is very well documented and has become an extremely important tool in modern day synthesis. Suzuki,[91-93] Negishi,[94,95] Heck,[96] Kumada[97-99] and Buchwald–Hartwig amination reactions[99-101] are just a few examples of the many powerful transformations possible using palladium catalysis (scheme 45).

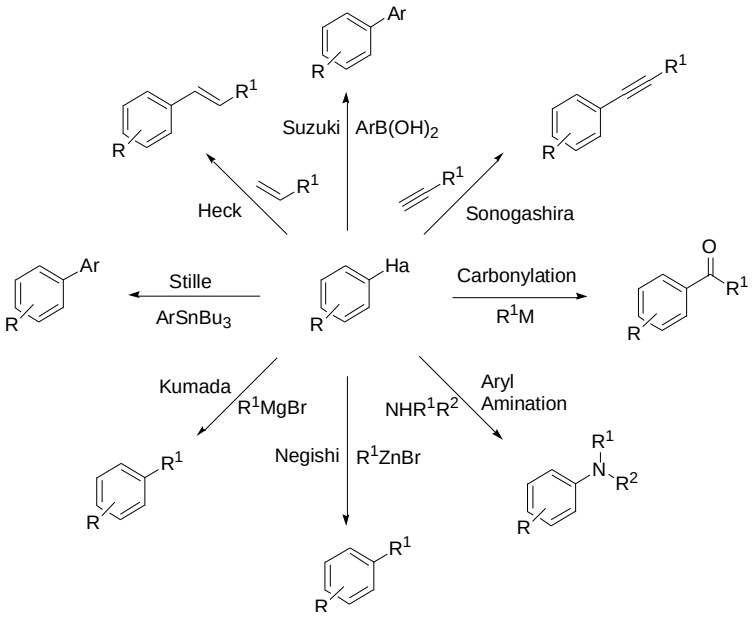

Scheme 45. Palladium catalysed reactions. Ha = Halide, R = Alkyl, Ar = Aryl.

An example of a palladium(0)-catalysed reaction is shown in scheme 46.[102] The catalytic cycle is initiated by formation of the Pd(0) active catalyst, either by reducing the Pd(II) precatalyst with phosphine or amine, or in the case shown, dissociation of NHC from the pre-catalyst $Pd(NHC)_2$ **117**, to give the catalytically active Pd(NHC) **118**. From this point onwards there are 4 stages to the catalytic cycle. The first is the oxidative addition of a palladium(0) active species to an sp or sp^2 carbon-halide bond, yielding a σ-aryl or σ-alkenylpalladium(II) complex **119**. This is the single most important reaction of palladium(0) complexes and involves oxidation of the metal from palladium(0) to palladium(II).[103] The resulting σ-aryl or

σ-alkenylpalladium(II) complexes formed can then participate in a wide variety of chemistry: alkene and CO insertion; hydrogenolysis; transmetallation with main group organometallics; addition of nucleophilic carbon, oxygen, sulfur or amine (latter shown in scheme 46) to form a four coordinate species **120**. Deprotonisation (if required) followed by *cis*-rearrangement then affords a three coordinate species primed for reductive elimination **121**, allowing formation of the coupled product **122** and regeneration of the palladium(0) catalyst **118** in the process.

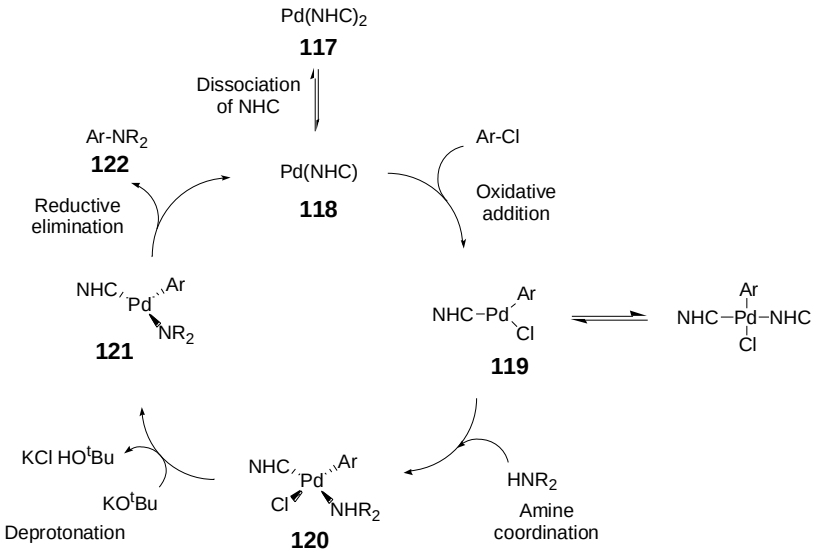

Scheme 46. Example of the possible mechanism for a Pd catalysed reaction, Aryl amination reaction shown.

The choice of aryl halide is important to the success of these reactions. It has been found that aryl halides containing a vacant low energy orbital (e.g. iodides, bromides) are, in general, more reactive than aryl halides containing a vacant high energy orbital (fluorides). This is a result of the vacant low energy orbital ((sp/sp^2) carbon–halide antibonding orbital) being closer in energy to the occupied high energy orbital of the Pd(0) nucleophile, allowing an efficient interaction between the two sets of orbitals, and therefore oxidative addition to take place. However, the difference in energy for aryl halides containing a vacant high energy orbital is too great for an efficient interaction and no reaction occurs. Additionally, carbon-halide bond strength is known to decrease as you descend group 7, resulting in the weaker bonds of carbon-iodides/bromides being more reactive than their fluoride counterpart.

3.1.1 Control of stereochemistry

Not only does palladium(0) catalysis allow for a vast array of different reactions, but also the potential control of the stereochemistry in the product. Whilst only readily available at sp and sp^2 centres, the extension of palladium chemistry to use a sp^3 centre would offer a powerful methodology for producing complex chiral molecules, provided the reactions proceeded with an absolute control of stereochemistry. A comparison of the oxidation addition of an active Pd(0) species into either a (sp/sp^2) carbon-halide bond or (sp^3) carbon-halide bond, finds that whilst the former occurs by a concerted process, the latter is stepwise (scheme 47). This is due to the inaccessibility of the (sp/sp^2)carbon-halide anti-bonding orbital for direct nucleophilic attack by Pd(0). However, in the case of the (sp^3)carbon-halide bond, the antibonding orbital is available for nucleophilic attack by Pd(0), which will result in an inversion of the stereochemistry of the product in relation to the starting material. Therefore in an analogous fashion with the use of the Mitsunobu reaction to invert the stereochemistry of alcohols, synthetic schemes can be designed which give both useful products, and also take advantage of the inversion of stereochemistry associated with Pd catalysed reactions using alkyl halides to give products of a desired stereochemistry.

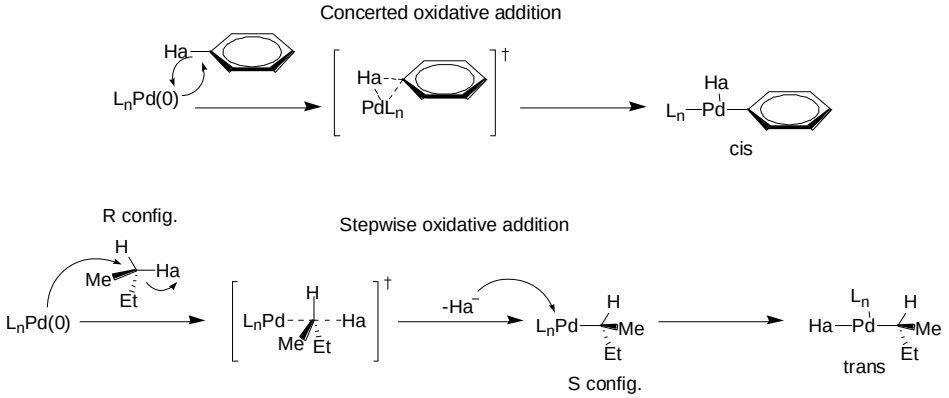

Scheme 47. Inversion of stereochemistry upon oxidative addition of Pd(0) into sp^3 carbon halide bond.

3.1.2 Choice of catalyst ligand

The choice of ligand bound to the metal in catalysis plays a very important role. Studies have shown that adjusting the properties of these ligands results in changes to the activity of the catalyst. Selectivity has found to be controlled by electronic and steric factors.[104] Therefore a proper choice of supporting ligand can affect both the oxidative addition and the reductive elimination steps, *via* preferential stabilisation of the metal complex at different stages of the catalytic cycle.[105] For instance, monodentate, bulky, electron-donating tertiary phosphines have generally been employed as ancillary ligands in coupling systems.[106] The increased steric bulk of the phosphine ligand favours the dissociation of excess phosphine and therefore formation of the catalytically active monodentate Pd(0) phosphine complex. Additionally, the electron-donating nature of the tertiary phosphine increases the electron density on the Pd centre, which raises the energy of its occupied high energy orbital. In doing so, this will decrease the difference in energy between the Pd(0)'s occupied high energy orbital and the aryl halides vacant low energy orbital (carbon–halide antibonding orbital), in turn increasing the orbitals ability to interact and form a bond.

Therefore bulky and electron-donating tertiary phosphines increase the reactivity of the Pd centre towards oxidative addition. However, whilst oxidative addition requires an occupied high energy orbital on the Pd centre, reductive elimination requires a vacant low energy orbital into which electron density can be donated. This means that reductive elimination will be increased by using ancillary ligands which remove electron density from the Pd centre, thus lowering the energy of this vacant orbital. By using bulky tertiary phosphine ligands which favour the formation of mono-ligated Pd(PR_3) over di-ligated Pd(PR_3)$_2$, reductive elimination is favoured. This is due to lowering of the energy of the vacant orbital on the Pd centre *via* the donation of electron density from only one PR_3 ligand as opposed to two. Additionally, phosphine ligands allow back-donation of electron density from the Pd centre, which again lowers the energy of the Pd's vacant orbital.

Catalytic activity is therefore a balance between the opposing factors contributing to oxidative addition and reductive elimination. Oxidative addition requires bulky,

electron-donating ligands, whilst reductive elimination requires bulky, electron-withdrawing ligands, and it is the use of ligands which give balance between these two processes which is important.

3.1.3 *N*-Heterocyclic carbene ligands

Although tertiary phosphine ligands are useful in controlling the reactivity in organometallic chemistry and homogeneous catalysis, they often undergo significant phosphorus-carbon bond degradation at higher temperatures. Unfortunately, this can result in deactivation of the catalyst; there is no longer control of oxidative addition and reductive elimination, or stabilisation of the metal centre by association of ligand. As a result, there is a need for strongly nucleophilic, electron rich ligands which can form stable bonds to the metal centre. *N*-Heterocyclic carbenes (NHCs) have been shown to be such ligands and combined with their behaviour as phosphine mimics, has enabled them to fulfil the role of alternative ligand.[107]

First reported by Wanzlick and Schonher[108] and by Olefe *et al*. in 1968, then isolated and characterised by Arduengo in 1991,[109] NHCs (figure 23) have since become ubiquitous ligands in both organometallic and inorganic coordination chemistry.[110] Their similarity to electron-rich organophosphines,[111] in terms of their metal coordination chemistry, ligand properties and in their metal complex synthesis was noted as early as 1993. NHCs were shown to bind to transition metals, in either high or low oxidation state, as well as to many main group elements such as beryllium, sulfur and iodine.

Figure 23. Basic structure of NHCs (R = ^{t}Bu, ^{i}Pr, Ms, Ad, Me, Bz).

NHCs are found to stabilise and activate diverse metal centres in many different key catalytic steps of organic synthesis.[110] Being strong σ-donors, they activate metal centres towards oxidative addition by donation of electron density onto the metal centre and thus raising the energy of the metals occupied high energy orbital. Additionally, NHCs such as IAd, IPr and IBu are found to be of sufficient steric bulk

to allow the formation of mono-ligated metal complexes, the active species in the oxidative addition step of many catalytic reactions.

Comparison of bond dissociation energies (BDEs) of metal bound NHCs and other ligands indicated that the NHCs were generally more coordinating than amines (NR_3), phosphines (PR_3) and CO (scheme 48). The finding that the BDEs calculated for the NHCs were considerably higher than for PR_3 (by almost 30 kJ mol^{-1} in some cases) was in agreement with the assumption that NHCs bind more tightly than phosphines to transition metals.

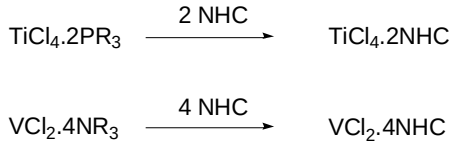

Scheme 48. Comparisons of NHCs binding with tertiary amines and phosphines.

It was initially thought that NHCs behaved like typical σ-donor ligands[112,113] such as amines, ethers and phosphines, which would classically donate two electrons. However, structural and thermodynamic studies led Nolan *et al.* to conclude that, with the exception of the most sterically bulky NHCs (e.g. adamantyl carbene), NHCs generally behave as better donors than the best of the phosphine donor ligands.[114,115]

This simplified picture is beginning to change and recent studies have suggested that NHC ligands are not simple σ-donors. Since there are filled π and empty π* orbitals on the NHC ring, these could contribute to the NHC-metal bond.[116,117] Meyer *et al*. found that NHC ligands could accept electron density from electron-rich group 11 metal atoms, *via* d → π* back bonding, and could thus stabilise an electron-rich metal centre containing high energy orbitals. They could also stabilise an electron-deficient metal centre, containing low energy orbitals, through a π → d bonding scheme back onto the metal. However, current opinion is divided, and it appears most likely that, depending on the metal centre in question, they can act as both π donors and acceptors.[118,119]

Reactions using saturated NHCs were found to give higher yields than for the corresponding unsaturated variants (table 9).[100] Theoretical studies using electron

density analysis has indicated that more electron density is back-donated from the metal centre to saturated NHCs than to unsaturated ones. Therefore unsaturated NHCs are both less σ-donating and less efficient π-acceptors, and hence weaker ligands than their saturated counterparts. In the case of the Pd-catalysed aryl amination reaction in table 9,[100] the strongly σ-donating saturated NHCs will impart more electron density onto the Pd centre, thus raising the energy of the Pd's occupied high energy orbital. This will close the gap in energy between the Pd(sat-NHC) high energy orbital and the aryl halides vacant low energy orbital (carbon–halide antibonding orbital), lowering the energy for oxidative addition, the rate determining step of the reaction. However, for the less σ-donating unsaturated NHCs, the opposite will happen. The occupied orbital of the Pd(unsat-NHC) will be lowered in energy and therefore there will be a bigger difference in energy to the vacant low energy orbital of the aryl halide.

Additionally, as already stated, sterically demanding NHCs such as IPr favour the formation of the mono-ligated Pd(NHC) complex, the active species in these reactions.[120] Shorter metal-carbon distances (0.01-0.02 Å) are predicted for saturated complexes, which enhances any steric effect already observed, again favouring formation of mono-ligated Pd(NHC). Additionally the more sterically encumbersome saturated NHCs favour formation of three coordinate Pd complexes, the species believed to be more react towards reductive elimination (see section 3.2.2).

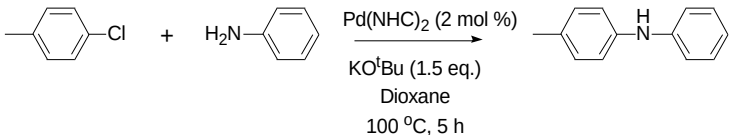

NHC	Yield (%)
SIPr	91
IPr	52
SIBu	30
IBu	19

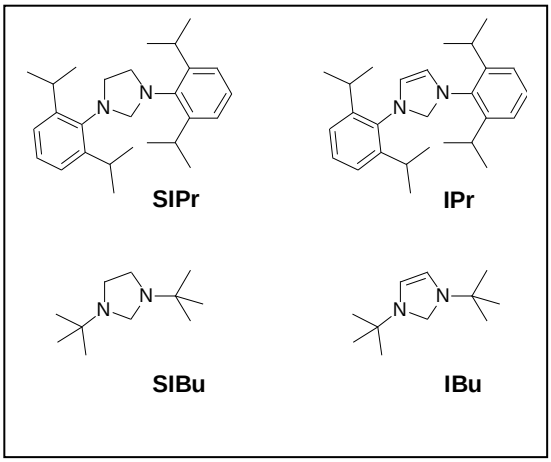

Table 9. Comparison of the effect on yield of various NHCs after 5 h.[100]

Therefore it is emerging that for the Pd-catalysed aryl amination reaction to be carried out in high yield and in an efficient time frame; the catalytic system employed must be able to form to the active mono-ligated Pd(NHC) quickly and in sufficient concentration, and contain NHC ligands both large in size and strongly σ-donating in nature. To increase the concentration and formation of the mono-ligated Pd(NHC) species, Caddick and Cloke *et al.*[121] and Organ *et al.*[95] have used precatalysts containing easily dissociable 'throw away' ligands and only one NHC (figure 24 – **123** and **124**). These pre-catalysts lead more quickly to the active mono-ligated Pd(NHC), and containing only one NHC, avoid the potential problem of excess NHC inhibiting the reaction.

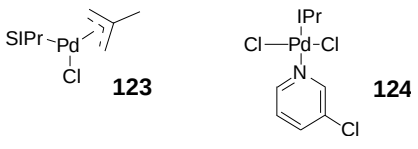

Figure 24. Pre-catalysts containing a single NHC.

3.2 Transition metal catalysed carbon(sp^3)-nucleophile bond formation

Whilst the literature contains an enormous number of examples of carbon(sp or sp^2)-nucleophile bond formation, for carbon(sp^3), in comparison, this is not the case. The presence of β-hydrogens on any carbon(sp^3) species usually results in fast β-hydride elimination to give an alkene product, rather than the slower transmetallation and reductive elimination (scheme 49). This alkene is then able to take part in a variety of side reactions: including insertion reactions into Pd(II) complexes, analogous to the Heck reaction.

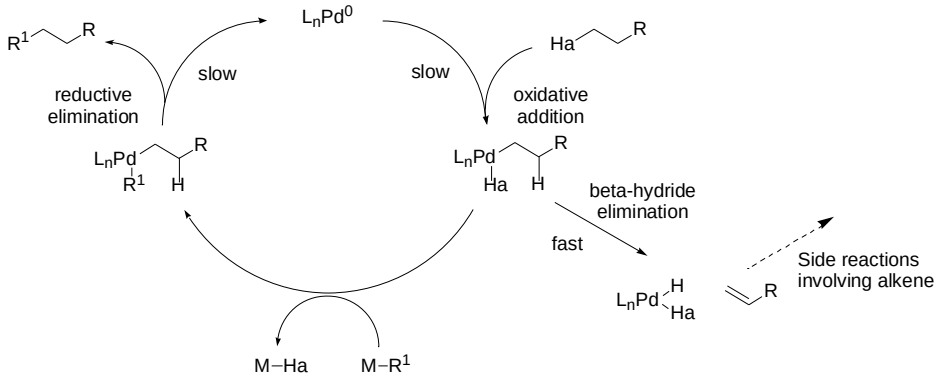

Scheme 49. Carbon(sp^3)-nucleophile bond formation.

Initial work carried out on carbon(sp^3)-nucleophile bond formation focused on substrates which did not contain any β-hydrogens (e.g. benzyl halides), so as to reduce the potential for β-hydride elimination. However, this severely limits the scope of the reaction. More recent research has instead focused on control of the selectivity of reductive elimination to β-hydride elimination by careful choice of catalyst and ligand system. Fu and Zhou,[122-124] for instance, discovered a Pd/PR_3 protocol (PR_3 = PCy_3 or $P(^tBu)_2Me$) which served as an effective catalyst for Suzuki reactions of primary and secondary alkyl bromides, chlorides and tosylates with trialkylboranes.

Fu found that the choice of ancillary ligand has a substantial impact on the success of these reactions; only trialkylphosphines of an appropriate size could produce catalysts active in Negishi couplings (table 10 entries 1 and 2),[124,125] whilst

triarylphosphines (entry 3), chelating electron-rich phosphines, NHCs (entry 5) and phosphites (entry 4) gave none of the desired coupled product.

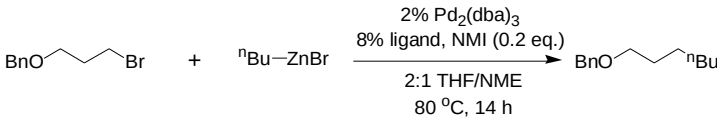

Entry	Ligand	Yield (%)
1	$PCyp_3$	70
2	$P(^tBu)_2Me$	55
3	PPh_3	5
4	$P(o\text{-tol})_3$	1
5	IMe	4

Table 10. An investigation of the effects of ancillary ligands on the yield of the Negishi reaction after 14 h.[125]

The trialkyl phosphine ligands, being strongly σ-donating, lower the energy for oxidative energy (by raising the energy of the Pd(0) occupied high energy orbital). However, the key to efficient selectivity is the inhibition of *β*-hydride elimination, due to the large size of the trialkyl phosphine ligand. *β*-hydride elimination requires a free coordination site on the metal centre. Therefore the use of large trialkyl phosphines which block this site will inhibit *β*-hydride elimination and instead favour reductive elimination.

Further work using excess diene has built on these principles, again by blocking the free coordination site on the metal centre. Knochel demonstated this using nickel complexes to catalyse Negishi reactions of both primary alkyl bromides and iodides with a range of organozinc reagents,[126] whilst Kambe reported a nickel complex that could catalyse the coupling of unfunctionalised Grignard reagents with primary alkyl bromides and tosylates (scheme 50).[127,128] Beller later went on to extend these reactions to include the use of alkyl chlorides with aryl Grignards.[129] Not only does

the added diene block the free coordination site on the metal, it also removes electron density from the metal centre, lowering the energy of the metals vacant orbital, thus favouring reduction of the metal. As β-hydride elimination is no longer available, the major reaction pathway becomes reductive elimination.

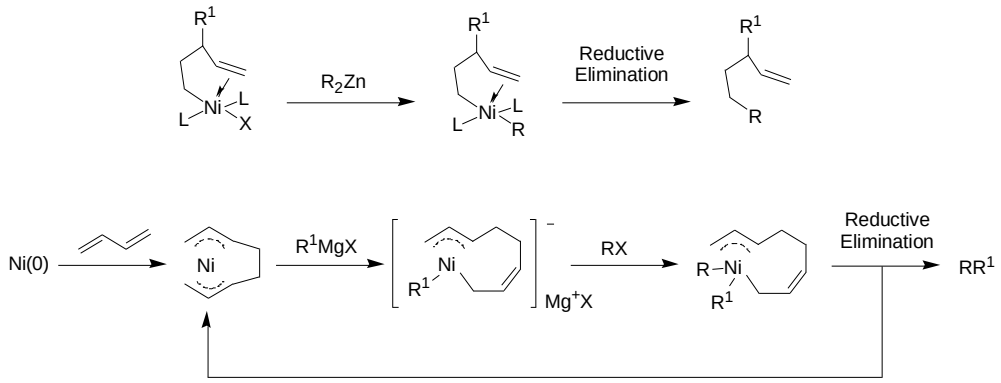

Scheme 50. Use of diene to block metal centres free coordination site and inhibit β-hydride elimination.[126-128]

Despite the considerable progress made towards alkyl-alkyl bond formation by control of β-hydride elimination, little success has been achieved concerning C(sp^3)-N bond formation

3.2.1 C(sp^3)-N bond formation; alkyl amination reaction

The Pd-catalysed alkyl amination cross-coupling has not previously been reported to any great extent, with only limited theoretical studies undertaken.[119,130] These have implied that in the corresponding sp^2 reaction (i.e. formation of an enamine), the participation of the π-system creates a lower-energy pathway for the reductive elimination step, which leads to the formation of the C-N bond. The lack of a π-system in the alkyl C-N bond formation might therefore be expected to inhibit such reactions.

A computational study of the oxidative addition of alkyl chlorides (chloromethane) to bis-carbene palladium complexes has been reported by Green *et al.*[119] The transition state for the oxidative addition of an alkyl chloride was found to be higher in energy than for the oxidative addition of the aryl chloride, indicating that this process would be significantly less favourable. This is consistent with the findings of Caddick and Cloke *et al.*, who observed difficulties in carrying out the oxidative

addition of neopentyl chloride to the $Pd(IBu)_2$ complex, forcing an alternative route to be devised.[131,132]

Research by Macgregor[130] described the use of DFT calculations to study the possibility of carbon-heteroatom bond formation *via* the reductive elimination reactions of *cis*-$Pd(PH_3)_n(CH_3)(X)$, where X = CH_3, OH and NH_2 and n = 1, 2 (scheme 51). This study led to a number of differences to Green's earlier work (although the ligand ancillary system in Macgregor's work was PH_3 as opposed to an NHC); the computed structures of the *cis*-$Pd(PH_3)_2(CH_3)(NH_2)$ reactants were all found to display slightly distorted square planar geometries. Reductive elimination appeared to be feasible from either of two isomers, a T_{CH3} or a T_{NH2} form in which the CH_3 or NH_2 was *trans* to the vacant site. Yet the T_{CH3} isomer **125** (isomer shown in scheme 51) was found to be ~13.8 kcal mol^{-1} more stable most probably due to the greater *trans* effect of CH_3 over NH_2 and the preference of CH_3 to be *trans* to the vacant site. The formation of the alkyl amine was also found to be an endothermic process (9.3 kcal mol^{-1}), as had been found by Green, Caddick and Cloke.

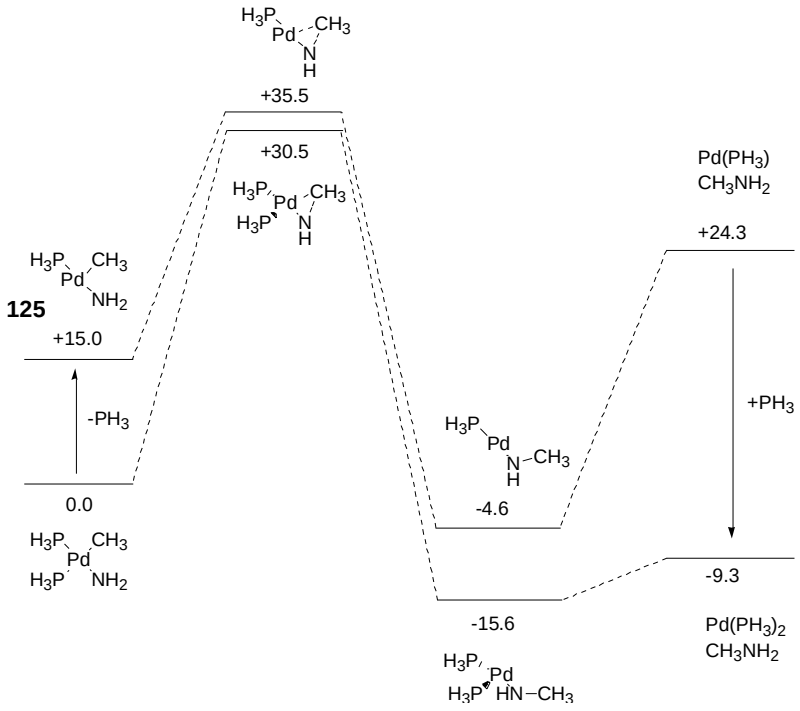

Scheme 51. Computed reaction profiles (kcal mol^{-1}) for C-N reductive elimination from the T_{CH3} isomer of $Pd(PH_3)_2(CH_3)(NH_2)$.[130]

In order to bring about the desired C(sp^3)-N bond formation experimentally, researchers have instead sought to oxidise the Pd(II) centre to Pd(IV), which would lower the energy of the vacant low energy orbital on Pd (scheme 52). However, upon investigation of the stereochemical course of this C-N bond formation in reactions of Pd(IV), Backvall,[133,134] Muniz[135,136] and Gaunt[137] all noted a clean inversion of configuration. This is indicative of a S_N2 type reaction, requiring first the dissociation of the amide from the Pd coordination sphere **126**, a process considered not to be a true coupling reaction.

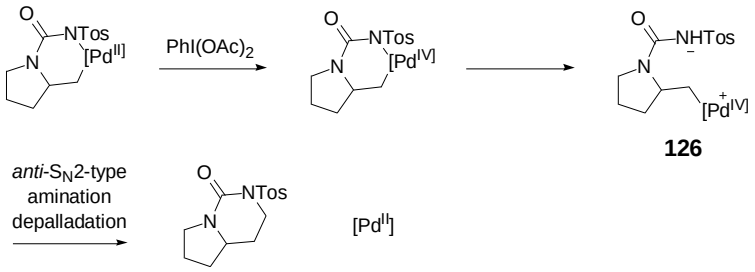

Scheme 52. Example of a Pd(IV) coupling reaction.

Caddick and Cloke have previously reported efforts towards developing a new protocol for catalytic alkyl amination reactions employing (NHC)–Pd complexes as catalysts.[131,132] These studies were undertaken using neopentyl chloride, an alkyl halide that does not contain β-hydrogens, so that oxidative addition could be thoroughly examined. The reaction investigated was the coupling of morpholine **127** to neopentyl chloride **128** using the palladium biscarbene complex $Pd(IBu)_2$ to give neopentyl morpholine **129** (scheme 53). Morpholine was chosen as it had exhibited the greatest reactivity in other coupling systems and as a result had become a standard choice in such reactions. Uncatalysed reaction conditions required the heating of morpholine (1 eq) and neopentyl chloride (1 eq) in a sealed bomb at 160 °C for three days to produce the neopentyl morpholine product,[138] conditions considerably more extreme than those employed with the palladium catalyst.

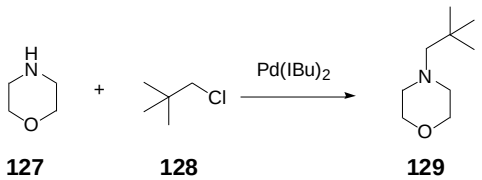

Scheme 53. Neopentyl chloride plus morpholine with $Pd(IBu)_2$ and base.

In order to maximise C–N bond formation, Caddick and Cloke employed IBu as ligand. McGuinness and Cavell *et al*.[139] had shown that sterically demanding substituents on metal-bound NHC ligands would hinder the close approach of the alkyl groups to the NHC, so the ^{t}Bu groups on the NHC should inhibit unwanted side-reactions of NHC with the neopentyl unit. It was also reasoned that the steric bulk of the neopentyl would prevent direct S_N2 attack by the amine on the initially formed insertion complex, and hence the only reaction able to occur would be the (sp^3)C–N reductive elimination from the metal-bound alkyl and amide.

Caddick and Cloke first investigated the oxidative addition of neopentyl halide to $Pd(IBu)_2$ by monitoring the reaction *via* ^{1}H NMR at room temperature. However, the formation of 2,5-dimethylhexane and $Pd(IBu)_2I_2$ as the major products implied an intermolecular exchange mechanism, as described by Cavell and McGuinness.[140] Additionally, at higher temperatures (75 °C) C-H activation of the *tert*-butyl group of IBu was observed; a process known to occur at iridium,[141] ruthenium[142,143] and nickel[144] centres, for both sp^2 and sp^3 C-H bonds. For Caddick and Cloke, C-H activation was followed by reductive elimination to yield neopentane. It was rationalised that this was a consequence of the concentration of NHC (2 eq) and if this was reduced (to 1 eq), both of these undesired processes could be reduced. Therefore an alternative route was devised to form an alkylpalladium halide NHC complex with only a single NHC attached **130**, which could then be used to investigate the reductive elimination step in an alkyl amination catalytic cycle (scheme 54).

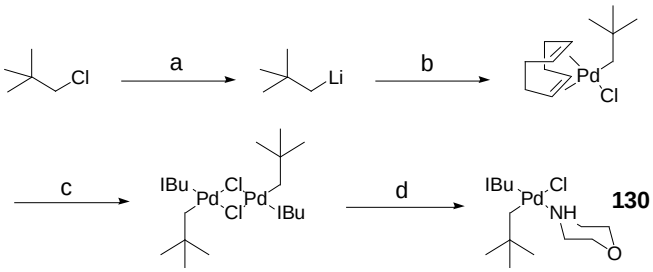

Li, 65 °C, 4 d; (b) $Pd(COD)Cl_2$, -78 °C to 21 °C, 5 h; (c) IBu, 0 °C, 30 min; (d) morpholine, 0 °C, 30 min.

Scheme 54. Route employed for the synthesis of alkyl palladium halide NHC complex.

Complex **130** was the first alkyl transmetallation product to be isolated and characterised.[131,132] It proved remarkably stable and did not undergo reductive

elimination despite having the required *cis* geometry. Furthermore, no evidence was found to suggest that deprotonation of the coordinated amine occurred when a variety of bases were added (KO^tBu, LHMDS, NaH, $NaOCEt_3$). Instead morpholine was liberated with additional formation of $Pd(IBu)_2$ and neopentane. Caddick and Cloke proposed that the electron donating effect of the alkyl group, combined with the strong σ-donation of IBu, led to an increase of the electron density on the metal centre. As a result, the nitrogen was more electron-rich, requiring less electron density from the bound hydrogen, which becomes less electropositive and thus harder to remove.

The aim of this project is to investigate the factors affecting the $C(sp^3)$-N coupling reaction, with an emphasis on gaining a greater understanding of the reductive elimination stage, using a combination of computational (DFT) and mass spectrometry analytical techniques. Before the theory behind these two methods is introduced, however, it is appropriate to discuss the factors affecting reductive elimination.

3.2.2 Reductive elimination reaction

The reductive elimination reaction is responsible for the formation of the new σ-bond in the product of the catalytic coupling process. The reaction involves the coupling of two covalent ligands and a formal reduction of the metal.[105] Reductive elimination reactions to form carbon-carbon and carbon-heteroatom bonds from aryl and vinyl complexes are typically more favourable than with alkyl complexes. In fact, examples of C-O and C-C bond formation involving alkyl carbons are very rare.[145]

Theoretical and early experimental studies have suggested that reductive elimination from metal complexes with more weakly electron-donating ligands is more favourable than from metal complexes with more strongly electron-donating ligands.[146-148] This is a result of the electron-withdrawing ligands removing electron density from the metal centre, lowering the energy of the metals vacant low energy orbital required for reductive elimination.

Reductive elimination is also more favourable for compounds in high and/or unstable oxidation states. In fact, oxidizing a stable complex to an unstable oxidation state can induce reductive elimination, a process called oxidatively induced reductive elimination (scheme 55).[149]

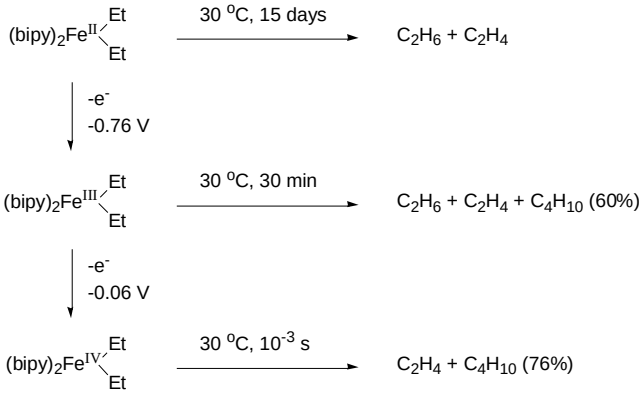

Scheme 55. Oxidatively induced reductive elimination.

It is generally true that reductive elimination from metal complexes with more hindered ancillary ligands is more favourable than from complexes with less hindered ancillary ligands. This effect arises from a relief of steric congestion upon generation of the coupled product and the reduced coordination number of the metal centre.[146] Additionally, hindered ancillary ligands force the two reacting groups (i.e. aryl and amide) into closer proximity, increasing the orbital overlap between the two groups, enabling reductive elimination to take place (figure 25 **131**<<**132**,**133**). As reductive elimination decreases the coordination number of the complex, steric hindrance will also affect the energy of the reactant more than the energies of the transition state and product.

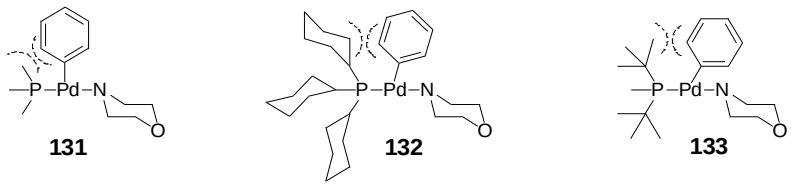

Figure 25. The use of hindered ancillary ligands to increase the orbital overlap between groups taking part in reductive elimination; Tolman's cone angle increases from left to right.

The use of hindered ancillary ligands will also favour the formation of three-coordinate organometallic complexes over four coordinate ones. This is important

because Yamamoto[150] and Stille[151] have shown that the reductive elimination to form C-C bonds from complexes containing mono- and bis- phosphines occurred considerably faster from three-coordinate monophosphine complexes than from the corresponding four-coordinate bisphosphines. Whilst it is believed that mono-ligated organometallic complexes are the active species from which oxidative addition takes place,[119,120] three-coordinate organometallic complexes are believed to be the species that from which reductive eliminations takes place. As already stated, reductive elimination is favoured for organometallic complexes containing a vacant low energy orbital, and disfavoured for complexes containing a vacant high energy orbital (figure 26). Therefore if only three ligands are bound to the metal **134**, less electron density will reside on the metal centre, the energy of the vacant orbital will be lowered, favouring reductive elimination. However, if four ligands are bound to the metal **135**, more electron density will be directed towards the metal centre, raising the energy of the vacant orbital, disfavouring reductive elimination. Additionally, ancillary ligands containing an empty orbital, such as trialkyl phosphine's, will be able to accept electron density back from the metal centre, lowering the energy of the metals vacant orbital further.

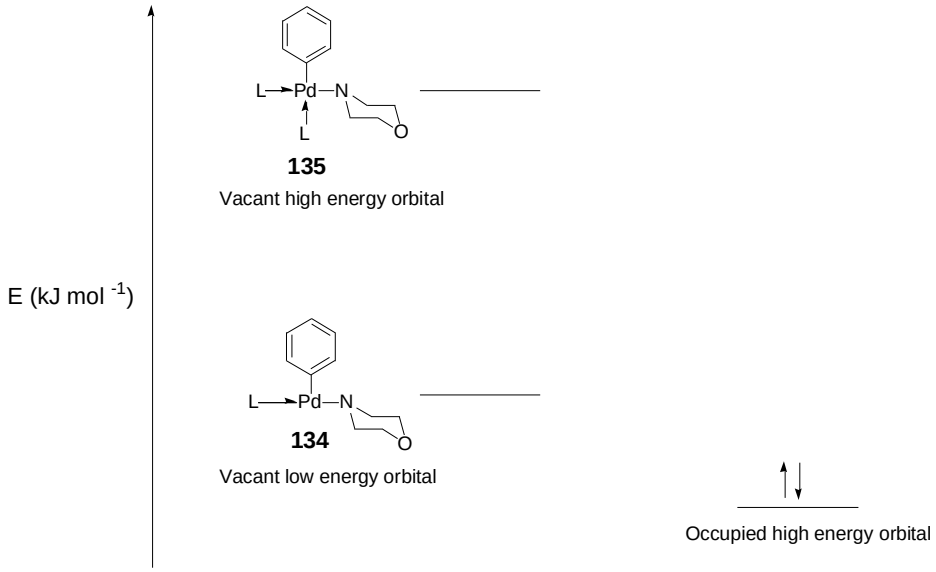

Figure 26. Differences in electron density of three and four-coordinate organometallic complexes; L = electron-donating ligand.

Arylpalladium halide complexes with a single phosphine have in fact been isolated but each complex contains an agostic interaction at the open site of a T-shaped geometry (figure 27).[152] Heating these three-coordinate species have been found to

cause reductive elimination, leading to the formation of aryl amines in reasonable yields. Hartwig *et al*. found that kinetic studies for this thermolysis were consistent with irreversible reductive elimination directly from the three-coordinate species.[153] It was even found that complexes with highly deactivating groups on both the palladium bound aryl ring and the nitrogen underwent such a reductive elimination.

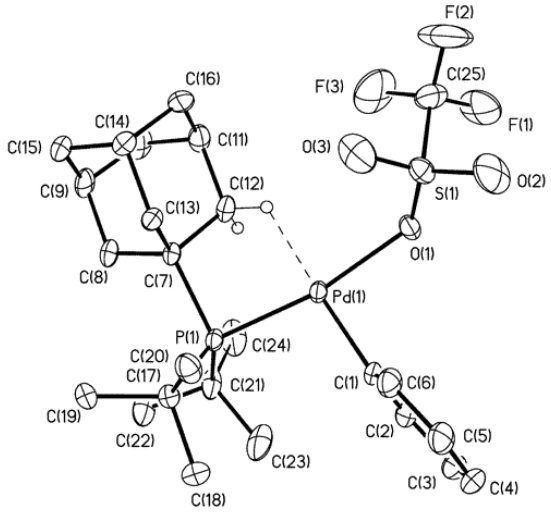

Figure 27. Ortep diagram of three coordinate Pd(Ph)(Br)(P(^{t}Bu)$_2$Ad).[152]

Thus an idea of the factors involved in reductive elimination has come to light. Organometallic complexes containing ancillary ligands both sterically cumbersome and electron-withdrawing in nature will favour reductive elimination; due to forcing the two reacting groups together, favouring formation of three coordinate over four coordinate complexes, and removing electron density from the metal centre, the latter two of which lower the energy of the vacant orbitals on the metal.

3.3 An introduction to computational chemistry

Computational chemistry uses the mathematical results of quantum mechanics incorporated into powerful computer programs to calculate the structures and properties of molecules and solids, which can then be applied to real world problems. The programs used are based on many different quantum chemical methods that solve the molecular Schrödinger equation (1). In quantum mechanics the Schrödinger equation describes the quantum state of a physical system, dependent or independent of time.

(1) $\hat{\mathrm{H}}\Psi = E\Psi$

Here E is the electronic energy, Ψ the wavefunction and $\hat{\mathrm{H}}$ the Hamiltonian energy operator, given by

(2) $\hat{\mathrm{H}} = E_{\mathrm{T}} + E_{\mathrm{V}} + E_{\mathrm{U}}$

E_{T} is the kinetic energy, E_{V} the nuclear-electron attraction energy (incorporating $v(r_i)$ the extential potential acting on electron *i*, dependent on the nuclei of charges Z_α), and E_{U} the electron-electron repulsion energy.

(3) $E_{\mathrm{T}} = \sum_{\mathrm{i}}^{\mathrm{n}} \left(-\frac{1}{2}\nabla_{\mathrm{i}}^{2}\right)$

(4) $E_{\mathrm{V}} = \sum_{i}^{n} v(r_i)$

(5) $E_{\mathrm{U}} = \sum_{i<j}^{n} \frac{1}{r_{ij}}$

(6) $v(r_i) = -\sum_{\alpha} \frac{Z_\alpha}{r_{i\alpha}}$

However, the major difficulty with the solution of this equation and the calculation of properties of chemical systems containing many electrons is how to accurately incorporate the numerous electron-electron interactions, which statistical methods model insufficiently accurately. This is no new problem. Understanding the planetary motion of the celestial bodies had troubled and attracted the best mathematical physicists, e.g. Newton and Laplace, for centuries.

Rather than dealing with these electron-electron interactions individually, or removing them from equations altogether, an approximate interaction energy can be assumed. Therefore whilst it is clear that a given electron moves under the influence of the nucleus, it can also be justifiable to suppose that it moves under the average influence of all the other electrons. This greatly simplifies the problem. The explicit electron-electron interactions are replaced by a mean field, *v*, in which all the electrons move. The solutions to the new form of this equation yield a set of *n* electronic orbitals $\psi_{\mathrm{i}}(\mathrm{r})$. However, since the field *v* depends on the electronic orbitals $\psi_{\mathrm{i}}(\mathrm{r})$, a chicken or egg paradox has been created. This is solved by stipulating that the field *v* generated from the orbitals $\psi_{\mathrm{i}}(\mathrm{r})$ must also be able to generate those orbitals.

Thus we have arrived at the Self–Consistent Field (SCF) or Hartree method,[154] which can be used iteratively to provide more accurate solutions of *E*.

If a molecule has *n* electrons with coordinates r_i, the total energy is found by solving the Schrodinger equation, $\hat{\mathrm{H}}\Psi = E\Psi$, where the Hamiltonian is,

$$(7) \qquad \hat{\mathrm{H}} = \tfrac{1}{2}\sum_i^n \nabla_i^2 - \sum_i^n v(r_i) - \sum_i^n \sum_{j>i}^n \left(\frac{1}{|r_i - r_j|}\right)$$

with $v(r_i)$ the classical electrostatic potential due to the nuclei, which are assumed to be fixed on the basis of the Born-Oppenheimer approximation. The complicating factor is the third term, which couples the motion of the electrons. Assuming that each electron moves in an average field due to all the others, the problem can be simplified to one whose solution yields *n* one-electron orbitals $\psi_i(r)$ using a simplified Hamiltonian,

$$(8) \qquad \hat{\mathrm{H}} = \tfrac{1}{2}\sum_i^n \nabla_i^2 - \sum_i^n v(r_i) - \sum_i^n v_1(r_i)$$

One of the difficulties arising from this analysis is the determination of a reasonable value for the average field υ_1. Since the 1920s much effort has gone into describing such a potential; Hohenberg and Kohn[155] proved an extraordinary result in which the unique potential (given by the variational principle), could be obtained from a unique density (*vide infra)*. Firstly, the energy expression used in quantum chemistry will be discussed.

It is convenient to separate the total electronic energy *E* of a chemical system into its components,

$$(9) \qquad E = E_{\mathrm{T}} + E_{\mathrm{V}} + E_{\mathrm{J}} + E_{\mathrm{X}} + E_{\mathrm{C}}$$

From left to right we have E_{T}, the kinetic energy of the electrons, E_{V} the coulomb energy of the electrons due to the attraction from the nucleus, E_{J} the coulomb energy the electrons have if moving in an average field, and $E_{\mathrm{X}} + E_{\mathrm{C}}$ which contains all the corrections due to the assumptions made. E_{X} is known as the exchange energy and is the larger correction. It accounts for the non-independent motion of the electrons due to their spin, the consequent stabilisation and a correction for self repulsion (the latter

being only a true correction in Hartree Fock theory). E_C, the correlation energy, is by far smaller and accounts for the correlated motion of all electrons. Although much smaller than E_X, E_C can be of the order of a chemical bond strength, and is thus of obvious chemical importance.

3.3.1 Density functional theory (DFT)

DFT has in the recent past emerged as an important computational method to predict chemical properties accurately and to analyse and interpret these in convenient and simple chemical terms. Examples of its use include the rational design of palladium NHC catalysts,[95] study of the chemical bonding in transition metal carbene complexes, and oxidative addition and reductive elimination reactions.[156]

The origins of the DFT analysis date back to the 1920s with Hartree,[154] who in 1928 first introduced the idea of an SCF and proposed a model in which the i^{th} electron in an atom moved completely independently of the others in an orbital $\psi_i(r)$. Therefore, in this completely uncorrelated model, the coulumbic electron-electron repulsion was taken to be only an average value. As a result, the total kinetic energy was simply the sum of all the kinetic energies of the electrons. Then in 1930 Fock[157] showed that the Hartree wavefunction violated the Pauli Exclusion Principle because it was not antisymmetric. By antisymmetrising the wavefunction he was able to describe how electrons with the same spin avoided one another.

In 1964 Hohenberg and Kohn[155] proved that there existed a universal functional of charge density, $F[\rho(r)]$, such that the expression

$$E \equiv \int v(r)\rho(r)dr + F[\rho(r)] \qquad (10)$$

has at its minimum value the correct ground-state energy associated with a given potential $v(r)$. They did this by first beginning with a collection of an arbitrary number of electrons, enclosed in a large box and moving under the influence of an external potential $v(r)$ and a mutual coulombic repulsion. The Hamiltonian would thus have the form,

$$\hat{H} = E_T + E_V + E_U \qquad (11)$$

Since the density $\rho(r)$ is a function of the wavefunction Ψ, so are the kinetic (E_T) and interaction energy (E_U),

$$F[\rho(r)] \equiv (\Psi, (E_T + E_U)\Psi) \quad (12)$$

where $F[\rho]$ is a universal function, valid for any number of particles and any external potential. With its aid and for a given potential $\upsilon(r)$, the energy functional $E_\upsilon[\rho]$ can be defined as,

$$E_v[\rho] = \int v(r)\rho(r)dr + F[\rho] \quad (13)$$

And so for the correct charge density $\rho(r)$, the energy functional $E_\upsilon[\rho]$ equals the correct ground-state energy E as long as the admissible functions are restricted by the condition,

$$N[\rho] \equiv \int \rho(r)dr = N \quad (14)$$

With N = the number of electrons in the system. Therefore if $F[\rho]$ were a known and sufficiently simple functional of the charge density ρ(r), the problem of determining the ground-state energy and density for a given potential would be rather easy since it required the minimisation of a functional of the three-dimensional density. The major complexity of the many-electron problem would be associated with the determination of the universal function $F[\rho]$. It was Kohn and Sham[158] who in 1965 discovered the correct form of this function.

Separating from $F[\rho]$ the classical coulomb energy E_J (where E_T has now become the kinetic energy in a system of non-interacting electrons $E_{T\text{-non}}$) gives,

$$F[\rho] = E_J + G[\rho] \quad (15)$$

$$= \frac{1}{2}\int \left(\frac{\rho(r)\rho(r^1)}{|r-r^1|}\right) drdr^1 + G[\rho] \quad (16)$$

And so substituting into equation 13 the energy functional becomes

$$E_v[\rho] = \int v(r)\rho(r)dr + \frac{1}{2}\iint \left(\frac{\rho(r)\rho(r^1)}{|r-r^1|}\right) drdr^1 + G[\rho] \quad (17)$$

$$= E_V + E_J + G[\rho] \quad (18)$$

(19) $$= E_{\mathrm{V}} + E_{\mathrm{J}} + (E_{\mathrm{T-non}} + E_{\mathrm{XC}})$$

where E_{J} is the classic coulomb potential. $E_{\mathrm{T\text{-}non}}$ is the kinetic energy of a system of non-interacting electrons of density $\rho(\mathrm{r})$ and E_{XC} is the exchange and correlation energy of an interacting system with density $\rho(\mathrm{r})$. It contains everything that cannot be evaluated, such E_{T}–$E_{\mathrm{T\text{-}non}}$ and the electron-electron interaction not included in E_{J}. This expression is a minimum for the correct density functional $\rho(\mathrm{r})$.

An approximation for $G[\rho]$ can be proposed, which leads to a scheme analogous to Hartree's method but contains the major part of the effects of exchange and correlation. Firstly it can be stated that,

(20) $$G[\rho] \equiv E_{\mathrm{T-non}}[\rho] + E_{\mathrm{XC}}[\rho]$$

For a sufficiently slow varying ρ(r), it can be shown that

(21) $$E_{\mathrm{XC}}[\rho] = \int \rho(r)\varepsilon_{XC}(\rho(r))dr$$

With the exchange correlation potential being

(22) $$\mu_{XC}(\rho) = \frac{d(\rho\varepsilon_{XC}(\rho))}{d\rho}$$

And for simplicity a modified external potential υ_{eff} can be stated as,

(23) $$v_{eff} = v(r) + \left(\frac{\rho(r^1)}{|r-r^1|}\right)dr^1 + \frac{d(\rho\varepsilon_{XC}(\rho))}{d\rho}$$

(24) $$= \phi(\mathrm{r}) + \mu_{XC}(\rho)$$

with $\phi(r)$ and $\mu_{XC}(\rho)$ the exchange and correlation contribution to the chemical potential of the uniform gas of density, ρ. Therefore for a given exchange and correlation functional, where μ_{XC} is the exchange-correlation potential, the correct charge density $\rho(r)$ which satisfies these equations is obtained by solving the series of one-particle Schrodinger-like equations,

(25) $$\left\{-\frac{1}{2}\nabla^2 + [\phi(r) + \mu_{\mathrm{XC}}(\rho(\mathrm{r}))]\right\}\psi_i(r) = \varepsilon_i\psi_i(r)$$

therefore

(26) $$\left\{-\frac{1}{2}\nabla^2 + v_{eff}\right\}\psi_i = \varepsilon_i\psi_i(r)$$

with

(27) $$\rho(r) = \sum_{i=1}^{N}|\psi_i(r)|^2$$

where *N* is the number of electrons. As in the Hartree Fock (HF) scheme, the Kohn Sham (KS) equations are a pseudo-eigenvalue problem and equations 23 and 26 have to be solved iteratively through an SCF procedure. Beginning with an estimated set of one-electron orbitals ψ_i, a charge density ρ(r) can be constructed from equation 27. This is then used to find the Kohn-Sham effective potential υ_{eff} and a new charge density ρ(r) is then calculated. Once a self-consistent charge density ρ(r) is established, the total energy can then be computed from,

$$E = \sum_{1}^{N}\varepsilon_i - \frac{1}{2}\iint\left(\frac{\rho(r)\rho(r^1)}{|r-r^1|}\right)drdr^1 + \int\rho(r)\left[\varepsilon_{XC}\left(\rho(r)\right) - \mu_{XC}(\rho(r))\right]dr$$

Or from equation 19,

$$E_\upsilon = E_{\mathrm{V}} + E_{\mathrm{J}} + (E_{\mathrm{T-non}} + E_{\mathrm{XC}})$$

Still, it should be kept in mind that the Kohn Sham orbitals have no physical significance other than in allowing one to construct the charge density.

Thus all density functional theory is based upon two powerful theorems proposed by Hohenberg and Kohn. First, the ground state charge density *(ρ)* is sufficient to describe all of the ground state properties of a system. Second, for any trial density, the energy is always greater than the true value, (known as the variational theorem). However, they left two unanswered questions, what was the form of $F[\rho]$ and how exactly could the charge density ρ(r) be determined? The answers came courtesy of the derivation of Kohn and Sham. This one-electron orbital treatment is rigorously correct and, provided that the correct exchange-correlation potential E_{XC} is used, the exact charge distribution ρ(r) any electronic system of interest can be determined exactly. However, this is the drawback in DFT. No one knows the precise form of the correct functional E_{XC} for atoms and molecules. Instead, approximations have to

be made to provide an expression for E_{XC} and depending on the system of interest, many are now available today.

3.3.2 The form of Exchange-Correlation energy E_{XC}

The reason for the problem of not knowing the exact explicit form of E_{XC} can be traced back to the non-homogeneity of the charge density in molecular systems. Neglecting this altogether gives one of the simplest forms of the functional which assumes that the charge density is constant or very slowly changing. Being only a local function of the charge density, $E_X[\rho]$, it is therefore known as a Local Density functional Approximation (LDA).

The LDA, however, does not take into consideration systems in an external magnetic field. To include these allows for the incorporation of additional physics into the equations and is in turn known as the Local Spin Density Approximations (LSDA). Further corrections over the years have enhanced the accuracy of these E_{XC} functionals. One particularly important correction was the addition of a gradient correction for the non-uniformity of the atomic and molecular densities, known as a Generalised-Gradient Approximation (GGA). Although many generalisations of the LDA were proposed, this was the first really practical one. In this method, $E_{XC}[\rho]$ and so $E_{XC}[\rho^{\alpha}, \rho^{\beta}]$ were evaluated not only from the local value of the electron density but also from the gradient of electron density at position r. This allowed not only an improvement of the E_X but also E_C. The recommended nonempirical GGA of Perdew, Burke and Ernzerhof (PBE)[159,160] will be the E_{XC} of choice employed in this study.

3.3.3 The Amsterdam density functional code

The DFT computational package used in this investigation is the Amsterdam Density Functional Package (ADF).[161] This is a particularly popular programme in the research areas of homogeneous and non-homogeneous catalysis, inorganic chemistry and heavy element chemistry. It has been used to deal with molecules on surfaces, in solvents and in protein environments, as well as periodic systems.

ADF works by a fragment oriented approach, with the poly-atomic system to be computed conceptually built up from fragments.[161] For a calculation, the volume around an atomic fragment, the atomic cell, is thus divided into different regions depending on the character of the region and these are then evaluated accordingly.

3.3.4 Basis sets

Atomic orbitals are mathematical functions which describe the behaviour of the electron density of the different orbitals. They consist of functions, a basis set, which combine to give an accurate representation of the way electrons behave in space. ADF takes advantage of Slater type functions (STOs) as basis functions, as these resemble the true atomic orbitals more closely than certain other basis functions (Gaussian Type Orbitals, GTOs). Although computationally expensive compared to GTOs, STOs are used to construct the total wavefunction of the molecule.

3.3.5 Relativistic effects

From calculations it is clear that the heavier the nucleus, Z, the larger the relativistic correction to the wavefunction, ψ. This is due to two effects. First, orbitals close to the nucleus (mainly s-orbitals) contract. Second, as the electron density close to the nucleus increases, more of the nuclear charge is shielded from the outer electrons, meaning that the effective charge experienced by these electrons is smaller. The d and f electrons are less attracted to the nucleus and the orbitals thus expand. Due to the fact that palladium is a relatively heavy transition metal, relativistic effects need to be included. Fortunately this is easy with ADF, which incorporates relativistic effects by a quasi-relativistic method based on the Zero-Order Regular Approximation (ZORA) to give accurate results. The calculation employed is very similar in structure to the non-relativistic one, having only a few additional terms in the Hamiltonian.[162]

3.3.6 Solvent effects

The computational description of molecules in a vacuum or in the gas phase has progressed remarkably over the past fifty years.[163] It has now reached a state which allows the calculation of the most interesting features of isolated systems or small

clusters by more or less sophisticated molecular orbital calculations. However, many biological and catalytic processes occur in solution where the chemical properties and processes are often very different from the gas phase. Due to the enormous importance of obtaining such information much effort has gone into the creation of solvent models able to carry out such tasks.

Chemistry in solution can be studied in ADF[164] *via* the Conductor like Screening Model (COSMO) of salvation.[163,165,166] The COSMO is a dielectric model in which the solute molecule is embedded in a molecule-shaped cavity surrounded by a dielectric medium with given dielectric constant ε.

3.3.7 Catalytic cycles

An investigation of the energies of active intermediates involved in a catalytic cycle is very desirable. It allows the calculation of enthalpy, entropy and free energy, which can then be used to determine the likelihood of a reaction taking place. ADF can be employed to help produce a catalytic cycle of the major steps involved the alkyl amination reaction and in particular the reductive elimination step. The key question is how we go about obtaining such information and a literature study of such catalytic cycles offers valuable insight.

A recent DFT report by Green described a study in which the key intermediates in the oxidative addition of aryl chlorides to palladium NHC complexes and the subsequent reductive elimination reaction was modelled.[119] Reaction energetics were calculated for various levels, zero point energy corrections were used to estimate the internal energy change at 0 K and frequency calculations used to obtain these zero point energies. Solvent corrections were then made to give an accurate Gibbs free energy. The major problem encountered was that the entropy term referred to that obtained in the gas phase and as a result did not take into account molecular tumbling in solution. This entropy term is usually found to consist of 30-60 % translational and rotational contributions, which would be reduced in solution due to the effect of solvent-solute interactions. This meant that depending on whether the reaction was by an associative or dissociative mechanism, the free energies would be either an overestimation or underestimation respectively. Similar problems were encountered

by Zhu and Ziegler whilst using DFT calculations to study the influence of different ligands on the rate and mechanism of methane activation by $PtCl_2X_2$.[167] They reported all free energies neglecting the electronic entropy energy term. Instead standard expressions were used to calculate the remaining gas-phase enthalpic and entropic contributions at non zero temperature, including the zero-point vibrational contribution.

TS structures are characterised using vibrational frequency analysis which should show one imaginary frequency corresponding to the mode of decomposition to the adjacent true minima (reactants and products). The creation of displacement structures along the reaction coordinate by adding +/- 5% to the TS geometry should then lead back to the starting material or forward to the product.

Therefore in the preparation of a theoretical catalytic cycle, a number of key steps are required. The structures of reactants, intermediates, transition states, and products all need to be fully optimised in the gas phase. Frequency calculations are then performed on all optimised structures to characterise the stationary points as minima or transition states, as well as for the calculation of gas phase Gibbs energies at 298.15 K. For all optimised structures, the Gibbs energies of solvation would then be computed in solvent (THF in the present study) at the gas-phase optimised geometries. The zero-point energy and internal energy corrections would then be added to the gas-phase energy to obtain the overall free energy, including entropic effects.

3.4 Mass spectrometry

Mass spectrometry (MS) is a scientific technique used to measure the mass of ions. As a tool it allows for the potential interception and characterisation of key intermediates, either as transient species or as protonated/deprotonated forms of neutral species. The process by which the mass spectrometer works begins with the ionisation of the molecule of interest. These ions are then accelerated to a beam of constant speed, and in the case of ESI and API (section 3.4.1), passed through a quadrupole mass analyser, which filters the ions according to their mass to charge ratio (m/z). Only ions of a certain m/z reach the detector for a given ratio of voltages:

other ions would have unstable trajectories and collide with the walls of the instrument. This process permits selection of an ion with a particular m/z and also allows the scanning of a range of m/z values by continuously varying the applied voltage.

3.4.1 Atmospheric pressure ionisation and electrospray ionisation

Two powerful and hence widely used ionisation methods are Atmospheric Pressure Ionisation (API) and Electrospray Ionisation (ESI), both of which enable the investigation of solutions by mass spectrometry. In principle, they allow the potential detection and study of reaction substrates and products and short-lived reaction intermediates.[87]

ESI protocol works by passing a solution of the analyte through a capillary held at high potential. The high voltage generates a cloud of highly charged droplets which passes through a potential and pressure gradient toward the analyser portion of the mass spectrometer. As the ions travel, the solvent evaporates which reduces the size of the droplets. This leads to an increasing charge-density on the shrinking solvent evaporate which then causes the droplets to subdivide. Eventually the ions become completely desolvated,[168,169] and it is these ions which are observed by the mass spectrometer. API, on the other hand, works by a different mechanism. Chemical ionisation of the solution takes place at atmospheric rather than high pressure, and is thus a soft process, inducing little or no fragmentation of the analyte. Rather than employing high voltages as in ESI, no voltages are applied in the spray formation in API and hence the neutral molecules are carried to the gas phase by a thermic process. Desolvation is achieved by heating the solution within the API assembly, normally maintained between 150 and 550 ^{o}C. Finally a corona discharge needle with an applied voltage between 300 and 5000 V then provides electrons that ionise the gaseous analyte *via* a series of gas phase ion/molecule reactions at atmospheric pressure.

The intensity of the detected gas-phase ions and the corresponding concentrations of these ions in the ESI and API are related. In cases where the solution contains compounds able to react with these ions, the intensities could change significantly

and much more complex relationships could prevail. Therefore there is a requirement to prove unambiguously that the species detected by ESI are those predominating in solution and more importantly, to confirm that they are indeed intermediates in the reaction path.[87] However, in practice this is not possible to do. MS is a violent technique, employing harsh conditions not experienced by molecules in solution. Care needs to be taken when proposing a structure for any species observed by MS; taking into account the fact that the species could have been formed as a result of the harsh conditions employed and not a result of any catalytic or reaction pathway.

Research groups using MS as a tool for monitoring reactions additionally employ MS/MS as a method to tentatively propose a possible structure for any species observed. In MS/MS ions of specific molecular weight are first filtered and then bombarded with Argon zero, a gas of high energy and purity, in order to induce collisions with the ions and cause them to fragment. The resulting fragmentation pattern can then be used to help determine, with higher accuracy than ESI alone, a potential structure for the species observed.

3.4.2 Offline and online screening

Currently there are two general methods to study reaction mechanisms: (1) Offline Screening and (2) Online Screening. In the offline screening method the reagents are mixed to produce the different intermediates and the solution composition is then determined over time as the reagents are progressively turned into products. This is accomplished by direct MS screening of the reaction mixtures during predefined intervals and then characterising the ions observed by MS/MS. This is only achievable if there is a reasonable concentration of intermediates in solution and if these species are not degraded within a few minutes. It is key that the time resolution matches the rate of the process to yield the desired information. Otherwise an inherent limitation is approached: it may not be possible to analyse the transient species due to their short lifetime in solution. The second method, although not available in this study, is Online Screening. Here the kinetic and mechanistic information for the reactants in solution is studied by coupling a reactor containing the reagents directly to the ion source. This allows screening of the reaction in real-

time and the trapping of any transient species, and is thus superior to the offline method.

3.4.3 Examples of MS use in monitoring reactions

There are many literature examples of the use of API and ESI online and offline methods as their many benefits have come to light.[170,171] Non-palladium containing reactions such as the Baylis-Hillman reaction, ring contractions, nucleophilic substitutions and α-methylenolation of keto esters, have all been studied extensively.[87] Those examples which study palladium chemistry or organometallics have all been published in the last eight or so years. One such study by Santos *et al*. looked at the active intermediates and reaction pathway of the Stille reaction.[172] They used online ESI(+)-MS(/MS) monitoring to intercept and characterise the catalytically active species $Pd^0(PPh_3)_2$, including the potential oxidative addition **136**, transmetallation **137** and reductive elimination products **138** (scheme 56).

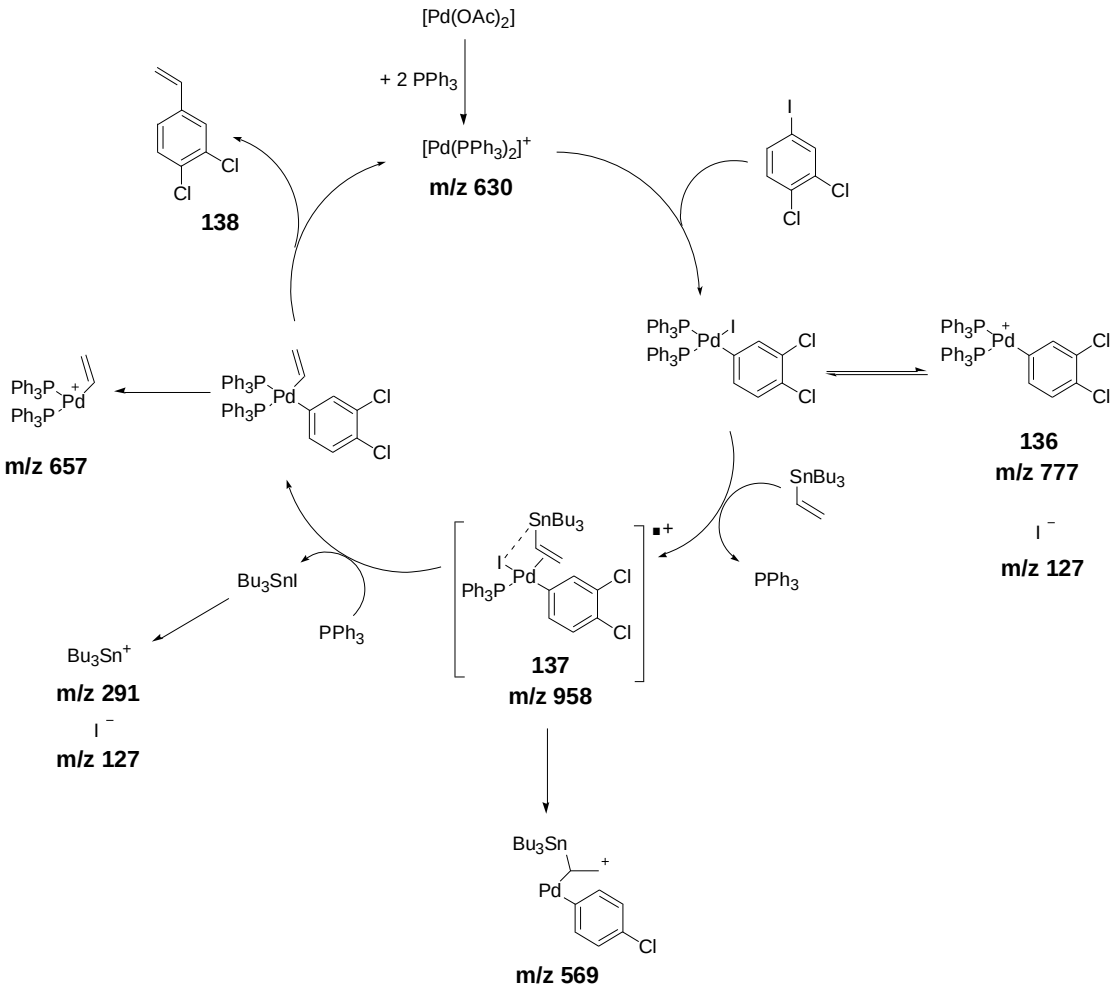

Scheme 56. Study of ESI-MS in the Stille reaction.

Using similar methods Santos *et al.* were further able to investigate the catalytic cycle proposed for the alkynylation of tellurides mediated by a $PdCl_2$ catalyst.[173] They were able to conclude from their study that the coupling of vinyl tellurides with alkynes *via* $PdCl_2$ greatly depended on the amount of Pd catalyst used and, more interestingly, on the presence of $CuCl_2$, which was used to reconvert Pd^0 back into Pd^{II}.

Eberlin and co-workers took the idea of using ESI-MS tandem mass spectrometry to study the Heck arylation using arenediazonium salts:[174] proposing the cationic intermediates **139**, **140**, **141** and **142** for the catalytic cycle (scheme 57). From these results a detailed catalytic cycle for the Heck reaction was proposed.

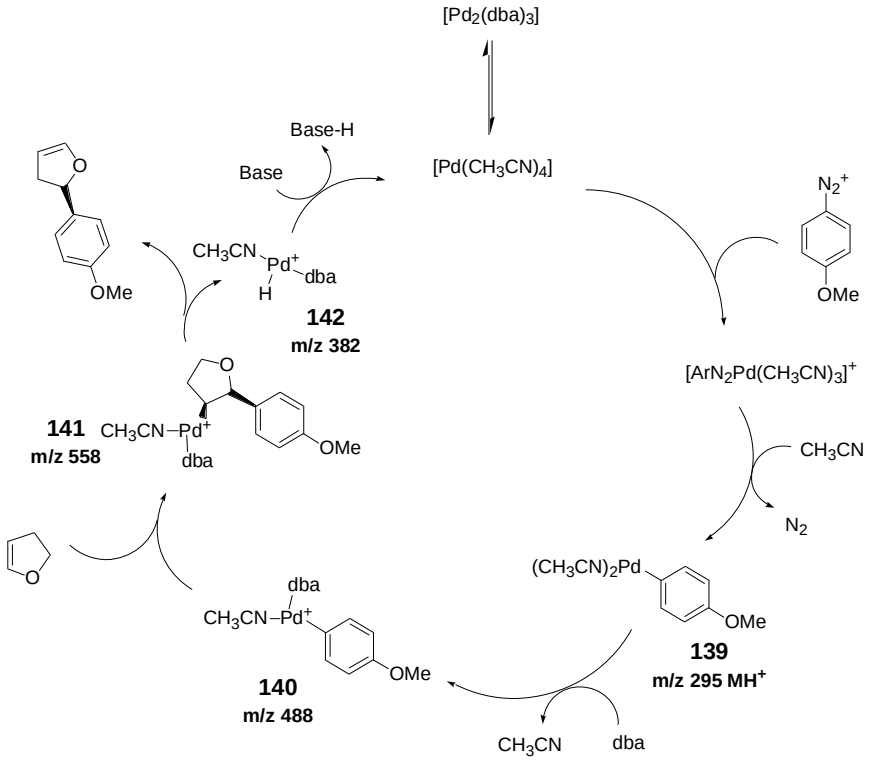

Scheme 57. Use of ESI-MS in the Heck reaction.

Aliprantis and Canary studied the Suzuki coupling of pyridyl halides with phenylboronic acids using offline ESI-MS techniques[175] and Markent and Pfaltz applied the Online principles for the parallel screening of the Pd-catalysed enantioselective allylation reaction of diethyl ethyl malonate with allylic esters, to further illustrate the scope of this method.[176]

The ability to isolate ionic species directly from crude reaction mixtures is an interesting feature of API-MS and ESI-MS. These new applications in the mechanistic chemistry of transient species undoubtedly appear an important tool in the future study of labile and sensitive intermediates in solution, especially since there is no need for the previous purifications, or isolation for further characterisation of active species, intermediates of reactions and products. However, the assumption is made that the species observed by MS are the same as those present in solution, which in reality can not be guaranteed.

Despite the literature precedent above, no MS studies have been carried out using Pd in conjunction with NHC ligands to the best of our knowledge. Thus not only would this work be useful in proposing the intermediates present in the Pd-catalysed alkyl

amination reaction but would also be the first ESI(+)-MS offline study employing the use of Pd bound NHCs. The presence of six naturally occurring Pd isotopes means that a very distinct and easily identifiable isotopic pattern would be available to ‘fish’ for ions of interest. The additional incorporation of an ionisable MS tag, such as a tertiary amine, to either of the reagents would allow further ease of identification.

4 An investigation of the potential energy surfaces available to Pd(L)(alkyl)(morpholide)

4.1 Studies on the reductive elimination of neopentyl morpholine from Pd(IBu)(neopentyl)(morpholide) complex

As noted in the introduction, previous attempts to deprotonate Pd(IBu)(neopentyl)(morpholine)(Cl) **130** (figure 28) had been unsuccessful.[131,132] One possible explanation is that the combined effects of the electron donating character of the alkyl substituent and the strong σ-donation of IBu increases the electron density at the metal centre, hence weakening the interaction with the amine lone pair. Assuming the proton abstraction is rate limiting, the pKa of the amino-proton would therefore increase making reductive elimination less likely to occur**.**

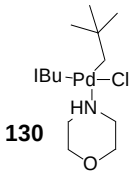

130

Figure 28. Pd(IBu)(neopentyl)(morpholine)(Cl) **130**.

4.1.1 Replacement of morpholine with lithium morpholide

Although the addition of base to **130** does not result in reductive elimination, a colour change from dark green to bright red was observed by Caddick and Cloke.[177] As this colour change occurred on addition of base, two possibilities arise; either the base does deprotonate the amine but reductive elimination doesn't take place; or the base itself binds to the Pd, both of which change the electronics of the Pd centre and hence the colour of the solution. To test both hypotheses, morpholine was replaced with lithium morpholide. Removal of the proton to give the pre-formed amide would overcome the problem of the deprotonation step and, upon addition of lithium morpholide to Pd(IBu)(neopentyl)(chloride) dimer **143**, synthesised using the method of Esposito,[132] would give direct access to tricoordinate Pd(IBu)(neopentyl)(morpholide) complex **144** which should be capable of reductive elimination (scheme 58). Alternatively if the base does indeed bind to the Pd centre,

then the addition of lithium morpholide to Pd(IBu)(neopentyl)(chloride) dimer **143**, would eliminate this problem because the addition of base (lithium morpholide in this case) would still give Pd(IBu)(neopentyl)(morpholide) **144**, the complex required for reductive elimination.

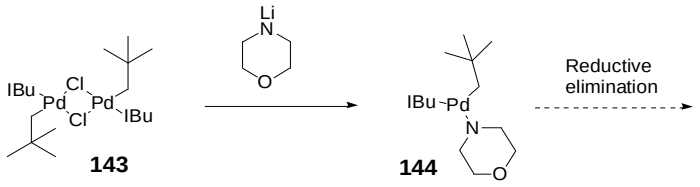

Scheme 58. Addition of lithium morpholide to Pd(IBu)(neopentyl)(chloride) dimer.

Interestingly, the addition of lithium morpholide to Pd(IBu)(neopentyl)(chloride) dimer **143** did result in a colour change from green to bright red, which was the same result as that obtained for the addition of base to Pd(IBu)(neopentyl)(morpholine)(Cl) **130**. Therefore if either hypotheses hold for the outcome of adding base to Pd(IBu)(neopentyl)(morpholine)(Cl) **130** (page 90), then these should also apply to the reaction of lithium morpholide and Pd(IBu)(neopentyl)(chloride) dimer **143**; either deprotonation can take place without leading to reductive elimination, or the base can bind to the Pd centre. In both cases this will lead to the formation of Pd(IBu)(neopentyl)(morpholide) **144**. However, reductive elimination was still found not to take place, either at room temperature or elevated temperature (60 °C, 90 °C, 120 °C). Instead $Pd(IBu)_2$ and morpholine was observed, followed by decomposition, after 2 h.

Upon addition of lithium morpholide to Pd(IBu)(neopentyl)(chloride) dimer **143** (figure 29), it was observed by ^{1}H NMR that the resultant reaction mixture contained more than one species (>1 NHC backbone and *tert*-butyl environment) (figure 30). However, the morpholide signal had split from two signals into four, possibly due to the morpholide protons residing in four different environments, indicative of binding to the Pd centre.[132] A comparison of figures 29 and 30 also finds that the NHC backbone has shifted 0.4 ppm upfield, the CH_2 of neopentyl 0.1 ppm upfield, whilst all *tert*-butyl groups have stayed approximately the same. This suggests the species present in figure 30 is different from that in figure 29.

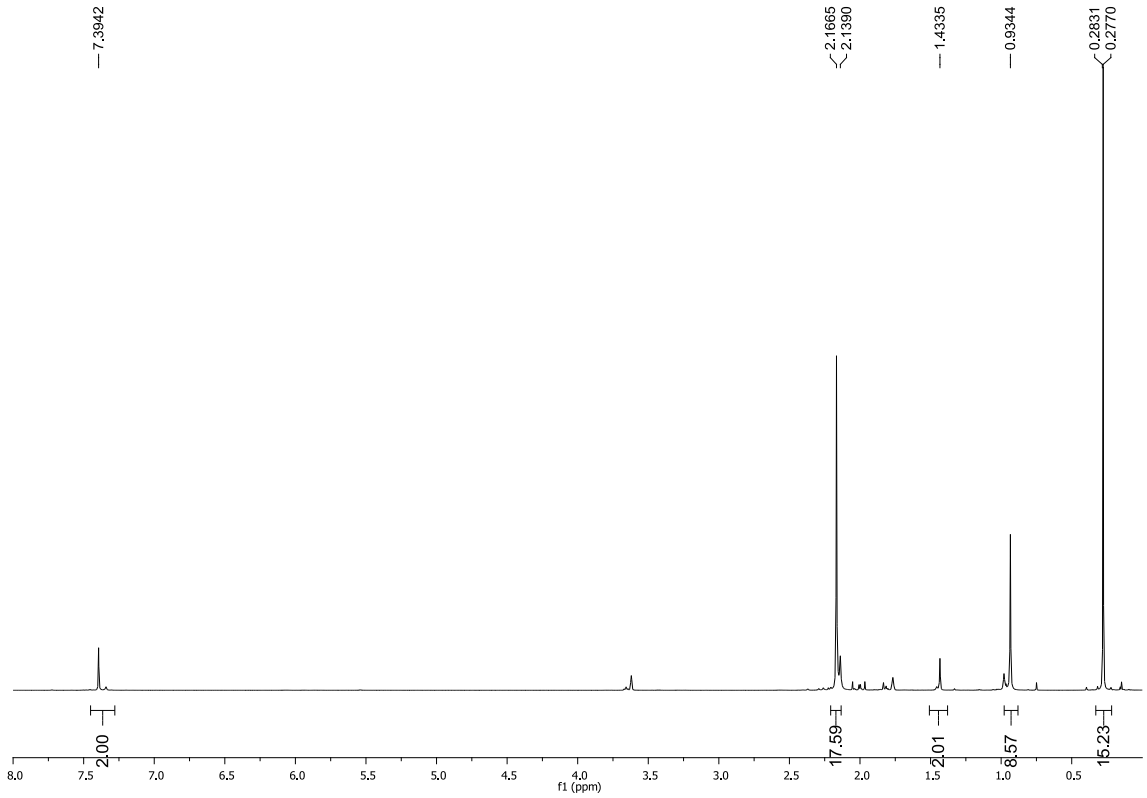

Figure 29. ^{1}H NMR of **143** in THF-d8.

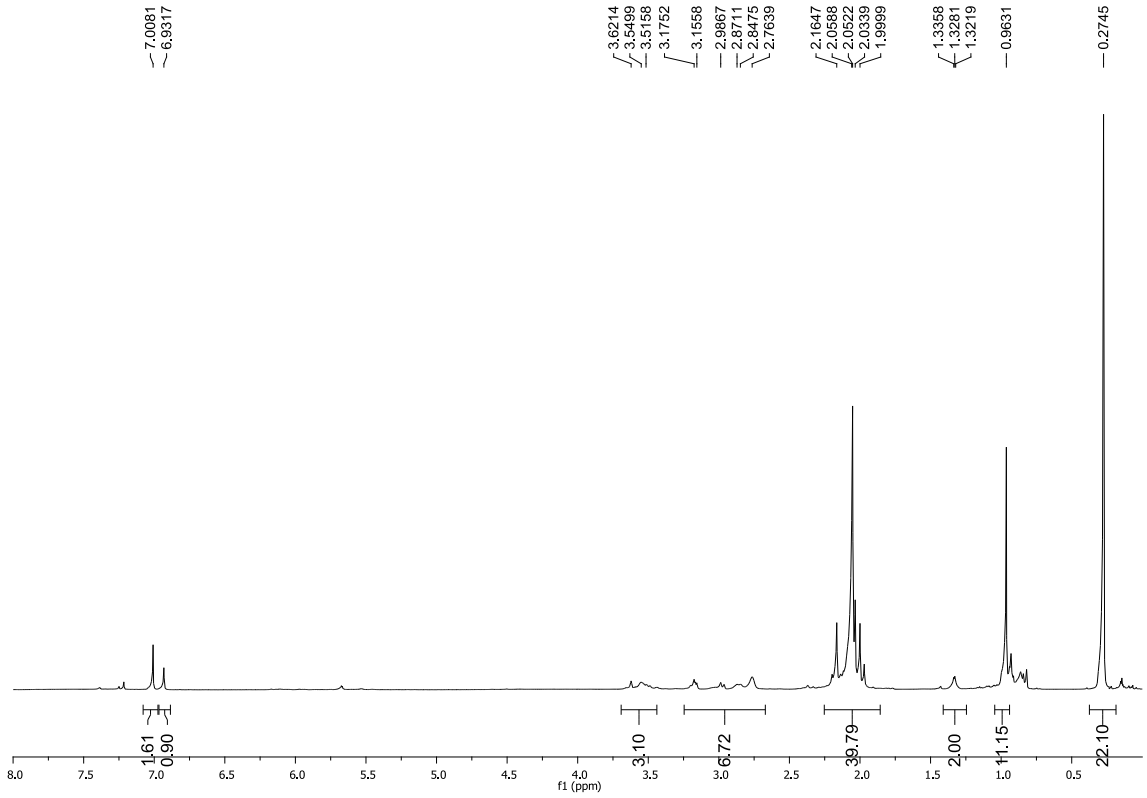

Figure 30. ^{1}H NMR of **144** in THF-d8 (THF-d8 solvent peaks at 3.62 and 1.90 ppm, $Si(Si(CH_3)_3)_4$ at 0.27 ppm).

It cannot be ruled out that the morpholide was not bound to two different species. A possible structure for these different species could be the *cis* and *trans* isomers of the three-coordinate Pd(IBu)(neopentyl)(morpholide) complex **144**, or the four coordinate Pd(IBu)$_2$(neopentyl)(morpholide) complex **145** (figure 31). If this were the case, all species could potentially give reductive elimination, upon *cis*-rearrangement and dissociation respectively.

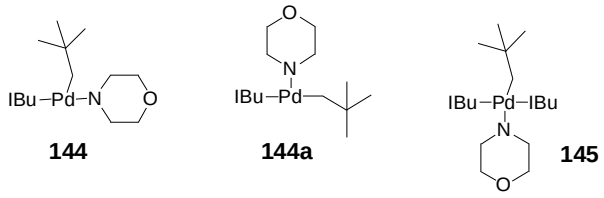

Figure 31. *cis* and *trans* isomers of **144** and four-coordinate Pd(IBu)$_2$(neopentyl)(morpholide) **145**.

Proposed complex **144** was found to decompose within 10 minutes at a temperature of 60 °C and above. However, below this temperature (21 °C and 40 °C) decomposition was found to occur after 2 h, meaning complex **144** was not a transient species but in fact present in significant concentration. This implies **144** is indeed stable towards reductive elimination. Whereas heating these three coordinate Pd complexes has been shown to induce reductive elimination,[153] this was found not to be the case. In order to promote reductive elimination, attention was focused on the ancillary ligand bound to the Pd.

4.1.2 Replacement of IBu with a range of ancillary ligand

IBu was replaced with a range of different ligands; PPh_3, DMPM (1,1-bis(dimethylphosphino)methane), $PCyp_3$ (tricyclopentylphosphine), PCy_3 (tricyclohexylphosphine), DPPM (1,1-bis(diphenylphosphino)methane), DPPP (1,3-bis(diphenylphosphino)propane), P^{t}BuMe$_2$ and IPr, in order to determine the effect it would have on the reaction. Previous work by Caddick and Cloke has found that, contrary to theory, the addition of an excess of ancillary ligand could help to drive the desired reductive elimination. For instance, the formation of neopentyl chloride and Pd(IBu)$_2$ from Pd(COD)(neopentyl)Cl and two equivalents of IBu has been reported (scheme 59).[132] This result is most certainly due to sterics, as two strongly σ-donating ligands would presumably raise the energy of the vacant orbital on the Pd

to too high a level for reductive elimination to take place. However, the two hindered IBu ligands would also force the neopentyl and chloride groups into very close proximity, forcing a reaction to take place.

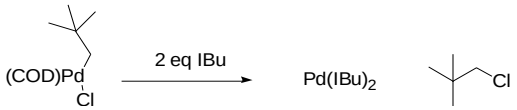

Scheme 59. Formation of neopentyl chloride with $Pd(IBu)_2$.[132]

Therefore to the reaction mixture obtained from the addition of lithium morpholide to Pd(IBu)(neopentyl)(chloride) dimer **143**, presuming to contain Pd(IBu)(neopentyl)(morpholide) **144**, was added one, two and four equivalents of alternative ancillary ligand. Whereas one equivalent would be expected to decrease electron density on the Pd centre (upon exchange with IBu, phosphine would remove electron density from the Pd *via* backbonding), two and four equivalents would be expected to impart more electron density onto the Pd centre. However, as shown by Caddick and Cloke,[132] the use of excess ancillary ligand could force the neopentyl and morpholide groups into closer proximity to react.

Upon addition of one, two and four equivalents of ancillary ligand to proposed species Pd(IBu)(neopentyl)(morpholide) **144,** the desired reductive elimination reaction was still not observed. Rather, a complex reaction mixture resulted, along with the formation of free morpholine and $Pd(IBu)_2$. Additionally in the case of PPh_3 and DPPP, crystals of $Pd(PPh_3)_4$ and $Pd(DPPP)_2$ were isolated.

In order to gain a greater understanding of the factors important for the reductive elimination of neopentyl morpholine from Pd(IBu)(neopentyl)(morpholide) **144**, and to investigate whether possible alternative reaction pathways existed, a DFT investigation was carried out. The aim of this investigation was to develop a series of potential energy surfaces for the possible reaction pathways available to **144**, which would allow the identification of key determinants for reductive elimination, as well as any other potential reaction pathway, and the selectivity issues involved.

4.2 A DFT investigation of the Pd catalysed reductive elimination of neopentyl morpholine from Pd(IBu)(neopentyl)(morpholide)

4.2.1 Geometry optimisation and analytical frequency calculations

In order to develop a potential energy surface for the reductive elimination of neopentyl morpholine from Pd(IBu)(neopentyl)(morpholide) **144**, the ground state energy of each proposed intermediate in the reductive elimination pathway was required, along with the energy of the transition state for reductive elimination. To find these energies, the geometries of all intermediates were first optimised to give the minimum energy ground state and transition state structures. Two types of ADF calculation enabled this to happen; a ground state energy geometry optimisation calculation optimised (corresponding to n_0 is figure 32) and a transition state geometry optimisation calculation (corresponding to the saddle point in figure 32).

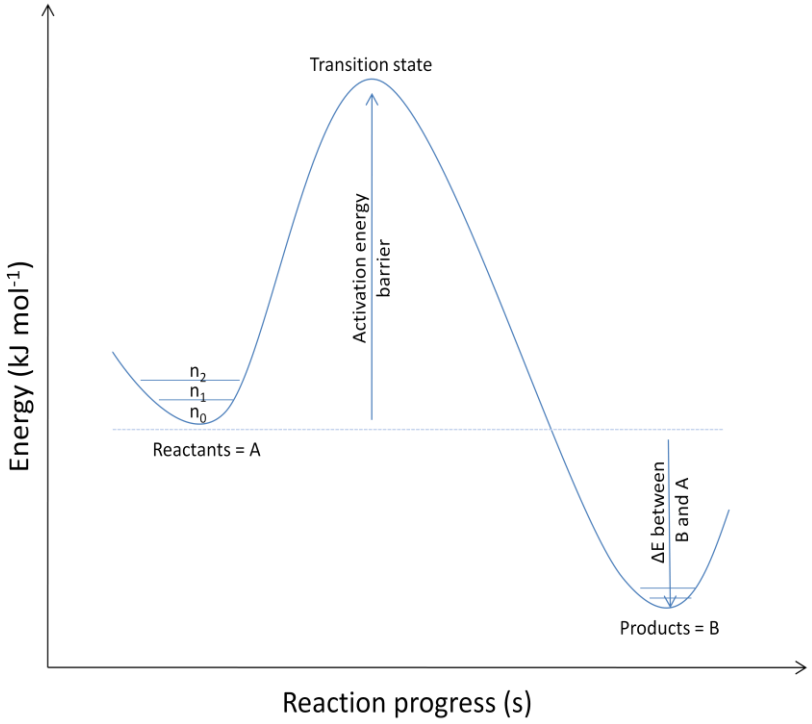

Figure 32. General reaction pathway for the conversion of reactants into products.

Strictly speaking, true ground state energies have all positive eigenvalues in the Hessian (the matrix of second derivatives of the total energy with respect to displacement of the nuclei) and hence all real vibrational frequencies. Transition

states, on the other hand, have a single negative eigenvalue in the Hessian, giving a single imaginary vibrational mode (associated with motion through the TS).

If a ground state geometry optimisation calculation was carried out on an intermediate with a geometry corresponding to the transition state, the geometry would try to rearrange to give the lowest energy structure (with only positive eigenvalues), corresponding to the structure of the starting material or the product (figure 33).

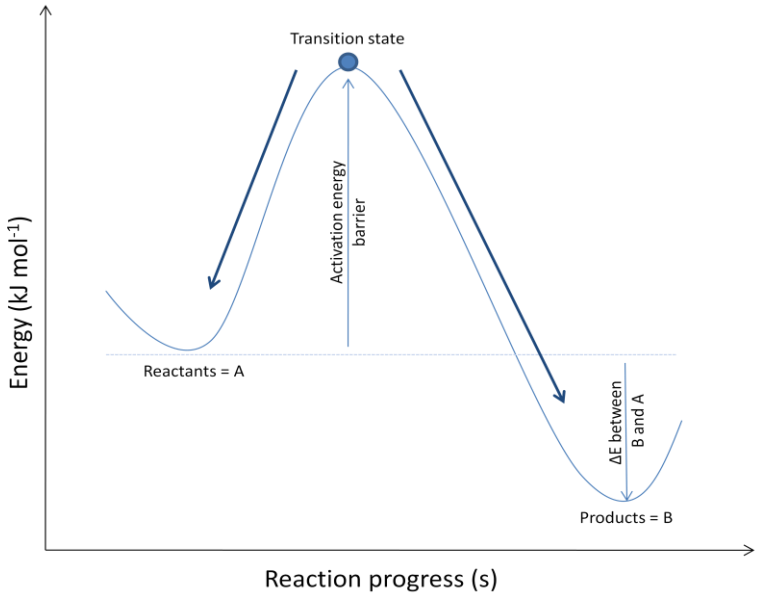

Figure 33. Geometry optimisation calculation carried out on a transition state structure.

If a transition state geometry optimisation calculation was carried out on an intermediate whose structure was that of the starting material or product, the transition state geometry would not be able to optimise; the energy of the intermediate would be at the bottom of the well (corresponding to only positive eigenvalues) and any rearrangement of the structure would be too small to reach the transition state structure (with a single negative eigenvalue in the Hessian) (figure 34). However, if the transition state geometry optimisation calculation was carried out on an intermediate whose energy corresponded to the saddle point in figure 34, the geometry would be able to converge to give a stable transition state structure (with a single negative eigenvalue in the Hessian).

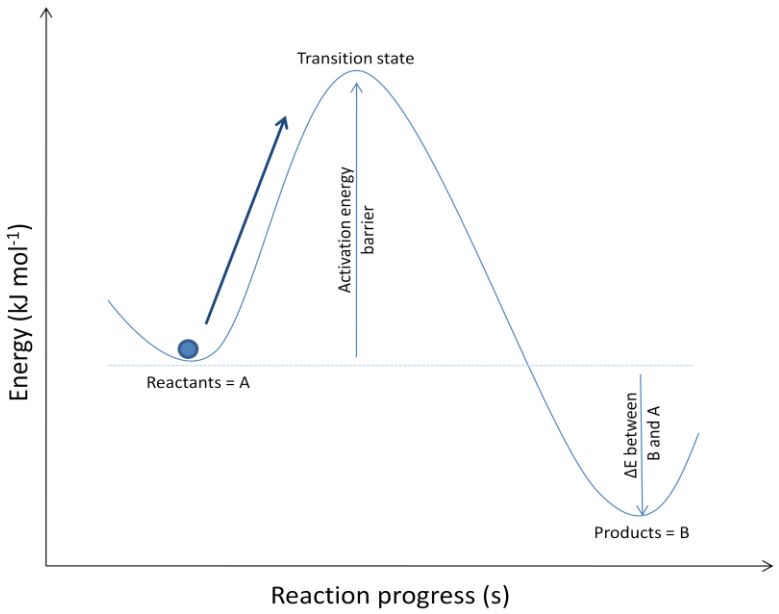

Figure 34. Transition state optimisation calculation carried out on a ground state energy structure.

4.2.1.1 Procedure for the development of potential energy surfaces

A comparison of the optimised geometries of Pd(IBu)(neopentyl)(morpholine)(Cl) **130** and $Pd(IBu)_2$ with that obtained experimentally[119,132] found that all bond lengths involving the Pd atom deviated by no more than 0.05 Å from their experimental values. With this information in hand, it was presumed that the geometry optimisations of the other intermediates would also be accurate to this degree.

Having optimised the geometry of all intermediates to obtain the minimum energy structures, n_0, an analytical frequency calculation was then carried out on these structures to obtain the zero-point energy correction for the ground state energy (zpe = n_1-n_0), as well as the enthalpic and entropic contributions to the energy. This was repeated using the cosmo solvent model, with THF chosen as the solvent, to give the minimum energies in solvent. However, analytical frequency calculations could not be carried out using the cosmo model for the transition state structure. Instead, the zero point energy, enthalpic and entropic corrections were taken from the gas phase optimised transition state structure, and applied to the solvent optimised transition state structure. Whilst not ideal, the fact that the geometries, energies and corrections for other intermediates were found to vary little, suggested that this would not affect the overall trend to changes in energy.

4.2.2 Reductive elimination of neopentyl morpholine from Pd(IBu)(neopentyl)(morpholine)

The study began with the attempted geometry optimisation of both *cis* and *trans* isomers of Pd(IBu)(neopentyl)(morpholine) **144** and **144a** (section 4.1.1, scheme 31), the species from which reductive elimination takes place.[119,130] However, it was found that both structures converged to the same geometry **144**, with IBu *trans* to the morpholide, a result of the greater *trans* influence of the strongly σ-donating neopentyl group. This species was found to have a distorted T-shaped geometry, due to the steric bulk of the neopentyl group (figure 35).

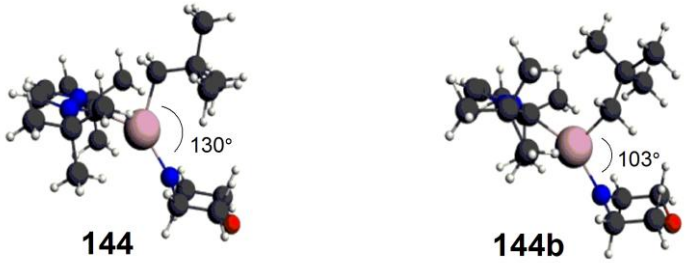

Figure 35. Geometry of Pd(IBu)(neopentyl)(morpholine) **144**.

The proposed steps involved in the reductive elimination of neopentyl morpholine are examined in scheme 60. It can be seen that elimination would first require rotation of the neopentyl group through ~ 90^{o} around the Pd–C bond to form **144b**, a rotamer of **144** with a (neopentyl)Pd(morpholide) bond angle of 103° (figure 35), formed at a cost of 8.1 kJ mol^{-1}. Further movement of the neopentyl group towards the morpholide would then lead to a reduction in the neopentyl-Pd-morpholide bond angle, and hence to transition state **TS-145**, 131.0 kJ mol^{-1} higher in energy than **144**. The neopentyl group can then pass to the nitrogen of the morpholide, to give Pd(0) complex **146**, 16.2 kJ mol^{-1} more stable than **144**. This increased stability is due to two reasons; the alleviation of strain associated with changing from a distorted T-shaped Pd(II) complex **144** to a 2-coordinate Pd(0) complex **146**; and the reduced electron density, and therefore lowering of the energy of the Pd orbitals, on having two formally neutral ligands bound to the Pd centre as opposed to the three ligands in **144** (one formally neutral and two formally negative). Finally neopentyl morpholine

129 can dissociate to give complex **147**, 35.6 kJ mol^{-1} more stable than Pd complex **144**.

4.2.3 Addition of THF to the free coordination site on Palladium

Whilst the employment of the cosmo solvent model describes the average solvent field observed by the complexes under investigation, it does not account for the exclusive binding of a molecule of solvent (in this case THF) to any free coordination sites on the Pd centre. An ideal calculation would combine an infinite field of solvent molecules, with additional free solvent molecules able to associate and dissociate from the Pd centre. However, this is very computationally expensive and not possible to do. Instead a single solvent molecule can be attached to the Pd centre and the energy of this complex calculated in an analogous fashion to those described previously.[119]

The attempted geometry optimisation of complex **146** to include a molecule of THF on the free coordination site of the Pd led to failure, with the molecule of THF repeatedly dissociating (figure 36). This is a result of the Pd centre being too sterically congested and therefore unable to support the addition of another ligand to its centre. The geometry optimisation of complex **147** containing a molecule of THF was also unsuccessful, with the molecule of THF again dissociating followed by calculation failure[178] (figure 36). In this case, however, steric congestion would not be the cause, as the Pd centre would only have two ligands attached. It is therefore believed that the strongly σ-donating NHC ligand forces the dissociation of the THF molecule due to the greater *trans* influence of the NHC.

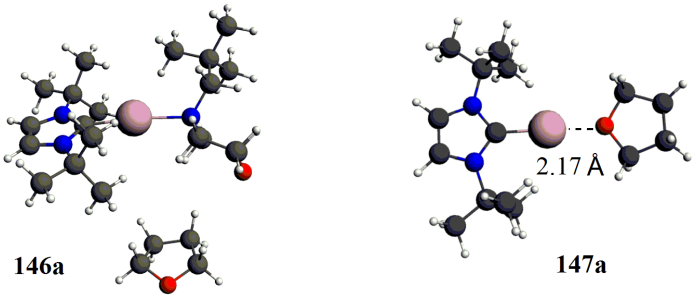

Scheme 36. Dissociation of THF to complexes **146** and **147**.

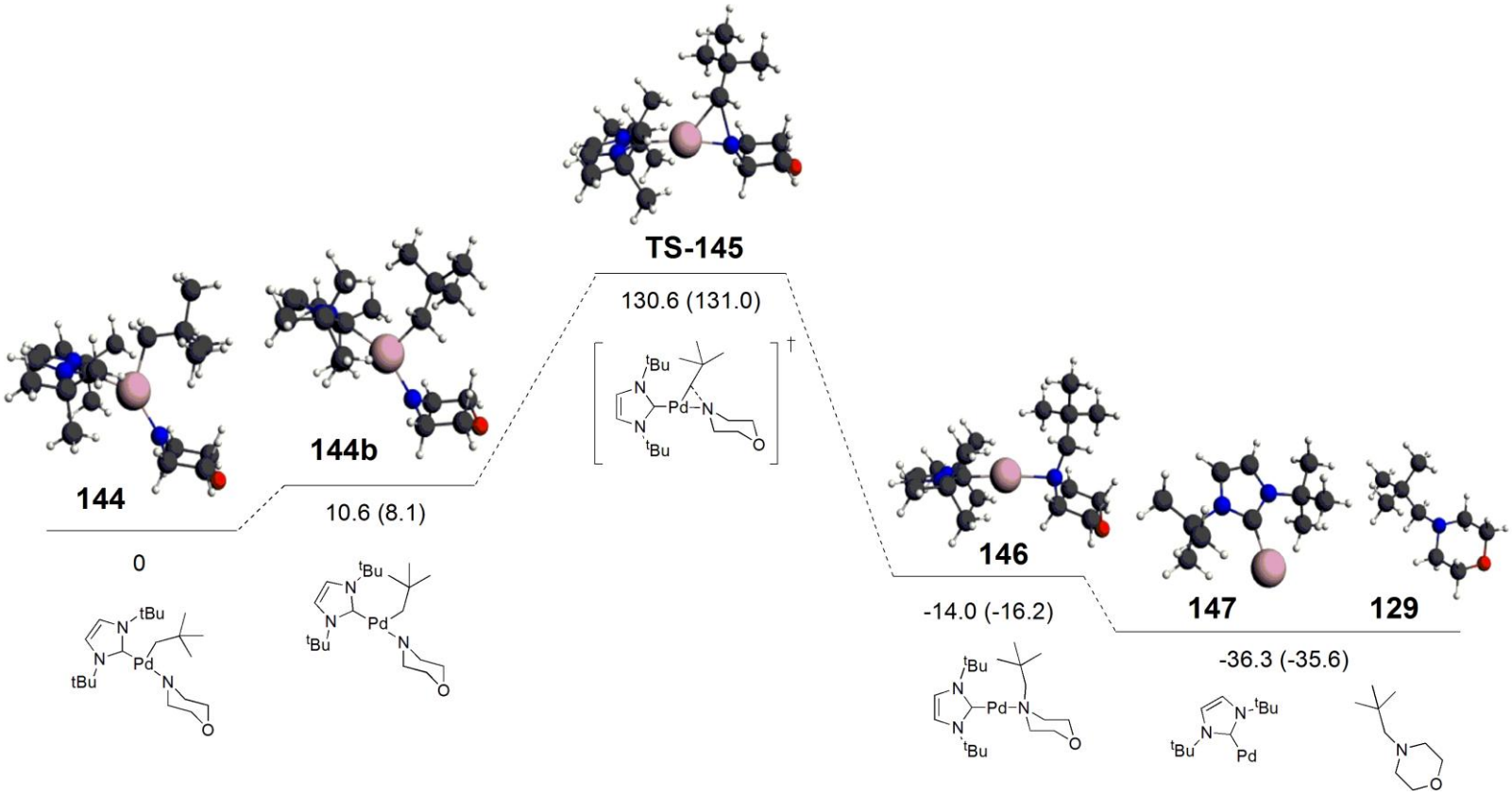

Scheme 60. Calculated relative energy level diagram (kJ mol^{-1}) of the stationary points on the potential energy surface for reductive elimination from **144**. The energies quoted are gas phase, including zero point, thermal and entropic corrections (at 298.15 K). Values in parentheses are derived from electronic energies computed with the inclusion of solvent effects, with zero point energies, thermal and entropic corrections taken from the gas phase calculations.

4.2.4 Association and dissociation of IBu to Pd(IBu)

The addition of IBu to Pd(IBu) **147** leads to the formation of $Pd(IBu)_2$ **148**, with an energy gain of 102.9 kJ mol^{-1} (scheme 61). The reverse of this process, the dissociation of IBu from $Pd(IBu)_2$ **148**, is known to occur at the beginning of many Pd(0) catalysed cycles with a similar energy to that calculated below (110 kJ mol^{-1}).[120] Hence there is no obvious reason why, on the basis of scheme 61, the reductive elimination stage of the alkyl amination reaction (*via* **TS-145**) should not take place.

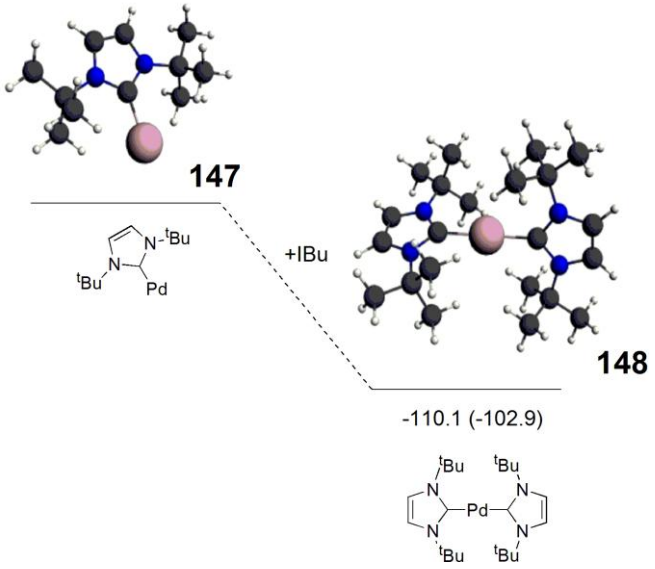

Scheme 61. Association of IBu to Pd(IBu). The energy quoted is calculated for the gas phase, and includes zero point, thermal and entropic corrections (at 298.15 K). The value in parenthesis is derived from the electronic energy computed with the inclusion of solvent effects, with zero point energy, thermal and entropic corrections taken from the gas phase calculation.

Following these calculations it was decided that further DFT studies were warranted in which (i) the neopentyl group was replaced with phenyl (for which the reductive elimination is known to take place) and (ii) the strongly σ donating IBu was replaced with a less donating trialkyl phosphine ($PCyp_3$). It was intended that these studies would offer a valuable insight into the differences in the activation energy of reductive elimination on changing the ancillary ligand and R group bound to the Pd.

4.3 Differences in the potential energy surfaces of Pd(IBu)(neopentyl)(morpholide), Pd(IBu)(phenyl)(morpholide) and Pd($PCyp_3$)(neopentyl)(morpholide)

Energy level diagrams with neopentyl replaced with phenyl and IBu with $PCyp_3$ are shown in scheme 62. It can be seen that the replacement of IBu by $PCyp_3$ gives an activation energy from **153** to **TS-154** still well in excess of 100 kJ mol^{-1}. By contrast, the activation energy from **149**, the three-coordinate phenyl complex known to undergo reductive elimination easily, is only 60.1 kJ mol^{-1} (to **TS-150**) in solution, substantially lower than the analogous steps on either the IBu or $PCyp_3$ neopentyl surfaces.

The much higher activation energy in the neopentyl systems may well result from steric factors. **144** is distorted by 40° from a typical T-shaped geometry on account of the steric bulk of the neopentyl group and hence, as discussed above, the neopentyl group must rotate in order to bring the neopentyl and morpholide ligands into sufficiently close proximity. This rotation is accompanied by the undesirable clash of the ^{t}Bu groups of the NHC with those of the neopentyl, and the combination of this congestion and the initial rotation may well have a significant effect on the energy of **TS-145**. Furthermore, the energy released on forming the two-coordinate species **151**, **146** and **155** from the preceding transition states is approximately 50% greater for the neopentyl systems, indicative of larger steric congestion in the neopentyl transition states **TS-145** and **TS-154** relative to the phenyl **TS-150**.

In order to probe the role of sterics in these reactions, the neopentyl of the Pd(IBu)(neopentyl)(morpholide) complexes was replaced with methyl, and the potential energy surface recalculated as above. On doing so it was found that the activation energy was reduced, but only by 102.9 kJ mol^{-1}; thus sterics could not account for all of the differences observed in the neopentyl/phenyl system and electronics must also play a role.

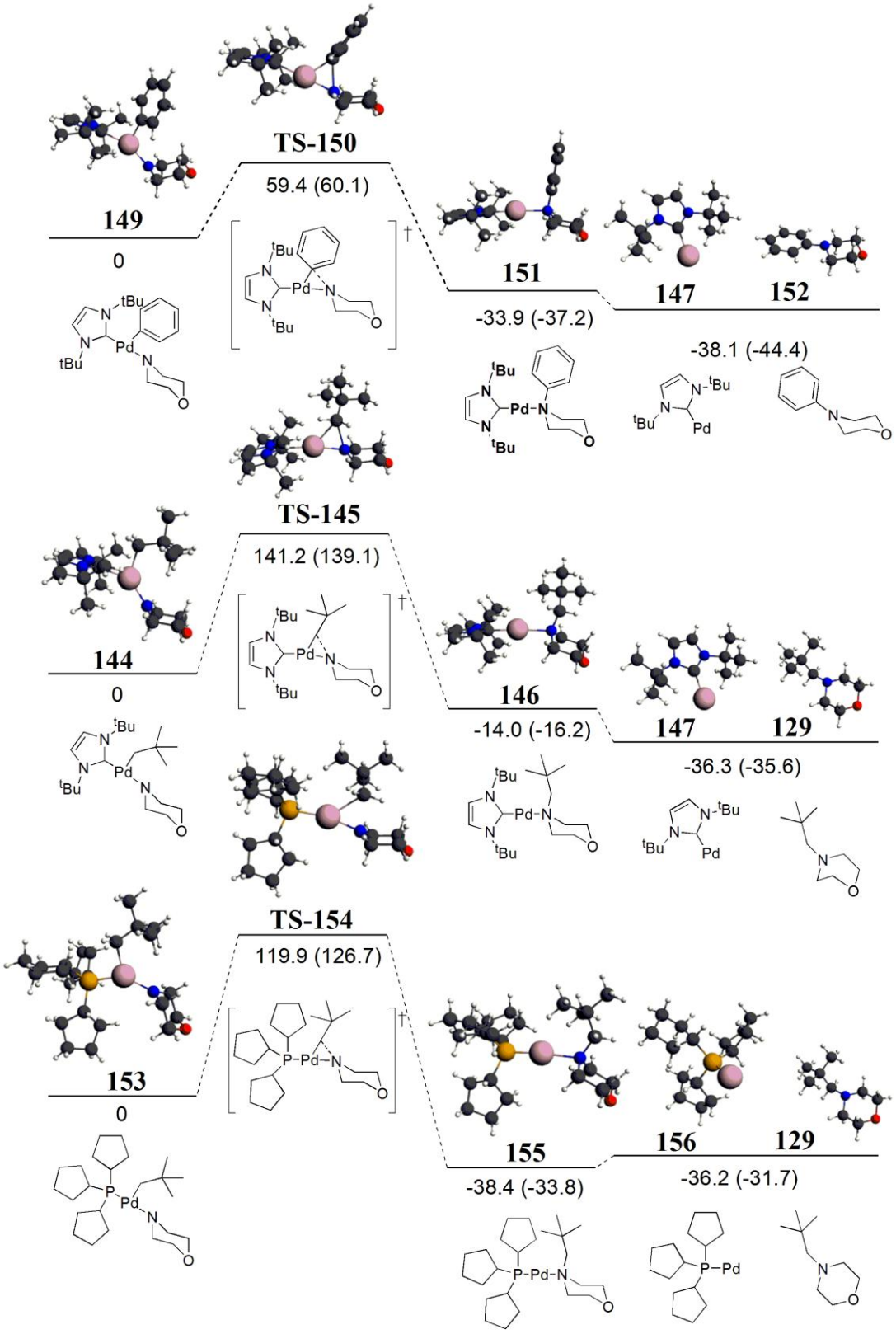

Scheme 62. Calculated energy level diagram (kJ mol^{-1}) of the stationary points on the potential energy surface for reductive elimination from **144**, **149** and **153**. The energies quoted are gas phase, including zero point, thermal and entropic corrections (at 298.15 K). Values in parentheses are derived from electronic energies computed with the inclusion of solvent effects, with zero point energies, thermal and entropic corrections taken from the gas phase calculations.

4.3.1 Differences in bond length between Pd(IBu)(neopentyl)(morpholide), Pd(IBu)(phenyl)(morpholide) and Pd(PCyp$_3$)(neopentyl)(morpholide)

Tables 11-13 present the calculated bond lengths for the structures discussed above. It is interesting to see how these bond lengths change as the reductive elimination progresses along the potential energy surface.

Pd(IBu)(neopentyl)(morpholide) complexes				
Bond	**130**	**144**	**TS-145**	**146**
Pd–N	2.170	2.004 (0.83)	2.026 (0.59)	2.250 (0.32)
Pd–C(neo)	2.120	2.097 (0.78)	2.408 (0.45)	-
C–N	-	(0.12)	(0.47)	(0.86)
Pd–C(IBu)	2.000	2.037	2.036	1.985

Table 11. Pd–ligand bond lengths (Å) and Mayer bond orders (in parentheses) for selected stationary points on the potential energy surfaces for Pd(IBu)(neopentyl)(morpholide) complexes.

In the IBu/neopentyl system, the Pd–N distance shortens significantly from the four coordinate species **130** to the three-coordinate **144**. This is in line with the idea that the amine is bound only datively to the Pd centre in **130**, but much more strongly upon deprotonation in **144**, with the latter being a traditional metal-amide bond. On progression to **TS-145** there is a slight lengthening in the Pd-N bond and then more significantly in **145**, as the amine becomes datively bound again before departing. There is little difference in the Pd–C(neopentyl) distance between the four- and three-coordinate species, but a very significant lengthening in **TS-145**, due to the movement of the neopentyl group towards the amine. By contrast, there is little change in the Pd–C (IBu) distance from **130** to **146**.

The analogous bond lengths in the PCyp$_3$ system behave similarly, with an increase in the Pd–N distance from **153** to **155**, and a reduction in Pd–P. There is also a significant lengthening in the Pd–C(neopentyl) distance on going from the

three-coordinate **153** to the transition **TS-154**, such that the Pd–C(neopentyl) distances in **TS-145** and **TS-154** are quite alike, ~ 2.4 Å. The distances in the phenyl complexes are also similar to their equivalents in the neopentyl compounds, with the notable exception of the Pd–C(phenyl). Whereas the analogous bond in the neopentyl complexes is lengthened very significantly in **TS-145** and **TS-154** relative to the preceding three-coordinate minima, that in **TS-150** is only 0.06 Å longer than in **151.**

$Pd(PCyp_3)$(neopentyl)(morpholide) complexes				
Bond	-	**153**	**TS-154**	**155**
Pd–N	-	2.007 (0.83)	2.037 (0.57)	2.294 (0.27)
Pd–C(neo)	-	2.075 (0.80)	2.436 (0.39)	-
C–N	-	(0.10)	(0.49)	(0.86)
Pd–P	-	2.239	2.522	2.199

Table 12. Pd–ligand bond lengths (Å) and Mayer bond orders (in parentheses) for selected stationary points on the potential energy surfaces for $Pd(PCyp_3)$(neopentyl)(morpholide) complexes.

Pd(IBu)(phenyl)(morpholide) complexes				
Bond		**149**	**TS-150**	**151**
Pd–N	-	1.993 (0.87)	2.017 (0.55)	2.210 (0.31)
Pd–C(phenyl)	-	2.011 (0.85)	2.071 (0.66)	-
C–N	-	(0.11)	(0.49)	(0.95)
Pd–C(IBu)	-	2.031	2.049	1.988

Table 13. Pd–ligand bond lengths (Å) and Mayer bond orders (in parentheses) for selected stationary points on the potential energy surfaces for Pd(IBu)(phenyl)(morpholide) complexes.

4.3.2 Differences in Mayer bond order of Pd(IBu)(neopentyl)(morpholide), Pd(IBu)(phenyl)(morpholide) and Pd($PCyp_3$)(neopentyl)(morpholide)

In addition to the bond length data discussed above, tables 11, 12 and 13 also report the intermediates' Mayer Bond Orders (MBOs).[179,180] MBOs contain all of the contributions to a bond between two atoms, *i.e.* they take account of all bonding and antibonding interactions in a single number and have been applied to a variety of systems by, for example, Bridgeman and co-workers.[181] In general, the greater the bond order, the higher the electron density and therefore the stronger the bond.

The MBOs in tables 11, 12 and 13 are, in general, rather similar in analogous complexes, with the exception of the Pd–C bond which weakens over the transition states. Specifically, the MBO for the weakening Pd–C bond in **TS-150** is significantly larger than for **TS-145** and **TS-154**, suggesting that the Pd–phenyl bond in **TS-150** is stronger than the Pd–alkyl bonds in the analogous transition states (the MBO for the Pd–C(Me) bond in the IBu/methyl transition state is the same as the Pd–C(neopentyl) MBO in **TS-145**). The stronger Pd–C(phenyl) bonding in the transition state, consistent with the shorter Pd–C bond in **TS-150** *vs* **TS-145** and **TS-154**, contributes significantly to the reduced activation energy on the phenyl potential energy surface.

4.4 A DFT investigation of the morpholide promoted C-H activation of neopentyl from Pd(IBu)(neopentyl)(morpholide)

No other reaction pathway is available for Pd(IBu)(aryl)(morpholine) **149** other than the reductive elimination of the aryl substituent. However, if another reaction pathway was available for complex **144**, then a selectivity issue would arise.

Pd(IBu)(neopentyl)(morpholide) **144** has three ^{t}Bu groups, two from the NHC and one from the neopentyl ligand. Although it has previously been reported that C–H activation of ^{t}Bu in IBu readily occurs,[144] this was not observed in our study nor could a transition state for such a process be found computationally, leaving only the neopentyl group as a C–H activation candidate. Several studies involving neopentyl-bound Ni and Pt have shown C–H activation to be a viable process,[182-184] often resulting in loss of 1,1-bis-dimethylcyclopropane from a metallocyclobutyl intermediate, a process which neighbouring group participation by the nitrogen of morpholide would facilitate. Therefore further computational studies were carried out to identify a mechanism to support the transfer of a hydrogen from neopentyl to the morpholide of Pd(IBu)(neopentyl)(morpholide) **144** resulting in subsequent dissociation of morpholine, followed by the loss of the neopentyl group and formation of $Pd(IBu)_2$ **148**. The results are shown in scheme 63.

The pathway begins with the transfer of a hydrogen atom from one of the neopentyl ^{t}Bu groups to the Pd centre, resulting in **TS-157**, a five coordinate transition state consisting of bound IBu, morpholide, hydride, and a metallocyclobutyl ring. The hydrogen lies in the same plane as the morpholide nitrogen and the neopentyl carbon atom to which it was previously bonded. Attempts to locate analogous transition states which do not involve the morpholide nitrogen proved unsuccessful, strongly suggesting that for the current system the presence of the nitrogen as a hydrogen acceptor is required. **TS-157** lies approximately 88 kJ mol^{-1} higher in energy than **144**, some 43 kJ mol^{-1} lower than the barrier for reductive elimination (**TS-145**, scheme 60). Furthermore, **144** is appropriately positioned for the C–H activation process whereas for reductive elimination, rotation of the bulky neopentyl group is first required. Additionally, the free rotation of the ^{t}Bu group means that there are

nine possible sites for C–H activation, compared with the one C centre for reductive elimination (see following paragraphs). From **TS-157**, movement of the hydrogen towards the nitrogen of the morpholide results in **158**, a four coordinate Pd species of similar energy to the starting complex **144**. Rotation and dissociation of morpholine, followed by loss of 1,1-bis-dimethylcyclopropane, gives Pd(IBu) **147**, 50.5 kJ mol^{-1} more stable than **144**.

Two factors need to be taken into account when discussing the selectivity of the reductive elimination and morpholide-promoted C-H activation reactions; the number of reaction sites available (1C *versus* 9H), and the activation energies of both processes, the latter of which provides the biggest contribution to reaction selectivity.[185] If the different carbon and hydrogen reaction sites could be considered equivalent, which in this case they cannot, and the activation energies of both processes were the same, which they aren't, then the rate of reaction would increase in proportional to the number of reaction sites available (i.e. 9H > 1C). Therefore morpholide-promoted C-H activation would be nines times faster than reductive elimination from the neopentyl carbon. However, the carbon and hydrogen reaction sites are not considered equivalent.

Fortunately, the difference in activation energy provides the biggest contribution to the reaction selectivity, assuming that the collision frequency is the same (equation 28, A_1=A). However, as there are nine hydrogens to only one carbon reaction centre, assuming the collision frequency is equivalent will mean that any affect on the rate constant of the reaction will be an underestimate. Neverless, taking the ratio of the rate constants (k_1/k) of morpholide-promoted C-H activation against reductive elimination finds morpholide-promoted C-H activation is favoured by 2.6 x 10^7.

(28) $$\frac{k_1}{k} = \frac{A_1}{A}\left(\frac{exp^{\left(\frac{-Ea_1}{RT}\right)}}{exp^{\left(\frac{-Ea}{RT}\right)}}\right) = exp\left(\frac{-Ea_1}{RT} - \frac{-Ea}{RT}\right)$$

$$= exp\left(\frac{-87.7\ kJ\ mol^{-1}}{8.314\ J\ K^{-1}mol^{-1}\ x\ 298\ K} - \frac{-130.0\ kJ\ mol^{-1}}{8.314\ J\ K^{-1}mol^{-1}\ x\ 298\ K}\right) = 2.6\ x\ 10^7$$

Not only is there a larger rate constant and lower activation energy barrier for C-H activation compared with reductive elimination, but the reaction also results in the

liberation of morpholine and 1,1-bis-dimethylcyclopropane, which is entropically more favourable than reductive elimination. The reverse of this process, the association of morpholine and insertion of Pd(0) into the cyclopropane ring of 1,1-bis-dimethylcyclopropane is highly unfavourable, both entropically and energetically. All of these factors therefore imply that the morpholide-promoted C-H activation of neopentyl would be selectively favoured over reductive elimination.

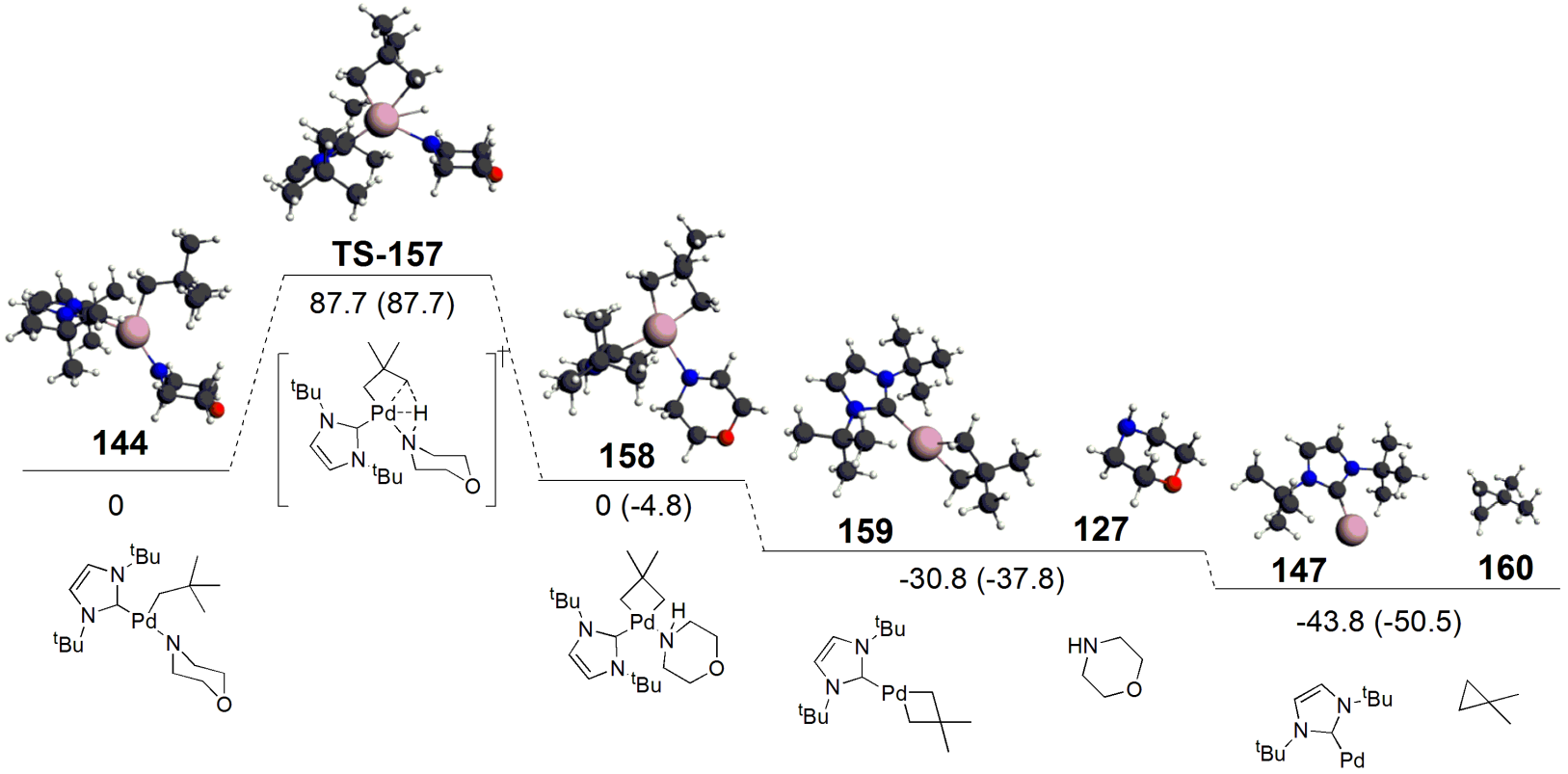

Scheme 63. Calculated relative energy level diagram (kJ mol^{-1}) of the stationary points on the potential energy surface for morpholide-promoted C-H activation of ^{t}Bu in **144**. The energies quoted are gas phase, including zero point, thermal and entropic corrections (at 298.15 K). Values in parentheses are derived from electronic energies computed with the inclusion of solvent effects, with zero point energies, thermal and entropic corrections taken from the gas phase calculations.

4.5 A DFT investigation of the Pd catalysed reductive elimination of 2-methylpropyl morpholine from Pd(IBu)(2-methylpropyl)(morpholide)

Schemes 60 and 63 suggest that reductive elimination is selectively less favourable in comparison with C–H activation; due to the lower activation energy barrier for C-H activation, 9:1 ratio of H:C reaction centres and larger rate constant calculated for C-H activation. However, the neopentyl compound does not possess β-hydrogens, and therefore it was decided to investigate the possible reaction pathways for a compound analogous to **144** which contains such hydrogens, Pd(IBu)(2-methylpropyl)(morpholide) **161**. This would allow the comparison of the potential surfaces not only for C–H activation and reductive elimination, but also for β-hydride elimination.

Scheme 64 shows the potential energy surface for the reductive elimination of 2-methylpropylmorpholine from Pd(IBu)(2-methylpropyl)(morpholide) **161** and table 14 the bond lengths and Mayer bond orders for the intermediates involved.

Pd(IBu)(2-methylpropyl)(morpholide) complexes			
Bond	**161**	**TS-162**	**163**
Pd–N	1.988 (0.87)	2.019 (0.56)	2.242 (0.32)
Pd–C(2-methylpropyl)	2.091 (0.81)	2.346 (0.39)	-
C–N	(0.10)	(0.51)	(0.85)
Pd–C(IBu)	2.012	2.033	1.986

Table 14. Pd–ligand bond lengths (Å) and Mayer bond orders (in parentheses) for selected stationary points on the potential energy surfaces for Pd(IBu)(2-methylpropyl)(morpholide) complexes.

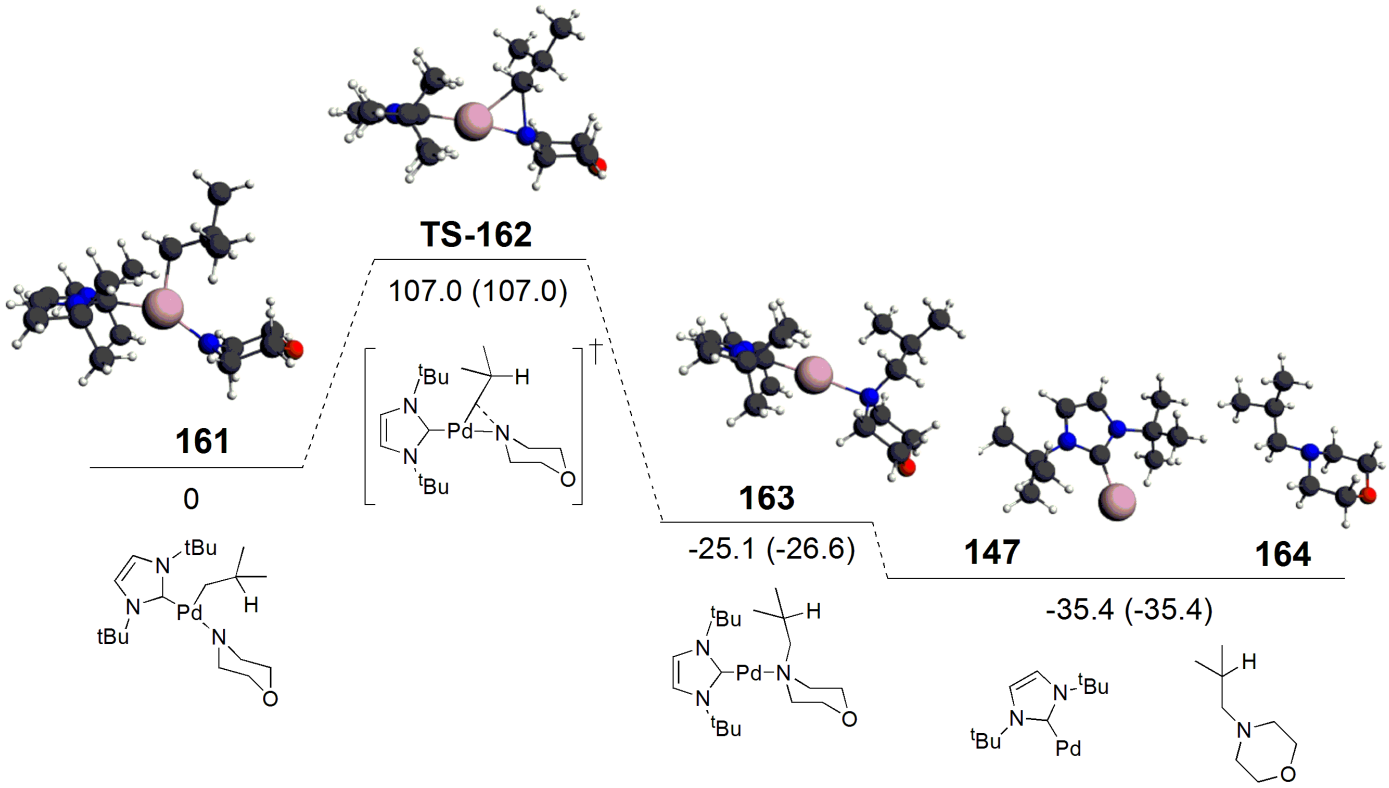

Scheme 64. Calculated relative energy level diagram (kJ mol^{-1}) of the stationary points on the potential energy surface for the reductive elimination of 2-methylpropyl morpholine from Pd(IBu)(2-methylpropyl)(morpholide) **161**. The energies quoted are gas phase, including zero point, thermal and entropic corrections (at 298.15 K). Values in parentheses are derived from electronic energies computed with the inclusion of solvent effects, with zero point energies, thermal and entropic corrections taken from the gas phase calculations.

Comparison of schemes 60 and 64 shows that the reductive elimination pathways for **144** and **161** are rather similar. 23 kJ mol^{-1} less is required to reach the transition state for reductive elimination (**TS-162**), than on the equivalent surface for the neopentyl derivative, possibly because there is one methyl group fewer in the 2-methylpropyl system and hence reduced steric congestion in the transition state. From **TS-162** the transfer of 2-methylpropyl to the morpholide nitrogen can take place, reducing Pd(II) to Pd(0) and lengthening Pd–morpholine bond from 2.019 to 2.242 Å (table 14). This is strongly exothermic (-133.6 kJ mol^{-1} in THF solution) and results in the formation of Pd(0) complex **163**, 26.6 kJ mol^{-1} more stable than **161**. The comparative process for the Pd neopentyl complex **144** was found to be 13.5 kJ mol^{-1} more exothermic, again a result of the increased steric bulk associated with the neopentyl group. Subsequent loss of 2-methylpropylmorpholine **164** finally leads to the formation of Pd(IBu) complex **147**, 35.4 kJ mol^{-1} more stable than Pd(IBu)(2-methylpropyl)(morpholide) **161**.

4.5.1 Morpholide promoted C-H activation of 2-methylpropyl from Pd(IBu)(2-methylpropyl)(morpholide)

The second process considered for **144** was the morpholide-promoted C–H activation of ^{t}Bu. To establish the effect of removing one of the three methyl groups from neopentyl, a potential surface for the 2-methylpropyl system **161** was developed, with the results presented in scheme 65. As with the reductive elimination, comparison of schemes 63 and 65 reveals rather similar surfaces. Indeed, the activation energy from **161** to **TS-165** is almost exactly the same as that between **144** and **TS-157** for the neopentyl system. That said, it might be expected that there is a rather larger dependence on the orientation of the alkyl group in **161** than in **144**, in that C–H activation requires a 2-methylpropyl methyl group to be adjacent to the morpholide N atom. There are, of course, only six such C–H bonds in **161** compared to the nine in **144**. Due to the activation barrier for the reaction being near identical, and considering the hydrogen reaction centres in **161** and **144** to be equivalent, means that the rate of C-H activation is directly proportional to the number of hydrogen reaction centres. Therefore the rate of reaction for C-H activation is 1.5 times faster for **144** than **161** (hydrogen ratio 3:2).

A comparison of the rate of reductive elimination against morpholide promoted C-H activation is less straightforward (see section 4.4, p108, paragraphs 2 and 3). Assuming in **161** that the single carbon reaction centre is equivalent to the six hydrogen reaction centres, which of course it is not, implies that the rate of morpholide promoted C-H activation from **161** is six times faster than reductive elimination.

The larger factor determining the rate of reaction is the activation energy. Again assuming the collision frequency is the same for the carbon and hydrogen reaction centres (A_1=A), finds that the ratio of rate constants (k_1/k) is 334 in favour of morpholide-promoted C-H activation (equation 29). However, as there are six hydrogens as opposed to one carbon, and assuming that the formation of a transition state consisting of a five membered ring is easier to obtain than a three-membered ring,[186] means that the collision frequency of the hydrogen reaction centres (A_1) will be higher than for the carbon reaction centres (A). The ratio found for the rate constants (k_1/k) will therefore be an underestimate, as $A_1 > A$ as opposed to $A_1 = A$.

(29) $$\frac{k_1}{k} = \frac{A_1}{A}\left(\frac{exp^{\left(\frac{-Ea_1}{RT}\right)}}{exp^{\left(\frac{-Ea}{RT}\right)}}\right) = exp\left(\frac{-Ea_1}{RT} - \frac{-Ea}{RT}\right)$$

$$= exp\left(\frac{-92.6\ kJ\ mol^{-1}}{8.314\ J\ K^{-1}mol^{-1}\ x\ 298\ K} - \frac{-107.0\ kJ\ mol^{-1}}{8.314\ J\ K^{-1}mol^{-1}\ x\ 298\ K}\right) = 334.3$$

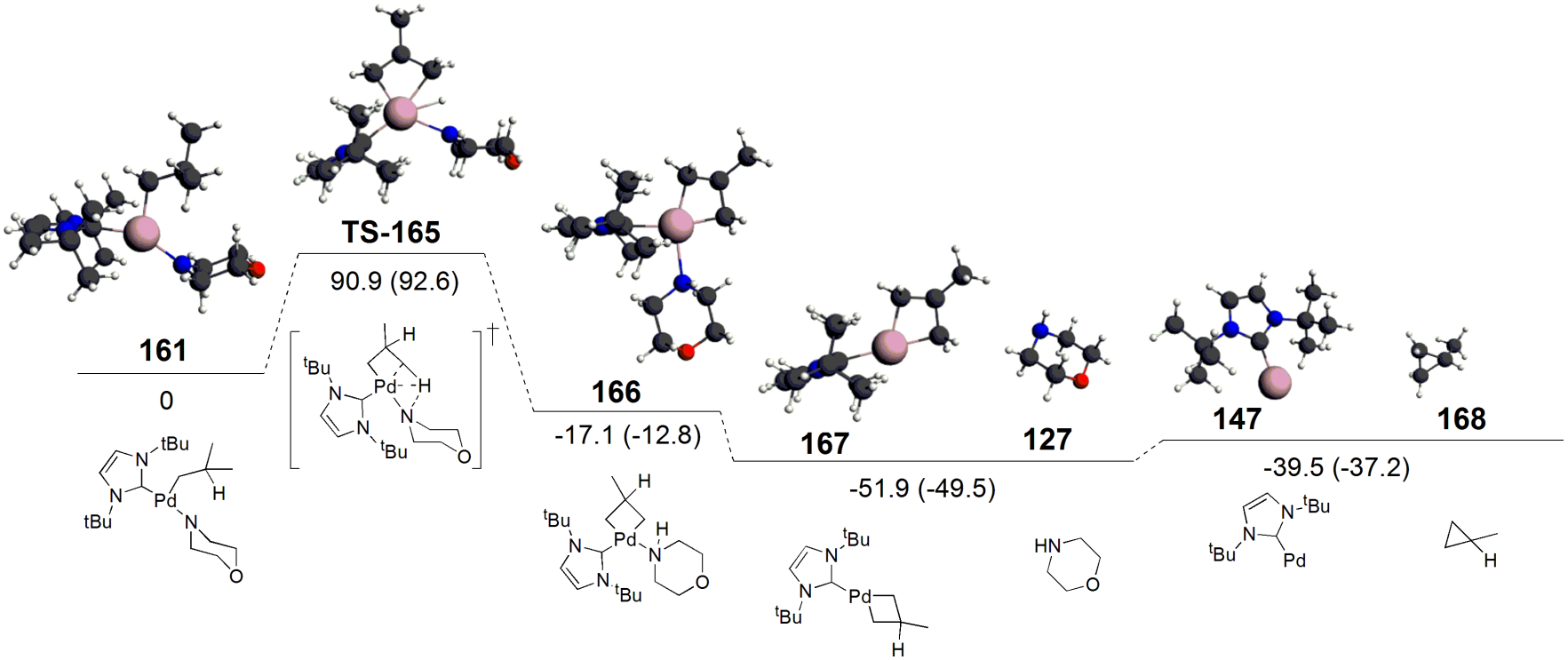

Scheme 65. Calculated relative energy level diagram (kJ mol^{-1}) of the stationary points on the potential energy surface for morpholide-promoted C-H activation of 2-methylpropane in **161**. The energies quoted are gas phase, including zero point, thermal and entropic corrections (at 298.15 K). Values in parentheses are derived from electronic energies computed with the inclusion of solvent effects, with zero point energies, thermal and entropic corrections taken from the gas phase calculations.

4.5.2 β-Hydride elimination of isobutene from Pd(IBu)(2-methylpropyl)(morpholide)

A third possible reaction of **161** is β-hydride elimination from 2-methylpropyl, and the potential surface for this process is shown in scheme 66. The activation energy to form **TS-169** is only 70.8 kJ mol^{-1} in solution, compared with 107.0 kJ mol^{-1} for reductive elimination (scheme 64 **TS-162**) and 92.6 kJ mol^{-1} for morpholide-promoted C–H activation (scheme 65 **TS-165**). Following β-hydride transfer, loss of either alkene or morpholine from complex **170** is possible. However, it was found that the most favourable reaction was loss of morpholine to form **171** (-71.7 kJ mol^{-1}), a result of the stronger bonding between Pd and the alkene (confirmed by calculation of the metal-alkene interaction energy (-199.9 kJ mol^{-1}) compared with the metal-morpholine interaction energy (-32.3 kJ mol^{-1})). This is consistent with our observation that a β-hydride transition state could be located only for morpholide-assisted loss of hydride.

As stated previously, the most likely reaction pathway is not only determined by the activation energy (although this provides the largest contribution) but also by the number of reaction centres available. In the case of **161** there is one hydogren available for β-hydride elimination, six for morpholide-promoted C-H activation and one carbon for reductive elimination. A comparison of β-hydride elimination against morpholide-promoted C-H activation therefore finds that the latter process is six times more likely to occur, whilst a comparison of β-hydride elimination against reductive elimination finds the rate of reaction the same, providing the assumption is made that the hydrogen and carbon reaction centres are equivalent in all cases.

Assuming the collision frequency is the same for all three processes, the difference in activation energy can be used to calculate the ratio of the rate constants for the respective reactions (equations 30, 31 and 32). Therefore, following this it was found that the ratio of the rate constants (k_1/k) is 6627 in favour of β-hydride elimination over morpholide-promoted C-H activation, and 2.2 x 10^6 in favour of β-hydride elimination over reductive elimination.

(30) $$\frac{k_1}{k} = \frac{A_1}{A}\left(\frac{exp^{\left(\frac{-Ea_1}{RT}\right)}}{exp^{\left(\frac{-Ea}{RT}\right)}}\right) = exp\left(\frac{-Ea_1}{RT} - \frac{-Ea}{RT}\right)$$

(31) $$= exp\left(\frac{-70.8\ kJ\ mol^{-1}}{8.314\ J\ K^{-1}mol^{-1}\ x\ 298\ K} - \frac{-92.6\ kJ\ mol^{-1}}{8.314\ J\ K^{-1}mol^{-1}\ x\ 298\ K}\right) = 6627.2$$

(32) $$= exp\left(\frac{-70.8\ kJ\ mol^{-1}}{8.314\ J\ K^{-1}mol^{-1}\ x\ 298\ K} - \frac{-107.0\ kJ\ mol^{-1}}{8.314\ J\ K^{-1}mol^{-1}\ x\ 298\ K}\right) = 2.2\ x\ 10^6$$

It is therefore found that the most favourable reaction of **161** is *β*-hydride elimination, followed by morpholide promoted C-H activation and then reductive elimination. The bulky 2-methylpropyl group impedes the formation of the reductive elimination transition state resulting in a higher activation energy for the coupling of 2-dimethylpropyl with morpholide. Whilst the energy for *β*-hydride elimination is lower than for morpholide-promoted C–H activation, the increased number of hydrogens available for the latter process does offset this energy difference. However, the largest contribution for determination the most likely reaction pathway is the activation energy, providing the difference in collision frequency is small. Therefore, despite the difference in number of reaction sites, *β*-hydride elimination is more still more favourable than morpholide-promoted C-H activation.

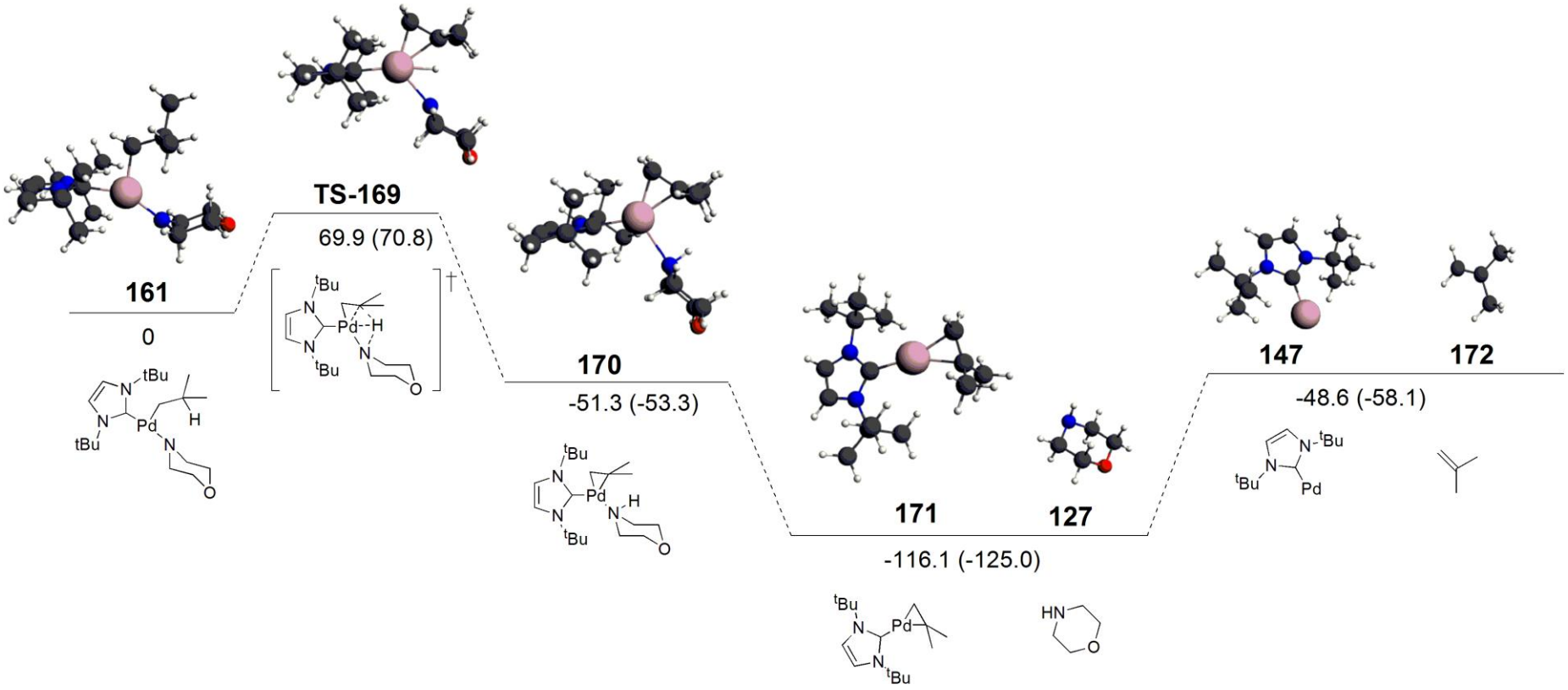

Scheme 66. Calculated relative energy level diagram (kJ mol^{-1}) of the stationary points on the potential energy surface for the *β*-hydride elimination reaction from 2-methylpropyl in **161**. The energies quoted are gas phase, including zero point, thermal and entropic corrections (at 298.15 K). Values in parentheses are derived from electronic energies computed with the inclusion of solvent effects, with zero point energies, thermal and entropic corrections taken from the gas phase calculations.

4.6 Comments and conclusions on the proposed potential energy surfaces of Pd(L)(alkyl)(morpholide)

By development of energy level diagrams for the stationary points on potential energy surfaces of a series of Pd catalysed reactions, all starting from a common intermediate, we have been able to determine the most likely pathway for reactions of Pd(IBu)(neopentyl)(morpholide) **144**. Unfortunately it seems that reductive elimination of neopentyl morpholine is not the most favoured pathway. In comparison, it was shown that the reductive elimination of phenyl morpholine was considerably lower in energy than the analogous neopentyl compound and was the only possible product available from Pd(IBu)(phenyl)(morpholide). Yet for Pd(IBu)(neopentyl)(morpholide) this was not the case; whilst searching for alternative reaction profiles, morpholide promoted C-H activation was discovered as an alternative reaction pathway, although experimentally the key product 1,1-dimethylcyclopropane could not be observed.

To compare these two possible reactions with the possible alternative, β-hydride elimination, a final series of potential energy pathways were developed using Pd(IBu)(2-methylpropyl)(morpholide) **161**. From this it was found that the most favourable pathway was indeed β-hydride elimination, followed by morpholide-promoted CH activation and finally reductive elimination. Therefore whilst the presence of β hydrogens has been known to be problematic when carrying out cross coupling reactions, the additional presence of hydrogens able to undergo C-H activation will also need to be considered.

In this study we have not observed any key Pd-bound intermediates other than Pd(IBu)(neopentyl)(morpholide), yet it would be very desirable to be able to identify them in future reactions. One technique which could possibly allow the characterisation of key intermediates from complex reaction mixtures is mass spectrometry (although not with 100% certainty - see section 3.4.1, p85), and is the final subject of this project.

5 The use of mass spectrometry in monitoring Pd catalysed reactions

Santos has shown that online ESI(+)-MS(/MS) monitoring of the Stille reactions can be used to intercept and characterise key reaction intermediates. These methods allow the study of transient reactive intermediates by preserving the inert atmosphere in which the reaction takes place. This is achieved by coupling the reactor containing all the reagents directly to the ion source. However, Santos' work did not extend to the use of offline ESI(+)-MS methods which require the transfer of a known amount of reaction mixture to the ion source by the experimentalist, a process that could possibly compromise the inert conditions under which the reaction takes place. A major concern of an offline method would thus be the neutralisation and degradation of key reactive intermediates upon transferring the reaction mixture to the ion source.

5.1 Pd catalysed aryl amination of 4-chlorotoluene and morpholine

The coupling of 4-chlorotoluene with morpholine was chosen as an ideal reaction to test the efficiencies of the offline ESI(+)-MS monitoring (scheme 67), as it is known to be a reliable high yielding process.[187] However, upon investigation of the intermediates present, the only potential palladium bound species observed was the pre-catalyst $Pd(IBu)_2$ **148** at 465 m/z. The reagents, 4-chlorotoluene and morpholine, and the product 4-*p*-tolyl-morpholine, were found to have too small a m/z ratio (below 250 m/z) to be monitored accurately by ESI(+)-MS. Below ~250 m/z the high abundance of solvent and free IBu peaks had a pronounced effect. The presence of free IBu at 180 m/z also 'swamped' the presence of any other signal, however, above 250 m/z the spectrum appeared cleaner. Major peaks at 465 m/z could potentially be attributed to $[Pd(IBu)_2]^+$ and at 558 m/z as $[Pd(IBu)_2(C_6H_4Me)]^+$ **173**, the oxidative addition product (minus Cl^-) of chlorotoluene or C-H activation product from the solvent toluene.

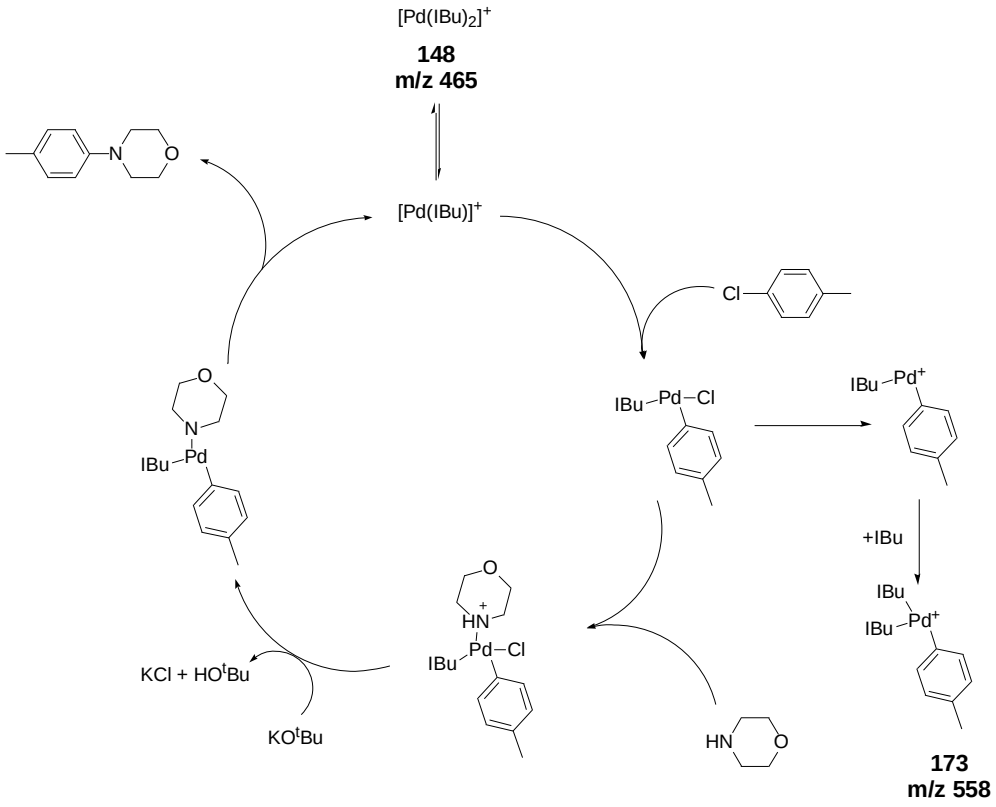

Scheme 67. Offline ES(+)-MS monitoring of the palladium catalysed reaction of 4-chlorotoluene with morpholine.

5.2 Synthesis of dansyl functionalised aryl amination reagents for MS analysis

Due to the difficulty in identifying the MS species below 250 m/z, alternative reagents were sought to allow the use of mass spectrometry to probe these coupling reactions. It was conceived that functionalisation of 4-chlorotoluene and morpholine in order to increase their mass above the 250 m/z threshold would in principle bring them in range to be observed by ESI(+)-MS.

The incorporation of functional groups that contain nitrogen, oxygen and sulfur would help to distinguish the transient reagent bound intermediates, due the increasing complexity of their isotope pattern. The additional restriction that the functional groups should act as an easy ionisable MS tag, such as a tertiary amine, would allow further ease of identification. Finally, restricting the functional group to one that has a simple ^{1}H and ^{13}C NMR spectrum, as well as fluorescent properties,

would add to its universal appeal. One such functional group that fills all of the above criteria is the fluorescent dansyl piperazine.[188]

5.2.1 Synthesis of dansyl piperazine and *N*-dansyl-4-chlorobenzylamine

Initial attempts to synthesise dansyl piperazine by reacting mono-Boc-piperazine **174** directly with dansyl chloride proved unsuccessful due to instability of the Boc group under the reaction conditions. Instead mono-Boc-piperazine **174** was protected to give the *N*-Boc-*N*-Cbz-piperazine **175** (scheme 68).[189] The Boc group was then removed and the mono-Cbz-protected-piperazine **176** reacted with dansyl chloride. Deprotection of the Cbz group by transfer-hydrogenation then furnished the required dansyl piperazine **178** in high yield.

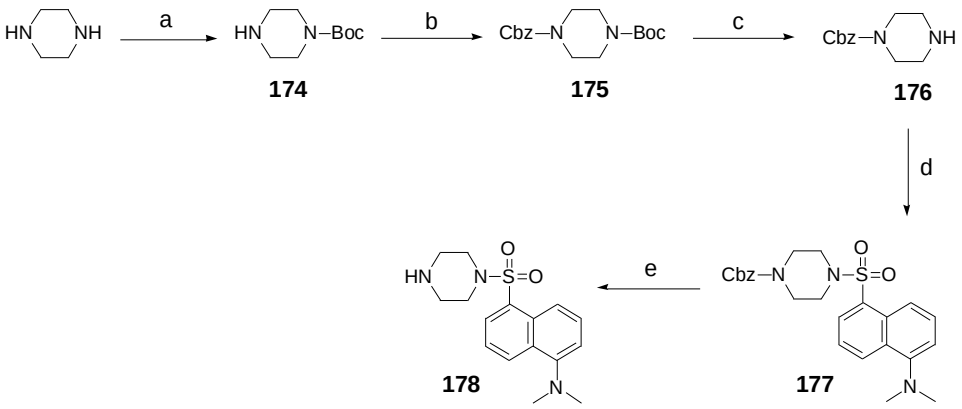

(a) Di-*tert*-dibutoxycarbonate, AcOH, 21 °C, 24 h, 82%; (b) benzyl chloroformate, NEt_3, 0 °C, 1 h, 99%; (c) TFA/CH_2Cl_2, 21 °C, 1 h, 97%; (d) dansyl chloride, DMAP, 0 °C, 24 h, 80 %; (e) Pd-C (5%), formic acid, EtOH, 95 °C, 3 h, 100%.

Scheme 68. Synthesis of dansyl piperazine.

The synthesis of *N*-dansyl-4-chloro-benzylamine **179** was accomplished by reaction of dansyl chloride with catalytic DMAP for 24 h (scheme 69).

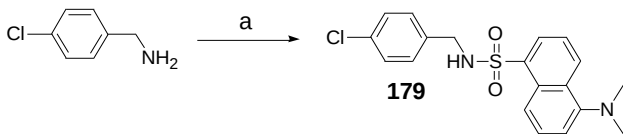

(a) Dansyl chloride, DMAP 0 °C, 24 h, 85%.

Scheme 69. Synthesis of *N*-dansyl-4-chloro-piperazine.

5.3 Offline ESI(+)-MS monitoring of the Pd catalysed aryl amination of chlorotoluene and dansyl piperazine

The initial palladium catalysed reaction of chlorotoluene and dansyl piperazine was found to occur in 80% isolated yield after 24 h (scheme 70). Using the same conditions, the reaction was repeated and monitored offline *via* ESI(+)-MS; 0.01 mL of reaction mixture was removed under a positive flow of argon, diluted with 0.99 mL of MeCN and injected directly into the ESI(+)-MS probe. This process was carried out after 1, 2, 4, 8 and 24 h intervals, and repeated at least three times for each time interval.

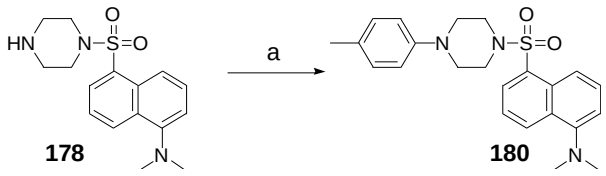

(a) 4-chlorotoluene, $Pd(IBu)_2$, KO^{t}Bu, 60 °C, 24 h, 80%.

Scheme 70. Palladium catalysed reaction of chlorotoluene with dansyl piperazine.

A major limitation with this approach is that the transient Pd bound species could decompose or react further during removal and transferring to the probe. However, there is a second limitation; the starting material, Pd bound species and product are of a different chemical nature, and therefore could exhibit different sensitivities towards the ESI(+)-MS, despite being in equal equivalents. For instance, the dansyl piperazine reagent **178** was found to be extremely sensitive towards MS ionisation and could be observed at very low concentration, due to containing a primary amine, whereas the product and any Pd-bound species would only contain a tertiary amine, which is less sensitive towards MS ionisation. Therefore, even if the reaction is 90% complete, the ratio of starting material:product cannot be used to determine an accurate percentage conversion. Unlike section 2.6, where the coupling of the small bromomaleimide reagent to the considerably larger Grb2 SH2 domain does not change the sensitivity of the Grb2 SH2 or the resultant protein-conjugate product towards MS ionisation, with dansyl piperazine **178** and the dimethyl-(5-(4-*p*-tolyl-piperazine-1-sulfonyl)-naphthalen-1-yl)-amine coupled product **180**, this is not the case. Not only are **178** and **180** both small in molecular weight, but also of a

sufficiently different chemical nature to affect their sensitivity towards MS ionisation.

Whilst percentage conversion cannot be accurately used to monitor reaction progress, thin layer chromatography can be combined with MS offline analysis to provide real time updates as to reaction progress. However, it should be noted that the aim of these MS experiments is not to monitor percentage conversion or reaction progress, but to observe and characterise any Pd-bound species present. Therefore whilst differences in MS ionisation are a limitation in this study, they do not affect the aims set out.

Scheme 71 shows the results for the offline ESI(+)-MS monitoring of the Pd-catalysed reaction of dansyl piperazine and chlorotoluene, and the possible structures for the species present.

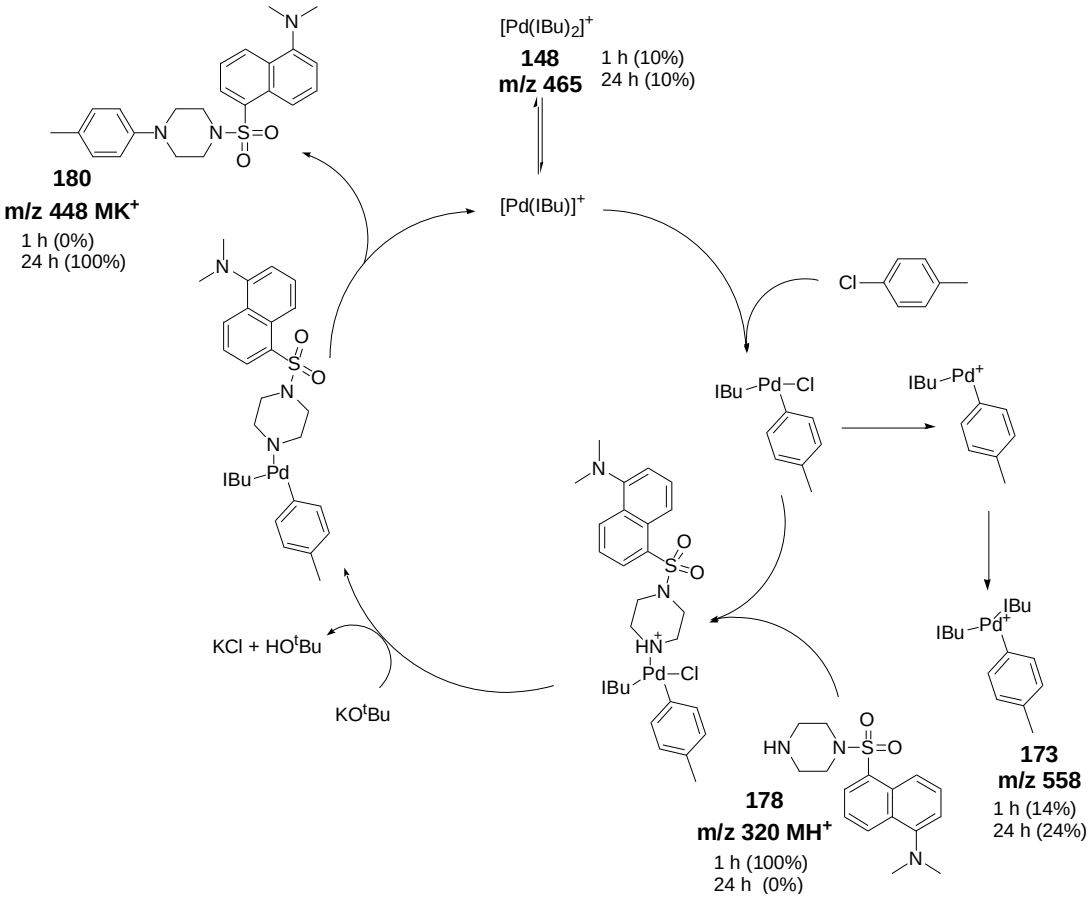

Scheme 71. Species observed in the offline monitoring of the palladium catalysed reaction of chlorotoluene with dansyl piperazine. Abundances shown in parenthesis.

A species, possible $[Pd(IBu)_2]^+$ **148**, was observed at 465 m/z along with the dansyl piperazine starting material **178** at 320 m/z. Disappointingly the only possible intermediate visible was the potential oxidative addition product $[Pd(IBu)_2(C_4H_4Me)]^+$ **173** at 558 m/z, whilst all intermediates containing the dansyl piperazine were absent. However, more positive was the observation of a peak for the dansyl piperazine **178** which decreased in abundance with time and was replaced by the aryl-amine coupled product **180** at 448 m/z (MK^+).

5.3.1 MS/MS analysis of the ionic species observed in the Pd catalysed aryl amination reaction of 4-chlorotoluene and dansyl piperazine

Despite the lack of transient palladium-bound species observed by ESI(+)-MS, further analysis using MS/MS was carried out on those species that were present, in order to investigate their fragmentation pattern and thus allow futher confirmation of their structure. However, the only species with a recognisable fragmentation pattern was the dansyl piperazine reagent **178** (figure 37).

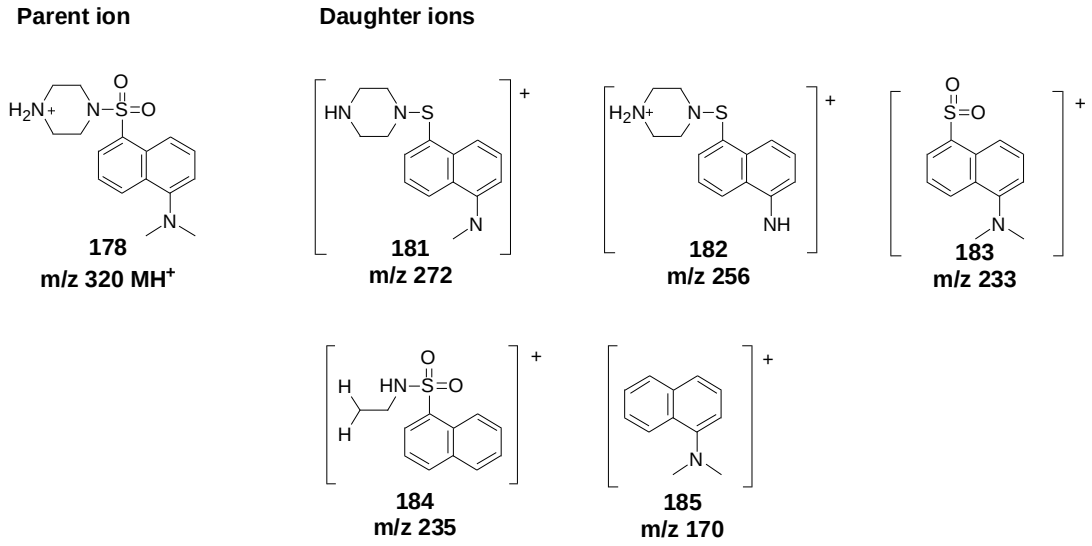

Figure 37. MS/MS induced fragmentation pattern of dansyl piperazine.

MS/MS fragmentation of dansyl piperazine proved remarkably successful. Loss of oxygen from sulfur was prevalent (**181** and **182)**, as was loss of methyl(s) from the dimethylamino moiety of the dansyl group (**181**, **182**, and **184**). Fragmentation of the

piperazine unit was also observed (**184**). However, by far the most abundant fragment was that which had lost both piperazine and SO_2 functionality **185**.

5.4 Offline ESI(+)-MS monitoring of the Pd catalysed aryl amination of *N*-dansyl-4-chloro-benzylamine and morpholine

The palladium catalysed reaction of *N*-dansyl-4-chloro-benzylamine and morpholine was found to give a yield of only a 15% after 24 h, although the product could not be obtained pure (scheme 72). This lower yield could be a result of the reaction requiring a longer time to go to completion.

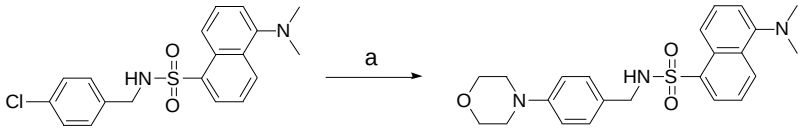

179 **186**

(a) Morpholine, $Pd(IBu)_2$, KO^tBu, 60 °C, 24 h.

Scheme 72. Pd-catalysed coupling of morpholine and and *N*-dansyl-4-chloro-benzylamine.

Pleasingly the introduction of *N*-dansyl-4-chloro-benzylamine **179** as reagent led to the observation of considerably more palladium-bound intermediates by offline ESI(+)-MS (scheme 73). Again a species with a m/z corresponding to $[Pd(IBu)_2]^+$ **148** was present at 465 m/z, along with the starting *N*-dansyl-4-chloro-benzylamine reagent **179** at 375 m/z, the latter of which was seen to disappear with time. The aryl-amine coupled product **186** was also observed 464 m/z (MK^+) and increased in abundance as the reaction progressed.

No oxidative addition product was observed for this reaction. However, palladium-bound species **173** was observed at 558 m/z, analogous to the previous two MS experiments. Whilst in the previous two cases this was assigned to the oxidative addition product, $[Pd(IBu)_2(C_4H_4Me)]^+$, in this experiment no such oxidative addition is available. Therefore this species could be the result of C-H activation of toluene by Pd(IBu), followed by addition of free IBu.

Interestingly, two new species were observed at 789 and 753 m/z, which could correspond to the transmetallation intermediates **187** and **188** respectively. In order

to investigate this further, the reaction conditions were varied and the effects monitored again by ESI(+)-MS.

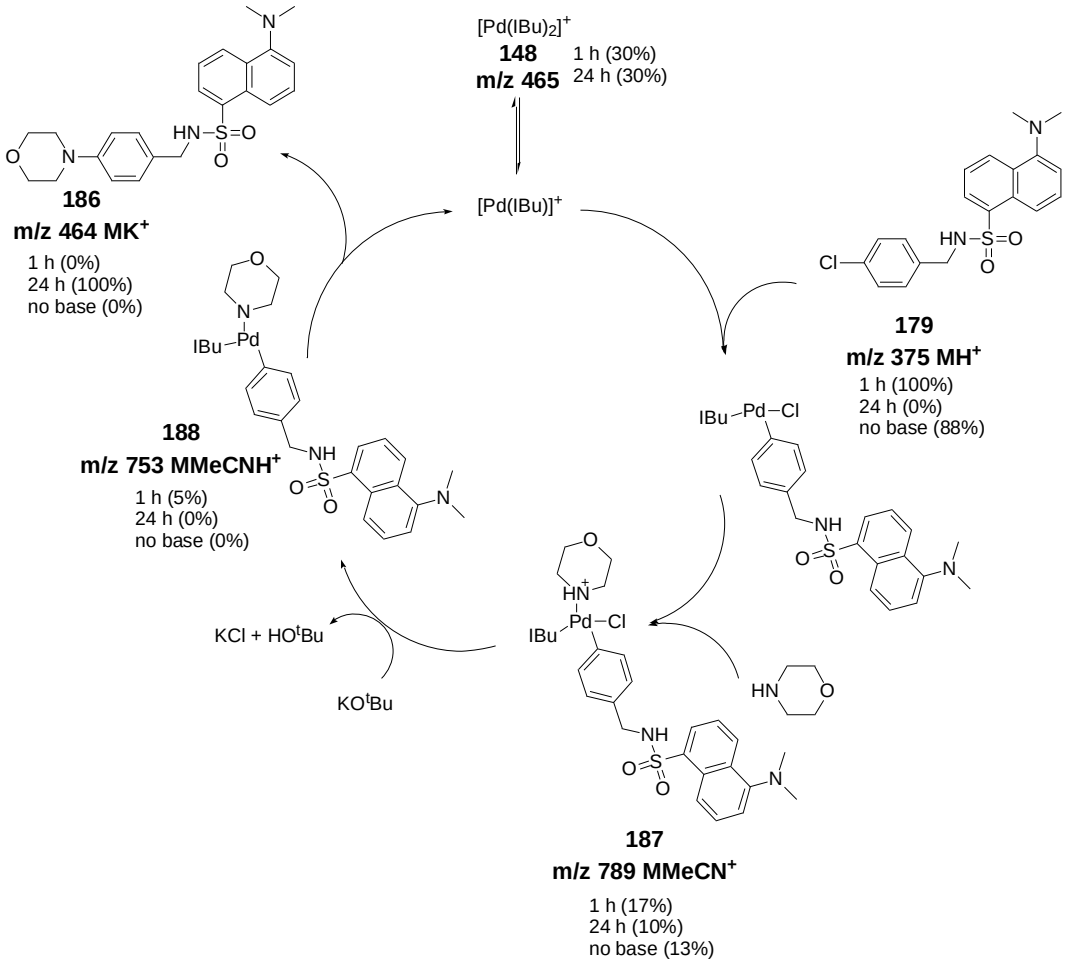

Scheme 73. Palladium bound species observed by ESI(+)-MS for the reaction of *N*-dansyl-4-chloro-benzylamine and morpholine. Abundances shown in parenthesis.

5.4.1 Effect of varying the conditions of the Pd catalysed aryl amination of *N*-dansyl-4-chloro-benzylamine and morpholine

Optimisation of the reaction conditions found a temperature of 60 °C was required for oxidative addition. Therefore the reaction was carried out at 21 °C and ESI(+)-MS used to monitor the presence of Pd bound species. It was observed that the only potential Pd bound species present were the pre-catalyst **148** and species **173**, indicating that the other Pd bound species could not be formed before oxidative addition had taken place. When the temperature was raised to 60 °C, however, the

proposed associated amine-intermediates **187** and **188** were observed, along with formation of product.

The order to which KO^{t}Bu was added to the reaction was varied. Normal experimental procedures required addition of KO^{t}Bu to a reaction mixture already containing *N*-dansyl-4-chloro-benzylamine **179**, morpholine and Pd(IBu)$_2$ **148**. However, the effect of adding KO^{t}Bu before Pd(IBu)$_2$ was found to be insignificant to the outcome of the reaction and the observance of any transient species. The equivalents of KO^{t}Bu were varied from 1 to 4 but showed no effect on species **187** and **188**. Finally, KO^{t}Bu was omitted from the reaction altogether. In the absence of KO^{t}Bu, no product was observed. Instead only starting material and proposed associated amine species **187** (789 m/z) was observed, due to lack of deprotonation taking place. When KO^{t}Bu was added, the reaction began to proceed through to the formation of product **186** (464 m/z), with loss of starting material **179** (375 m/z) and amine species **187** (789 m/z), all of which was observed by MS.

5.4.2 MS/MS analysis of the ionic species observed in the Pd catalysed aryl amination reaction of *N*-dansyl-4-chloro-benzylamine and morpholine

Whilst the MS/MS analysis of the dansyl piperazine reagent **178** produced fragmentation patterns that were useful for analytical purposes, *N*-dansyl-4-chloro-benzylamine **179** failed to give such useful fragments under similar conditions (figure 38). The only potentially recognisable fragments observed resulted from loss of oxygen from sulfur or loss of methyl from the dimethylamino moiety, both of which were in line with previous MS/MS analysis in section 5.3.1. However, whilst the *N*-dansyl-4-chloro-benzylamine **179** reagent did not fragment well, the transient palladium-bound species faired better.

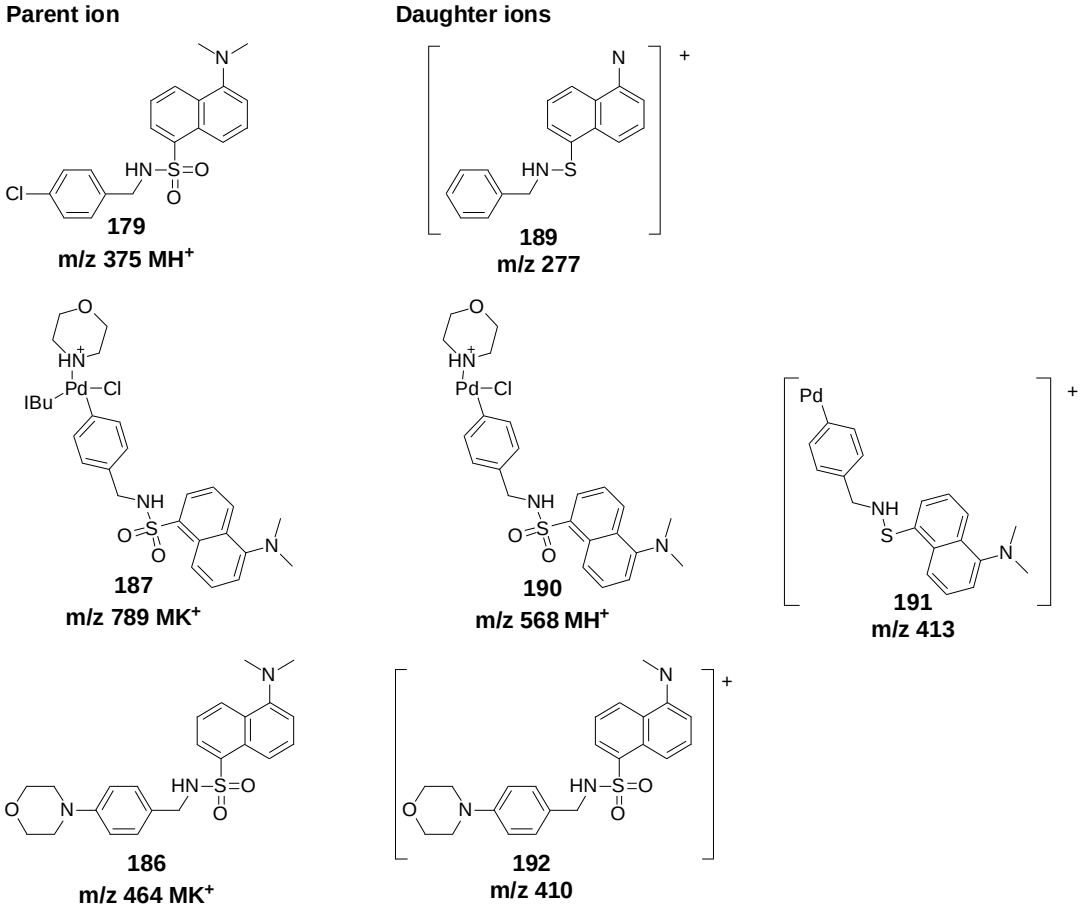

Figure 38. MS/MS induced fragmentation pattern of *N*-dansyl-4-chloro-benzylamine and associated intermediates from palladium catalysed aryl amination reaction.

The proposed amine-bound palladium species **187** produced two fragments; the first potentially corresponding to having lost IBu **190** and the second having potentially having lost morpholine, IBu, Cl and the oxygens from sulfur **191**. The coupled product **186** was also found to fragment, with loss of a single methyl group from the dimethylamino moiety **192**. This was most probably due to its similarity with the starting material and thus inability to fragment in a conceivable way.

5.5 Offline ESI(+)-MS monitoring of the Pd catalysed aryl amination of *N*-dansyl-4-chloro-benzylamine and dansyl piperazine

In order to compare the ionisability of the dansyl functionalised reagents, an experiment was carried out using both reagents. The palladium-catalysed reaction of *N*-dansyl-4-chloro-benzylamine and dansyl piperazine is shown in scheme 74. However, this combination of reagents resulted in a complex reaction mixture, of which only 10% product could be obtained and not pure. This was possibly a direct result of the large size of both dansyl functionalised reagents, inhibiting the approach and binding of the reagents to the palladium centre. Fortunately, ESI(+)-MS is an extremely sensitive process, and the reaction could be monitored offline to investigate if the reaction was actually taking place (scheme 75).

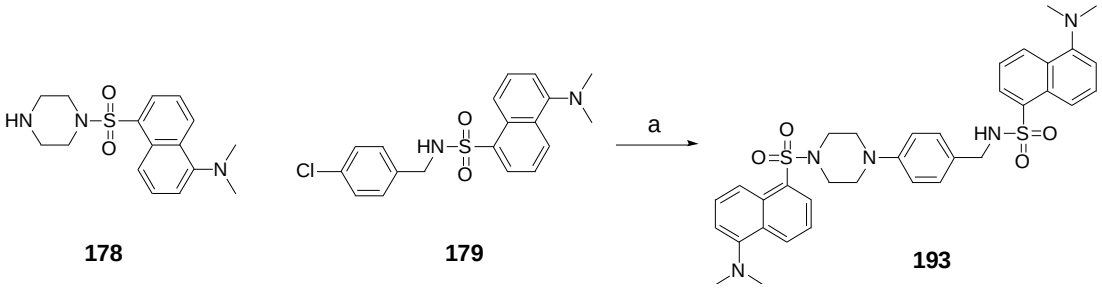

178 **179** **193**

(a) $Pd(IBu)_2$, KO^tBu, 60 °C, 24 h.

Scheme 74. Pd-catalysed coupling of *N*-dansyl-4-chloro-benzylamine with dansyl piperazine.

The offline ESI(+)-MS analysis failed to find any transient Pd bound species from the reaction. Again, both starting materials **178** and **179** were present at the beginning, only to decrease in abundance as the reaction progressed, whilst the opposite was found for the bisdansyl functionalised product **193**. Interestingly the dansyl piperazine **178** starting material was found to decrease to 0% abundance after 24 h, whilst the less sensitive chlorobenzylamine **179** did not, suggesting that either decomposition of **178** occurred or it was able to react further to an unknown and un-observable species.

The product **193** mass to charge ratio was found to be 657 m/z, indicative of the singly charged ion. No doubly charged ion of 328 m/z, or for any reaction intermediates, was observed during this experiment, indicating that the tertiary amine

present in the dansyl functional group was not protonated. This could have been a result of the conjugation of the amine with the π-system of the dansyl unit, with the majority of the electron density channelled into the SO_2NR moiety *via* the aromatic ring.

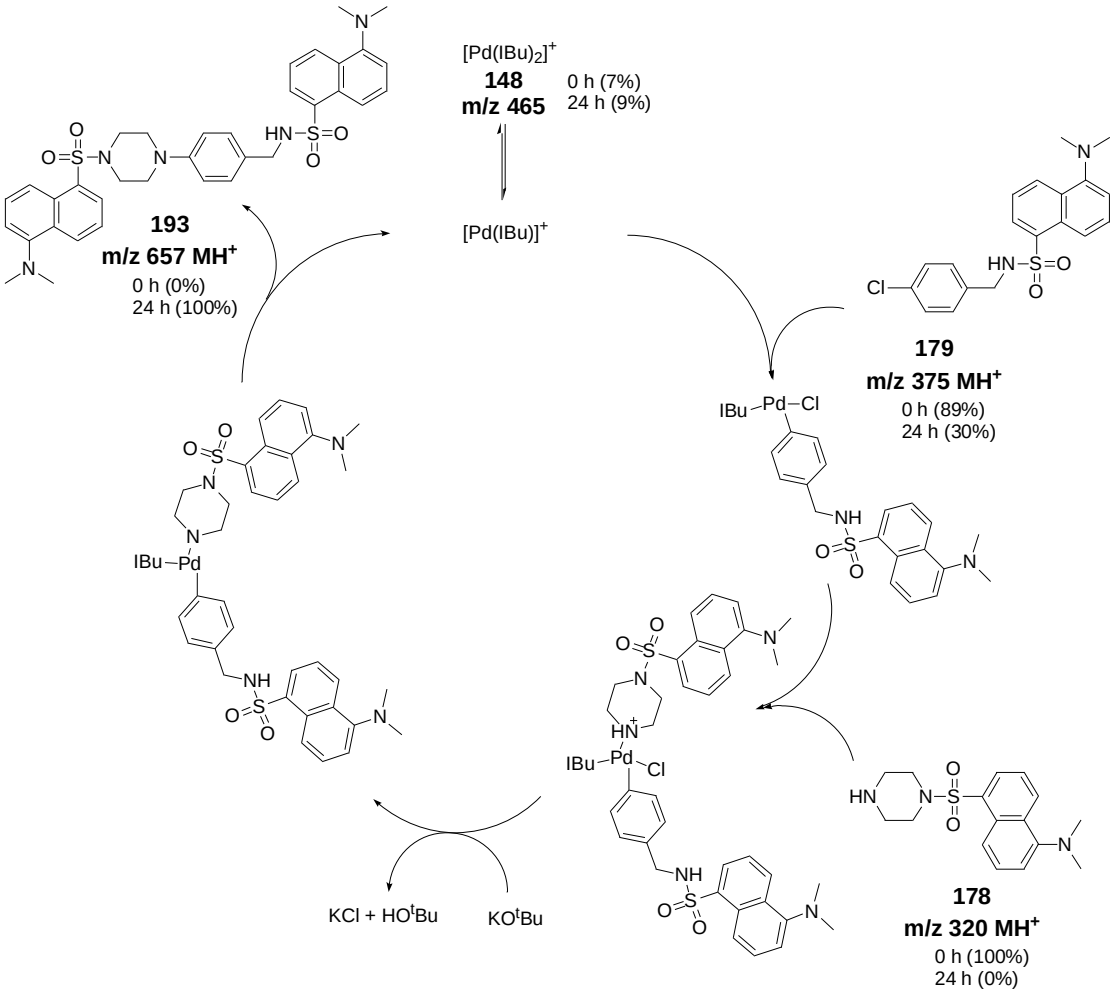

Scheme 75. Palladium catalysed reaction of *N*-dansyl-4-chloro-benzylamine and dansyl piperazine. Abundances shown in parenthesis.

Whilst the reactions of (1) dansyl piperazine and chlorotoluene and (2) dansyl piperazine and *N*-dansyl-4-chlorobenzylamine were unsuccessfully monitored using offline ESI(+)-MS techniques, the reaction of morpholine with *N*-dansyl-4-chlorobenzylamine had shown some success. Therefore attention was turned to the troublesome alkyl amination reaction. It was hoped that the observation of any intermediates present would shed light on the inability of the tricoordinate palladium complex, Pd(IBu)(neopentyl)(morpholide) **144,** to undergo reductive elimination. It

would also be of interest to see whether any of the intermediates proposed in the DFT study would be visible and thus provide potential confirmation of the reaction pathway taken.

5.6 Offline ESI(+)-MS monitoring of the reductive elimination stage of the Pd catalysed alkyl amination reaction

Offline ESI(+)-MS analysis for the reaction of Pd(IBu)(neopentyl)(Cl) dimer with lithium morpholide, or morpholine and base, led in both cases to a complex reaction mixture with a considerable number of unidentifiable Pd-bound species present (scheme 58, p 90). Further MS/MS analysis of these intermediates led in all cases to fragmentation to an unidentified ion, the m/z of which did not correspond with any proposed complex. The only potentially recognisable palladium-bound species was the corresponding monomer **194** of Pd(IBu)(neopentyl)(chloride) dimer (scheme 76).

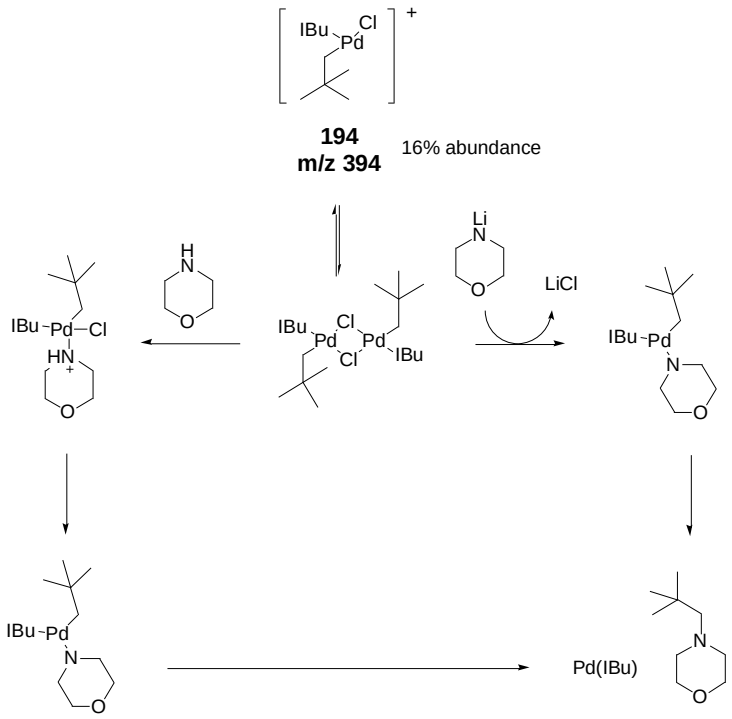

Scheme 76. Palladium catalysed alkyl amination reaction.

Following this, morpholine was replaced with the previously successful dansyl piperazine **178** and the ESI(+)-MS reactions repeated. The increased m/z of the amine reagent would provide additional information as to the amines fate, as would

its easily recognisable MS/MS fragmentation pattern. However, upon carrying out the ESI(+)-MS experiment, the only notable observation was that of free dansyl piperazine reagent **178**. No other information could be ascertained from this study. A ^{1}H NMR experiment confirmed that no reaction had taken place, returning only starting material, most likely due to the sterical congestion created on binding dansyl piperazine to Pd(IBu)(neopentyl)(Cl) monomer **194** (scheme 77).

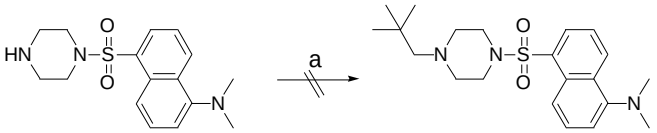

178 **195**

(a) [Pd(IBu)(neopentyl)(Cl)]$_2$, KO^{t}Bu, 21 °C to 60 °C, 24 h.

Scheme 77. Palladium catalysed alkyl amination reaction of Pd(IBu)(neopentyl)(morpholine) with dansyl piperazine.

5.7 Comments and conclusions of the offline ESI(+)-MS and MS/MS analysis of Pd catalysed aryl and alkyl aminaton reactions

Initially the study of the palladium catalysed aryl amination reaction was intended to assess the potential utility of offline ESI(+)-MS to screen for the presence of any transient palladium bound species in the reaction mixture. This process was then to be applied to the alkyl amination reaction in an attempt to observe any species that might offer insight into the reductive elimination step. However, during this initial study many factors came to light which would influence the observation of any potential species or catalytic process.

Size of reagent and intermediate was found to be very important. Below a threshold of 250 m/z, solvent and free IBu ‘swamped’ the MS signal. Above this threshold, however, the complex palladium isotopic pattern enabled the observation of a number of palladium bound species. By variation of the temperature and base (KO^{t}Bu), the intensity of these species could be varied, allowing a possible assignment of these species. With the completion of the initial offline experiments, the application of this method to the reductive elimination stage of the palladium catalysed alkyl amination reaction was investigated.

Unfortunately no useful Pd-bound species could be seen by ESI(+)-MS. The complex reaction mixture resulted in a considerable number of species, none of which could be assigned with confidence by ESI(+)-MS or MS/MS. The use of dansyl piperazine also failed to produce any results, due to its inability to bind to the palladium centre of Pd(IBu)(neopentyl)(Cl) monomer formed *in situ* from Pd(IBu)(neopentyl)(Cl) dimer.

In order to investigate the potential for offline ESI(+)-MS reaction monitoring further, and in particular its use in the alkyl amination reaction, different mass spectrometry tags would be required that would allow efficient reaction coupling. The dansyl linkers used in this study were found to be unsuitable, due to their large size. However, the reaction failure could also be due to the system in question, as reductive elimination was initially found not to take place. Therefore in future work, attention needs to be paid to the reagents in the alkyl amination reaction and the catalyst system used, in order to find success in both offline ESI(+)-MS reaction monitoring and in finding a system of general use.

6 Experimental section

6.1 General methods and experimentation

All the starting materials including solvents were used as received without further purification, unless otherwise stated. Where necessary, reactions were carried out under argon, unless otherwise stated. Specially dried (anhydrous) solvents were used when necessary.

Reactions were monitored by TLC analysis carried out on SIL G/UV_{254} silica plates purchased from VWR, and were visualized under a UV lamp operating at short and long wavelength ranges. Visualisation was aided by dipping plates into an alkaline potassium permanganate solution. Flash column chromatography was carried out with Kieselgel 60M 0.04/0.063mm (230-400 mesh) silica gel. All yields quoted are isolated yields, unless otherwise stated, and when multiple products are obtained, data are presented in terms of order isolated.

^{1}H and ^{13}C NMR spectra were recorded at room temperature on a Bruker Avance 400 instrument operating at a frequency of 400 MHz for ^{1}H and 100 MHz for ^{13}C, a Bruker Avance 500 instrument operating at a frequency of 500 MHz for ^{1}H and 125 MHz for ^{13}C, and a Bruker Avance 600 instrument operating at a frequency of 600 MHz for ^{1}H and 150 MHz for ^{13}C. $CDCl_3$, CD_3OD and DMSO-d6 were used as the deuterated solvents for all spectra run. Peaks are reported as singlet (s), doublet (d), triplet (t), quartet (q), quintet (quintet), broad (br) or multiplet (m). All chemical shifts are reported in parts per million (ppm) relative to residual protiated signals of the solvent, and coupling constants (J) are in Hertz (Hz). Infra-red spectra were run on a PerkinElmer Spectrum 100 FT-IR spectrometer operating in ATR mode with frequencies given in reciprocal centimeters (cm^{-1}). Mass spectra and high resolution mass data were recorded on a VG70-SE mass spectrometer (EI and ESI(+) mode). Melting points were taken on a Gallenkamp heating block and are uncorrected. Lyophilised somatostatin was purchased from Sigma-Aldrich and used without further purification. Grb2 SH2 domain model protein **37** was obtained from the Waxman group.[67]

LC-MS was performed on protein samples using a Waters Acquity uPLC connected to Waters Acquity Single Quad Detector (SQD). Column: Acquity uPLC BEH C18 1.7µm 2.1 x 50 mm. Wavelength: 254 nm. Mobile Phase: 95:5 Water (0.1% Formic Acid): MeCN (0.1% Formic Acid) Gradient over 4 min (to 5:95 Water (0.1% Formic Acid): MeCN (0.1% Formic Acid). Flow Rate: 0.6 mL/min. MS Mode: ES+. Scan Range: m/z = 85-2000. Scan time: 0.25 sec. Data obtained in continuum mode. The electrospray source of the MS was operated with a capillary voltage of 3.5 kV and a cone voltage of 50 V. Nitrogen was used as the nebulizer and desolvation gas at a total flow of 600 L/h.Total mass spectra for protein samples were reconstructed from the ion series using the MaxEnt 1 algorithm pre-installed on MassLynx software.

Density Functional Theory (DFT) calculations were performed using the Amsterdam Density Functional (ADF) quantum chemistry package[161] with the PBE Generalized Gradient Approximation (GGA) exchange correlation functional.[159,160] TZ2P Zero-Order Regular Approximation (ZORA) all electron basis sets were used on all atoms. Scalar relativistic effects were accounted for by the ZORA. The integration grid parameter was set to 6.0, and the geometry convergence was 10^{-3} au $Å^{-1}$. All geometries were optimised without symmetry constraints. Analytical harmonic frequency calculations were used to characterise stationary points as either true minima or transition states by the observation of 0 or 1 imaginary vibrational modes respectively. Solvent effects (tetrahydrofuran) were included by the COnductor-like Screening Model (COSMO)[163,190] with the following values for the atomic radii: Pd = 2.3 Å, O = 1.72 Å, Cl = 2.05 Å, N = 1.83 Å, P = 2.0 Å, C = 2.0 Å and H = 1.3 Å. The solvent radius and dielectric constant used were r = 3.18 Å and ε = 7.58. Entropic, internal and zero-point energy corrections were taken from gas-phase calculations and applied to both gas-phase and solvent optimised geometries and transitions states. Schlenk line manipulations involved the use of oven-dried glassware or glassware that had been flame dried under vacuum. Glassware was repeatedly evacuated and purged with dry argon. Glove box manipulations were performed in a Mbraun or a Miller Howe glove box under an atmosphere of dinitrogen. Alkyl halides, PPh_3, DMPM (1,1-bis(dimethylphosphino)methane), $PCyp_3$ (tricyclopentylphosphine), PCy_3 (tricyclohexylphosphine), DPPM (1,1-bis(diphenylphosphino)methane), DPPP (1,3-bis(diphenylphosphino)propane),

P^tBuMe_2 were purchased from commercial sources (Aldrich). Amines were distilled at reduced pressure. The *N*-heterocyclic carbenes IBu and IPr were prepared according to literature procedure.[191,192] Anhydrous solvents were obtained from Anhydrous Engineering (USA) solvent systems after drying on alumina granules or pellets. NMR solvents were purified by refluxing over a suitable drying agent, then vacuum transferred to an ampoule and stored under dinitrogen in a glove box.

6.2 Experimental data

6.2.1 Route 1 to mono- and di- bromomaleimides

N-(2-(2-(2-Amino-ethoxy)-ethoxy)-ethyl)-4-hydroxy-butyramide[80] 80

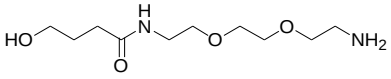

Dihydro-furan-2-one (1.72 g, 20.0 mmol, 1 eq) was added to a solution of 2-(2-(2-aminoethoxy)ethoxy)ethanamine (2.96 g, 20.0 mmol, 1 eq) and H_2O (1 mL) and the reaction mixture heated at 90 °C for 15 h under argon. The solvent was removed *in vacuo* and the product purified by column chromatography (5:2:2:1 Et_2O/MeOH/MeCN/Et_3N) to yield **80** as a light yellow oil (3.47 g, 14.8 mmol, 74% yield). ^{1}H NMR (500 MHz, $CDCl_3$) δ 6.99 (br, 1H, N*H*), 3.61-3.57 (m, 4H, OCH_2CH_2O), 3.54-3.52 (m, 6H, CH_2OCH$_2$CH$_2$OCH_2 & CH_2OH), 3.35 (t, J = 5.5 Hz, 2H, C(O)NHCH_2), 2.81 (t, J = 5.5 Hz, 2H, OCH$_2$CH_2NH$_2$), 2.27 (t, J = 6.0 Hz, 2H, C(O)CH_2CH$_2$), 1.79 (quintet, J = 6.0 Hz, 2H, C(O)CH$_2$CH_2); ^{13}C NMR (125 MHz, CD_3OD) δ 175.98 (s), 73.45 (t), 71.32 (t), 71.27 (t), 70.59 (t), 62.23 (t), 42.06 (t), 40.33 (t), 33.58 (t), 29.79 (t); IR (neat) 3000, 1739, 1366, 1217 cm^{-1}; HRMS (CI) calcd for $C_{10}H_{23}N_2O_4$ $[M+H]^+$ 235.1658, observed 235.1661.

(2-(2-(2-(4-Hydroxy-butyrylamino)-ethoxy)-ethoxy)-ethyl)-carbamic acid *tert*-butyl ester 73

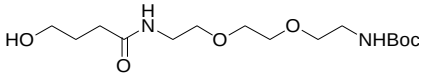

Di-*tert*-butyl-dicarbonate (93.0 mg, 0.43 mmol, 1 eq) in CH_2Cl_2 (5 mL) was added dropwise to solution of *N*-(2-(2-(2-amino-ethoxy)-ethoxy)-ethyl)-4-hydroxy-butyramide **80** (100 mg, 0.43 mmol, 1 eq) and NEt_3 (60.0 µL, 0.43 mmol, 1 eq) in CH_2Cl_2 (10 mL) and the reaction mixture stirred at 21 °C for 15 h. The solvent was then removed *in vacuo* and the product purified by column chromatography (5:2:2:1 Et_2O/MeOH/MeCN/Et_3N) to yield **73** as a light yellow oil (140 mg, 42.1 mmol, 98% yield). ^{1}H NMR (600 MHz, $CDCl_3$) δ 3.56 (t, J = 6.5 Hz, 2H, CH_2OH), 3.53 (bs, 4H, OCH_2CH_2O), 3.47 (t, J = 5.0 Hz, 4H, CH_2OCH$_2$CH$_2$OCH_2), 3.35 (t, J = 5.0 Hz, 2H,

C(O)NHCH_2), 3.23 (t, J = 5.0 Hz, 2H, C(O)NHCH_2), 2.27 (t, J = 6.5 Hz, 2H, C(O)CH_2CH$_2$), 1.78 (quintet, J = 6.5 Hz, 2H, C(O)CH$_2$CH_2), 1.35 (s, 9H, C(CH_3)$_3$); ^{13}C NMR (150 MHz, $CDCl_3$) δ 173.92 (s), 156.13 (s), 79.44 (s), 71.32 (t), 70.24 (t), 69.63 (t), 68.56 (t), 61.65 (t), 40.39 (t), 38.04 (t), 33.74 (t), 28.22 (q), 27.99 (t); IR (neat) 3324, 2932, 1690, 1640 cm^{-1}; HRMS (CI) calcd for $C_{15}H_{31}N_2O_6$ $[M+H]^+$ 335.2182, observed 335.2177.

6.2.1.1 Synthetic route for 2-(2-(2-Hydroxy-ethoxy)-ethoxy)-ethyl)-carbamic acid *tert*-butyl ester 85

Methanesulfonic acid 2-(2-(2-hydroxy-ethoxy)-ethoxy)-ethyl ester[81]

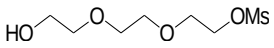

Methanesulfonyl chloride (2.70 g, 23.6 mmol, 1 eq) was added dropwise to a solution of 2-(2-(2-hydroxy-ethoxy)-ethoxy)-ethanol (3.54 g, 23.6 mmol, 1 eq) and NEt_3 (3.3 mL, 23.6 mmol, 1 eq) in THF (25 mL) at 0 °C whereby a white precipitate was formed. The reaction mixture was warmed to 21 °C and stirred for 24 h. The precipitate was then filtered, the filtrate concentrated *in vacuo* and the liquid purified by column chromatography (8:2 EtOAc/PE) to give product as a colourless liquid (1.75 g, 7.68 mmol, 33 % yield). ^{1}H NMR (500 MHz, $CDCl_3$) δ 4.31 (m, 2H, CH_2OMs), 3.73 (m, 2H, CH_2OH), 3.65 (t, J = 4.0 Hz, 2H, OCH_2), 3.62 (m, 4H, OCH_2), 3.52 (t, J = 4.0 Hz, 2H, OCH_2), 3.02 (s, 3H, CH_3); ^{13}C NMR (150 MHz, $CDCl_3$) δ 72.40 (t), 70.39 (t), 70.01 (t), 69.35 (t), 68.74 (t), 61.37 (t), 37.36 (q); IR (neat) 3448, 2939, 1739, 1347 cm^{-1}; HRMS (CI) calcd for $C_7H_{17}O_6S$ $[M+H]^+$ 229.07458, observed 229.07412.

2-(2-(2-Amino-ethoxy)-ethoxy)-ethanol[81]

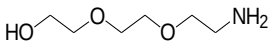

Sodium azide (324 mg, 4.98 mmol, 1.5 eq) was added to a stirred solution of methanesulfonic acid 2-(2-(2-hydroxy-ethoxy)-ethoxy)-ethyl ester (0.76 g, 3.31 mmol, 1 eq) in MeCN (15 mL) and the reaction mixture refluxed for 36 h. H_2O (10 mL) was then added and the organic product extracted into CH_2Cl_2. After drying with $MgSO_4$, the solvent was removed *in vacuo*. The liquid was redissolved in the

minimum amount of EtOAc and passed through a short plug of silica, before again being concentrated *in vacuo*. THF (30 mL) was added to this liquid, followed in one portion by triphenylphosphine (3.91 g, 14.9 mmol, 4.5 eq) and the reaction mixture stirred at 21 °C for 4 h. The solvent was removed *in vacuo* and the residue purified by column chromatography (3:3:1 $CHCl_3$/MeOH/NEt_3) to give the amino-alcohol product as a light yellow oil (387 mg, 2.6 mmol, 78 % yield). ^{1}H NMR (500 MHz, $CDCl_3$) δ 3.44 (m, 4H, OCH_2), 3.36 (q, J = 4.5 Hz, 2H, OCH_2), 3.32 (m, 3H), 2.85 (m, 3H), 2.52 (bs, 2H, NH_2); ^{13}C NMR (125 MHz, $CDCl_3$) δ 72.80 (t), 72.59 (t), 70.22 (t), 70.09 (t), 61.13 (t), 41.24 (t); IR (neat) 3300, 3007, 2868, 1739 cm^{-1}; HRMS (CI) calcd for $C_6H_{16}NO_3$ $[M+H]^+$ 150.11302, observed 150.11365.

(2-(2-(2-Hydroxy-ethoxy)-ethoxy)-ethyl)-carbamic acid *tert*-butyl ester[81] 85

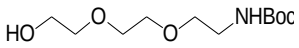

KOH (0.61 g, 10.9 mmol, 1.1 eq) was added to a solution of 2-(2-(2-Amino-ethoxy)-ethoxy)-ethanol (1.47 g, 9.90 mmol, 1 eq) in H_2O (10 mL) and the reaction mixture stirred for 5 min at 21 °C. It was then cooled to 0 °C and di-*tert*-butyl-dicarbonate (2.37 g, 10.6 mmol, 1.1 eq) in dioxane (5 mL) was added dropwise. After 1 h the solution was warmed to 21 °C and stirred for another 4 h. The mixture was then extracted with CH_2Cl_2, dried with $MgSO_4$ and the solvent removed *in vacuo* to give a residue. Purification by column chromatography (8:2 EtOAc/PE) gave product **85** as a yellow oil (2.48 g, 9.90 mmol, 100 % yield). ^{1}H NMR (600 MHz, $CDCl_3$) δ 3.75 (q, J = 4.5 Hz, 2H, HOCH_2), 3.65 (m, 4H, OCH_2), 3.61 (q, J = 4.5 Hz, 2H, OCH_2), 3.56 (t, J = 4.5 Hz, 2H, OCH_2), 3.31 (t, J = 4.5 Hz, 2H, NCH_2), 1.44 (s, 9H, C(CH_3)$_3$); ^{13}C NMR (125 MHz, $CDCl_3$) δ 155.72 (s), 78.82 (s), 72.03 (t), 69.97 (t), 69.89 (t), 69.82 (t), 61.12 (t), 39.93 (t), 28.02 (q); IR (neat) 3339, 2932, 1688, 1519 cm^{-1}; HRMS (ES+) calcd for $C_{11}H_{23}NO_5Na$ $[M+Na]^+$ 272.1474, observed 272.1482.

Trifluoro-acetate-2-(2-(2-(3,4-dibromo-2,5-dioxo-2,5-dihydro-pyrrol-1-yl)-ethoxy)-ethoxy)-ethyl-ammonium 87

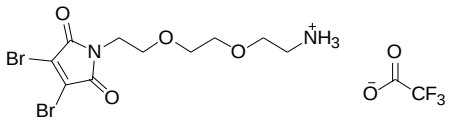

DIAD (324 mg, 1.60 mmol, 1 eq) was added dropwise to a stirred solution of triphenylphosphine (420 mg, 1.60 mmol, 1 eq) in dry THF (10 mL) at -78 ºC under argon and the reaction mixture stirred at this temperature for 1 h, whereby a white precipitate was formed. **(**2-(2-(2-Hydroxy-ethoxy)-ethoxy)-ethyl)-carbamic acid *tert*-butyl ester **85** (0.60 g, 2.40 mmol, 1.5 eq) in dry THF (5 mL) was then added, followed by 3,4-dibromo-pyrrole-2,5-dione (408 mg, 1.60 mmol, 1 eq) in one portion. The reaction was stirred for 15 min at -78 °C until the solution became clear and then at 21 °C for an additional 15 h. The solvent was then removed *in vacuo* to give a residue which was re-dissolved in CH_2Cl_2 (5 mL). To this solution TFA (5 mL) was added and the reaction mixture stirred at 21 °C for 15 h. Toluene was then added (5 mL) and the solvent removed *in vacuo* to give a yellow oil. Purification by column chromatography (2:98 MeOH/CH_2Cl_2) gave product **87** as a light yellow oil (0.75 g, 1.50 mmol, 94% yield). ^{1}H NMR (600 MHz, $CDCl_3$) δ 7.82 (br, 3H, NH_3), 3.81 (t, J = 5.5 Hz, 2H, OCH$_2$CH_2NH$_3$), 3.68 (t, J = 5.5 Hz, 2H, OCH$_2$CH_2O), 3.64 (t, J = 5.5 Hz, 2H, OCH_2CH$_2$O), 3.60 (bs, 4H, CH_2OCH$_2$CH$_2$OCH_2), 3.18 (br, 2H, C(O)NCH_2); ^{13}C NMR (150 MHz, $CDCl_3$) δ 164.11 (s), 129.44 (s), 69.99 (t), 69.59 (t), 67.79 (t), 66.44 (t), 39.76 (t), 38.75 (t); IR (neat) 3450, 2970, 1726, 1205 cm^{-1}; HRMS (CI) calcd for $C_{10}H_{16}N_2O_4Br_2$ $[M+H]^+$ 384.9399, observed 384.9402.

6.2.2 Route 2 to mono- and di- bromomaleimides

2,3-dibromo-maleic anhydride[69] 90

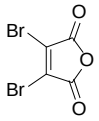

Under an inert atmosphere, a solution of maleic anhydride (1.50 g, 15.3 mmol, 1 eq), aluminium trichloride (300 mg, 0.21 mmol, cat.) and bromine (4.95 g, 30.6 mmol, 2 eq) was heated at 160 °C in a sealed ampule (*note* - *blast shield*) for 16 h. Upon cooling to 21 °C the reaction mixture was stirred for a further 24 h and carefully opened to air. EtOAc was added and the solid filtered off and repeatedly washed with further EtOAc. The filtrate was finally concentrated *in vacuo* to give the title compound **90** was a yellow solid which was used without further purification (3.05 g, 11.9 mmol, 78% yield). m.p 107-110 °C; ^{13}C NMR (150 MHz, CD_3OD) δ 163.33 (s),

125.28 (s); IR (MeOH) 1769, 1706, 1590 cm^{-1}; HRMS (CI) calcd for $C_4O_3Br_2$ $[M]^+$ 253.82087, 253.82082 observed.

3-(3,4-Dibromo-2,5-dioxo-2,5-dihydro-pyrrol-1-yl)-propionic acid 91

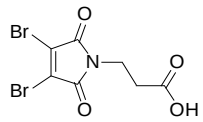

A mixture of *β*-alanine (1.00 g, 11.2 mmol, 1 eq) and 2,3-dibromo-maleic anhydride **90** (2.84 g, 11.2 mmol, 1eq) in AcOH (10 mL) was heated to 150 °C for 3 h. The reaction mixture cooled to 21 °C and the precipitate filtered off and recrystallised in hot EtOAc to yield product **91** as a yellow solid (2.85 g, 8.74 mmol, 78%). m.p. > 250 °C (dec); ^{1}H NMR (500 MHz, DMSO-d6) δ 12.38 (s, 1H, OH), 3.67 (t, J = 7.0 Hz, 2H, CH_2), 2.53 (t, J = 7.0 Hz, 2H, CH_2); ^{13}C NMR (125 MHz, DMSO-d6) δ 171.96 (s), 164.00 (s), 129.24 (s), 35.00 (t), 32.07 (t); IR (MeOH) 3363, 2800, 1725 cm^{-1}; HRMS (CI) calcd for $C_7H_6NO_4Br_2$ $[M+H]^+$ 325.86636, observed 325.86743.

6.2.3 Route 3 to mono- and di- bromomaleimides

***tert*-Butyl *N*-(2-(2-(2-aminoethoxy)ethoxy)ethyl)carbamate[82] 75**

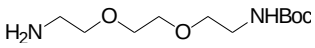

A solution of di-*tert*-butyl-dicarbonate (1.10 g, 5.00 mmol, 1 eq) in CH_2Cl_2 (5 mL) was added dropwise to a solution of 2-[2-(2-aminoethoxy)ethoxy]ethanamine (7.32 mL, 50.0 mmol, 10 eq) in CH_2Cl_2 (15 mL). The resulting reaction mixture was stirred at 21 °C for 24 h. The CH_2Cl_2 was then removed *in vacuo* to leave a colourless residue. Addition of EtOAc (125 mL) caused formation of a white precipitate, which was washed with a saturated solution of Na_2CO_3 (3 x 50 mL), dried over $MgSO_4$, and concentrated *in vacuo*. Further purification by column chromatography (8:2 CH_2Cl_2/MeOH) furnished the desired monoprotected amine **75** as a colourless oil (0.69 g, 2.80 mmol, 56% yield). ^{1}H NMR (500 MHz, $CDCl_3$) δ 5.27 (bs, 1H, N*H*), 3.54-3.52 (m, 4H, OCH_2), 3.47-3.42 (m, 4H, OCH_2), 3.23-3.22 (m, 2H, NCH_2), 2.80 (t, J = 5.0, 2H, NCH_2), 2.05 (bs, 2H, N*H*), 1.35 (s, 9H, CH_3);

^{13}C NMR (125 MHz, $CDCl_3$) δ 156.08 (s), 79.09 (s), 73.19 (t), 70.21 (t), 70.16 (t), 41.59 (t), 40.32 (t), 28.40 (q), * 1 *t* missing; IR (neat) 3344, 2869, 1692 cm^{-1}; HRMS (CI) calcd for $C_{11}H_{25}N_2O_4$ $[M + H]^+$ 249.18143, observed 249.18251.

tert-Butyl-_N_-(2-(2-(2-(5-(2-oxo-1,3,3a,4,6,6a-hexahydrothieno(3,4-d)imidazol-6-yl)pentanoylamino)ethoxy)ethoxy)ethyl)carbamate[83] 92

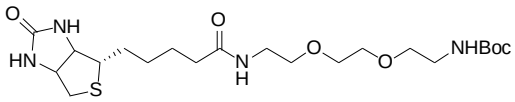

A solution of biotin (0.59 g, 2.42 mmol, 1.5 eq), HBTU (0.79 g, 2.10 mmol, 1.3 eq) and DIEA (0.45 mL, 2.60 mmol, 1.6 eq) in DMF (15 mL) was stirred for 20 min at 21 °C before being added dropwise to a solution of *tert*-butyl-*N*-(2-(2-(2-aminoethoxy)ethoxy)ethyl)carbamate **75** (400 mg, 1.61 mmol, 1 eq) in DMF (10 mL). The reaction mixture was stirred for 2 h at 21 °C, after which the DMF was removed *in vacuo* to give a yellow residue. The crude product was purified by column chromatography (gradient 2-10% MeOH/CH_2Cl_2) to yield **92** as a white solid (0.61 g, 1.29 mmol, 80% yield). m.p. 106-108 °C; $[\alpha]_D^{20.0}$ +23.0 (*c* 0.6, CH_2Cl_2); ^{1}H NMR (500 MHz, $CDCl_3$) δ 4.55 (dd, J = 5.0, 7.5 Hz, 1H, NHC(O)NHC*H*), 4.36 (dd, J = 5.0, 7.5 Hz, 1H, NHC(O)NHC*H*), 3.62 (bs, 6H, OCH_2), 3.59-3.55 (m, 2H, OCH_2), 3.46 (m, 2H, NCH_2), 3.31 (m, 2H, NCH_2), 3.17 (dt, 3.0, 5.0 Hz, 1H, SC*H*), 2.92 (dd, J = 5.0, 13.0 Hz, 1H, SCH*H*), 2.79 (d, J = 13.0 Hz, 1H, SC*H*H), 2.27 (t, J = 7.0 Hz, 2H, NHC(O)CH_2CH$_2$CH$_2$), 1.71 (m, 4H, NHC(O)CH$_2$CH_2CH_2CH$_2$), 1.47 (br, 11H, C(CH_3)$_3$ & NHC(O)CH$_2$CH$_2$CH$_2$CH_2); ^{13}C NMR (125 MHz, $CDCl_3$) δ 173.69 (s), 163.92 (s), 155.99 (s), 79.14 (s), 70.03 (t), 69.69 (br t), 61.58 (d), 60.06 (d), 55.19 (d), 40.16 (t), 39.96 (t), 38.91 (t), 35.44 (t), 28.09 (q), 27.80 (t), 27.67 (t), 25.23 (t), * 2 t absent; IR (neat) 3307, 2933, 1691 cm^{-1}; HRMS (ES) calcd for $C_{21}H_{38}N_4O_6NaS$ $[M+Na]^+$ 497.2410, observed 497.2423.

2-(2-(2-(5-(2-oxo-1,3,3a,4,6,6a-hexahydrothieno(3,4-d)imidazol-6-yl)pentanoylamino)ethoxy)ethoxy)ethylammonium; 2,2,2-trifluoroacetate[83] 93

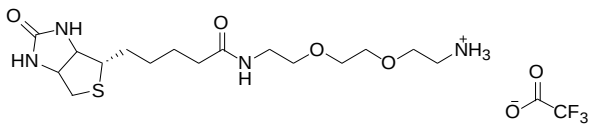

A solution of *tert*-butyl *N*-(2-(2-(2-(5-(2-oxo-1,3,3a,4,6,6a-hexahydrothieno(3,4-d)imidazol-6-yl)pentanoylamino)ethoxy)ethoxy)ethyl)carbamate **92** (0.61 g, 1.29 mmol) in CH_2Cl_2 (5 mL) and TFA (5 mL) was stirred at 21 °C for 24 h. Toluene was then added (x2) and the solvent removed *in vacuo* to yield **93** as an oil (0.63 g , 1.29 mmol, 100% yield). $[\alpha]_D^{20.0}$ +41.0 (*c* 0.49, MeOH); ^{1}H NMR (400 MHz, CD_3OD) δ 4.53 (dd, J = 5.0, 7.5 Hz, 1H, NHC(O)NHC*H*), 4.33 (dd, J = 5.0, 7.5 Hz, 1H, NHC(O)NHC*H*), 3.71 (t, J = 5.0 Hz, 2H, $OCH_2CH_2NH_3$), 3.65 (br, 4H, OCH_2), 3.57 (t, J = 5.0 Hz, 2H, OCH_2), 3.38 (t, J = 5.0 Hz, 2H, OCH_2), 3.22 (dt, J = 5.0, 8.5 Hz, 1H, SC*H*), 3.13 (t, J = 5.0 Hz, 2H, $C(O)NHCH_2CH_2O$), 2.94 (dd, J = 5.0, 13.0 Hz, 1H, SCH*H*), 2.74 (d, J = 13.0 Hz, 1H, SC*H*H), 2.24 (t, J = 7.5 Hz, 2H, $NHC(O)CH_2CH_2CH_2$), 1.76-1.43 (m, 6H, $NHC(O)CH_2CH_2CH_2CH_2$); ^{13}C NMR (100 MHz, CD_3OD) δ 174.98 (s), 164.76 (s), 69.92 (t), 69.83 (t), 69.22 (t), 66.46 (t), 62.08 (d), 60.36 (d), 55.59 (d), 39.65 (t), 39.24 (t), 38.77 (t), 35.29 (t), 28.29 (t), 28.06 (t), 25.44 (t); IR (MeOH) 3300, 2941, 1686 cm^{-1}; HRMS (ES) calcd for $C_{16}H_{31}N_4O_4S$ $[M+H]^+$ 375.2066, observed 375.2060.

***N*-(2-(2-(2-(3,4-dibromo-2,5-dioxo-pyrrol-1-yl)ethoxy)ethoxy)ethyl)-5-(2-oxo-1,3,3a,4,6,6a-hexahydrothieno(3,4-d)imidazol-6-yl)pentanamide 60**

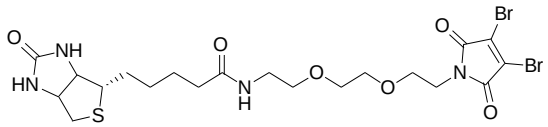

Dibromomaleic anhydride **90** (108 mg, 0.42 mmol, 1 eq) was added in one portion to a solution of 2-(2-(2-(5-(2-oxo-1,3,3a,4,6,6a-hexahydrothieno(3,4-d)imidazol-6-yl)pentanoylamino)ethoxy)ethoxy)ethylammonium 2,2,2-trifluoroacetate **93** (205 mg, 0.42 mmol, 1 eq) in AcOH (10 mL) and the reaction mixture heated to 170 °C for 2 h. Upon cooling to 21 °C toluene was added and the AcOH azeotropically removed *in vacuo* (x2) to give crude product. Column chromatography (gradient 2-7% MeOH/CH_2Cl_2) yielded pure product **60** as a white solid (123 mg, 0.20 mmol, 48% yield). m.p. 100-102 °C; $[\alpha]_D^{20.0}$ +71.0 (*c* 0.15, MeOH); ^{1}H NMR (600 MHz, CD_3OD) δ 4.53 (dd, J = 5.0, 8.0 Hz, 1H, NHC(O)NHC*H*), 4.34 (dd, J = 5.0, 8.0 Hz, 1H, NHC(O)NHC*H*), 3.82 (t, J = 5.5 Hz, 2H, OCH_2), 3.70 (t, J = 5.5 Hz, 2H, OCH_2), 3.63 (m, 2H, OCH_2), 3.59 (m, 2H, OCH_2), 3.53 (t, J = 5.5 Hz, 2H, NCH_2), 3.37 (t, J

= 5.5 Hz, 2H, NCH_2), 3.24 (dt, J = 5.0, 8.0 Hz, 1H, SC*H*), 2.96 (dd, J = 5.0, 13.0 Hz, 1H, SCH*H*), 2.73 (d, J = 13.0 Hz, 1H, SC*H*H), 2.26 (t, J = 7.5 Hz, 2H, NHC(O)CH_2CH$_2$CH$_2$), 1.74 (m, 4H, CH_2CH$_2$CH_2), 1.49 (quintet, J = 7.5 Hz, 2H, CH$_2$CH_2CH$_2$); ^{13}C NMR (150 MHz, CD_3OD) δ 174.83 (s), 164.71 (s), 164.06 (s), 129.00 (s), 69.80 (t), 69.72 (t), 69.24 (t), 67.19 (t), 61.97 (d), 60.22 (d), 55.64 (d), 39.67 (t), 39.03 (t), 38.56 (t), 35.42 (t), 28.39 (t), 28.11 (t), 25.47 (t); IR (MeOH) 2970, 1724, 1365, 1217 cm^{-1}; HRMS (ES) calcd for $C_{20}H_{28}N_4O_6NaSBr_2$ $[M+Na]^+$ 631.9916, observed 631.9937.

_N_-(2-(2-(2-(3-bromo-2,5-dioxo-pyrrol-1-yl)ethoxy)ethoxy)ethyl)-5-(2-oxo-1,3,3a,4,6,6a-hexahydrothieno(3,4-d)imidazol-6-yl)pentanamide 61

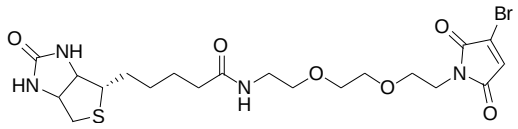

Monobromomaleic anhydride (45.0 mg, 0.25 mmol, 1 eq) was added in one portion to a solution of 2-(2-(2-(5-(2-oxo-1,3,3a,4,6,6a-hexahydrothieno(3,4-d)imidazol-6-yl)pentanoylamino)ethoxy)ethoxy)ethylammonium 2,2,2-trifluoroacetate **93** (124 mg, 0.25 mmol, 1 eq) in AcOH (10 mL) and the reaction mixture heated to 170 °C for 3 h. Upon cooling to 21 °C toluene was added and the AcOH azeotropically removed *in vacuo* (x2) to give crude product. Column chromatography (gradient 2-10% MeOH/CH_2Cl_2) yielded **61** as a white solid (70.0 mg, 0.13 mmol, 52% yield). m.p. 95-98 °C; $[\alpha]_D^{20.0}$ +65.1 (*c* 0.15, MeOH); ^{1}H NMR (600 MHz, CD_3OD) δ 7.17 (s, 1H, C*H*CBr), 4.51 (dd, J = 5.0, 8.0 Hz, 1H, NHC(O)NHC*H*), 4.33 (dd, J = 5.0, 8.0 Hz, 1H, NHC(O)NHC*H*), 3.77 (t, J = 5.5 Hz, 2H, OCH_2), 3.68 (t, J = 5.5 Hz, 2H, OCH_2), 3.63 (m, 2H, OCH_2), 3.58 (m, 2H, OCH_2), 3.53 (t, J = 5.5 Hz, 2H, NCH_2), 3.37 (t, J = 5.5 Hz, 2H, NCH_2), 3.24 (td, J = 5.0, 8.0 Hz, 1H, SC*H*), 2.95 (dd, J = 5.0, 12.5 Hz, 1H, SCH*H*), 2.73 (d, J = 12.5 Hz, 1H, SC*H*H), 2.26 (t, J = 7.0 Hz, 2H, NHC(O)CH_2CH$_2$CH$_2$), 1.69 (m, 4H, CH_2CH$_2$CH_2), 1.47 (quintet, J = 7.0 Hz, 2H, CH$_2$CH_2CH$_2$); ^{13}C NMR (150 MHz, CD_3OD) δ 176.12 (s), 170.13 (s), 166.97 (s), 166.08 (s), 133.63 (s), 132.05 (d), 71.22 (t), 71.11 (t), 70.61 (t), 68.69 (t), 63.35 (d), 61.61 (d), 57.03 (d), 41.09 (t), 40.31 (t), 39.09 (t), 36.75 (t), 29.78 (t), 29.50 (t), 26.87

(t); IR (MeOH) 3355, 2970, 1737 cm^{-1}; HRMS (ES) calcd for $C_{20}H_{29}N_4O_6$ NaSBr $[M+Na]^+$ 555.0889, observed 555.0905.

6.2.4 Synthesis of fluorescein maleimide reagents

3,4-dibromo-1-(3',6'-dihydroxy-3-oxo-spiro(isobenzofuran-1,9'-xanthene)-5-yl)pyrrole-2,5-dione 62

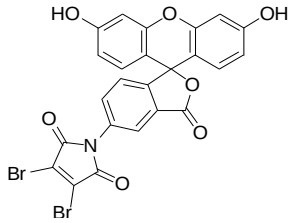

Dibromomaleic anhydride **90** (77.0 mg, 0.30 mmol, 1 eq) was added in one portion to a solution of fluoresceinamine (105 mg, 0.30 mmol, 1 eq) in AcOH (10 mL) and the reaction mixture was stirred for 6 h at 21 ºC. The solid was then filtered off, washed with EtOAc, and redissolved in AcOH (10 mL). The reaction mixture was then heated to 170 °C for 3 h. Upon cooling to 21 °C toluene was added and the AcOH azeotropically removed *in vacuo* (x2) to give **62** as an orange solid (148 mg, 0.25 mmol, 84% yield). m.p. > 220 °C (dec); ^{1}H NMR (400 MHz, CD_3OD) δ 8.07 (d, J = 1.5 Hz, 1H, Ar*H*), 7.82 (dd, J = 1.5, 8.0 Hz, 1H, Ar*H*), 7.34 (d, J = 8.0 Hz, 1H, Ar*H*), 6.71 (d, J = 2.5 Hz, 2H, Ar*H*), 6.59 (d, J = 9.0 Hz, 2H, Ar*H*), 6.57 (dd, J = 2.5, 9.0 Hz, 2H, Ar*H*); ^{13}C NMR (150 MHz, CD_3OD) δ 170.23 (s), 164.34 (s), 161.63 (s), 154.18 (s), 152.93 (s), 134.59 (s), 134.19 (d), 131.01 (s), 130.35 (d), 129.25 (s), 126.25 (d), 123.63 (d), 113.84 (d), 111.02 (s), 103.55 (d), * 1 s absent; IR (MeOH) 3063, 2924, 1725, 1588 cm^{-1}; HRMS (ES) calcd for $C_{24}H_{12}NO_7Br_2$ $[M+H]^+$ 583.8980, observed 583.8964.

3-bromo-1-(3',6'-dihydroxy-3-oxo-spiro(isobenzofuran-1,9'-xanthene)-5-yl)pyrrole-2,5-dione 63

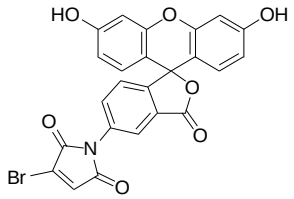

Monobromomaleic anhydride (77.0 mg, 0.30 mmol, 1 eq) was added in one portion to a solution of fluoresceinamine (105 mg, 0.30 mmol, 1 eq) in AcOH (10 mL) and the reaction mixture was stirred for 24 h at 21 °C. The solid was then filtered off, washed with EtOAc, and redissolved in AcOH (10 mL). The reaction mixture was then heated to 170 °C for 3 h. Upon cooling to 21 °C toluene was added and the AcOH azeotropically removed *in vacuo* (x2) to give **63** as a yellow solid (98.0 mg, 0.19 mmol, 65% yield). m.p. > 220 °C (dec); ^{1}H NMR (600 MHz, CD_3OD) δ 8.00 (d, J = 1.5 Hz, 1H, Ar*H*), 7.78 (dd, J = 1.5, 8.0 Hz, 1H, Ar*H*), 7.73 (s, 1H, C*H*), 7.44 (d, J = 8.0 Hz, 1H, Ar*H*), 6.69 (d, J = 2.0 Hz, 2H, Ar*H*), 6.62 (d, J = 8.5 Hz, 2H, Ar*H*), 6.59 (dd, J = 2.0, 8.5 Hz, 2H, Ar*H*); ^{13}C NMR (150 MHz, CD_3OD) δ 168.36 (s), 168.07 (s), 164.91 (s), 160.06 (s), 152.23 (s), 151.95 (s), 134.10 (s), 133.46 (d), 133.33 (s), 131.36 (d), 129.58 (s), 127.58 (d), 125.25 (s), 122.73 (d), 113.21 (d), 109.52 (s), 102.74 (d), * 1 d absent; IR (MeOH) 3063, 2449, 1722, 1578 cm^{-1}; HRMS (ES) calcd for $C_{24}H_{13}NO_7Br$ $[M+H]^+$ 505.9875, observed 505.9852.

6.2.5 Studies on the chemical modification of Grb2 SH2 domain

General method for modification of Grb2 SH2 domain 37 with bromomaleimide reagent at pH 8

To a solution of Grb2-SH2 (L111C) **37** (100 μL, [protein] 2.0 mg/mL, 100 mM sodium phosphate, 150 mM NaCl, pH 8.0) at 0 °C was added bromomaleimide reagent (5 μL, 5.64 mM solution in DMF). The mixture was vortexed for 1 s then maintained at 0 °C for 2 h. Analysis using LCMS showed that Grb2-bromomaleimide-conjugate had been formed in quantitative yield.

General method for modification of Grb2 SH2 domain 37 with bromomaleimide reagent at pH 7

To a solution of Grb2-SH2 (L111C) **37** (100 μL, [protein] 1.1 mg/mL, 100 mM sodium phosphate, 150 mM NaCl, pH 7.0) at 0 °C was added bromomaleimide reagent (5 μL, 6.20 mM solution in DMF). The mixture was vortexed for 1 s then maintained at 0 °C for 2 h. Analysis using LCMS showed that Grb2-bromomaleimide-conjugate had been formed in quantitative yield.

General method for the BME mediated cleavage of Grb2-bromomaleimide conjugates at pH 8

The solution containing Grb2-bromomaleimide conjugate was treated with BME (5 μL, 282 mM solution in H_2O) at 0 °C. The mixture was vortexed for 1 s and maintained at 0 °C for 4 h, after which the mixture was analyzed by LCMS. Analysis showed that the Grb2-SH2 (L111C) **37** (mass = 14170) was formed in quantitative conversion.

General method for the BME mediated cleavage of Grb2-bromomaleimide conjugates at pH 7

The solution containing Grb2-bromomaleimide conjugate was treated with BME (5 μL, 155 mM solution in H_2O) at 0 °C. The mixture was vortexed for 1 s and maintained at 0 °C for 4 h, after which the mixture was analyzed by LCMS. Analysis showed that the Grb2-SH2 (L111C) **37** (mass = 14170) was formed in quantitative conversion.

6.2.6 Studies on the chemical modification of Somatostatin

General method for the bridging of somatostatin 112 with dibromomaleimide reagents

Lyophilized somatostatin (mass = 1638) was solubilized in buffer (50 mM sodium phosphate, pH 6.2, 40% MeCN, 2.5% DMF) to yield a concentration of 152.6 μM (0.25 mg/mL) and reduced with 1.1 equiv of TCEP for 1 h at 21 °C. Completeness of the reduction was confirmed by LCMS (mass = 1640); 1.1 equiv of dibromomaleimide reagent was added and the reaction maintained at 21 °C for 1 h. Quantitative insertion of the maleimide into the disulfide bond to give somatostatin-bridged-conjugate was confirmed by LCMS. *Note - Insertion of the fluorescein dibromomaleimide into the disulfide bond to give conjugate **113** was confirmed by LCMS (mass = 2066)* M^{+1} *peak of product above spectrometer threshold,* M^{+2} *(m/z = 1033) and* M^{+3} *(m/z = 689) clearly visualized]*.

General method for the BME mediated cleavage of somatostatin-bridged-conjugates

The solution of somatostatin-bridged-conjugate was treated with BME (100 equiv) and the reaction maintained at 21 °C for 1 h. Analysis by LCMS showed complete cleavage of the conjugate, yielding reduced somatostatin **114** (mass = 1640).

6.2.7 Synthetic route for Pd(IBu)(neopentyl)(Cl) dimer 143

Neopentyl Lithium[132]

Lithium wire (0.59 g, 84.4 mmol, 4.5 eq) was cut up into small segments, added to a schlenk tube and sealed under argon. Hexane (20 mL) was added, followed by neopentyl chloride (1.99 g, 18.8 mmol, 1 eq) and the reaction mixture stirred for 5 d at 60 °C under argon and reduced pressure. After this time, the purple solution was filtered through flame-dried celite and the solvent removed in vacuo to yield a white solid which was used without further purifaction (0.95 g, 12.2 mmol, 65%). ^{1}H NMR (400 MHz, C_6D_6) δ 1.12 (s, 9H, C(C*H*$_3$)$_3$), -0.68 (s, 2H, C*H*$_2$); ^{13}C NMR (400 MHz, C_6D_6) δ 37.00 (q), 26.31 (s), 23.32 (t). *Neopentyl lithium found to be too reactive to obtain MS and IR.*

Pd(1,5-COD)(neopentyl)(chloride)[132]

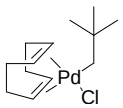

Pd(COD)Cl_2 (300 mg, 1.05 mmol) was placed in a schlenk tube and dried under vacuum for 1 h before use. It was then suspended in Et_2O (20 mL), cooled to -75 °C, covered in tin foil and neopentyl lithium (0.08 g, 1.05 mmol) in Et_2O (5 mL) added dropwise via cannula over a period of 1.5 h. The dark reaction mixture was stirred at -78 °C for a further 1 h and then slowly warmed to 21 °C over 1 h. The reaction mixture was then stirred at this 21 °C for 3 h. It was then filtered through flame-dried celite and the yellow-orange solvent removed in vacuo to yield product as a brown solid (0.16 g, 0.5 mmol, 48%). ^{1}H NMR (400 MHz, $CDCl_3$) δ 5.90 (q, J = 15

Hz, 2H, CH_2CH), 5.17 (q, J = 15 Hz, 2H, CH_2CH), 2.61 (m, 4H, $CHCH_2$), 2.44 (m, 4H, $CHCH_2$), 2.23 (s, 2H, CH_2), 1.13 (s, 9H, $C(CH_3)_3$); ^{13}C NMR (100 MHz, $CDCl_3$) δ 125.41 (d), 100.74 (d), 37.43 (s), 35.91 (q), 32.94 (t), 27.36 (t); LRMS (ES+) 285.1 $[M–Cl]^+$ 100%.

Pd(IBu)(neopentyl)(Cl) dimer[132] 143

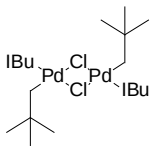

Pd(1,5-COD)(neopentyl)(chloride) (0.18 g, 0.5 mmol, 1 eq) was dissolved in THF (15 mL), cooled to 0 °C and IBu (0.09 g, 0.5 mmol, 1eq) in THF (5 mL) was added via cannula. The reaction mixture was stirred at 0 °C for 30 min, and then 21 °C for 15 min. The reaction mixture was filter cannulared to new a schlenk, the solvent removed *in vacou* and the residue washed with Et_2O (15 mL) and hexane (2x10 mL), to yield the desired product as a white powder (298 mg, 0.38 mmol, 76%). ^1H NMR (400 MHz, THF-d8) δ 7.39 (s, 2H, CH), 2.17 (s, 18H, $C(CH_3)_3$ - IBu), 1.43 (s, 2H, CH_2), 0.93 (s, 9H, $C(CH_3)_3$ – neopentyl); ^{13}C NMR (100 MHz, THF-d8) δ 170.00 (s), 118.20 (d), 59.11 (s), 35.21 (s), 31.9 (q), 29.89 (q); LRMS (CI) 500.0 [M-Cl, IBu, $CH_2C(CH_3)_3]^+$ 100%.

6.2.8 ^1H NMR reaction of Pd(IBu)(neopentyl)(Cl) dimer 143 and lithium morpholide

Pd(IBu)(neopentyl)(morpholide) 144

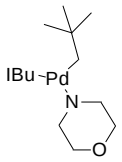

In a glove box lithium morpholide (8.00 mg, 0.08 mmol, 2 eq) was added to an NMR tube containing Pd(IBu)(neopentyl)(chloride) dimer **143** (32.0 mg, 0.04 mmol, 1 eq) and tetrakis(trimethylsilyl)silane (10.0 mg, 0.03 mol, 0.79 eq) in THF-d8 (1 mL) and

an ^{1}H NMR run after 10 min, 30 min, 60 min, 90 min, and there after at 30 min intervals. ^{1}H NMR shown in figure 30.

6.2.9 Synthesis of dansyl piperazine and *N*-dansyl-4-chlorobenzylamine

Piperazine-1-carboxylic acid *tert*-butyl ester 174

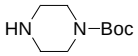

Di-*tert*-butyl-dicarbonate (4.05 g, 18.6 mmol) in acetic acid (15 mL) was added dropwise over 7 h to a stirred solution of piperazine (1.60 g, 18.6 mmol) in acetic acid (30 mL) at 21 °C and the resulting reaction mixture stirred for a further 15 h. The reaction mixture was then poured onto water, causing a precipitate to form (di-boc-protected piperazine 0.59 g, 3.15 mmol, 17% yield). The filtrate was basidified by addition of $NaOH_{(aq)}$, the organic material extracted into CH_2Cl_2, and then dried with $MgSO_4$. Filtration and removal of solvent *in vacuo* led to the isolation of desired piperazine-1-carboxylic acid *tert*-butyl ester **174** (2.84 g, 15.2 mmol, 82% yield) which was used without further purification. ^{1}H NMR (600 MHz, $CDCl_3$) δ 3.35 (t, J = 5.0 Hz, 4H, C(O)NC*H*$_2$CH$_2$), 2.78 (t, J = 5.0 Hz, 4H, C(O)NCH$_2$C*H*$_2$), 1.72 (bs, 1H, N*H*), 1.43 (s, 9H, C(C*H*$_3$)$_3$); ^{13}C NMR (125 MHz, $CDCl_3$) δ 155.0 (s), 79.8 (s), 45.6 (t), 28.5 (q),[*] *1 t absent*; IR (neat) 3331, 2976, 2860, 1682 cm^{-1}; HRMS (ES+) calcd for $C_9H_{19}N_2O_2$ $[M+H]^+$ 187.1447, observed 187.1450.

Piperazine-1,4-dicarboxylic acid benzyl ester *tert*-butyl ester[189] 175.

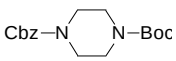

Benzyl chloroformate (0.51 g, 3.01 mmol) in CH_2Cl_2 (10 mL) was added to a stirred solution of piperazine-1-carboxylic acid *tert*-butyl ester **174** (0.51 g, 2.74 mmol) and NEt_3 (330 mg, 3.29 mmol) in CH_2Cl_2 (20 mL) at 0 °C under argon. The reaction mixture was then stirred at 21 °C for 1 h before being concentrated *in vacuo*. The resulting residue was taken up in EtOAc (30 mL) and washed sequentially with $KHSO_4$ (1M, 2 x 30 mL), $NaHCO_3$ (1M, 30 mL) and brine (15 mL). Drying with $MgSO_4$, followed by filtration and removal of solvent *in vacuo* led to the isolation of

the desired piperazine-1,4-dicarboxylic acid benzyl ester *tert*-butyl ester **175** (0.87 g, 2.74 mmol, 99% yield) which was used without further purification. ^{1}H NMR (600 MHz, $CDCl_3$) δ 7.32 (m, 5H, Ar*H*), 5.10 (s, 2H, NC(O)OC*H*$_2$), 3.39 (m, 4H, C(O)NCH$_2$C*H*$_2$NC(O)), 3.41 (m, 4H, C(O)NC*H*$_2$CH$_2$NC(O)), 1.42 (s, 9H); ^{13}C NMR (150 MHz, $CDCl_3$) δ 155.9 (s), 154.3 (s), 136.2 (s), 128.7 (d), 128.5 (d), 127.9 (d), 79.9 (s), 67.1 (t), 43.3 (bs, *note 2x t*), 28.4 (q); IR (neat) 2978, 2864, 2250, 1686, 1457, 1416 cm^{-1}; HRMS (ES+) calcd for $C_{17}H_{24}N_2O_4Na$ $[M+Na]^+$ 343.1634, observed 343.1635.

Trifluoro-acetate-4-benzyloxycarbonyl-piperazin-1-ium[189] 176

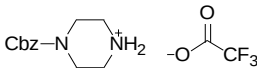

TFA (2.5 mL) was added dropwise to a stirred solution of piperazine-1,4-dicarboxylic acid benzyl ester *tert*-butyl ester **175** (0.87 g, 2.74 mmol) in CH_2Cl_2 (10 mL) at 0 °C. The reaction mixture was then stirred for 1 h at 21 °C and concentrated *in vacuo* affording trifluoro-acetate-4-benzyloxycarbonyl-piperazin-1-ium **176** (0.58 g, 2.65 mmol, 97% yield), which was used without further purification. ^{1}H NMR (600 MHz, $CDCl_3$) δ 7.28 (m, 5H, Ar*H*), 5.08 (s, 2H, NC(O)OC*H*$_2$), 3.71 (t, J = 5.0 Hz, 4H, C(O)NCH$_2$C*H*$_2$NH$_2^+$), 3.14 (bs, 4H, C(O)NC*H*$_2$CH$_2$NH$_2^+$), 2.27 (s, 1H, N*H*); ^{13}C NMR (125 MHz, $CDCl_3$) δ 154.9 (s), 135.6 (s), 129.2 (d), 128.8 (d), 128.3 (d), 68.5 (t), 43.7 (bs, *note 2x t*); IR (neat) 3034, 2839, 2496, 1670, 1431 cm^{-1}; HRMS (ES+) calcd for $C_{12}H_{17}N_2O_2$ $[M+H]^+$ 221.1290, observed 221.1291.

4-(5-dimethylamino-naphthalene-1-sulfonyl)-piperazine-1-carboxylic acid benzyl ester[188] 177

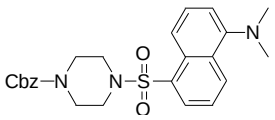

Dansyl chloride (1.22 g, 0.45 mmol) was added in one portion to a stirred solution of trifluoro-acetate-4-benzyloxycarbonyl-piperazin-1-ium **176** (0.10 g, 0.45 mmol), DMAP (3.00 mg, 0.03 mmol) and NEt_3 (46.0 mg, 0.46 mmol) in CH_2Cl_2 (25 mL) at 0 °C under argon. The now bright yellow reaction mixture was warmed to 21 °C and

stirred for 15 h. Distilled H_2O was added and the organic material extracted with CH_2Cl_2, which was then dried with $MgSO_4$. Filtration and removal of solvent *in vacuo* afforded desired 4-(5-dimethylamino-naphthalene-1-sulfonyl)-piperazine-1-carboxylic acid benzyl ester **177** (1.63 g, 0.36 mmol, 80% yield) which was used without further purification. ^{1}H NMR (500 MHz, $CDCl_3$) δ 8.56 (d, J = 8.5 Hz, 1H, Ar*H*), 8.38 (d, J = 8.5 Hz, 1H, Ar*H*), 8.19 (d, J = 8.5 Hz, 1H, Ar*H*), 7.54 (t, J = 7.5 Hz, 2H, Ar*H*), 7.31 (m, 5H, Ar*H*), 7.20 (d, J = 7.5 Hz, 1H, Ar*H*), 5.07 (s, 2H, NC(O)OC*H*$_2$), 3.54 (t, J = 5.0 Hz, 4H, C(O)NCH$_2$C*H*$_2$NSO$_2$), 3.18 (bs, 4H, C(O)NC*H*$_2$CH$_2$NSO$_2$), 2.90 (s, 6H, N(C*H*$_3$)$_2$); ^{13}C NMR (125 MHz $CDCl_3$) δ 171.2 (s), 151.9 (s), 136.3 (s), 132.5 (s), 131.0 (d), 130.8 (d), 130.4 (s), 130.1 (s), 128.6 (d), 128.3 (d), 128.1 (d), 123.3 (d), 119.5 (d), 115.4 (d), 67.5 (t), 45.5 (q), 43.5 (bs, *note 2x t*) * *1x d from dansyl absent*; IR (neat) 3457, 3016, 2970, 1739, 1435, 1366 cm^{-1}; HRMS (ES+) calcd for $C_{24}H_{28}N_3O_4S$ $[M+H]^+$ 454.1801, observed 454.1810.

Formate-4-(5-dimethylamino-naphthalene-1-sulfonyl)-piperazin-1-ium[188] 178

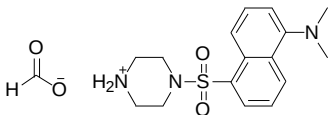

5% Palladium on carbon (160 mg) was added to a stirred solution of 4-(5-dimethylamino-naphthalene-1-sulfonyl)-piperazine-1-carboxylic acid benzyl ester **177** (1.00 g, 2.21 mmol) and formic acid (0.02 mL) in Et_2O (50 mL) and the reaction heated to 95 °C for 3 h. Following this the reaction mixture was cooled to 21 °C and filtered through a short plug of Celite, with copious washing by Et_2O to ensure all product flushed through. The filtrate was washed with distilled water, dried with $MgSO_4$, filtrated and the solvent removed *in vacuo* to afford **178** (0.67 g, 2.21 mmol, 100% yield) as a yellow solid. ^{1}H NMR (500 MHz, $CDCl_3$) δ 8.56 (d, J = 8.5 Hz, 1H, Ar*H*), 8.43 (d, J = 8.5 Hz, 1H, Ar*H*), 8.19 (dd, J = 1.0, 7.5 Hz, 1H, Ar*H*), 7.53 (dt, J = 2.0, 7.5 Hz, 2H, Ar*H*), 7.18 (d, J = 7.5 Hz, 1H, Ar*H*), 3.15 (t, J = 5.0 Hz, 4H, C(O)NCH$_2$C*H*$_2$NSO$_2$), 2.88 (bs, 10H, N(C*H*$_3$)$_2$ & C(O)NC*H*$_2$CH$_2$NSO$_2$), 1.63 (s, 2H, N*H*$_2$); ^{13}C NMR (125 MHz, $CDCl_3$) δ 151.7 (s), 132.7 (s), 130.7 (d), 130.6 (s), 130.13 (s), 128.0 (d), 123.2 (d), 119.9 (d), 115.3 (d), 46.5 (t), 45.6 (t), 45.5 (q), * *1 d absent*; IR (neat) 3292, 2947, 2849, 1454 cm^{-1}; HRMS (ES+) calcd for $C_{16}H_{22}N_3O_2S$ $[M+H]^+$ 320.1433, observed 320.1425.

5-Dimethylamino-naphthalene-1-sulfonic acid 4-chloro-benzylamide 179

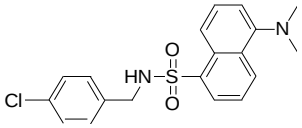

Dansyl chloride (0.72 g, 2.67 mmol) was added in one portion to a stirred solution of 4-chloro-benzylamine (0.38 g, 2.67 mmol), DMAP (17.0 mg, 0.13 mmol) and NEt_3 (0.41 mL, 2.94 mmol) in CH_2Cl_2 (30 mL) at 0 °C. The reaction mixture was then warmed to 21 °C and stirred for 15 h. Distilled H_2O was added and the organic material extracted into CH_2Cl_2, which was then dried with $MgSO_4$. Filtration and removal of solvent *in vacuo* then afforded **179** (0.85 g, 2.30 mmol, 85% yield) as a yellow solid. ^{1}H NMR (500 MHz, $CDCl_3$) δ 8.54 (d, J = 8.5 Hz, 1H, Ar*H*), 8.25 (m, 2H, Ar*H*), 7.56 (t, J = 8.0 Hz, 1H, Ar*H*), 7.50 (t, J = 8.0 Hz, 1H, Ar*H*), 7.20 (d, J = 7.5 Hz, 1H, Ar*H*), 7.09 (d, J = 8.5 Hz, 2H, Ar*H*), 6.97 (d, J = 8.5 Hz, 2H, Ar*H*), 4.05 (d, J = 6.5 Hz, 2H, $S(O)_2NHCH_2$), 2.91 (s, 6H, $N(CH_3)_2$); ^{13}C NMR (125 MHz, $CDCl_3$) δ 151.0 (s), 134.6 (s), 133.6 (s), 132.0 (s), 130.7 (d), 130.0 (d), 129.9 (s), 129.2 (d), 128.6 (d), 128.0 (s), 123.2 (d), 118.6 (d), 115.2 (d), 46.7 (t), 45.5 (q), * *1 d absent*; IR (neat) 3286, 2971, 1738 cm^{-1}; HRMS (ES+) calcd for $C_{19}H_{20}N_2O_2SCl$ $[M+H]^+$ 375.0934, observed 375.0930.

6.2.10 General procedure for Pd catalysed aryl amination reaction

$Pd(IBu)_2$ (3.00 mg) was added in one portion to a stirred solution of amine (0.10 mmol), aryl halide (0.10 mmol) and KO^tBu (0.12 mmol) in toluene (5 mL) under argon and the reaction mixture heated to 60 °C for 24 h. The reaction mixture was then filtered through Celite. Distilled water (5 mL) was added and the organic layer separated, washed with brine, dried with $MgSO_4$, filtered and concentrated to yield product.

Dimethyl-(5-(4-*p*-tolyl-piperazine-1-sulfonyl)-naphthalen-1-yl)-amine[188] 180

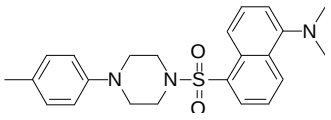

Product isolated as a yellow solid, 32.0 mg, 0.08 mmol, 80% yield.

^{1}H NMR (500 MHz, $CDCl_3$) δ 8.56 (d, J = 8.5 Hz, 1H, Ar*H*), 8.45 (d, J = 8.5 Hz, 1H, Ar*H*), 8.23 (dd, J = 1.0, 7.5 Hz, 1H, Ar*H*), 7.53 (m, 2H, Ar*H*), 7.16 (d, J = 7.5 Hz, 1H, Ar*H*), 7.02 (d, J = 8.0 Hz, 2H, Ar*H*), 6.75 (bs, 2H, Ar*H*), 3.33 (bs, 4H, $C(O)NCH_2CH_2NSO_2$), 3.12 (bs, 4H, $C(O)NCH_2CH_2NSO_2$), 2.87 (s, 6H, $N(CH_3)_2$), 2.24 (s, 3H, CH_3); ^{13}C NMR (125 MHz $CDCl_3$) δ 151.2 (s), 132.5 (s), 130.9 (s), 130.8 (d), 130.6 (s), 130.1 (s), 129.8 (d), 128.1 (d), 123.3 (d), 119.9 (d), 117.3 (s), 115.4 (d), 50.0 (t), 45.7 (t), 45.5 (q), 29.8 (q) * *2x d absent*; IR (neat) 3300, 2944, 2832, 1574 cm^{-1}; HRMS (ES+) calcd for $C_{23}H_{28}N_3O_2S$ $[M+H]^+$ 410.1902, observed 410.1939.

5-Dimethylamino-naphthalene-1-sulfonic acid 4-morpholin-4-yl--benzylamide 186

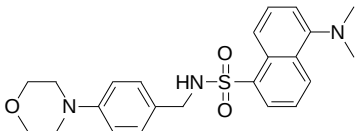

Product could not be obtained pure.

5-Dimethylamino-naphthalene-1-sulfonic acid 4-[4-(5-dimethylamino-naphthalene-1-sulfonyl)-piperazin-1-yl]-benzylamide 193

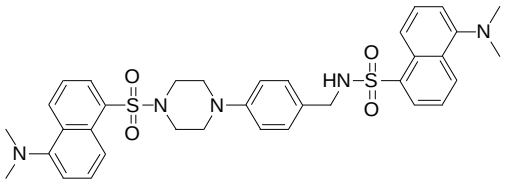

Product could not be obtained pure.

6.2.11 General procedure for ESI(+)-MS Pd catalysed aryl amination reaction

In a dry glove box $Pd(IBu)_2$ (3.00 mg) was added in one portion to an ampoule containing a solution of amine (0.10 mmol), aryl halide (0.10 mmol) and KO^tBu (14.0 mg, 0.12 mmol) in toluene (5 mL). The ampoule was then taken out of the glove box, attached to a schlenk line and heated to 60 °C. After 1, 2, 4, 8, and 24 h

intervals, 0.01 mL of reaction mixture was removed under a positive flow of argon, diluted with 0.99 mL of MeCN (HPLC grade) and injected directly into the ESI(+)-MS probe. This process was repeated at least three times for each time interval.

7 References

1. Alberts, B. J., A.; Lewis, J.; Raff, M.; Roberts, K.; Walter, P. *Molecular biology of the cell*. Garland Science: 2002.
2. Chalker, J. M.; Bernardes, G. J. L.; Lin, Y. A.; Davis, B. G. *Chem. Asian. J.* **2009**, 4, (5), 630.
3. de Graaf, A. J.; Kooijman, M.; Hennink, W. E.; Mastrobattista, E. *Bioconjugate. Chem.* **2009**, 20, (7), 1281.
4. Zhu, H.; Bilgin, M.; Bangham, R.; Hall, D.; Casamayor, A.; Bertone, P.; Lan, N.; Jansen, R.; Bidlingmaier, S.; Houfek, T.; Mitchell, T.; Miller, P.; Dean, R. A.; Gerstein, M.; Snyder, M. *Science.* **2001**, 293, (5537), 2101.
5. MacBeath, G.; Schreiber, S. L. *Science.* **2000**, 289, (5485), 1760.
6. King, H. D.; Dubowchik, G. M.; Walker, M. A. *Tetrahedron. Lett.* **2002**, 43, (11), 1987.
7. Griep, M. A.; Mesman, T. N. *Bioconjugate. Chem.* **1995**, 6, (6), 673.
8. Wong, L. S.; Khan, F.; Micklefield, J. *Chem.Rev.* **2009**, 109, (9), 4025.
9. Cheung, C. L.; Camarero, J. A.; Woods, B. W.; Lin, T. W.; Johnson, J. E.; De Yoreo, J. J. *J. Am. Chem. Soc.* **2003**, 125, (23), 6848.
10. Ferrero, V. E. V.; Andolfi, L.; Di Nardo, G.; Sadeghi, S. J.; Fantuzzi, A.; Cannistraro, S.; Gilardi, G. *Anal. Chem.* **2008**, 80, (22), 8438.
11. Strachan, E.; Mallia, A. K.; Cox, J. M.; Antharavally, B.; Desai, S.; Sykaluk, L.; O'Sullivan, V.; Bell, P. A. *J. Mol. Recognit.* **2004**, 17, (3), 268.
12. Ziegler, M.; Xiao, R.; Penefsky, H. S. *J. Biol. Chem.* **1994**, 269, (6), 4233.
13. Turina, P.; Capaldi, R. A. *J. Biol. Chem.* **1994**, 269, (18), 13465.
14. Aggeler, R.; Chicascruz, K.; Cai, S. X.; Keana, J. F. W.; Capaldi, R. A. *Biochemistry.* **1992**, 31, (11), 2956.
15. Skakoon, E. N.; Dunn, S. D. *Arch. Biochem. Biophys.* **1993**, 302, (1), 272.
16. Rana, T. M.; Meares, C. F. *J. Am. Chem. Soc.* **1990**, 112, (6), 2457.
17. Ermacora, M. R.; Delfino, J. M.; Cuenoud, B.; Schepartz, A.; Fox, R. O. *P. Natl. Acad. Sci. USA.* **1992**, 89, (14), 6383.
18. McLachlin, D. T.; Dunn, S. D. *Protein. Expres. Purif.* **1996**, 7, (3), 275.
19. Bernardes, G. J. L.; Chalker, J. M.; Errey, J. C.; Davis, B. G. *J. Am. Chem. Soc*. **2008**, 130, (15), 5052.

20. Chapman, C. J.; Hargrave, J. D.; Bish, G.; Frost, C. G. *Tetrahedron.* **2008**, 64, (40), 9528.
21. Chapman, C. J.; Matsuno, A.; Frost, C. G.; Willis, M. C. *Chem. Commun.* **2007**, (38), 3903.
22. Navarre, L.; Martinez, R.; Genet, J. P.; Darses, S. *J. Am. Chem. Soc.* **2008**, 130, (19), 6159.
23. Chapman, C. J.; Wadsworth, K. J.; Frost, C. G. *J. Organomet. Chem.* **2003**, 680, (1-2), 206.
24. Collier, P. N.; Campbell, A. D.; Patel, I.; Taylor, R. J. K. *Tetrahedron. Lett.* **2000**, 41, (36), 7115.
25. Tedaldi, L. M.; Smith, M. E. B.; Nathani, R. I.; Baker, J. R. *Chem. Commun.* **2009**, (43), 6583.
26. Hermanson, G. T. *Bioconjugate techniques*. Academic press: 1996.
27. Ellman, G. L. *Arch. Biochem. Biophys.* **1959**, 82, (1), 70.
28. Annis, I.; Chen, L.; Barany, G. *J. Am. Chem. Soc.* **1998**, 120, (29), 7226.
29. Nielsen, M. L.; Vermeulen, M.; Bonaldi, T.; Cox, J.; Moroder, L.; Mann, M. *Nat. Methods.* **2008**, 5, (6), 459.
30. Lundell, N.; Schreitmuller, T. *Anal. Biochem.* **1999**, 266, (1), 31.
31. Davis, N. J.; Flitsch, S. L. *Tetrahedron. Lett.* **1991**, 32, (46), 6793.
32. Macmillan, D.; Bill, R. M.; Sage, K. A.; Fern, D.; Flitsch, S. L. *Chem. Biol.* **2001**, 8, (2), 133.
33. Simon, M. D.; Chu, F. X.; Racki, L. R.; de la Cruz, C. C.; Burlingame, A. L.; Panning, B.; Narlikar, G. J.; Shokat, K. M. *Cell.* **2007**, 128, (5), 1003.
34. Smith, H. B.; Hartman, F. C. *J. Biol. Chem.* **1988**, 263, (10), 4921.
35. Vives, E.; Lebleu, B. *Tetrahedron. Lett.* **2003**, 44, (29), 5389.
36. Cardoza, J. D.; Kleinfeld, A. M.; Stallcup, K. C.; Mescher, M. F. *Biochemistry.* **1984**, 23, (19), 4401.
37. Konno, K.; Morales, M. F. *P. Natl. Acad. Sci. USA.* **1985**, 82, (23), 7904.
38. Bigelow, D. J.; Inesi, G. *Biochemistry.* **1991**, 30, (8), 2113.
39. Yen, T. Y.; Yan, H.; Macher, B. A. *J. Mass. Spectrom.* **2002**, 37, (1), 15.
40. Smyth, D. G.; Nagamatsu, A.; Fruton, J. S. *J. Am. Chem. Soc.* **1960**, 82, (17), 4600.
41. Stekhoven, F. S.; Bonting, S. L. *Physiol. Rev.* **1981**, 61, (1), 1.

42. Feng, Y.; Forgac, M. *J. Biol. Chem.* **1992**, 267, (9), 5817.
43. Deweille, J. R.; Muller, M.; Lazdunski, M. *J. Biol. Chem.* **1992**, 267, (7), 4557.
44. De Lorimier, R. M.; Tian, Y. J.; Hellinga, H. W. *Protein. Sci.* **2006**, 15, (8), 1936.
45. Misra, A. *Bioorgan. Med. Chem. Lett.* **2007**, 17, (13), 3749.
46. Hall, D. A.; Ptacek, J.; Snyder, M. *Mech. Ageing. Dev.* **2007**, 128, (1), 161.
47. Huang, J.; Zhu, H.; Haggarty, S. J.; Spring, D. R.; Hwang, H.; Jin, F. L.; Snyder, M.; Schreiber, S. L. *P. Natl. Acad. Sci. USA.* **2004**, 101, (47), 16594.
48. Zhu, H.; Snyder, M. *Curr. Opin. Chem. Biol.* **2001**, 5, (1), 40.
49. Kusnezow, W.; Hoheisel, J. D. *J. Mol. Recognit.* **2003**, 16, (4), 165.
50. Kusnezow, W.; Jacob, A.; Walijew, A.; Diehl, F.; Hoheisel, J. D. *Proteomics.* **2003**, 3, (3), 254.
51. Angenendt, P.; Glokler, J.; Murphy, D.; Lehrach, H.; Cahill, D. J. *Anal. Biochem.* **2002**, 309, (2), 253.
52. Charles, P. T.; Taitt, C. R.; Goldman, E. R.; Rangasammy, J. G.; Stenger, D. A. *Langmuir.* **2004**, 20, (1), 270.
53. Stillman, B. A.; Tonkinson, J. L. *Biotechniques.* **2000**, 29, (3), 630.
54. Zhu, H.; Snyder, M. *Curr. Opin. Chem. Biol.* **2003**, 7, (1), 55.
55. Dunn-Dufault, R.; Pollak, A.; Fitzgerald, J.; Thornback, J. R.; Ballinger, J. R. *Nucl. Med. Biol.* **2000**, 27, (8), 803.
56. Hnatowich, D. J. *Nucl. Med. Commun.* **1994**, 15, (8), 575.
57. Hnatowich, D. J.; Virzi, F.; Rusckowski, M. *J. Nucl. Med.* **1987**, 28, (8), 1294.
58. Reznik, G. O.; Vajda, S.; Cantor, C. R.; Sano, T. *Bioconjugate. Chem.* **2001**, 12, (6), 1000.
59. Lal, S. P.; Christopherson, R. I.; dos Remedios, C. G. *Drug. Discov. Today.* **2002**, 7, (18), S143.
60. Kissel, M.; Peschke, P.; Subr, V.; Ulbrich, K.; Strunz, A. M.; Kuhnlein, R.; Debus, J.; Friedrich, E. *Eur. J. Nucl. Med. Mol. I.* **2002**, 29, (8), 1055.
61. Rubin, R. H.; Fischman, A. J.; Needleman, M.; Wilkinson, R.; Callahan, R. J.; Khaw, B. A.; Hansen, W. P.; Kramer, P. B.; Strauss, H. W. *J. Nucl. Med.* **1989**, 30, (3), 385.

62. Goh, A. S. W.; Aw, S. E.; Sundram, F. X.; Ang, E. S.; Goh, S. K.; Leong, K. H. *Nucl. Med. Commun.* **1990**, 11, (12), 843.
63. Palmer, T. N.; Caride, V. J.; Caldecourt, M. A.; Twickler, J.; Abdullah, V. *Biochim. Biophys. Acta.* **1984**, 797, (3), 363.
64. Roberts, D. D.; Lewis, S. D.; Ballou, D. P.; Olson, S. T.; Shafer, J. A. *Biochemistry.* **1986**, 25, (19), 5595.
65. Gartner, C. A.; Elias, J. E.; Bakalarski, C. E.; Gygi, S. P. *J. Proteome. Res.* **2007**, 6, (4), 1482.
66. Smith, M. E. B.; Schumacher, F. F.; Ryan, C. P.; Tedaldi, L. M.; Papaioannou, D.; Waksman, G.; Caddick, S.; Baker, J. R. *J. Am. Chem. Soc.* **2010**, 132, (6), 1960.
67. Papaioannou, D. Thesis. University College London.
68. Cho, I. H.; Paek, E. H.; Lee, H.; Kang, J. Y.; Kim, T. S.; Paek, S. H. *Anal. Biochem.* **2007**, 365, (1), 14.
69. Dubernet, M.; Caubert, V.; Guillard, J.; Viaud-Massuard, M. C. *Tetrahedron.* **2005**, 61, (19), 4585.
70. Kalgutkar, A. S.; Crews, B. C.; Marnett, L. J. *J. Med. Chem.* **1996**, 39, (8), 1692.
71. Reddy, P. Y.; Kondo, S.; Fujita, S.; Toru, T. *Synthesis.* **1998**, (7), 999.
72. Reddy, P. Y.; Kondo, S.; Toru, T.; Ueno, Y. *J. Org. Chem.* **1997**, 62, (8), 2652.
73. Walker, M. A. *Tetrahedron. Lett.* **1994**, 35, (5), 665.
74. Sun, C. Z.; Wirsching, P.; Janda, K. D. *Bioorgan. Med. Chem.* **2003**, 11, (8), 1761.
75. Schwartz, A. L.; Lerner, L. M. *J. Org. Chem.* **1974**, 39, (1), 21.
76. Pfeifer, S.; Lutz, J. F. *Chem. Eur. J.* **2008**, 14, (35), 10949.
77. Bilitewski, U. *Anal. Chim. Act.* **2006**, 568, (1-2), 232.
78. Mehrvar, M.; Bis, C.; Scharer, J. M.; Moo-Young, M.; Luong, J. H. *Anal. Sci.* **2000**, 16, (7), 677.
79. Misra, A.; Dwivedi, P. *Anal. Biochem.* **2007**, 369, (2), 248.
80. Tang, W.; Fang, S. Y. *Tetrahedron. Lett.* **2008**, 49, (41), 6003.
81. Lebeau, L.; Oudet, P.; Mioskowski, C. *Helv. Chim. Acta.* **1991**, 74, (8), 1697.

82. Guy, J.; Caron, K.; Dufresne, S.; Michnick, S. W.; Skene, W. G.; Keillor, J. W. *J. Am. Chem. Soc.* **2007**, 129, (39), 11969.
83. Trester-Zedlitz, M.; Kamada, K.; Burley, S. K.; Fenyo, D.; Chait, B. T.; Muir, T. W. *J. Am. Chem. Soc.* **2003**, 125, (9), 2416.
84. McKay, A. R. Personal communication. In 2010.
85. Daniel, J. M.; Friess, S. D.; Rajagopalan, S.; Wendt, S.; Zenobi, R. *Int. J. Mass. Spectrom.* **2002**, 216, (1), 1.
86. Jecklin, M. C.; Schauer, S.; Dumelin, C. E.; Zenobi, R. *J. Mol. Recognit.* **2009**, 22, (4), 319.
87. Santos, L. S. *Eur. J. Org. Chem.* **2008**, (2), 235.
88. http://www.ncsu.edu/labwrite/res/gt/gt-stat-home.html
89. Diedrich, F.; Stang, P. J. *Metal-catalysed cross-coupling reactions*. Wiley-VCH: Weinheim: 1998.
90. Tsuji, J., *Palladium reagents and catalysts*. Wiley: Chichester: 1995.
91. Bellina, F.; Carpita, A.; Rossi, R. *Synthesis.* **2004**, (15), 2419.
92. Miyaura, N.; Suzuki, A. *Chem.Rev.* **1995**, 95, (7), 2457.
93. Suzuki, A. *J. Organomet. Chem.* **1999**, 576, (1-2), 147.
94. O'Brien, C. J.; Kantchev, E. A. B.; Valente, C.; Hadei, N.; Chass, G. A.; Lough, A.; Hopkinson, A. C.; Organ, M. G. *Chem. Eur. J.* **2006**, 12, (18), 4743.
95. Organ, M. G.; Avola, S.; Dubovyk, I.; Hadei, N.; Kantchev, E. A. B.; O'Brien, C. J.; Valente, C. *Chem. Eur. J.* **2006**, 12, (18), 4749.
96. Beletskaya, I. P.; Cheprakov, A. V. *Chem.Rev.* **2000**, 100, (8), 3009.
97. Hartwig, J. F. *Accounts. Chem. Res.* **1998**, 31, (12), 852.
98. Tamao, K.; Sumitani, K.; Kumada, M. *J. Am. Chem. Soc.* **1972**, 94, (12), 4374.
99. Wolfe, J. P.; Wagaw, S.; Marcoux, J. F.; Buchwald, S. L. *Accounts. Chem. Res.* **1998**, 31, (12), 805.
100. Arentsen, K.; Caddick, S.; Cloke, F. G. N. *Tetrahedron.* **2005**, 61, (41), 9710.
101. Caddick, S.; Geoffrey, F.; Cloke, N.; Hitchcock, P. B.; Leonard, J.; Lewis, A. K. D.; McKerrecher, D.; Titcomb, L. R. *Organometallics.* **2002**, 21, (21), 4318.

102. Lewis, A. K. D.; Caddick, S.; Esposito, O.; Cloke, F. G. N.; Hitchcock, P. B. *Dalton. T.* **2009**, (35), 7094.
103. Sclosser, M. H., L. S.; Lipshutz, B. H.; Marshall, J. A.; Nakamura, E.; Negishi, E.; Reetz, M. T.; Semmelhack, M. F.; Smith, K.; Yamamoto, H. *Organometallics in synthesis; a manual*. Wiley: 2004.
104. Hillier, A. C.; Grasa, G. A.; Viciu, M. S.; Lee, H. M.; Yang, C. L.; Nolan, S. P. *J. Organomet. Chem.* **2002**, 653, (1-2), 69.
105. Hartwig, J. F. *Inorg. Chem.* **2007**, 46, (6), 1936.
106. Parshall, G. W. I., S D. *Homogeneous catalysis, the applications and chemistry of catalysis by soluble transition metal complexes*. Wiley. New York: 1992.
107. Herrmann, W. A.; Ofele, K.; Von Preysing, D.; Schneider, S. K. *J. Organomet. Chem.* **2003**, 687, (2), 229.
108. Wanzlick, H. W.; Schonher, H. J. *Ange. Chem. Int. Ed.* **1968**, 7, (2), 141.
109. Arduengo, A. J.; Harlow, R. L.; Kline, M. *J. Am. Chem. Soc.* **1991**, 113, (1), 361.
110. Herrmann, W. A. *Ange. Chem. Int. Ed.* **2002**, 41, (8), 1290.
111. Herrmann, W. A.; Mihalios, D.; Ofele, K.; Kiprof, P.; Belmedjahed, F. *Chem. Ber. Recl.* **1992**, 125, (8), 1795.
112. Jafarpour, L.; Stevens, E. D.; Nolan, S. P. *J. Organomet. Chem.* **2000**, 606, (1), 49.
113. Tafipolsky, M.; Scherer, W.; Ofele, K.; Artus, G.; Pedersen, B.; Herrmann, W. A.; McGrady, G. S. *J. Am. Chem. Soc.* **2002**, 124, (20), 5865.
114. Huang, J. K.; Schanz, H. J.; Stevens, E. D.; Nolan, S. P. *Organometallics.* **1999**, 18, (12), 2370.
115. Bourissou, D.; Guerret, O.; Gabbai, F. P.; Bertrand, G. *Chem.Rev.* **2000**, 100, (1), 39.
116. Hu, X. L.; Castro-Rodriguez, I.; Olsen, K.; Meyer, K. *Organometallics.* **2004**, 23, (4), 755.
117. Hu, X. L.; Tang, Y. J.; Gantzel, P.; Meyer, K. *Organometallics.* **2003**, 22, (4), 612.
118. Fantasia, S.; Petersen, J. L.; Jacobsen, H.; Cavallo, L.; Nolan, S. P. *Organometallics.* **2007**, 26, (24), 5880.

119. Green, J. C.; Herbert, B. J.; Lonsdale, R. *J. Organomet. Chem.* **2005**, 690, (24-25), 6054.
120. Lewis, A. K. D.; Caddick, S.; Cloke, F. G. N.; Billingham, N. C.; Hitchcock, P. B.; Leonard, J. *J. Am. Chem. Soc.* **2003**, 125, (33), 10066.
121. Cawley, M. J.; Cloke, F. G. N.; Fitzmaurice, R. J.; Pearson, S. E.; Scott, J. S.; Caddick, S. *Org. Biomol. Chem.* **2008**, 6, (15), 2820.
122. Saito, B.; Fu, G. C. *J. Am. Chem. Soc.* **2007**, 129, 9602.
123. Saito, B.; Fu, G. C. *J. Am. Chem. Soc.* **2008**, 130, (21), 6694.
124. Zhou, J. R.; Fu, G. C. *J. Am. Chem. Soc.* **2003**, 125, (48), 14726.
125. Zhou, J. R.; Fu, G. C., *J. Am. Chem. Soc.* **2003**, 125, (41), 12527.
126. Devasagayaraj, A.; Studemann, T.; Knochel, P. *Ange. Chem. Int. Ed.* **1995**, 34, (23-24), 2723.
127. Terao, J.; Ikumi, A.; Kuniyasu, H.; Kambe, N. *J. Am. Chem. Soc.* **2003**, 125, (19), 5646.
128. Terao, J.; Watanabe, H.; Ikumi, A.; Kuniyasu, H.; Kambe, N. *J. Am. Chem. Soc.* **2002**, 124, (16), 4222.
129. Frisch, A. C.; Shaikh, N.; Zapf, A.; Beller, M. *Ange. Chem. Int. Ed.* **2002**, 41, (21), 4056.
130. Macgregor, S. A.; Neave, G. W.; Smith, C. *Faraday. Discuss.* **2003**, 124, 111.
131. Esposito, O.; Gois, P. M. P.; Lewis, A.; Caddick, S.; Cloke, F. G. N.; Hitchcock, P. B. *Organometallics.* **2008**, 27, (24), 6411.
132. Esposito, O.; Lewis, A.; Hitchcock, P. B.; Caddick, S.; Cloke, F. G. N. *Chem. Commun.* **2007**, (11), 1157.
133. Backvall, J. E. *Tetrahedron. Lett.* **1978**, (2), 163.
134. Backvall, J. E. *Accounts. Chem. Res.* **1983**, 16, (9), 335.
135. Muniz, K.; Hovelmann, C. H.; Streuff, J. *J. Am. Chem. Soc.* **2008**, 130, (2), 763.
136. Streuff, J.; Hovelmann, C. H.; Nieger, M.; Muniz, K. *J. Am. Chem. Soc.* **2005**, 127, (42), 14586.
137. Jordan-Hore, J. A.; Johansson, C. C. C.; Gulias, M.; Beck, E. M.; Gaunt, M. J. *J. Am. Chem. Soc.* **2008**, 130, (48), 16184.
138. Eckert, T. S.; Rominger, R. L. *J. Org. Chem.* **1987**, 52, (24), 5474.

139. McGuinness, D. S.; Saendig, N.; Yates, B. F.; Cavell, K. J. *J. Am. Chem. Soc.* **2001**, 123, (17), 4029.
140. McGuinness, D. S.; Cavell, K. J.; Skelton, B. W.; White, A. H. *Organometallics.* **1999**, 18, (9), 1596.
141. Burling, S.; Mas-Marza, E.; Valpuesta, J. E. V.; Mahon, M. F.; Whittlesey, M. K. *Organometallics.* **2009**, 28, (23), 6676.
142. Zhang, C. Y.; Zhao, Y.; Li, B.; Song, H. B.; Xu, S. S.; Wang, B. Q. *Dalton. T.* **2009**, (26), 5182.
143. Haller, L. J. L.; Page, M. J.; Macgregor, S. A.; Mahon, M. F.; Whittlesey, M. K. *J. Am. Chem. Soc.* **2009**, 131, (13), 4604.
144. Caddick, S.; Cloke, F. G. N.; Hitchcock, P. B.; Lewis, A. K. D. *Ange. Chem. Int. Ed.* **2004**, 43, (43), 5824.
145. Calhorda, M. J.; Brown, J. M.; Cooley, N. A. *Organometallics.* **1991**, 10, (5), 1431.
146. Mann, G.; Baranano, D.; Hartwig, J. F.; Rheingold, A. L.; Guzei, I. A. *J. Am. Chem. Soc.* **1998**, 120, (36), 9205.
147. Widenhoefer, R. A.; Buchwald, S. L. *J. Am. Chem. Soc.* **1998**, 120, (26), 6504.
148. Driver, M. S.; Hartwig, J. F. *J. Am. Chem. Soc.* **1997**, 119, (35), 8232.
149. Lau, W.; Huffman, J. C.; Kochi, J. K. *Organometallics.* **1982**, 1, (1), 155.
150. Tatsumi, K.; Hoffmann, R.; Yamamoto, A.; Stille, J. K. *B. Chem. Soc. Jpn.* **1981**, 54, (6), 1857.
151. Moravskiy, A.; Stille, J. K. *J. Am. Chem. Soc.* **1981**, 103, (14), 4182.
152. Stambuli, J. P.; Incarvito, C. D.; Buhl, M.; Hartwig, J. F. *J. Am. Chem. Soc.* **2004**, 126, (4), 1184.
153. Yamashita, M.; Hartwig, J. F. *J. Am. Chem. Soc.* **2004**, 126, (17), 5344.
154. Hartree, D. R. *Proc. Camb. Phil. Soc.* **1928**, 24, 89.
155. Hohenberg, P.; Kohn, W. *Phys. Rev. B.* **1964**, 136, (3B), B864.
156. Frenking, G.; Sola, M.; Vyboishchikov, S. F. *J. Organomet. Chem.* **2005**, 690, (24-25), 6178.
157. Fock, V. *Z. Physik.* **1930**, 61, 126.
158. Kohn, W.; Sham, L. J. *Phys. Rev.* **1965**, 140, (4A), 1133.
159. Perdew, J. P. B. K.; Ernzerhof, M. *Phys. Rev. Lett.* **1996**, 77, 3865.

160. Perdew, J. P. B. K.; Ernzerhof, M. *Phys. Rev. Lett.* **1997**, 78, 1396.
161. SCM, T. C. Http://www.Scm.Com.
162. Velde, G. T.; Bickelhaupt, F. M.; Baerends, E. J.; Guerra, C. F.; Van Gisbergen, S. J. A.; Snijders, J. G.; Ziegler, T. *J. Comput. Chem.* **2001**, 22, (9), 931.
163. Klamt, A. *J. Phys. Chem.* **1995**, 99, (7), 2224.
164. Pye, C. C.; Ziegler, T. *Theor. Chem. Acc.* **1999**, 101, (6), 396.
165. Klamt, A.; Jonas, V. *J. Chem. Phys.* **1996**, 105, (22), 9972.
166. Klamt, A.; Schuurmann, G. *J. Chem. Soc. Perk. T. 2.* **1993**, (5), 799.
167. Zhu, H.; Ziegler, T. *Organometallics.* **2007**, 26, (9), 2277.
168. Santos, L. S.; Knaack, L.; Metzger, J. O. *Int. J. Mass. Spectrom.* **2005**, 246, (1-3), 84.
169. Santos, L. S.; Knaack, L.; Metzger, J. O. *Int. J. Mass. Spectrom.* **2006**, 248, (3), 155.
170. Ferraz, H. M. C.; Pereira, F. L. C.; Goncalo, E. R. S.; Santos, L. S.; Eberlin, M. N. *J. Org. Chem.* **2005**, 70, (1), 110.
171. Domingos, J. B.; Longhinotti, E.; Brandao, T. A. S.; Bunton, C. A.; Santos, L. S.; Eberlin, M. N.; Nome, F. *J. Org. Chem.* **2004**, 69, (18), 6024.
172. Santos, L. S.; Rosso, G. B.; Pilli, R. A.; Eberlin, M. N. *J. Org. Chem.* **2007**, 72, (15), 5809.
173. Raminelli, C.; Prechtl, M. H. G.; Santos, L. S.; Eberlin, M. N.; Comasseto, J. V. *Organometallics.* **2004**, 23, (16), 3990.
174. Sabino, A. A.; Machado, A. H. L.; Correia, C. R. D.; Eberlin, M. N. *Ange. Chem. Int. Ed.* **2004**, 43, (34), 4389.
175. Aliprantis, A. O.; Canary, J. W. *J. Am. Chem. Soc.* **1994**, 116, (15), 6985.
176. Markert, C.; Pfaltz, A. *Ange. Chem. Int. Ed.* **2004**, 43, (19), 2498.
177. Lewis, A. K. D. Personal communication. In 2008.
178. *ADF output file, error message; Incompatible hessians in GetHessian.*
179. Mayer, I. *Int. J. Quant. Chem.* **1984**, 26, (1), 151.
180. Mayer, I. *Chem. Phys. Lett.* **1983**, 97, (3), 270.
181. Bridgeman, A. J.; Cavigliasso, G.; Ireland, L. R.; Rothery, J. *J. Chem. Soc. Dalton Trans.* **2001**, (14), 2095.

182. Brainard, R. L.; Miller, T. M.; Whitesides, G. M. *Organometallics.* **1986**, 5, (7), 1481.
183. Diversi, P.; Fasce, D.; Santini, R. *J. Organomet. Chem.* **1984**, 269, (3), 285.
184. Miyashita, A.; Ohyoshi, M.; Shitara, H.; Nohira, H. *J. Organomet. Chem.* **1988**, 338, (1), 103.
185. Rowley, D. M. Personal communication. In 2010.
186. Baldwin, J. E. *J. Chem. Soc. Chem. Commun.* **1976**, (18), 734.
187. Caddick, S.; Cloke, F. G. N.; Clentsmith, G. K. B.; Hitchcock, P. B.; McKerrecher, D.; Titcomb, L. R.; Williams, M. R. V. *J. Organomet. Chem.* **2001**, 617, (1), 635.
188. Stauffer, S. R.; Hartwig, J. F. *J. Am. Chem. Soc.* **2003**, 125, (23), 6977.
189. Lowik, D.; Lowe, C. R. *Eur. J. Org. Chem.* **2001**, (15), 2825.
190. Schuurmann, A. K. a. G. *J. Chem. Soc., Perkin Trans 2.* **1993**, 5, 799.
191. Arduengo, A. J.; Dias, H. V. R.; Harlow, R. L.; Kline, M. *J. Am. Chem. Soc.* **1992**, 114, (14), 5530.
192. Arnold, P. L.; Cloke, F. G. N.; Geldbach, T.; Hitchcock, P. B. *Organometallics.* **1999**, 18, (16), 3228.